THE LASER POWERED INTERORBITAL VEHICLE

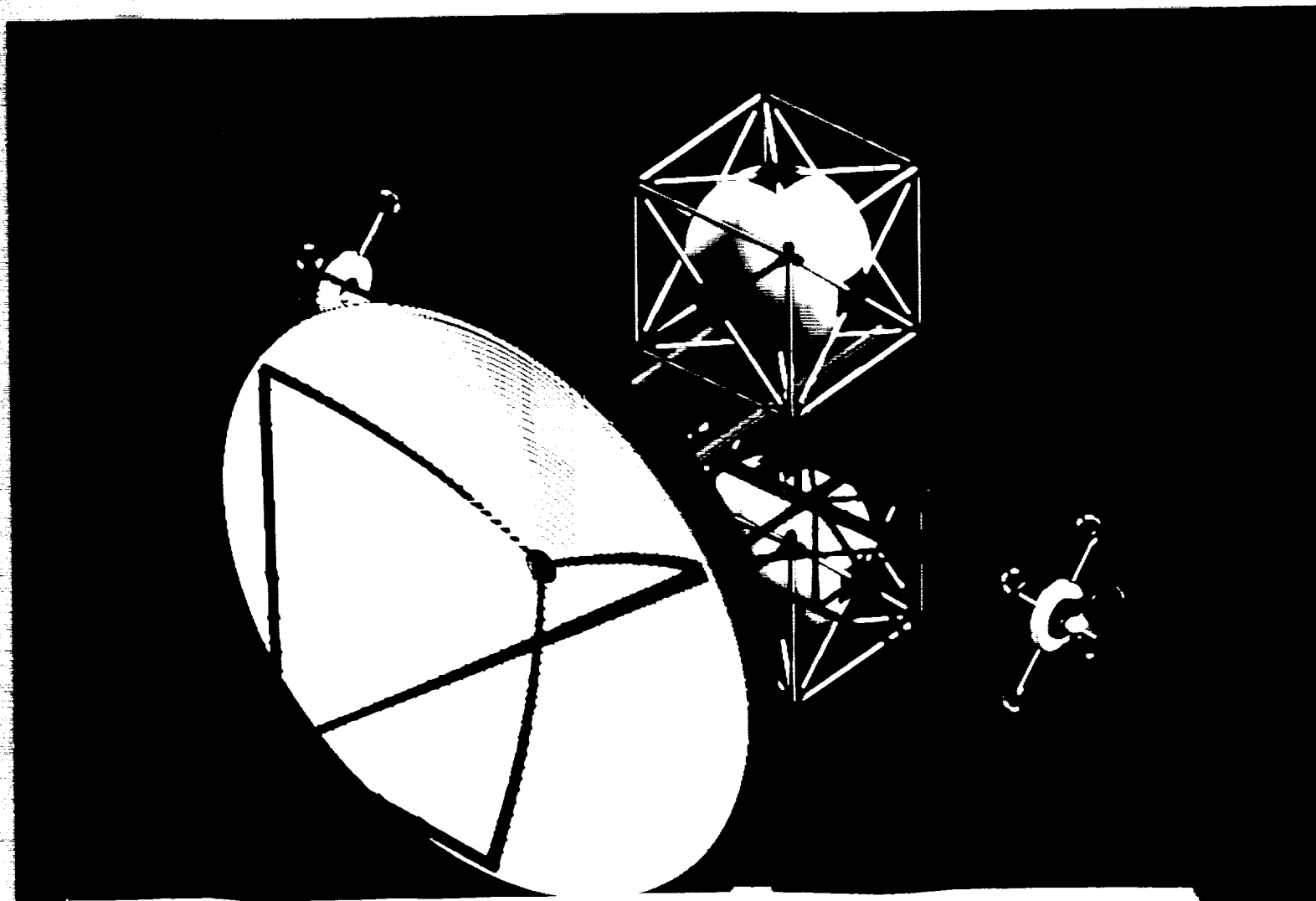

NASA/USRA

ADVANCED SPACE DESIGN PROGRAM

NASW-4435

Department of Aerospace and Ocean Engineering

Virginia Polytechnic Institute & State University

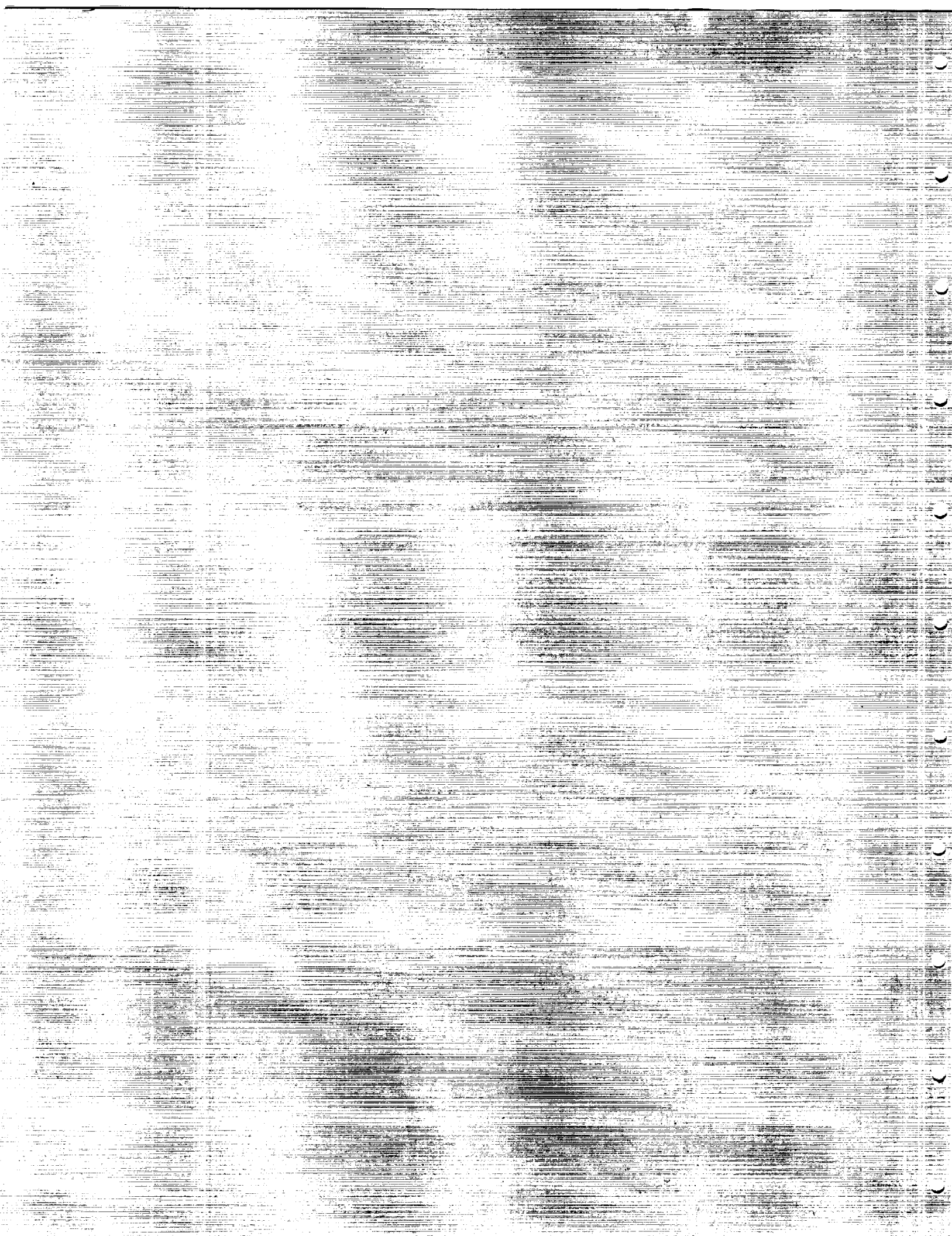

THE LASER POWERED INTERORBITAL VEHICLE

June, 1989

VPI & SU Aerospace Senior Design Team

ACKNOWLEDGEMENTS

We gratefully acknowledge the financial support provided by the National Aeronautics and Space Administration and Universities Space Research Association. Special thanks are also due to Jim Youngblood at NASA Langley Research Center for his technical advice and assistance during this project.

NASA/USRA

ADVANCED SPACE DESIGN PROGRAM

LASER POWERED INTERORBITAL VEHICLE

Design Team:

Michael T. Clarke
John J. Cooper
Gary P. Eggleston
Michael A. Farkas
Dan C. Hunt
Jeff King
Hai Nguyen
Greg Rahal
Kyi Saw
Robert Tipton
John P. Tirone
Hiep Vu

Project Advisor: Dr. A. K. Jakubowski

June 1989

Department of Aerospace and Ocean Engineering

Virginia Polytechnic Institute & State University

Blacksburg, VA

Table of Contents

List of Illustrations

List of Tables

Abstract

This report presents a preliminary design of a low-thrust Laser Powered Interorbital Vehicle (LPIV) intended for cargo transportation between an earth space station and a lunar base. The LPIV receives its power from two iodide laser stations, one orbiting the earth and the other located on the surface of the moon. The selected mission utilizes a spiral trajectory, characteristic of a low-thrust spacecraft, requiring 8 days for a lunar rendezvous and an additional 9 days for return. The ship's configuration consists primarily of an optical train, two hydrogen plasma engines, a 37.1 m box beam truss, a payload module, and fuel tanks. The total mass of the vehicle fully loaded is 63300 kg.

A single plasma, regeneratively cooled engine design is incorporated into the two 500 N engines. These are connected to the spacecraft by turntables which allow the vehicle to thrust tangentially to the flight path. Proper collection and transmission of the laser beam to the thrust chambers is provided through the optical train. This system consists of the 23 m diameter primary mirror, a convex parabolic secondary mirror, a beam splitter and two concave parabolic tertiary mirrors.

The payload bay is capable of carrying 18000 kg of cargo. The module is located opposite of the primary mirror on the main truss. Fuel tanks carrying a maximum of 35000 kg of liquid hydrogen are fastened to tracks which allow the tanks to be moved perpendicular to the main truss. This capability is required to prevent the center of mass from moving out of the thrust vector line.

The laser beam is located and tracked by means of an acquisition, pointing and tracking system which can be locked onto the space-based laser station. Correct orientation of the spacecraft with the laser beam is maintained by control moment gyros and reaction control rockets. Aditionally an aerobrake configuration was designed to provide the option of using the atmospheric drag in place of propulsion for a return trajectory.

NOMENCLATURE

LEO:	Low Earth Orbit
LLO:	Low Lunar Orbit
LPIV:	Laser Powered Interorbital Vehicle
SIGHT:	Simulated Interactive GrapHical Trajectory (System)
TOF:	Time Of Flight
GEO:	Geosynchronous Earth Orbit
AOTV:	Aero-assisted Orbital Transfer Vehicle
EVA:	Extra-Vehicle Activity
FS:	Factor of Safety
IBP:	Inverse Bremsstrahlung Process
RCS:	Reaction and Control System
CMG:	Control Moment Gyros
CG:	Center of Gravity
MLI:	Multi-Layered Insulation
APT:	Acquisition, Pointing, and Tracking
LPS:	Laser Powered Station
APD:	Avalanche PhotoDiode
FOV:	Field Of View
TTC:	Telemetry, Tracking, and Command
FDMA:	Frequency-Division Multiple Access
ASK:	Amplitude Shift Keying
FSK:	Frequency Shift Keying
PSK:	Phase Shift Keying
QPSK:	Quarternary Phase Shift Keying
BER:	Bit Error Rate
TPS:	Thermal Protection System
TOF:	Time of Flight
CTE:	Coefficient of Thermal Expansion

SYMBOLS

P	power
T	thrust
g	gravitational constant
m	mass
I_{sp}	specific impulse
T_o	stagnation temperature
P_o	stagnation pressure
A_e/A	nozzle area ratio
H	efficiency
u	velocity of propellant
V	ship velocity
K	Kelvin
I_i	mass moment of inertia about i-axis
$\dot{m}$	mass flow
$\dot{q}$	heat flux
σ	Stefan-Boltzman constant
k	thermal conductivity
h_{fg}	heat of vaporization
q	solar radiation constant
ε	emissivity
V_{cs}	circular velocity
r	radial distance
Db	decibels
G	antenna gain
lamda	wavelength
B	bandwidth
C/N	carrier - noise ratio
lbm	pound mass
L/D	Lift to drag ratio
C_p	coefficient of pressure
α	angle of attack
C_L, C_D, C_M, $C_{y\beta}$, $C_{H\beta}$, $C_{l\beta}$	stability derivatives

INTRODUCTION

FOUNDATIONS OF THE LASER POWERED VEHICLE

Although the concept of wireless power transmission was conceived in the late 1800's, the technology to achieve this was not developed until the mid 1900's. The concept of laser powered vehicles makes use of this principle to eliminate the need for an onboard power source. This idea is quite useful for space applications since it eliminates the need for fuel oxidizers, thereby reducing the vehicle's overall mass.

The laser powered spacecraft receives its power from a remote laser station through an optical train which receives and then focuses the incoming laser beam. Thrust is obtained by directing the beam into the engine's chamber. A plasma is initiated in the chamber, raising the temperature of the propellant which is then exhausted through a propulsive nozzle to produce thrust.

For quite some time now this country's space program has developed the means to create and utilize craft for space exploration, but up to now these vehicles have been equipped with chemical rockets requiring very large quantities of propellant. The electrical rockets provide a potential for significant reduction of fuel requirements, however, they can develop very low thrust and consequently, result in very long trip times. Laser propulsion can provide an ideal compromise by combining significant propellant savings with low to medium thrust levels resulting in reasonably short trip times.

Without the added mass of fuel oxidizers, a vehicle of the same size can transport more cargo, or go farther on the same initial amount of propellant. Laser propulsion provides a means for high efficiency, low thrust spaceflight as a result of its high specific impulse, (I_{SP}). I_{SP} on the order of 1000-2000 sec are common for this type of propulsion as compared to chemical rockets which possess I_{SP} on the order of 400 secs.

PROJECT PROPOSAL

Requirements and objectives for the preliminary design of a Laser-Propelled Interorbital Vehicle (LPIV) have been established in consultation with NASA Langley Research Center. The LPIV will be used for transportation between low Earth and Moon orbits. Power will be provided via two iodide laser stations (1.315μm wavelength), one being a direct solar-pumped laser orbiting the Earth and the other a nuclear-powered laser placed on the lunar surface. The maximum beam power provided by the laser stations is 15 megawatts. An additional requirement is that the LPIV be capable of transporting payloads of 16000 to 18000 kg on each leg of its mission. The LPIV itself is to be reusable with allowances for the periodic maintenance of components needing refurbishment. An aero-assisted version utilizing a rigid aeroshell is to be considered along with an all-propulsive version. The all-propulsive system may include hybrid systems that combine laser and other engine types. The technology level for the LPIV construction is assumed to be one projected for the 2010-2020 time frame. The important design objectives for the LPIV are as follows:

1. Minimize propellant requirements and vehicle dry mass
2. Minimize size of laser stations

3. Minimize trip times

Once the requirements of the proposal had been established, a review of literature was initiated with an emphasis placed on studies done regarding the optical train (Ref. Minovich), and the plasma engines (Ref. Keefer).

EVOLUTION OF THE LPIV DESIGN CONFIGURATION

The initial task involved in developing a laser-powered spacecraft is the design of the optical system required to capture and focus the incoming laser beam. The optical system will use a combination of highly reflective parabolic and planar mirrors in order to capture the incoming laser beam.

Using the criteria established by NASA/VPI Dept. of Aerospace Engineering as guidelines, two design configuration concepts were considered. Following the 1988 VPI design team proposal (Ref. SLICK), the first scheme utilized an off-center primary mirror design to capture and then focus the power beam into a single laser engine. The term "off-center" refers to the fact that the secondary mirror is situated off the axis of the primary mirror. Calculations done indicated a primary mirror diameter of 23 meters was needed in order to successfully capture the incoming beam. Auxiliary planar mirrors were to direct a focused beam into the combustion chamber of the main engine. The optical assembly was supported by an L-shape triangular truss which pivoted and rotated about a turret at its base. The placement of the auxiliary mirrors followed directly from the focal length of the primary mirror.

For optimum structural stability, the shape of the truss was hexagonal, measuring 30 meters across and approximately 5 meters in height. The truss housed the LPIV's two spherical fuel tanks as well as two cylindrical cargo bays. These were mounted on the interior structure. Figure 1 shows a general schematic of the vehicle. The advantage of this configuration was that the vehicle only needed to roll about one axis in order to receive the incoming laser beam from all directions, along with a corresponding optical train (primary plus two tertiary mirrors) rotation. However, this design necessitated engine gimballing in order to maintain thrust alignment with the vehicle's center of mass. It also demanded large structural mass to support the off-center primary mirror.

The most appealing feature associated with the off-centered configuration was the ease with which it could intercept the incoming laser beam. This idea brought to mind the concept of a fixed primary mirror, wherein the entire vehicle rotates in order to catch the laser beam. The concept, similar to that proposed by Minovich, eliminates the need for a complicated mirror support assembly, as well as stabilizes the location of the vehicle's center of mass by using a mirror which is symmetric about an axis in-line with the ship's center of mass. The problem of gimballing the engines to alter the thrust is eliminated by: a) using two engines situated at each end of a main truss structure, with each capable of 360° rotation, and b) providing a means of maintaining the craft's center of mass at a fixed point, midway between the engine-turntable rotation centers. The mirror's mass could then be counterbalanced by proper positioning of the payload or by allowing the fuel tanks to move as propellant is used.

The fixed mirror geometry required a new technique to direct the beam into the engine chambers. The use of two engines instead of one also dictated the use of a beam splitter in the optical train to divide the beam into two equal components. With proper placement of the secondary mirror, the selected layout for the optical system allowed the laser beam to be redirected through an opening located at the center of the primary mirror, where it is then divided by the beam splitter and reflected into each of the two engine chambers. The geometry of this design is represented in Figure 2. The location of the optical system, engine placement, as well as general propellant and payload locations are shown.

To capture the incoming laser and to align the thrust vector with the trajectory path, the vehicle utilizes a control moment gyro/reaction control rocket system for synchronized turntable rotation of the engines. This engine rotation provides the LPIV with thrust vectoring capabilities, and the fixed mirror geometry reduces structural degradation due to vibrations, possible with an off center

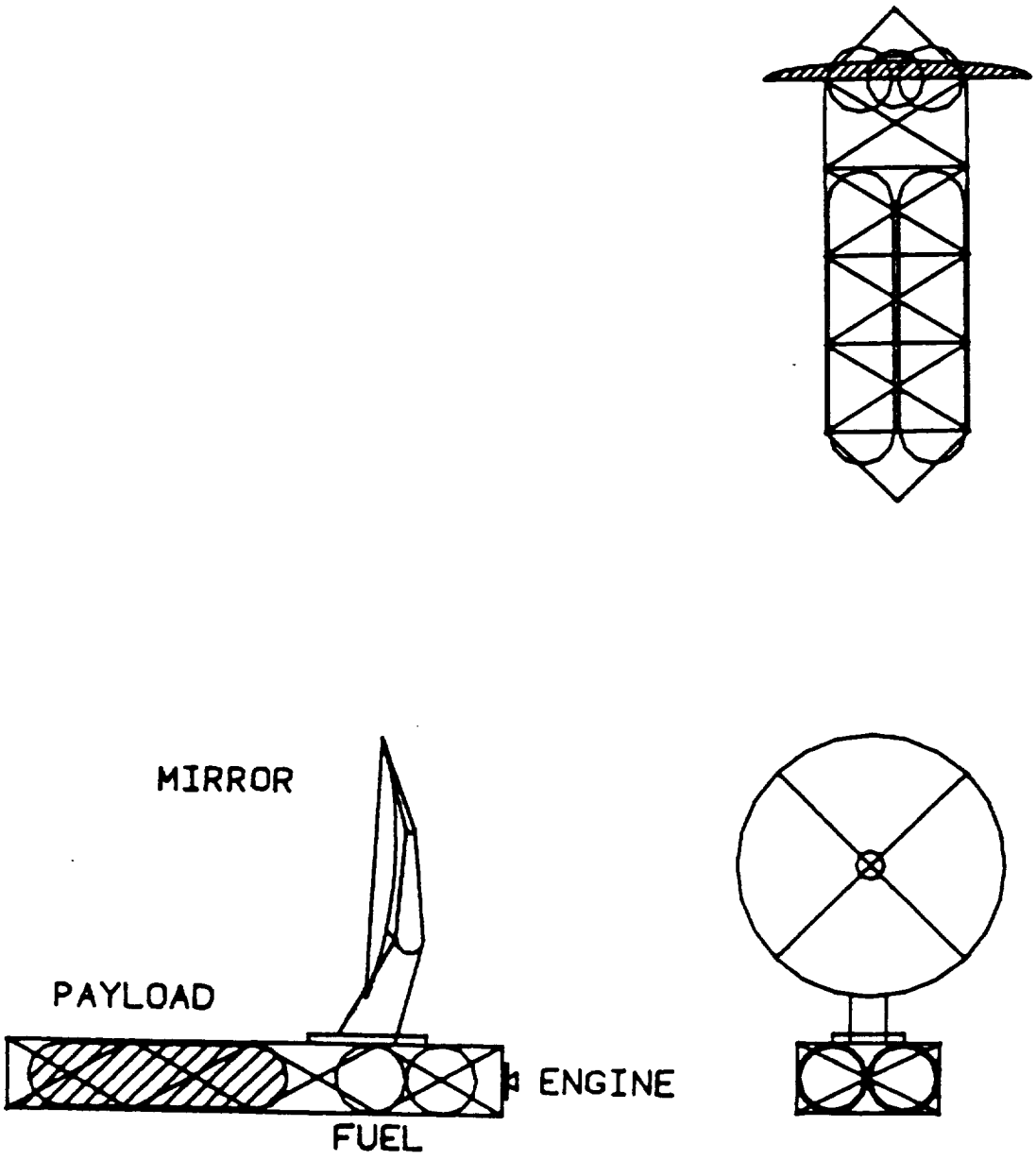

Figure 1. Initial Configuration of the LPIV

mirror configuration. Also, less support structure is needed in comparison with the off-center design. Figure 3, shows the final configuration in 3 view representation; showing the payload, the engine assemblies located at the ends of the main truss and the fuel tanks mounted on the track mechanism.
The next most important feature of the LPIV are the laser sustained plasma engines which provide the vehicle with thrusting capabilities. The two 500 Newton engines are mounted on turntables located at each end of the main truss structure. The turntables allow the engines to rotate through 360°. Rotations of both engines are precisely synchronized to ensure symmetric thrusting.

As part of this project, an aerobraked option of the LPIV was considered in addition to a non-aerobraked or all-propulsive version. The advantage of an aerobrake is the use of a planetary atmosphere to create drag on the vehicle, thereby decelerating the vehicle without expending propellent in retro burns. This technique lowers the fuel mass consumed on each return mission. Unfortunately, the addition of this feature onto the LPIV increases the vehicle dry mass as well as subjects it to extensive thermal and gravitational loads, requiring additional support structure. The first configuration considered a raked elliptical conic section for the aerobrake (Ref. Scott). It provided excellent stability and aeromanuvering capabilities, due to its asymmetry about the LPIV's primary axis. This geometry however, was not suitable for the two engine configuration due to the instability occurring when the engines are rotated. The fact that the aeroshell was not symmetric about the LPIV's roll axis created difficulties in maintaining a stable center of mass. By choosing a symmetric geometry, these problems were alleviated and the benefits obtained by the LPIV's fixed mirror design were not sacrificed. Figure 4 shows the orthographic views of the aero-assisted version with Figure 5 being an overall isometric representation.

GENERAL MISSION SCENARIO

The mission is assumed to begin in Low Earth Orbit (LEO), with a final destination being intercept into a Low Lunar Orbit (LLO). The initial orbit is oriented with the proposed Earth-orbiting Space Station, or roughly 220 nautical miles above the Earth's surface. The LPIV is powered by the solar pumped laser station and respective relay stations which orbit the Earth in the equatorial plane at an altitude of one earth radius. The vehicle is designed for cargo transportation between the LEO and low lunar orbit. The payload it will handle consists primarily of maintenance supplies and provisions on the outbound mission, and oxygen manufactured at the lunar base on the return trip.

The mission scenario is broken into three phases: departure, coast and capture, for both the aero-assisted and the non-aerobrake versions. The trajectory for departure follows a low-thrust spiral, taking into account the neccessary condition of intermittent power as a result of laser station-solar power interruption. A coast period will begin at an altitude of approximately 100000 kilometers, with enough total energy to reach the Moon's orbit. A third phase for navigation is initiated near the moon in order to match the spacecraft's velocity with the specified LLO circular speed; this is followed by an appropriate docking procedure. The return flight follows a similar outline with only minor adjustments made to account for the different profile on the power supply. The trajectory for the full mission is shown in Figure 6.

In this report, the evolution and final selection of a non-aerobraked and an aeroassisted vehicle are presented. Table 1 gives a mass breakdown of the non-aerobraked LPIV. In the chapters which follow, a comprehensive preliminary study of the mission, configuration and sub- ystems of the spacecraft is presented.

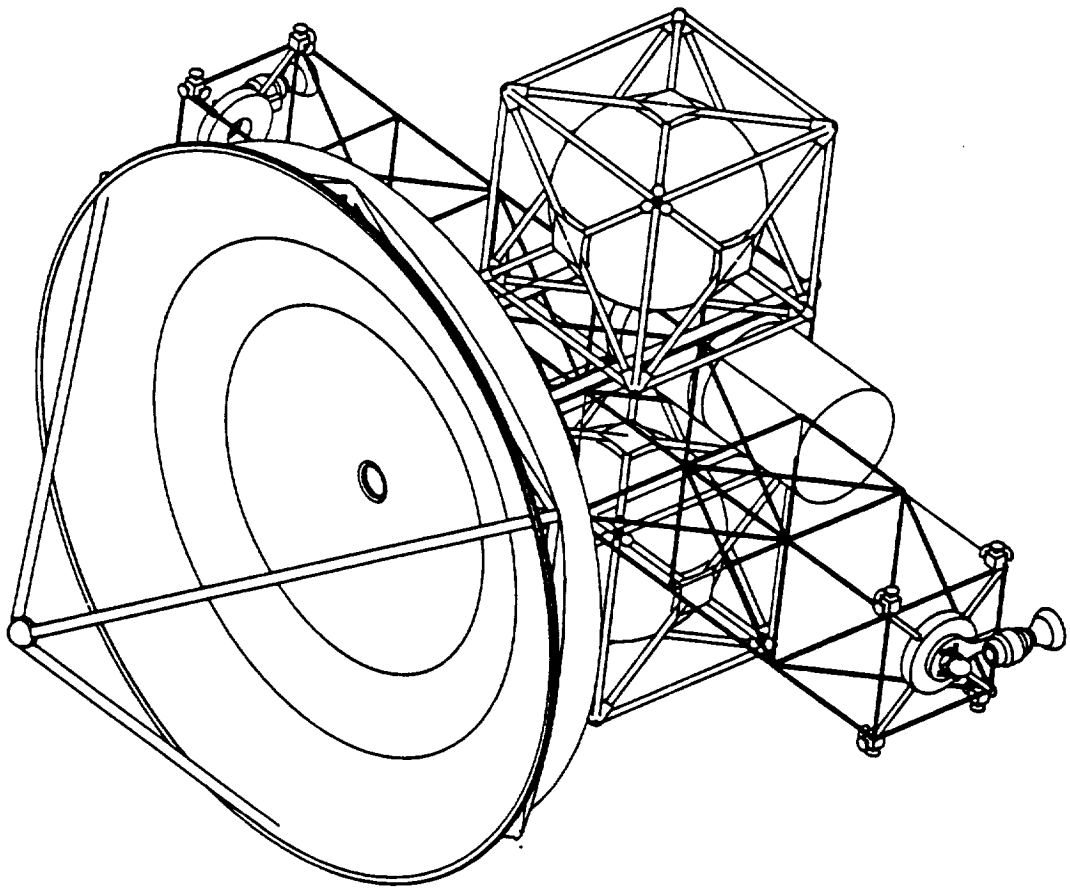

Figure 2. Isometric View of the LPIV

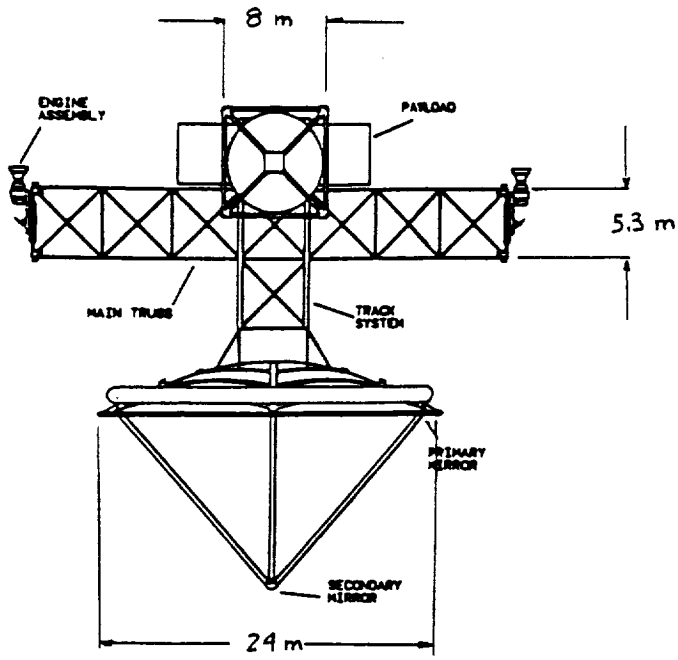

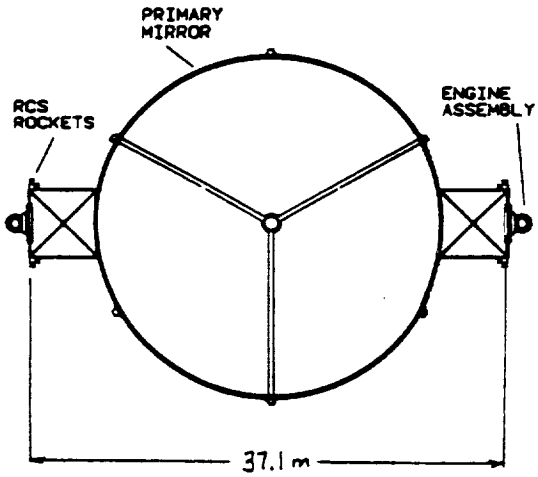

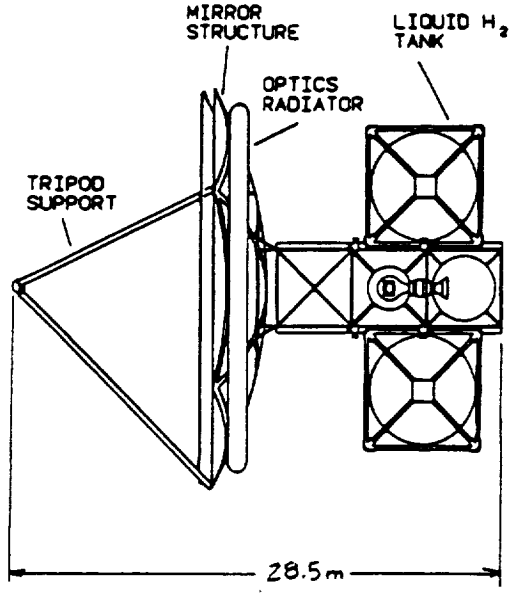

Figure 3. Three Views of the Non-aeroassisted LPIV

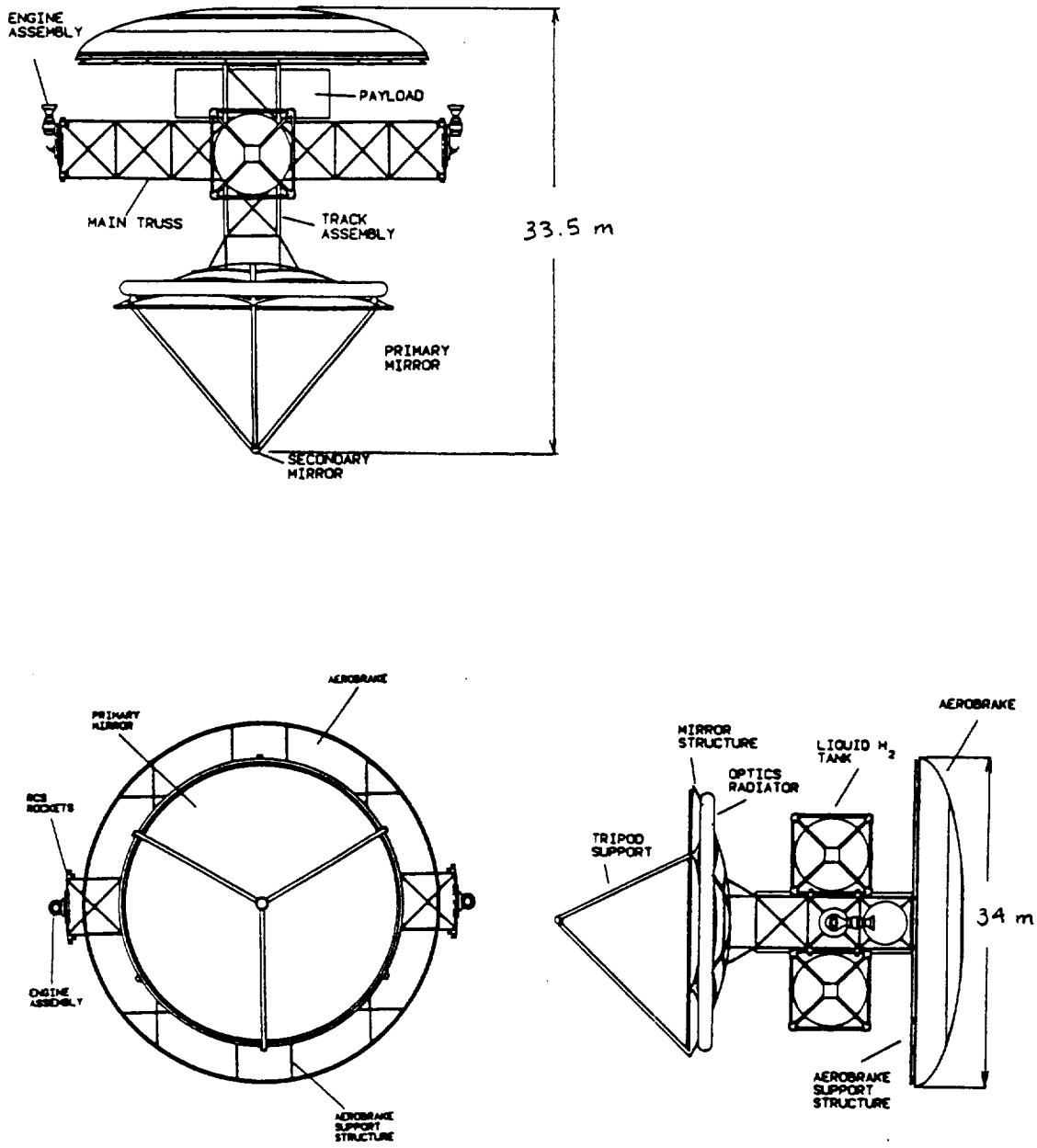

Figure 4. Three Views of the Aeroassisted LPIV

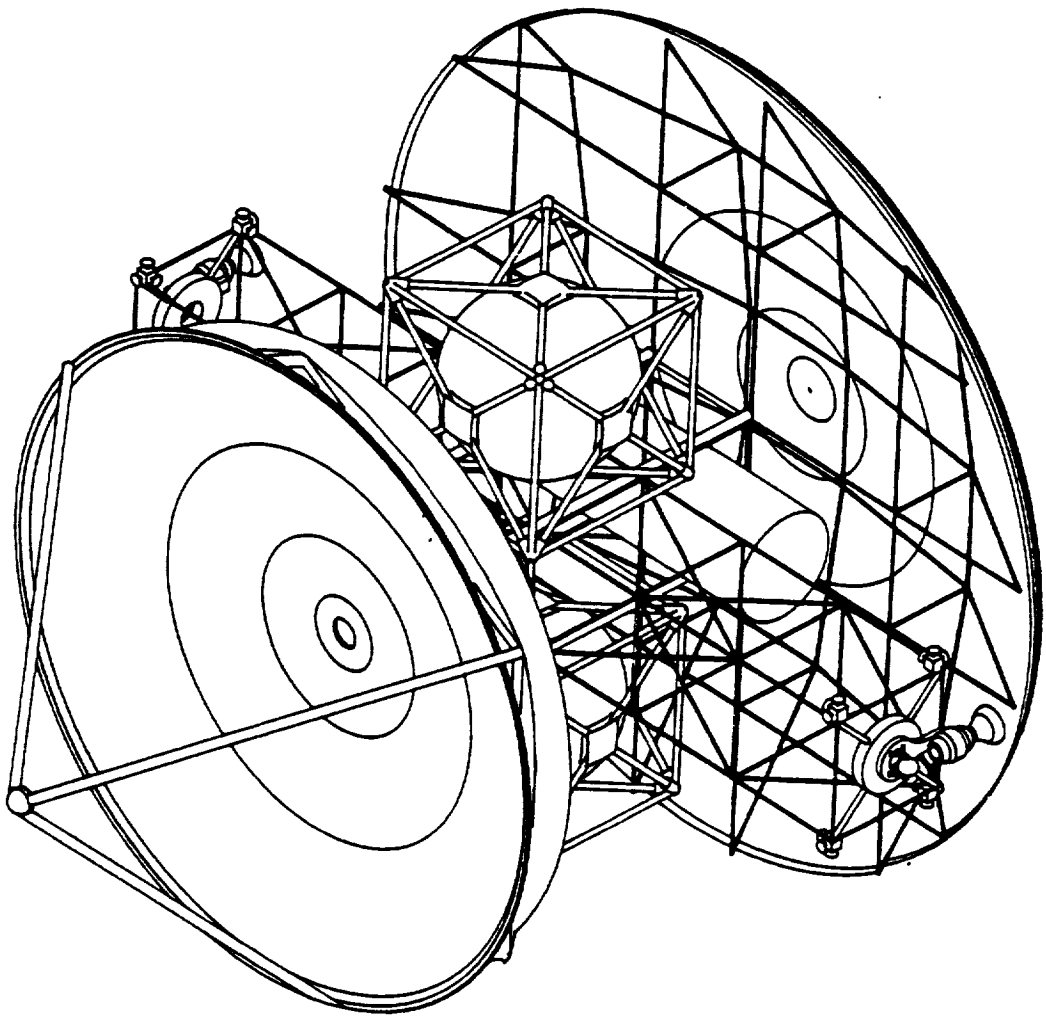

Figure 5. Isometric View of the Aeroassisted LPIV

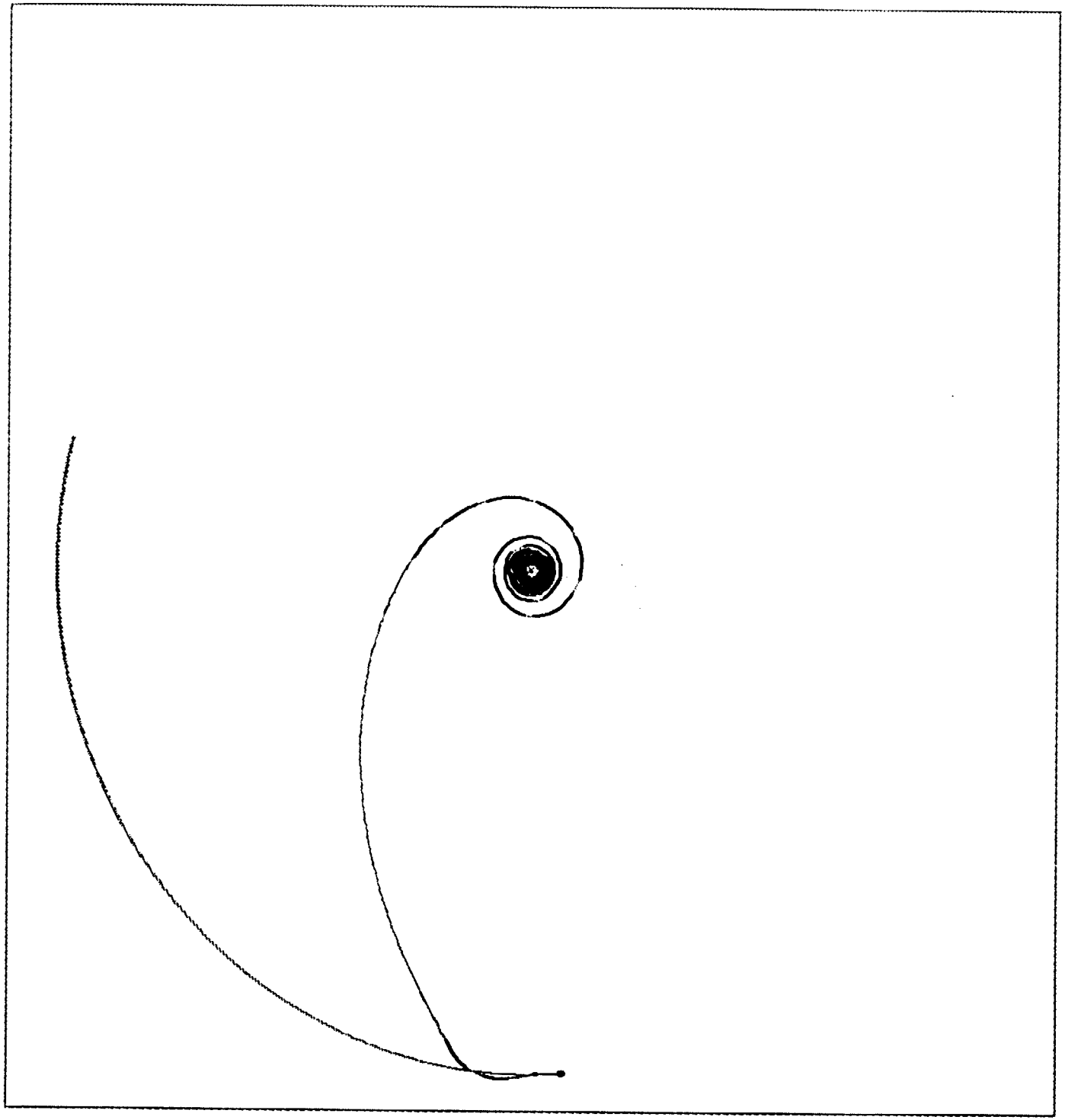

FIGURE 6

Table 1. LPIV Total Mass Breakdown

Subsystem	Mass (kg)
Main Truss	734
Propellant Tanks	1293
RCS and CMG's	1022
Engines	200
Turntables	547
Docking Mechanism	90
Optical System	5400
Acquisition, Pointing and Tracking (APT)	105
Communications	70
Payload Module	649
Vehicle Dry Mass	12300
Propellant Mass	35000
Payload Mass	16000
Total Vehicle Mass	63300

ORBITAL MECHANICS AND TRAJECTORY ANALYSIS

INTRODUCTION

In designing the mission of the LPIV the following objectives were considered: minimizing trip time, minimizing fuel consumption for a given mission, and optimizing the LPIV trajectory. Orbital mechanics and trajectory analysis were used to provide a way to meet these objectives. These analyses were performed using a multi-functional mission simulation and analysis system named SIGHT. The evolution of that system and the problems that necessitated the innovation of SIGHT will be discussed in this chapter. Conclusions and results of the analysis as well as future recommendations and proposals for the LPIV mission will also be presented.

MISSION ASSUMPTIONS AND REQUIREMENTS

The fundamental purpose of the LPIV spacecraft is to transport 16000 kg of cargo between Low Earth Orbit (LEO) and Low lunar Orbit (LLO). The transport will service the proposed earth-orbiting space station and the lunar orbiting station. In the proximity of the Earth, the LPIV's propulsion system is energized by a solar-pumped iodide laser orbiting equatorially at an altitude of one earth radius (6373 km). In the vicinity of the Moon, the LPIV will receive energy from a nuclear-powered station on the lunar surface.

The earth orbiting laser station cannot provide continuous energy to the LPIV due to the passage of the station through the earth's shadow. This station-solar occultation means that on-demand power near the Earth for the LPIV cannot be provided. This situation exists for seventeen percent of the orbit or forty minutes out of the two hundred forty minute orbital period of the laser power station (Figure 7). Whenever the spacecraft is not in line of sight with the orbiting power station because of Earth interference, one of two optical relay stations are used (Figure 8). Designed to reflect and redirect the beam, the relays are placed in the same reference orbit at 115 degrees lead and 115 degrees lag with respect to the power station. The relay stations are utilized only when direct beam capture between the laser station and the LPIV is prohibited.

EVOLUTION OF TRAJECTORY DETERMINATION

Prior to the development of the program SIGHT, three primary mission scenarios were successively investigated to provide orbital mechanics data for the design mission. These were the following: a multi-elliptical orbital transfer, an approximate spiral method, and an Eulerian numerical integration applied to the equations of motion of the spacecraft.

Multi-Impulsive Elliptical Transfer

Since the vehicle employs a power-limited, low-thrust propulsion system, a trajectory determined by a minimum energy Hohmann transfer is impossible without the aid of an impulsive chemical rocket. Therefore, as a starting point to this low-thrust trajectory problem, the use of a multi-

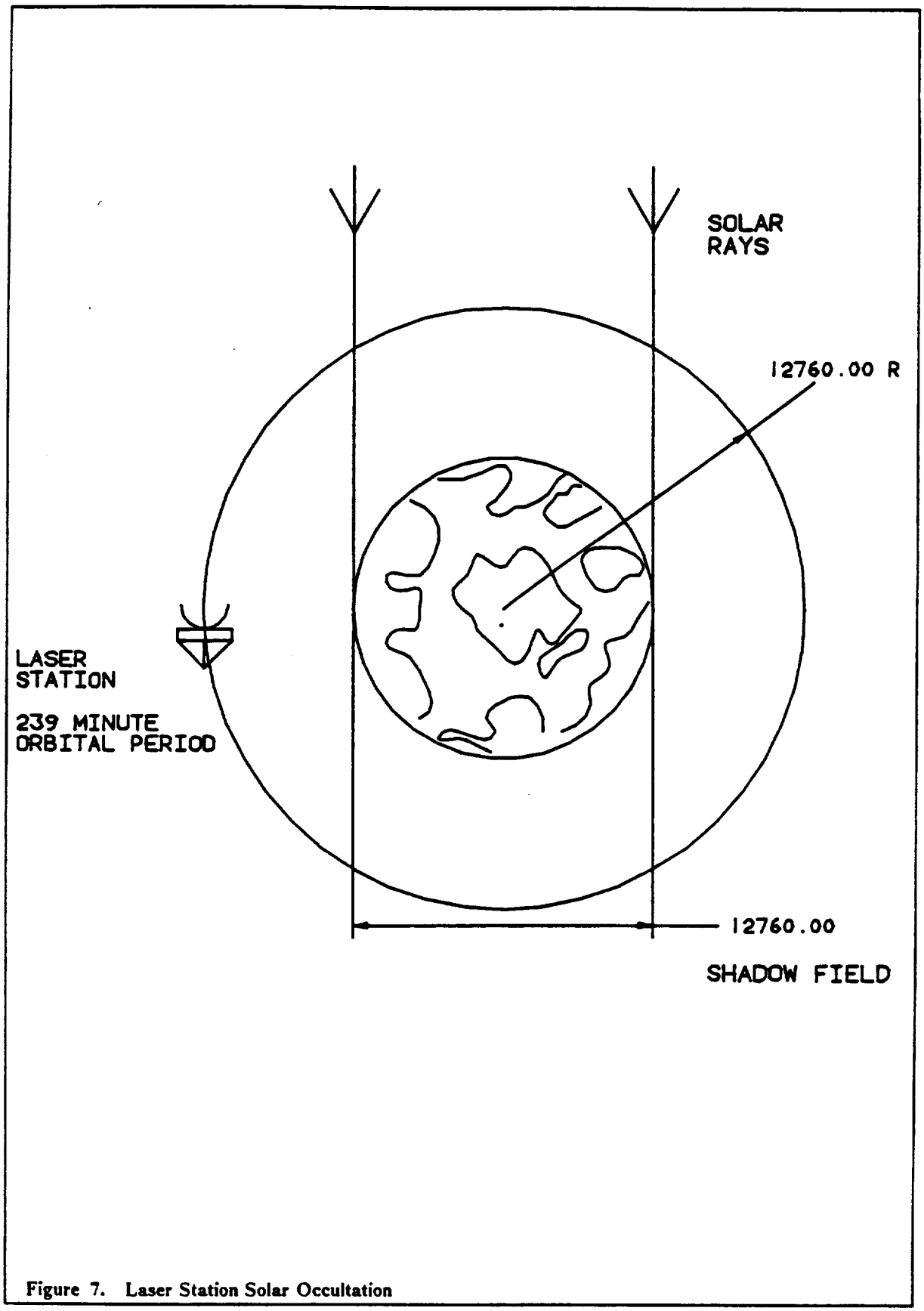

Figure 7. Laser Station Solar Occultation

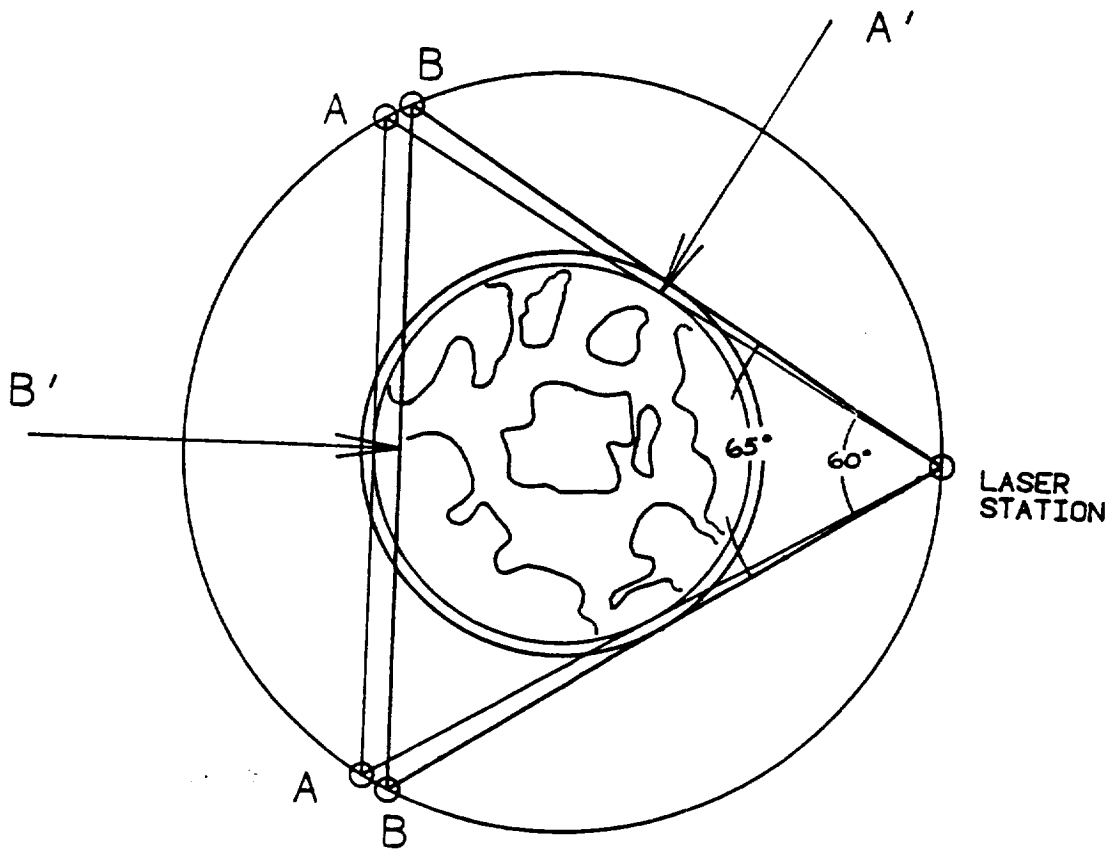

Figure 8. Laser Station and Beam Relay Configuration

elliptical transfer was first considered. (Ref. SLICK) This scheme suggested an analysis involving a series of elliptical orbits followed by a translunar chemical rocket injection and a final LLO capture.

The method requires successive perigee burn arcs to lift the apogee of the orbit to a desired intermediate orbit (Figure 9). By assuming constant thrust over an arc of 120 degrees centered at perigee, an equivalent impulsive thrust is computed by integrating the thrust through the time of the burn. This integration results in an equivalent change in velocity, delta-V, which is assumed to act at perigee. Applying this delta-V, the impulsive thrust trajectories yield increasingly eccentric elliptical paths with common perigee locations. Another series of burns are then required to circularize into the reference orbit.

To extend the apogee out to a radial distance equal to the Moon's orbit would require a great deal of time because of the number of ellipses; therefore, an alternate approach was considered. In this scenario the LPIV uses GEO as the intermediate orbit and without circularization, fires an impulsive chemical rocket to put the vehicle into a trans-lunar trajectory. Following the injection another impulsive thrust at the vicinity of the moon puts the LPIV into a LLO.

This method takes too much time and does not reflect the true potential that exists in a low- thrust vehicle. Table 2 reflects the data for this mission.

Table 2. Multi-Impulsive Elliptical Transfer

	Delta-V (km/sec)	TOF (days)
LEO to GEO	0.931	6.34
Translunar injection	1.053	5.67
LLO capture	1.188	-

Spiral Trajectory Approximation

A more feasible approach developed by Ernst Stuhlinger assumes the vehicle to travel in segments of spirals as opposed to elliptical paths. (Figure 10). Stuhlinger's method simplifies the spiral trajectory of a low-thrust vehicle using a stepwise approach. The following simplifications are used: (1) The moon moves in a circular orbit about the Earth, (2) The ship's motion is always treated as a two- body problem, (3) The thrust of the propulsion system is constant with the propellant masses decreasing linearly with time, and (4) The thrust vector is tangential to the trajectory. (Ref. Stuhlinger)

The motion of the ship is determined by the laws of mechanics. According to Stuhlinger these equations lend themselves easily to stepwise integration with given initial conditions, as shown in Appendix A. Instead of computing this spiral by direct integration of the equations of motion, a simpler method is employed by replacing one revolution of the spiral by a circle having the average spiral radius. A disadvantage of this method is that the solution loses accuracy when the spiral becomes wider. For this reason the spiral is only considered out to an intermediate distance where once again our method is to employ a translunar chemical thrust injection. Upon nearing the moon's orbit, an impulsive thrust is used to produce a capture orbit ending at LLO with the appropriate circular speed. Data for these maneuvers are shown in Table 3.

Table 3. Stepwise Spiral Trajectory

	Delta-V (km/sec)	TOF (days)
LEO to GEO	3.12	2.73
Translunar injection	1.012	4.40
LLO capture	1.486	1.81

Numerical Integration Method

Since the error involved using Stuhlinger's method is undetermined, the data referring to the spiral trajectory is possibly inaccurate. In addition, the method assumes constant thrust, disregarding the condition of solar oculation, when the laser station is in the shadow of the Earth, unable to power the spacecraft. Numerical integration of the equations of motion is the next approach.

Utilizing an Eulerian method of approximation, the integration routine calculates the vehicle's position and velocity using small time intervals in the equations of central force motion (See Appendix A). In addition to previous considerations, this algorithm assumes that the vehicle will thrust only when the laser power station is not in the Earth's shadow. The resulting trajectory is a spiral of which an intermediate orbit, GEO, is again chosen to initiate an impulsive burn for translunar flight, followed by a subsequent impulse to circularize at LLO. Data for this mission is shown in Table 4 with a summary of all preliminary missions referenced in Table 5.

Table 4. Eulerian Approximation Method

	Delta-V (km/sec)	TOF (days)
LEO to GEO	3.21	3.03
Translunar injection	1.012	4.40
LLO capture	1.486	1.81

Table 5. Summary of Preliminary Outbound Missions

	Delta-V (km/sec)	Fuel Required (kg)	TOF(days)
Multiple Ellipse	3.172	51023	10.71
Stepwise Spiral	5.618	30700	8.94
Eulerian Method	5.708	28546	9.24

Up to this point the mission analysis had still failed to deliver a feasible low-thrust trajectory rendezvous and capture into LLO. The Eulerian method might well have been adapted for such an application; however, after research into numerical routines, a much more accurate and efficient numerical integration technique was applied. Not only does the method yield feasible results, it emphasizes the potential of the laser- powered vehicle and eliminates the undesirable requirement of chemical rocket injections for transit or circularization.

SIGHT

SIGHT is a multi-functional mission simulation and analysis system for the determination of orbital mechanics and spacecraft dynamics. SIGHT provides three dimensional real-time simulation of the orbital paths and rotations of multiple bodies. The system uses a numerical solution to the restricted three body problem and introduces algorithms for guidance, navigation and control. The purpose of SIGHT is to create, model and analyze complex scenarios of thrusting and non-thrusting structures.

In the past, little attention has been given to the guidance and control of low thrust Earth-Lunar trajectories or to the consideration of simultaneous gravitational effects of the Earth and Moon (Ref. Korsmeyer). The trajectory determination, guidance and navigation are all closely related problems. The SIGHT system accomplishes three-body trajectory analysis as well as basic orbital changes and circularization.

Background on Orbital Motion

Definition of Coordinate System

The reference frame is an inertial earth-centered orthogonal XYZ system. The orbital plane of the Earth and Moon is specified to be in the XY plane, the inclination of the Earth's equator then is eighteen and one-third degrees. A valid assumption is that precession of the ascending and descending nodes of the Moon and lunar libration do not to occur. It is also customary to assume that the X-axis is pointed colinear with the autumnal or vernal equinox. These reference locations represent the apparent point of intersection with the sun's motion on the ecliptic with the celestial equator. This assumption is only necessary if the accurate positioning of the stars which are added to the display for visual perspective.

In this chapter, positions and velocities of the bodies in the system are referenced with respect to the inertial frame. Results are presented with vector magnitudes irrespective of orientation.

Laws Governing Orbiting Bodies

The basics laws governing orbiting bodies have been known since the time of Newton. One of the basic laws formulated by Newton is the law of gravity, stating that any two bodies attract one another with a force proportional to the product of their masses and inversely proportional to the square of their distance. Expressed in vector notation this law becomes:

$$\vec{F}_g = -\frac{GMm}{r^3}\vec{r} \tag{1}$$

where $\vec{r}$ is the vector between masses M and m. G is the universal gravitation constant.

Due to the vector nature of force, this law may be extrapolated to a system with multiple bodies. The equation of force for N-bodies becomes:

$$\vec{F}_g = -Gm_i \sum_{j=1}^{n} \frac{m_j}{r_{ji}^3}\vec{r}_{ji} \tag{2}$$

This formula can easily be converted to an acceleration for the i-th body by merely dividing through by the i-th mass. This general formula for acceleration in a N-body system is:

$$\ddot{\vec{r}} = -G \sum_{j=1}^{n} \frac{m_j}{r_{ji}^3}\vec{r}_{ji} \tag{3}$$

Basic simplifying assumptions were made for this formula governing the orbital model. First, all bodies are assumed to be point masses. Secondly, gravitation is the only force that perturbs the N-body system.

This model may deviate siginifcantly from a realistic environment for two reasons. Contrary to the first assumption, a planetary body is not spherical but oblate and bulges at the equator. This asphericity causes perturbative effects for orbiting bodies. Secondly, the system is prone to other accelerations due to thrust if a spacecraft is concerned, or other effects due to solar pressure or atmospheric drag. Considering these other effects, we may group the other accelerations into one term
$\vec{a}_\tau$. The equation governing our system will become:

$$\ddot{\vec{r}} = -\frac{GM}{r^3}\vec{r} + \vec{a}_\tau \tag{4}$$

Description of Computational Technique

Background on Mathematical and Computational Methods

The general equation of motion in (4), is a second order non-linear differential equation. Rewritten in general mathematical notation this formula can be expressed as:

$$\ddot{\bar{r}} = \bar{f}(\bar{r}, t) + \bar{u}(\bar{r}, t) \tag{5}$$

In modern day engineering systems, this is referred to as an input-output problem. The $\bar{f}(\bar{r}, t)$ function is determined by physical mechanism and the $\bar{u}(\bar{r},t)$ term is the input function.

In our application, $\bar{f}(\bar{r}, t)$ is determined by the law of gravitation. This function will later be extended to include other accelerations due to solar pressure and atmospheric drag. The $\bar{u}(\bar{r}, t)$ term will be assumed as a function governing the thrust over a specific time interval. Traditionally, analytical solutions of this equation could be determined by Euler's variation of parameters or other techniques. These methods are still considered feasible when $\bar{u}(\bar{r},t)$ is equal to zero. Analytical solutions are considered difficult when the solutions for various control functions are desired, or when complex adaptive control functions are employed.

When $\bar{u}(\bar{r},t)$ operates over short time intervals velocity effects may be assumed to be impulsive. For high thrust applications such as chemical rockets, adequate approximations can be obtained by assuming that a change in velocity occurs at a point as opposed to a time interval. Impulsive velocity changes become inadequate when a low-thrust power supply or long duration reaction and control system maneuvers are involved. Other complications will result with constraints of power supply that are time and position dependent on other elements in the system. Examples are solar sails and the laser propulsion system that is addressed in this paper.

Application of Numerical Methods

Second-order differential equations can be written as two coupled first-order equations by introducing an additional variable. This means that the equations must be solved simultaneously. The two first order formulas are:

$$\dot{\vec{r}} = \vec{v} \qquad\qquad \dot{\vec{v}} = \vec{a}_\tau - \frac{GM}{r^3}\vec{r} \tag{6}$$

To describe an object in the Cartesian coordinate system, these functions become six equations.

$$\begin{aligned} \dot{x} &= v_x & \dot{v}_x &= a_{\tau x} - \frac{GM}{r^3}x \\ \dot{y} &= v_y & \dot{v}_y &= a_{\tau y} - \frac{GM}{r^3}y \\ \dot{z} &= v_z & \dot{v}_z &= a_{\tau z} - \frac{GM}{r^3}z \end{aligned} \tag{7}$$

There exists several numerical methods for the solution of a first order differential equation. In general, these methods discretize the dependent variable range and using slope information determine a value at a specified position. These calculated values have a certain error due to discretization and round-off. Therefore it is important to choose a method where this error value is stable and within a tolerable limit.

These numerical techniques can be divided into single-step and multi-step methods. Multi-step methods make use of the information at previous time steps to determine the value at the current step. One of the best multi-step methods is the Adams-Moulton predictor corrector method.

The Adams-Moulton Method is computationally fast and unconditionally stable. It has variable step-size and truncation error proportional to fifth-power of the step size (Ref. NASA SP-33). The

advantage of using a multi-step method is the ability to obtain tolerable solutions using one equation for each discretatization step.

The fourth-order Adams-Moulton formulas are (Ref. Boyce):

Basic Multistep Formula

$$y_{n+1} = y_n + \frac{h}{24}(55\dot{y}_n - 59\dot{y}_{n-1} + 37\dot{y}_{n-2} - 9\dot{y}_{n-3}) + \frac{251}{720}h^5\frac{d^5x(\zeta)}{dt^5} \tag{8a}$$

Predictor

$$y_{n+1} = y_{n-3} + \frac{4h}{3}(2\dot{y}_n - \dot{y}_{n-1} + 2\dot{y}_{n-2}) \tag{8b}$$

Corrector

$$y_{n+1} = y_n + \frac{h}{24}(9\dot{y}_{n+1} + 19\dot{y}_n - 5\dot{y}_{n-1} + \dot{y}_{n-2}) \tag{8c}$$

A numerical solution for the trajectory can be determined utilizing this method and solving simultaneously for the six equations in (7). This method may then be applied to each body in the system. Updates to the acceleration vector due to thrust and other time dependent quantities such as spacecraft mass, may be computed after each time step. In this manner, the only necessary assumptions are that perturbing masses are stationary and time-dependent quantities are constant over the time interval. Selecting a small time step minimizes any significant errors.

Guidance and Control

Orbits for non-thrusting orbital bodies are determined by the form of equation (6) where $\bar{u}(\bar{r},t)$ is zero. Solutions to this equation are determined by initial-values of position and velocity. The motion is governed only by physical mechanism of gravity and perhaps atmospheric drag or solar pressure.

The analysis of thrusting trajectories include the definition of parameterized functions of thrust. The thrust is determined by position and velocities of the spacecraft or other bodies in the system at a specific instant of time (t). This might include a plane change, or a burn to obtain maximum change in specific energy. Constraints such as plume impingement factors might also be defined.

Spacecraft navigation involves the imposition of boundary conditions on the equation of motion governing the body. A $\bar{u}(\bar{r},t)$ function must be determined that causes the differential equation to converge to an answer. If a minimum fuel constraint is implied, the control function becomes the optimum solution for fuel consumption. Another constraint which may be imposed is a minimum time of flight requirement.

SIGHT introduces a basic algorithm that utilizes a user defined boundary condition based on a destination orbit. During the trajectory determination, the program will analyze current values of position and velocity with the rendezvous orbit. When the spacecraft is inside a determined thrust window, the system will calculate a thrust vector for each discretized time step that tends to converge the current values of position and velocity with those of the the desitination orbit. In this manner, a control function is determined by iteration. This function is not necessarily the optimum solution but is valid for preliminary fuel mass requirements and time of flight estimates.

APPLICATION OF SIGHT TO THE LPIV MISSION ANALYSIS

Mission Description

Primary analysis of the LPIV mission was accomplished using SIGHT. This allowed for a solution in three dimensions, with perturbations by multiple gravitational masses, modeling of six simultaneously moving bodies, and power interruption caused by solar occultation of the earth laser station. The laser station and relays are in circular equatorial orbits. The LPIV begins at LEO with an inclination of twenty-eight degrees off the Earth's equator or approximately forty-seven degrees with respect to the XY plane. The LPIV mission trajectory consisted of three separate phases: departure, coasting, and capture. These three phases are used for the outbound flight path as well as the return trajectory.

The first phase, departure, involves the time from the beginning of the mission leaving LEO, to a specified distance out from the Earth. This distance is defined as the point where the spacecraft achieves an enough specific energy capable of achieving a translunar trajectory. The vehicle is thrusting continuously during this initial phase, except when the power station is incapable of firing the laser. The path it will follow is the low-thrust spiral. The spiral orbit takes full advantage of the I_{sp} of the low-thrust propulsion system and as well gives the maximum increase in velocity in the shortest possible time. In addition, a small portion of the thrust will be dedicated to plane-change since the LPIV must precess about forty-seven degrees throughout its journey.

Figure 11 is an isometric view of the orbital system in the first phase. The change of color in the spacecraft trajectory indicates the transition between thrust and coast periods. The orbits of the laser station and beam relays are displayed. The beam path from the laser station to the LPIV has been modeled. The beam path algorithm allows monitoring of the angle of orientation that the LPIV must maintain for laser beam capture. This information enables estimates of the reaction and control system and moment gyros necessary for spacecraft pointing and tracking.

The second phase is a coasting period in which the vehicle has gained enough energy from the continuous burning phase to cross the Moon's orbit without any further thrust. During this portion the propulsion system is inactive and only minor control rockets are required to navigate.

The final phase of the flight consists of rendezvous and final capture. By reinitiating the thrust when the LPIV reaches a predetermined orbit window near the Moon, the vehicle will perform appropriate navigation maneuvers in order to intercept the Moon's orbit and finally rendezvous with LLO. Therefore, navigation and rendezvous are accomplished through utilization of the laser propulsion system. Navigation procedure is discussed in a later section along with the docking procedure.

In Figure 12, a top view of the LPIV trajectory is displayed. This view shows phase two and three of the LPIV trajectory, and includes the moon and its corresponding orbit. It can be observed here that the major portion of the LPIV mission is a coast phase after the LPIV has reached lunar intercept orbit velocity. In Figure 13, a close-up view of the navigation phase can be observed. In this view the LPIV has thrusted to put the spacecraft into a lunar intercept orbit.

The aforementioned scheme is applicable in the return flight from LLO back to the Space Station at LEO. Only slight modifications are necessary in terms of the time and position that the laser engines fire.

Mission Results

The LPIV's initial low earth orbit has an inclination of 28.5 degrees off the Earth's equator, corresponding to the orbiting Space Station. It is assumed that a docking vehicle, dedicated to the service and payload handling of the LPIV, will be in orbit near the Space Station. The LPIV will

begin its journey by firing the twin hydrogen plasma engines and thrusting with 1000 N opposite and parallel to its line of velocity.

The trajectory will follow a spiral outward, thrusting continuously except for periods of intermittent coasting when the laser power station is in the Earth's shadow. At approximately 94000 km radially outward from the Earth, the LPIV has reached enough speed to continue without additional power assist to a lunar orbit intercept. The time of flight required to conclude this first phase is seventy-seven hours, as indicated in Table 6. Once this point is reached, the laser propulsion system remains inactive until the final phase of the trajectory. The vehicle follows an elliptical path as it coasts to the specified lunar orbit and begins phase three, lower lunar intercept.

The return trajectory was formulated using a reverse computational procedure. The LPIV was initialized with its dry weight and payload mass (24000 kg). The beginning orbit was at 6859 km or the destination of the return mission. The LPIV then proceeded to thrust with 1000 N in the same manner as previously stated. The principle difference was a negative massflow term that increased the fuel mass of the spacecraft on the outbound spiral. When the spacecraft had reached the necessary mechanical energy for a coast orbit to lunar intercept, the current fuel mass represented the amount necessary for the decelerating spiral return trajectory. Results of this procedure may be seen in Table 7.

In Figure 14, a plot showing the velocity versus position is presented. In this graph, we may see that the optimal place to begin a plane change occurs when the LPIV reaches approximately 50000 km. From this distance out to 94000 km, there is decreased rate of change in total LPIV velocity due to the inverse relation of the laws of motion. In Figure 15 a graph of position versus time is shown. Also provided is a graph of the total spacecraft mass compared to the radial position (Figure 16).

Aerobraked Trajectories

NASA is considering the use of Aero-assisted Orbital Transfer Vehicles (AOTV). An aerobraked maneuver involves using the drag pressure of the the upper atmosphere to decelerate the spacecraft for correct orbit insertion. The obvious advantage to aerobraking is significant decrease in fuel consumption. A second configuration of the LPIV utilizing a rigid shell aerobrake has been addressed. SIGHT has been adapted to analyze the aero-assisted lunar return trajectory. The drag is a function of the atmospheric density, relative spacecraft velocity, relative speed of the rotating atmosphere, frontal spacecraft area and drag coefficient. The formula used for an approximate deceleration is:

$$\ddot{\bar{r}} = -\frac{1}{2} C_D \frac{A}{m} \rho v_a \dot{\bar{r}}_a \tag{9}$$

C_D = nondimensional drag coefficient

A = cross sectional area of vehicle perpendicular to direction of motion

m = vehicle mass

ρ = atmospheric density at vehicle altitude

v_a = scalar of velocity relative to rotating atmosphere

ORIGINAL PAGE
COLOR PHOTOGRAPH

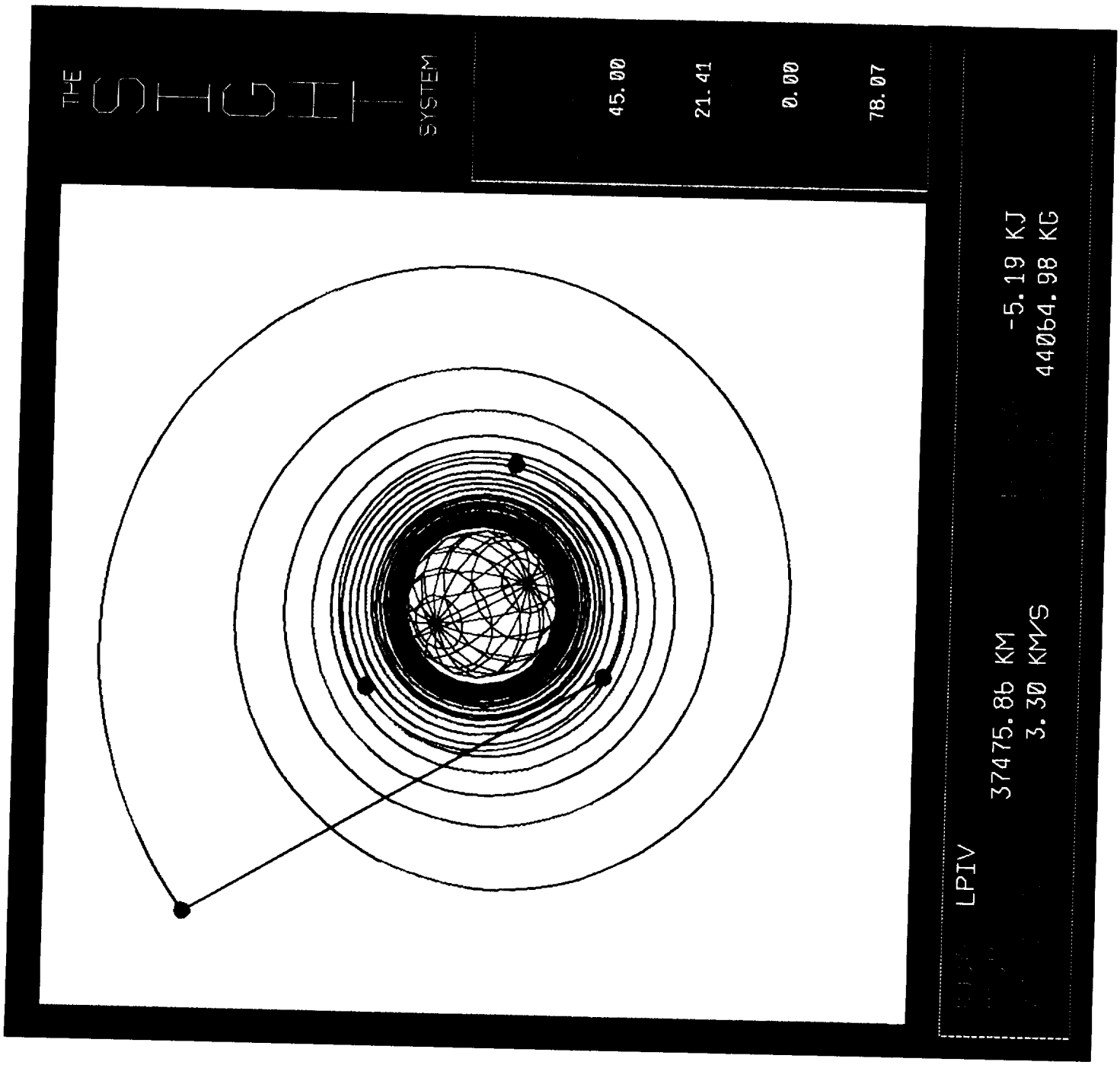

FIGURE 11

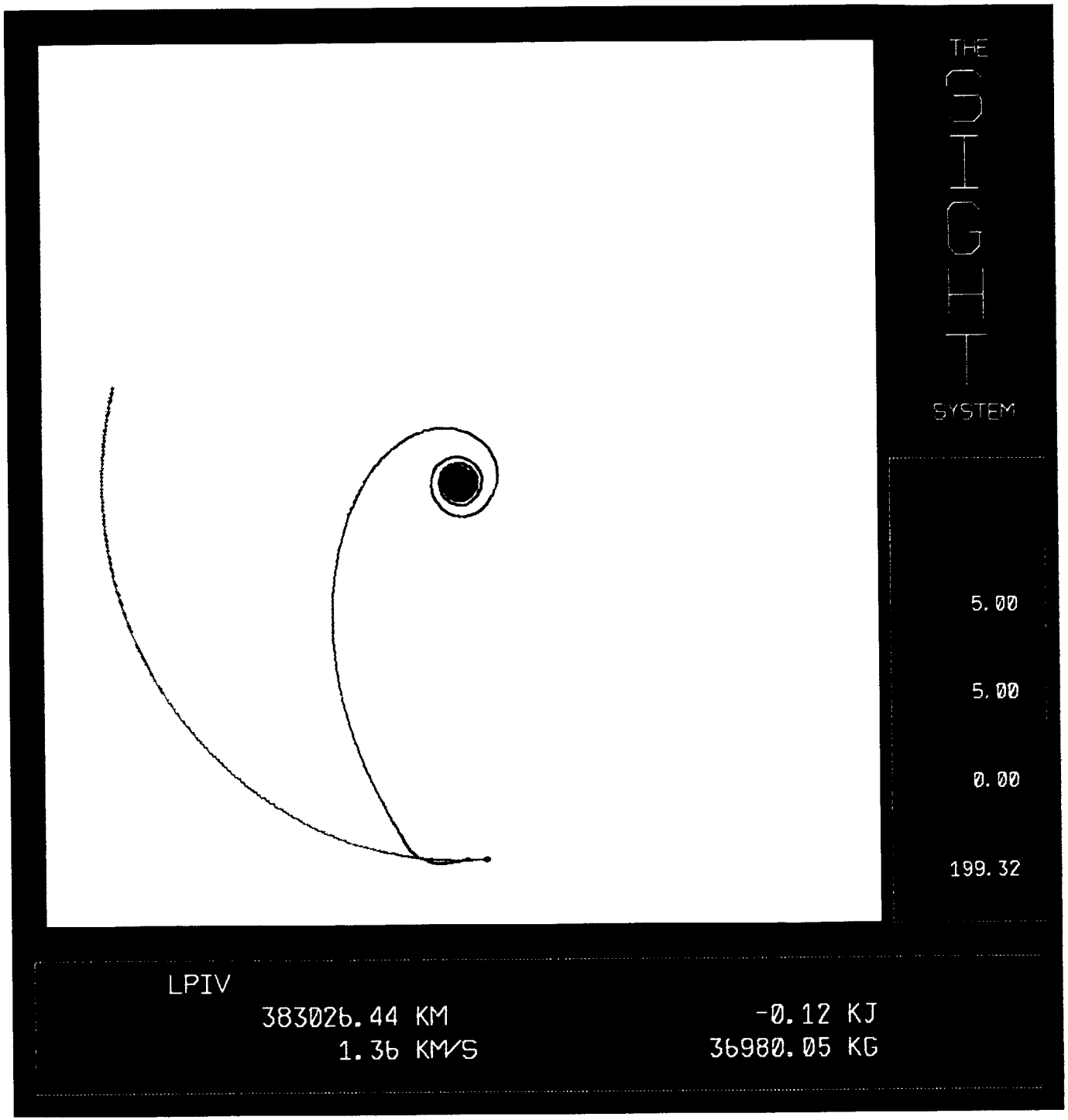

ORIGINAL PAGE
COLOR PHOTOGRAPH

FIGURE 12

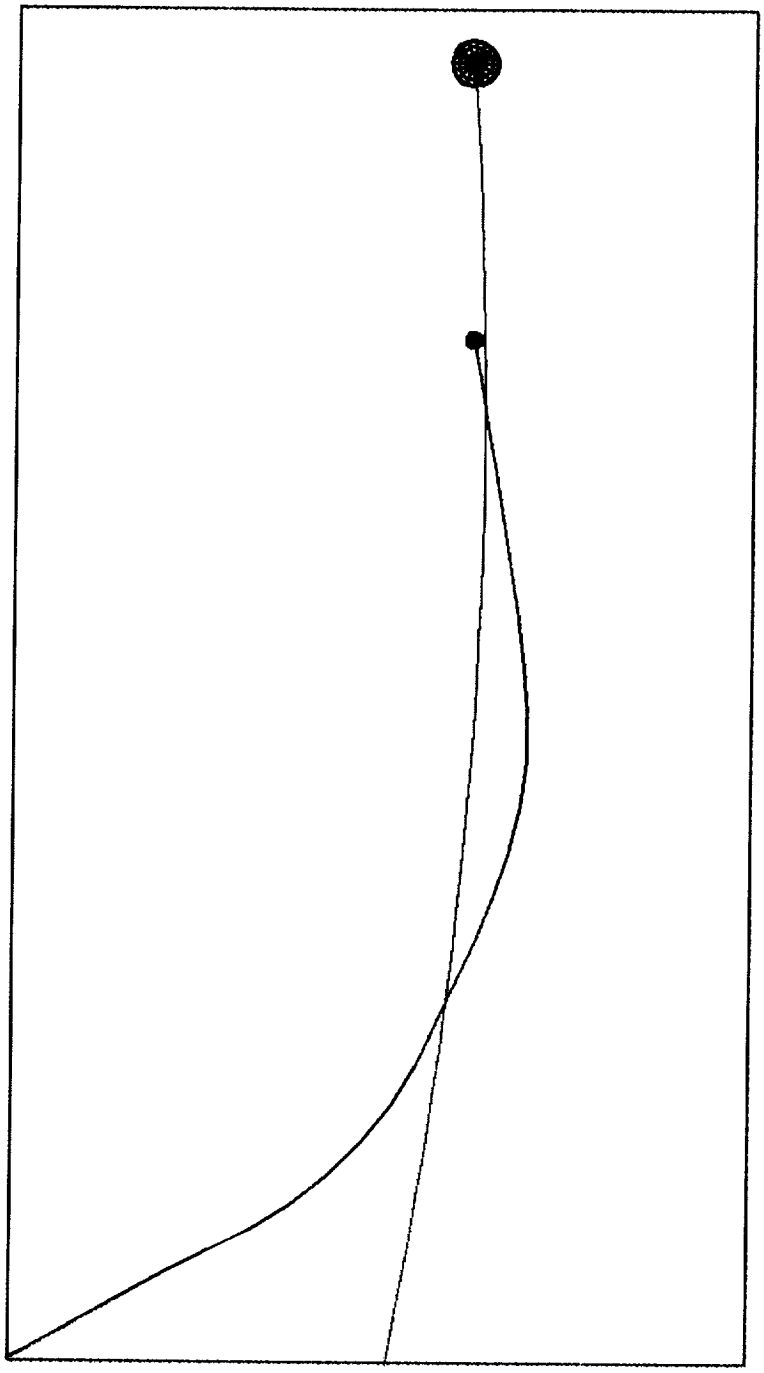

ORIGINAL PAGE
COLOR PHOTOGRAPH

FIGURE 13

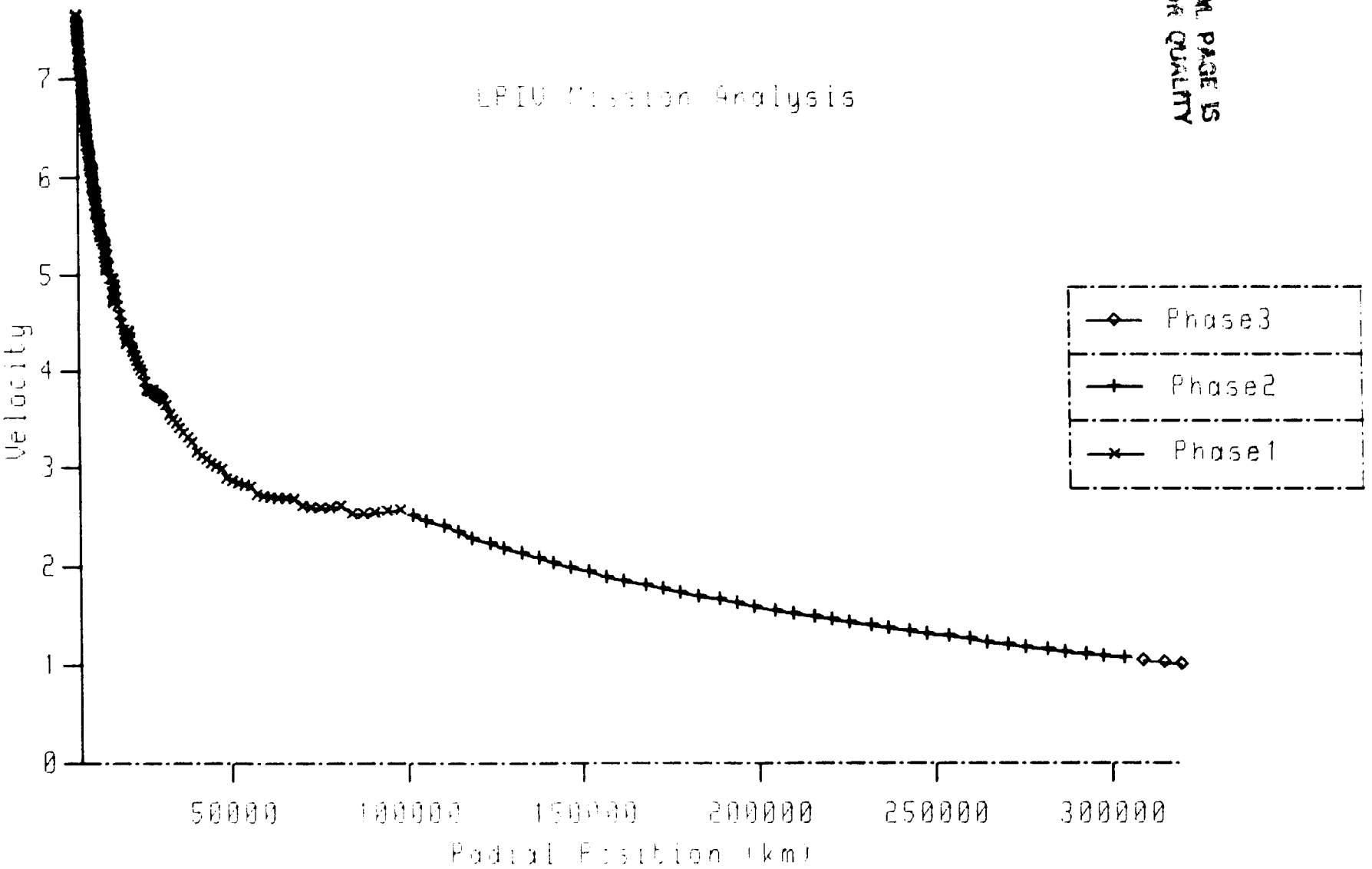

FIGURE 14

ORIGINAL PAGE IS
OF POOR QUALITY

ORIGINAL PAGE IS
OF POOR QUALITY

FIGURE 15

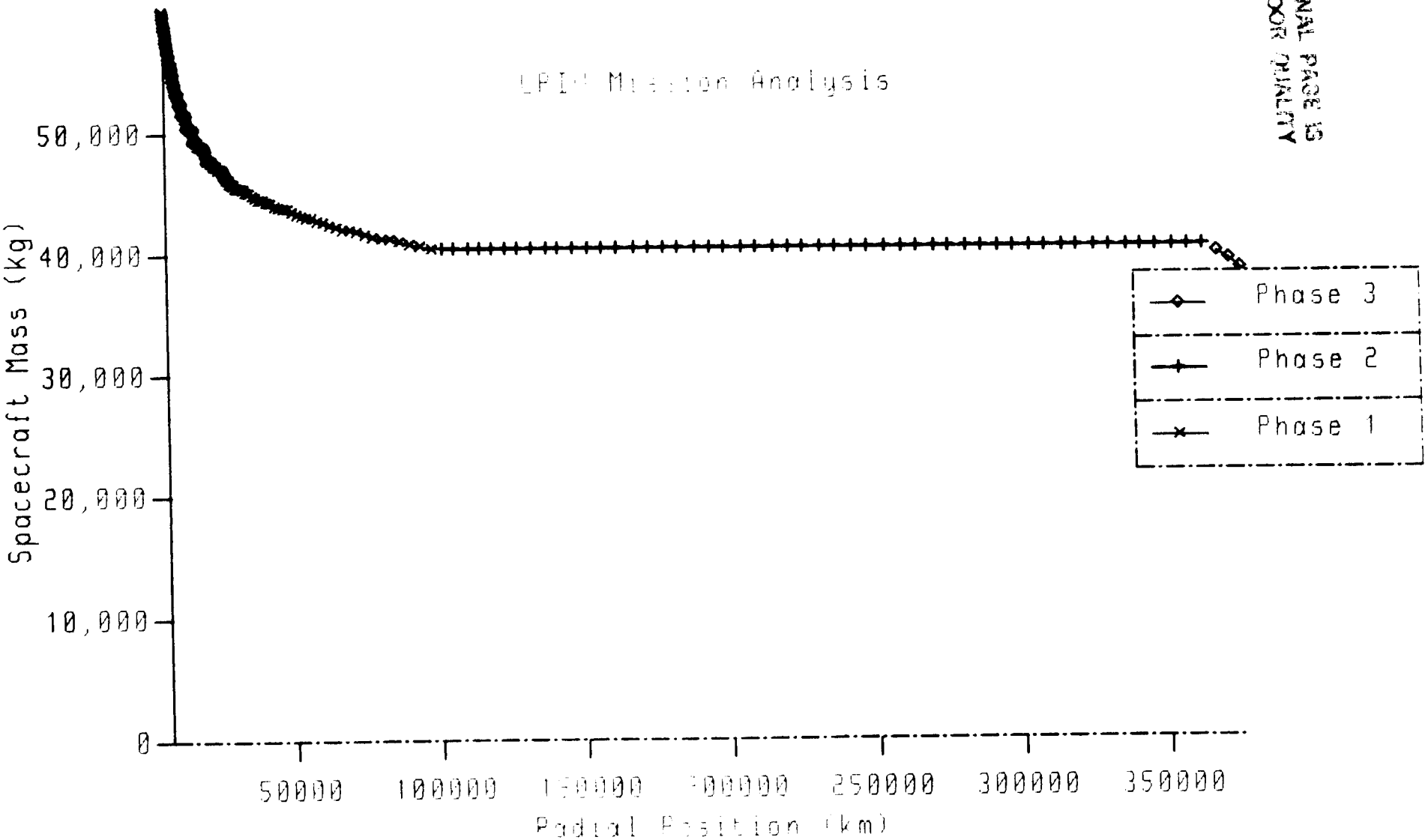

FIGURE 16

Table 6. Outbound Trajectory

Phase I -- Departure Initial Conditions	
Mass:	59000 kg
Radial Distance:	6859 km
Velocity	7.624 km/s
Inclination:	28.5 degrees with respect to the equator
Thrust:	1000 N
Time of Flight:	0 hours
Phase II -- Translunar Injection	
Mass:	43145 kg
Radial Distance:	94000 km
Velocity	2.524 km/s
Inclination:	5.12 degrees with respect to the equator
Thrust:	0 N
Time of Flight:	77.5 hours
Phase III -- Lunar Orbit Intercept	
Mass:	41784 kg
Radial Distance:	384400 km
Velocity	1.01 km/s
Inclination:	5.12 degrees with respect to the equator
Thrust:	1000 N
Time of Flight:	165 hours

Table 7. Return Trajectory

Phase I -- Lunar Orbit Departure Initial Conditions	
Mass:	41784 kg
Radial Distance:	384400 km
Velocity	1.01 km/s
Inclination:	5.12 degrees with respect to the equator
Thrust:	1000 N
Time of Flight:	0 hours
Phase III -- Earth Capture Initial Conditions	
Mass:	40242 kg
Radial Distance:	94000 km
Velocity	2.62 km/s
Inclination:	5.12 degrees with respect to the equator
Thrust:	1000 N
Time of Flight:	127 hours
Phase III -- Earth Capture Terminal Conditions	
Mass:	26903 kg
Radial Distance:	6859 km
Velocity	7.624 km/s
Inclination:	28.5 degrees with respect to the equator
Thrust:	0 N
Time of Flight:	201 hours

FUTURE RECOMMENDATIONS

A potential improvement would be the placement of the orbiting earth laser station in a polar orbit precessing with a rate that keeps the orbital plane normal to the sun's rays. This would reduce the dependence on the beam relays to possibly one or none. Additionally, the solar pumped laser could stay charged indefinitely.

The nuclear-fueled laser station on the lunar surface may be more strategically placed on the dark side of the Moon. In this location, the station may be used more efficiently for the LPIV's laser energized burns. The resulting thrusting arcs for the LPIV craft would tend to lift the apogee toward the Earth instead of away.

In the future, optimal control functions may be determined for a variety of constraints. It will become desirable to develop adaptive guidance algorithms which consider structural limits and margins as well as spacecraft performance characteristics. This would allow solutions to be derived using control functions which consider heating constraints during aero-assisted trajectories. This investigation could lead to computer-based adaptive guidance and targeting algorithms for an autonomous LPIV spacecraft.

SUMMARY

The investigation of orbital mechanics and trajectory analysis for the LPIV spacecraft has yielded a feasible laser-propelled low-thrust trajectory. The first obvious advantage of this mission scenario is the ellimination of dependence on hybrid or chemical thrusting systems. In addition, this mission represents a fast and efficient transport method for shuttling cargo between the Earth and Moon. The research has also led to the development of a software system, SIGHT, that will serve as a platform to facilitate the comprehensive study of the spacecraft dynamics and navigation characteristics as well as guidance and control.

OPTICS

INTRODUCTION

The optical system is the most critical subsystem of the LPIV. It provides the only link between the engines and their power source, located thousands of kilometers away. The function of the optical system is to intercept the laser beam which may be as much as 24 meters wide, and focus the beam to a few centimeters in the chamber of the engines. Here the energy is used to heat the hydrogen propellant which is then expanded through the nozzle. Three objectives were considered in the design of the optical system: maximizing energy transmitted to the engines, minimizing deformtions due to inertial and thermal loading, and minimizing the overall mass of the system. These objectives are addressed in this chapter in the discussions on mirror geometry and placement, material selection, support structures, and construction.

EVOLUTION

Evolution of the Optical Path

The first step in the design of the LPIV's optical system is to determine the optical path traced by the laser beam as it travels from the collector to the thrust chamber. The initial vehicle configuration employed offset parabolic mirrors for the primary and secondary reflectors and required two additional mirrors to direct the beam into the engine. A convergent lens was then used to bring the beam to a focus in the engine chamber. This asymetric design presented problems in maintaining the center of mass in the line of thrust. To solve this problem, a symmetric configuration was considered.

With the symmetric design, the secondary mirror is supported on the centerline of the primary mirror. When the beam is intercepted, it is reflected to the secondary mirror and back through the central opening in the primary mirror. A beam splitter is located behind the mirror's support structure. When the beam strikes the splitter, it is divided into two beams of equal power which are directed to the tertiary mirrors at each end ot the main truss. These mirrors focus the beams into the plasma chambers of engines where their energy is converted to thrust power by the hydrogen propellant. With this design, if the incoming beam were captured symmetrically on the primary mirror the most energetic central portion of the beam would be obstructed by the secondary mirror. In order to make an efficient use of the energy available, the beam must be collected off center. This requires adding area to the primary mirror which increases its mass.

The selected configuration of the spacecraft introduced some important features. The primary and secondary mirrors were arranged into a Cassegrain configuration with the secondary mirror suspended in front of the primary mirror by means of a tripod support structure. Next, two engines were introduced instead of one which demanded that the power of the laser beam be split and transferred to two different focusing points. The division of the power required the use of a beam splitter (Figure 17).

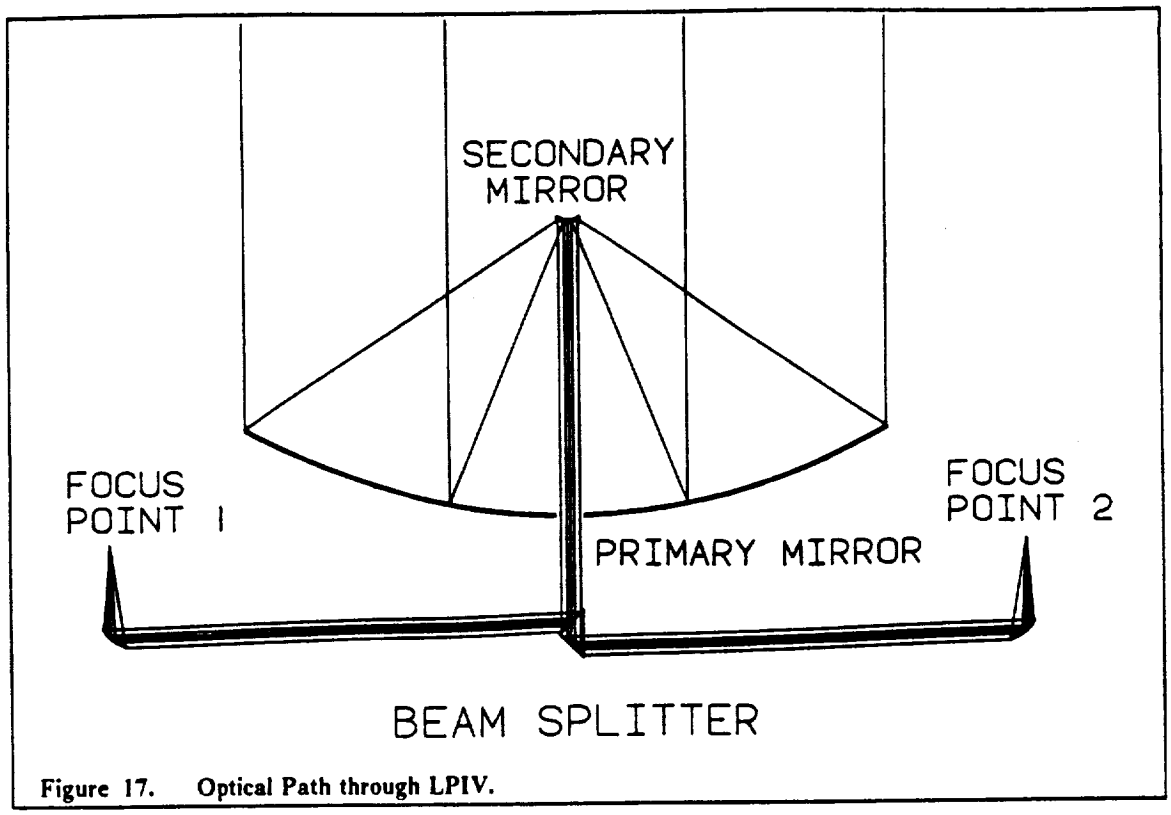

Figure 17. Optical Path through LPIV.

Possible Degradation of the Optical System

An important factor which may effect the efficiency of beam transmission throughout the optical train is degradation of the reflecting surfaces. During the vehicle's life such degradation may be caused by the reactivity of materials with the atomic oxygen that occurs during long term exposure to the atmosphere in Low Earth Orbit (LEO). Micrometeoriods also degrade space systems by leaving small holes and surface imperfections where atomic oxygen can cause further corrosion. Other adverse conditions apparent in space are ultraviolet radiation, charged particle radiation, and space debris. Another factor is thermal cycling, which is naturally induced as the vehicle travels in and out of the shadow of the earth, causing structural fatigue. The LPIV's optical train is expected to operate unrefurbished for approximately two years with a maximum power loss of ten percent through the entire laser path; therefore, these conditions must be taken into serious consideration when selecting a material for the mirror surface.

Evolution of the Primary Mirror Design

The primary mirror assembly serves as a concentrating reflector which will intercept the laser beam from the remote power station orbiting the Earth radius, or sitting on the lunar surface. Three types of primary reflectors were considered for this function. The first design considered was a lightweight inflatable mirror which can be deployed in space. The second type was a rigid mirror with a polished metal surface. The third type was also rigid but used a dielectric reflective surface.

The inflatable concentrator considered was made from a Mylar transparent film and a Kapton reflecting surface (Figure 18). This mirror design was attractive because it made possible the launching of a compact package, consisting of the stowed mirror and its deployment apparatus into space. Deployment of the mirror would be done by inflating an aluminum torus beyond its yield strength, enabling it to maintain its shape after depressurization. The cavity created between the Mylar film and Kapton surface is then filled with hydrogen gas to produce the geometric shape needed for the reflective surface. The rigidized torus maintains the shape of the reflecting surface

and allows for attachment of the mirror to the spacecraft. The main benefits of an inflatable mirror are its low specific mass (Table 8) and its ease of deployment in space. The primary disadvantage of this concentrator was the relatively low reflectivity (Table 8) compared with rigid mirrors. This is due to the absorbtion of energy by the transparent film which the beam must pass through twice. This absorption will cause a significant reduction of power transferred to the engine. The second disadvantage was that this scheme could not be used in an aerobraking version of the LPIV without adding a significant amount of support structure because the inertial loads would deform the reflector.

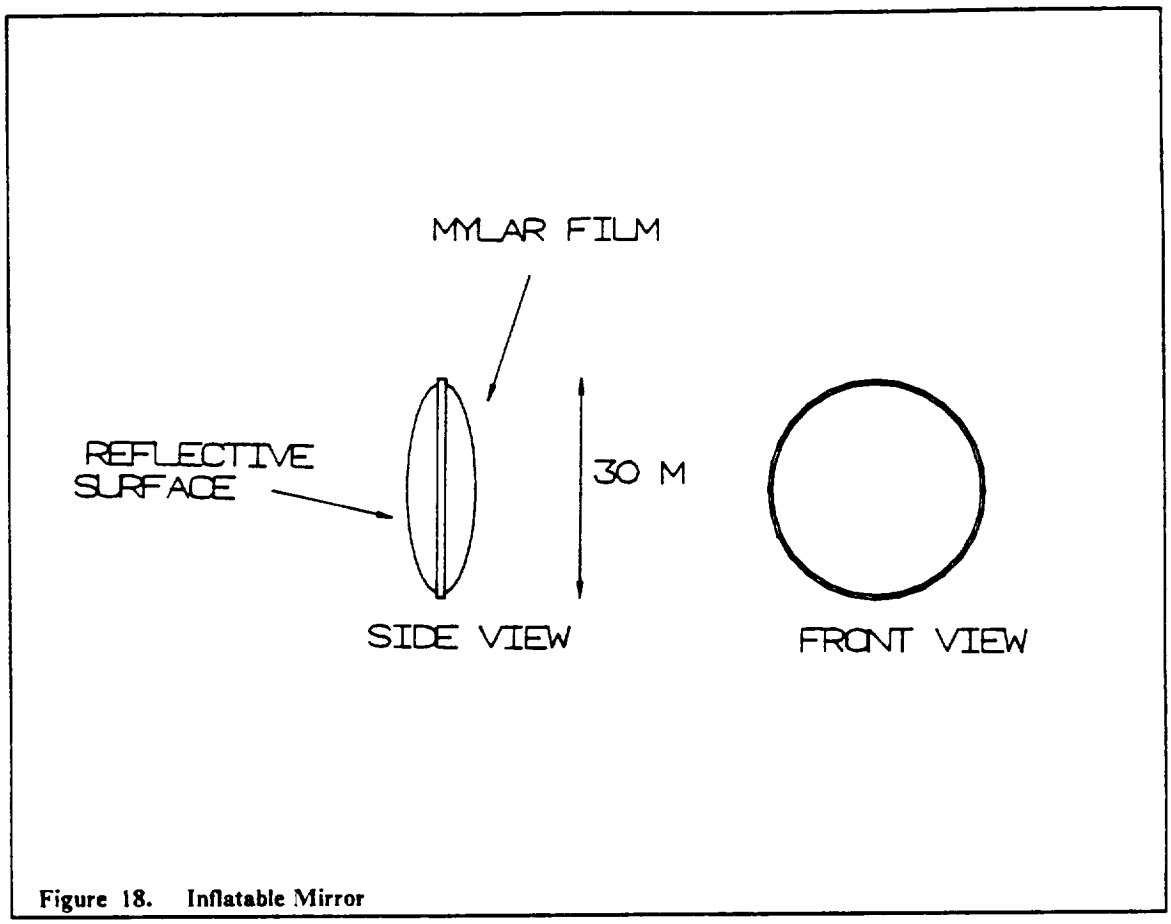

Figure 18. Inflatable Mirror

The rigid mirrors considered are not as easily deployed and would require assembly in space but can be made to achieve a much higher reflectivity. A polished metal mirror using common materials such as aluminum, silver, and copper can produce optimum reflectivities of up to 99%. However, to achieve a highly reflective surface the thickness of metal required would result in an undesirably high mass. These materials have a high thermal coefficient of expansion which means that the mirror would encounter significant deformations in the surface shape due to the heat absorbed.

The third concentrator design, selected for our vehicle, consists of a reflective surface of dielectric materials. The main advantage of a dielectric mirror is its high degree of reflectivity for a narrow range of wavelength, possibly as high as 99.9+ %. Dielectrics employ alternating layers of high and low refractive index materials that provide multiple reflections, all in phase (Figure 19). The dielectrics must be applied in vapor form to a facesheet material, in order to achieve the required thickness of 0.3 micrometers. The facesheet acts as a substrate for the dielectrics and as a heat sink. For this application, a scheme of ten dielectric layers will be used to produce a high degree of reflectivity, reducing the heat absorbed by the facesheet, and alleviating the need for primary mirror cooling. Overall, the dielectric mirror was selected because it provided the LPIV with a very efficient and relatively light primary mirror.

Table 8. Primary mirror surface data.

Collector Type	reflectivity%	Mass/unit area (kg/m^2)
Inflatable	95%	0.50
Metallic	98%	30.0
Dielectric	99.9 + %	9.77

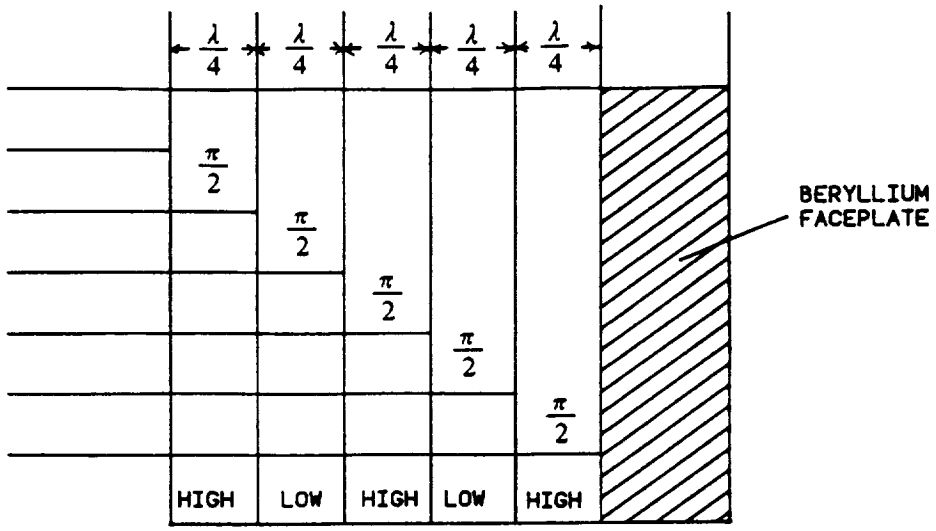

Figure 19. Sample five layer dielectric surface.

Primary mirror geometry

Once the type of mirror and optical path have been selected, the mirror shape needs to be determined. Two conical shapes commonly used for radiation and radio wave collection are spherical and parabolic profiles. The manufacture of spherical mirrors is basically simple but aberration and low efficiency at shorter focal lengths prompted the selection of a parabolic contour for the LPIV application. The parabolic contour allows the beam to be focused with minimal energy loss.

PRIMARY MIRROR DESIGN

The initial task in designing the primary mirror was to calculate the maximum diameter required to collect the laser beam. This calculation was accomplished by considering the maximum distance at which the beam would be received, beam divergence, wave front error and beam jitter. The maximum distance the laser was required to travel is 110000 km. This distance was determined by considering the maximum distance of the vehicle from the earth during thrusting and the location of the laser power station and/or relays. The wave front error is caused by imperfections of the laser transmitting mirror. The beam jitter is caused by fluctuations in the emission intensity produced by non-linearity in the refractive index of the lasers active medium. Beam divergence error is the

amount the diameter of the beam will increase as the beam travels through space. The equation used to determine the beam diameter (Irvine) is:

Total divergence $S_t = [(1.3S_o)^2 + S_j^2 + S_w^2]^{0.5}$ rad

Where: $S_o = 0.4138(\lambda/D)$ (diffraction half- angle)
$S_j = 0.05 \times 10^{-6}$ rad (beam jitter assumed)
$S_w = \lambda/(20D)$ (wave front error)
$\lambda = 1.315$ micrometers (wavelength)
D = 30 m (laser transmitter mirror diameter)
Spot size $D_{spot} = 4S_tR$
Where: R = 110000 km (maximum firing distance)

The above equation yields a maximum spot diameter of 24.0 m. It should be emphasized that for most of the thrusting operation, the spot diameter will be smaller, or even significantly smaller, due to the focusing ability of the laser transmitting system. Sizing of the mirror was based on the spot diameter, the minimum acceptable power requirements and the amount of offset necessary to make use of the peak intensity of the beam. After examining these factors, a mirror diameter of 24 m was decided upon. A primary consideration in the selection of the mirror size was that fringe intensity of the beam spot is much less than the peak intensity.

Before determining the contour of the mirror, placement of the secondary mirror needed to be determined. In determining placement of the secondary mirror,

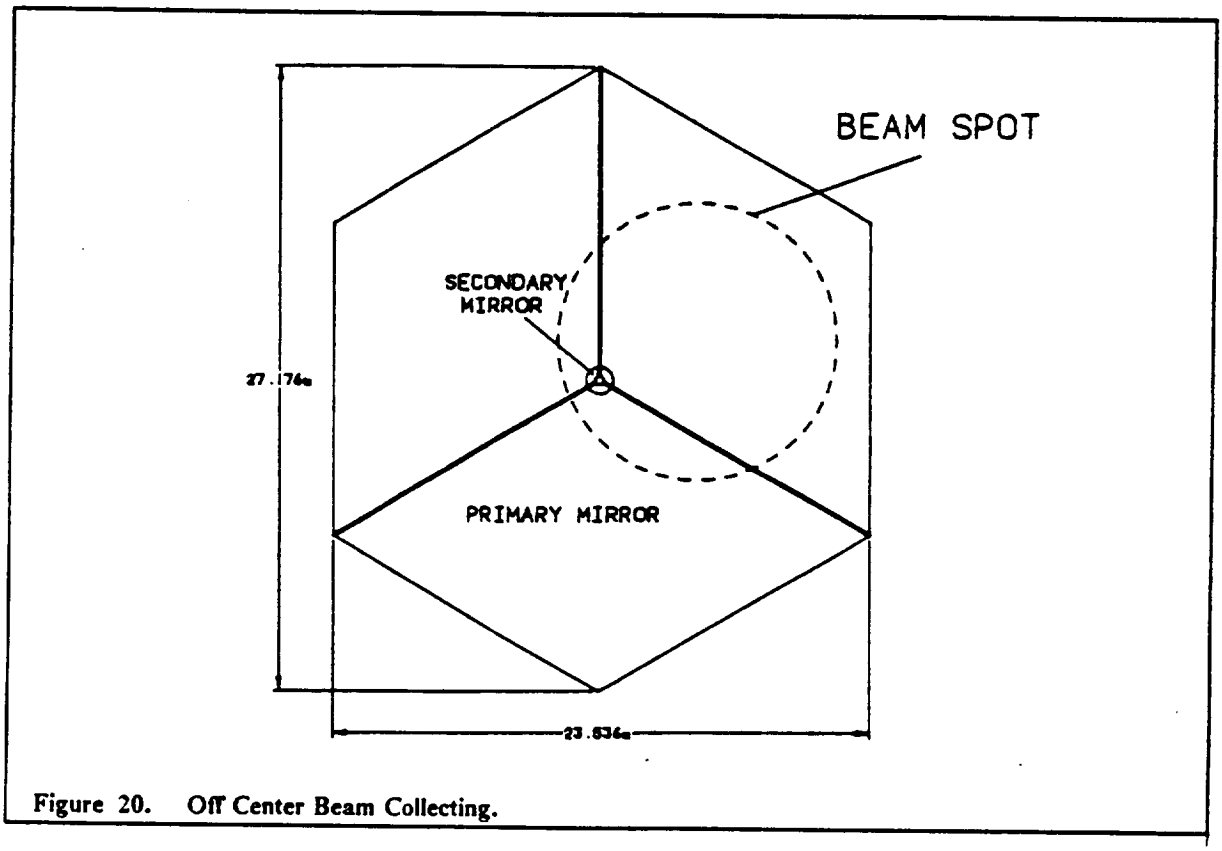

Figure 20. Off Center Beam Collecting.

it was required to consider the effects of thermal and inertial loads on the structural members. From these considerations a focal length approximately equal to the radius of the primary mirror was selected. Using the mirror diameter and desired focal length , the following equation for the primary mirror contour was obtained:

$$z = 0.02x^2 + 0.02y^2$$

Once the mirror geometry was determined, the primary mirror surface and support structure needed to be selected. The mirror surface that best meets the design criteria is multilayered coatings of dielectrics, as described in the evolution section. The selection of the facesheet material is critical because the dielectrics must be applied in vapor form to the facesheet. The choice is based on the following criteria: material specific heat (Cp), surface smoothness and density.

Surface smoothness is an important characteristic because the dielectric layers are extremely thin, 0.3 micrometers, propagating any errors that occur in the facesheet. For a given amount of absorbed energy, the temperature variaton in the material depends on the specific heat. Therefore, a material with a higher specific heat is desirable. The two materials considered are beryllium and fused silica. The beryllium was chosen because it has a higher Cp (1825.4 J/kg/K) and a lower density (1850 kg/m^3) than fused silica. Properties of berylliun can be seen in Table 2.

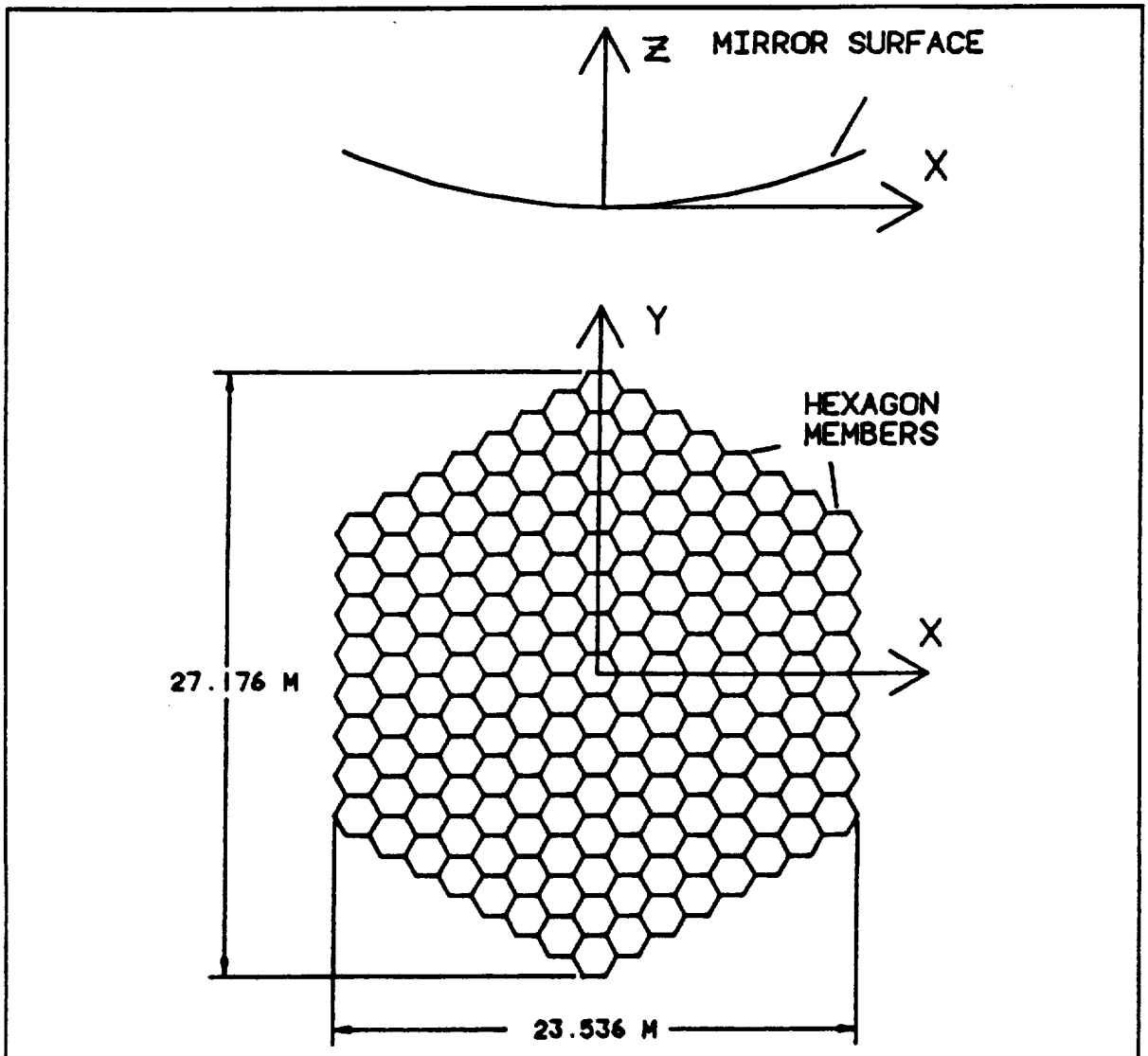

Figure 21. Primary Mirror

Two designs were considered for the support structure of the mirror - a radial panel design and a hexagon panel design. The hexagon panel was selected as the basic surface element (Figure 22) because it allows for more uniform manufacturing and a simpler supporting truss structure. For structural stability and ease of attachment, a derivative of a honeycomb type structure is used for the panel design (Figure 22).

Table 9.	Properties of beryllium.	
	Density	1850 kg/m^3
	Coefficient of thermal expansion	8.4 x 10^{-6} /K
	Specific heat	1825 W/kg/K
	Maximum temperature	1120 K
	Thermal diffusivity	6.22 m^2/sec
	Thermal conductivity	155 W/m/K

The structure consists of two perforated graphite epoxy panels (Figure 22) connected to the surface layer by fused silica pegs. The panels have a side length of 1.1806 m and contains 546 fused silica pegs that are adhered to the individual panels with epoxy. The pegs are 2 mm in diameter and 13.0 mm long, and their main purpose is to provide stability while not significantly affecting the overall mass (Table 11). One advantage of this type of structure is that a parabolic surface shape can be closely approximated by varying the length of the pegs and curving the beryllium facesheet. This change in curvature can be accomplished without adding any complexity to the support structure since only the front of the panel is curved.

The majority of these panels can be assembled before being launched into orbit. Each panel will be fastened to six small angular C-beams using two spring pins in each C-beam. These pins will allow for easy removal and replacement of panels having suffered damage or degradation during the service. Once the C-beams are attached to the panels, the beams may be fastened to each other using machine bolts. To allow for transporting in the space shuttle payload bay the entire mirror assembly will be broken down into six identical sub assemblies, and assembled in space. The remaining C-beams will be connected along those six joints by a latch jaw assembly.

The surface area of the primary mirror was calculated to be 456 m^2 which requires 126 hexagon panels. The mass of the surface of the primary mirror was calculated to be 2730.9 kg resulting in a surface mass density of 5.9888 kg/m^2 The spring pins and the C-beams used to attach the panels together and support them will be discussed in more detail in the mirror support structure section.

SECONDARY MIRROR

The geometry of the secondary mirror was determined from the following criteria. Its function is to redirect the converging light rays from the primary mirror in paraxial fashion toward a circular hole at the center of the primary mirror. In order for the beam reflected, from the secondary mirror, to be paraxial, the primary and secondary mirror must share a common focal point. Therefore, a convex, parabolic surface was employed.

Secondary Mirror Surface:
$z = 0.54x^2 + 0.54y^2$
Diameter: 1.2 m

The secondary mirror is mounted 12.13 m along the focal path of the primary mirror at the end of a tripod support axis structure. As stated, the beam is paraxial once it is reflected from the surface of the secondary mirror and it has a diameter of 1.1 m. The diameter of this beam is directly related to the initial spot size of the incoming laser beam on the primary mirror.

The construction of the secondary mirror consists of ten dielectric layers coated on a 2.5 cm thick beryllium slab which serves as a facesheet and structural support for mounting (Figure 23). Since dielectrics were chosen for the the reflective surface, the secondary mirror has an initial reflectivity of 99.9%. However, due to degradation it is assumed that the reflectivity will decrease to 98.5% during its service life. Therefore, a cooling system will be attached to the back of the beryllium facesheet.

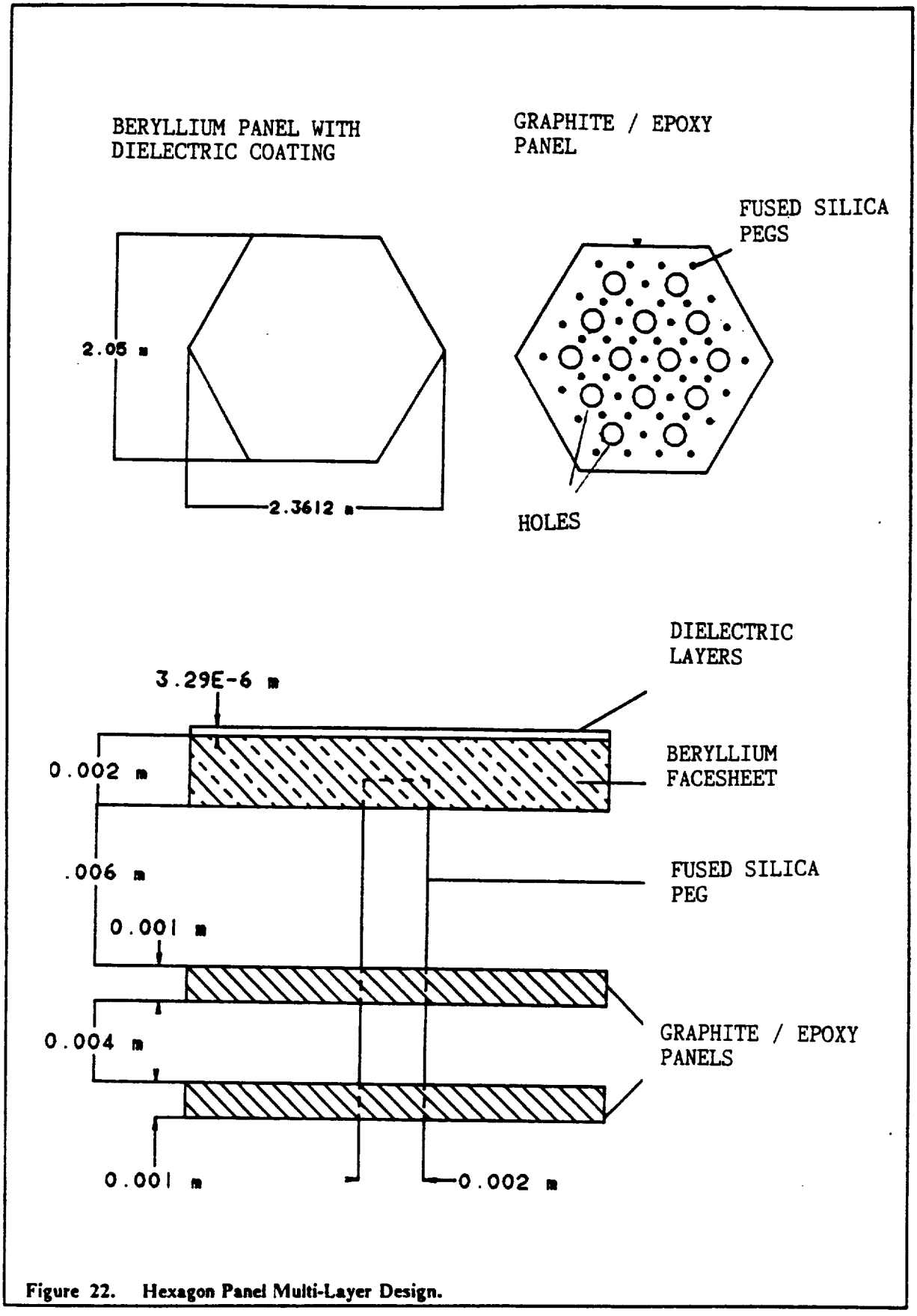

Figure 22. Hexagon Panel Multi-Layer Design.

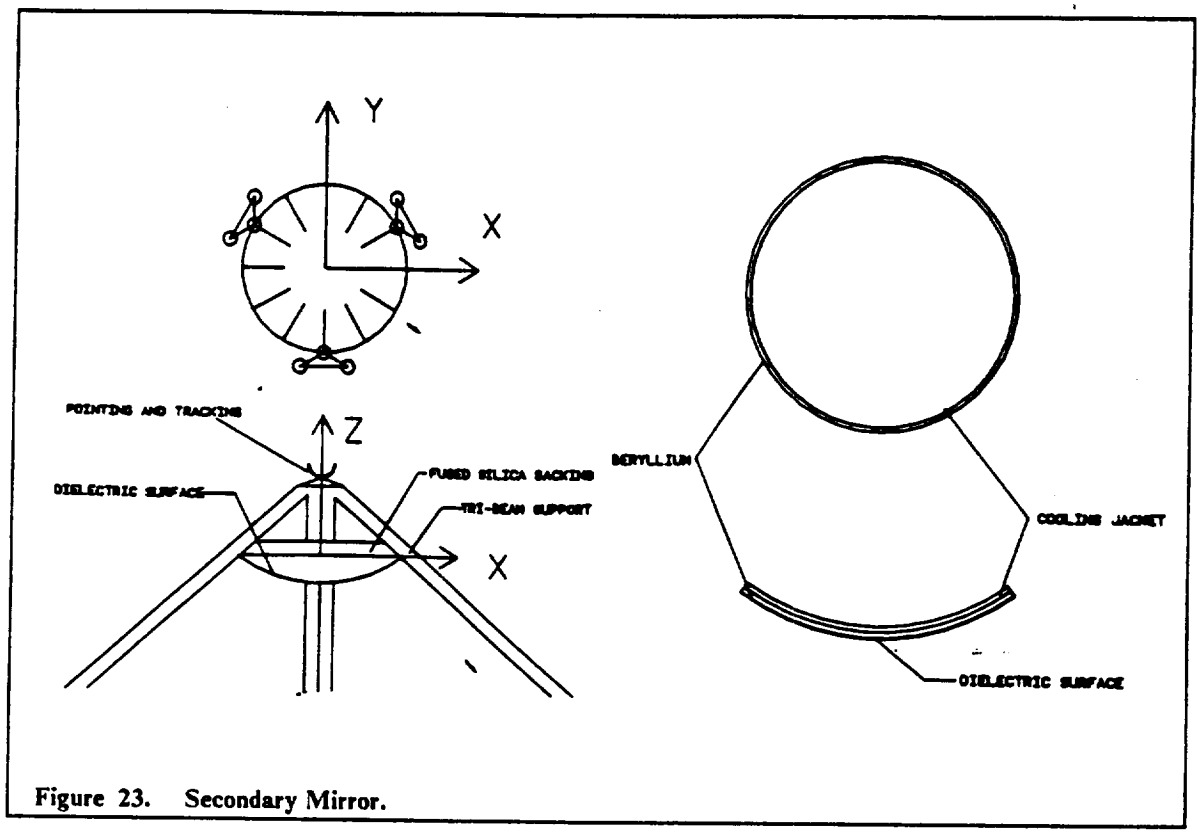

Figure 23. Secondary Mirror.

BEAM SPLITTER

A beam splitter is incorporated into the design of the LPIV's optical train to allow equal power to be transferred to each of its two engines. The beam splitter is located behind the primary mirror in the center of the main truss. The beam splitter consists of two mirrors joined at a right angle, the first being a slotted, 50 percent open surface to reflect exactly one half of the incident radiation toward one engine. The second, aft surface reflects the remaining half of the laser beam toward the second engine. The assembly is then rotated to an angle of 0.749 degrees. This rotation is needed to insure symmetric positioning of the two tertiary mirrors.

The front reflective surface of the beam splitter is constructed from dielectric layers coated on a grated beryllium facesheet (Figure 24). Diffraction of light passing through the slots calculated from

$$d(\sin(\theta) - \sin(\alpha)) = m \times \lambda$$

d = distance between centers of slits
θ = angle light is deffracted
α = angle of incidence
m = the order
λ = wavelength of the laser

Using d = 0.06 m, alpha = 45.749 °, m = 1 and $\lambda = 1.315 \times 10^{-6}$ m the light passing through the grated section is deffracted 0.0018 ° which offsets the center of the beam approximately 1mm in the thrust chamber. Dielectrics are also used for the aft reflective surface layered over a beryllium facesheet to send the rest of the beam to the engine. The length of the sides and base of the beam splitter are 1.23 m and 2.4 m, respectively, in order to accommodate any size of concentrated beam reflected from the secondary mirror.

The structure which supports the beam splitter is fastened directly to the beryllium facesheets. Graphite/Epoxy C-beams are connected to the beryllium by bolts which then allows for the structure to be attached to a box assembly. Finally, the box assembly is then secured to the main truss by eight circular beams (Figure 24).

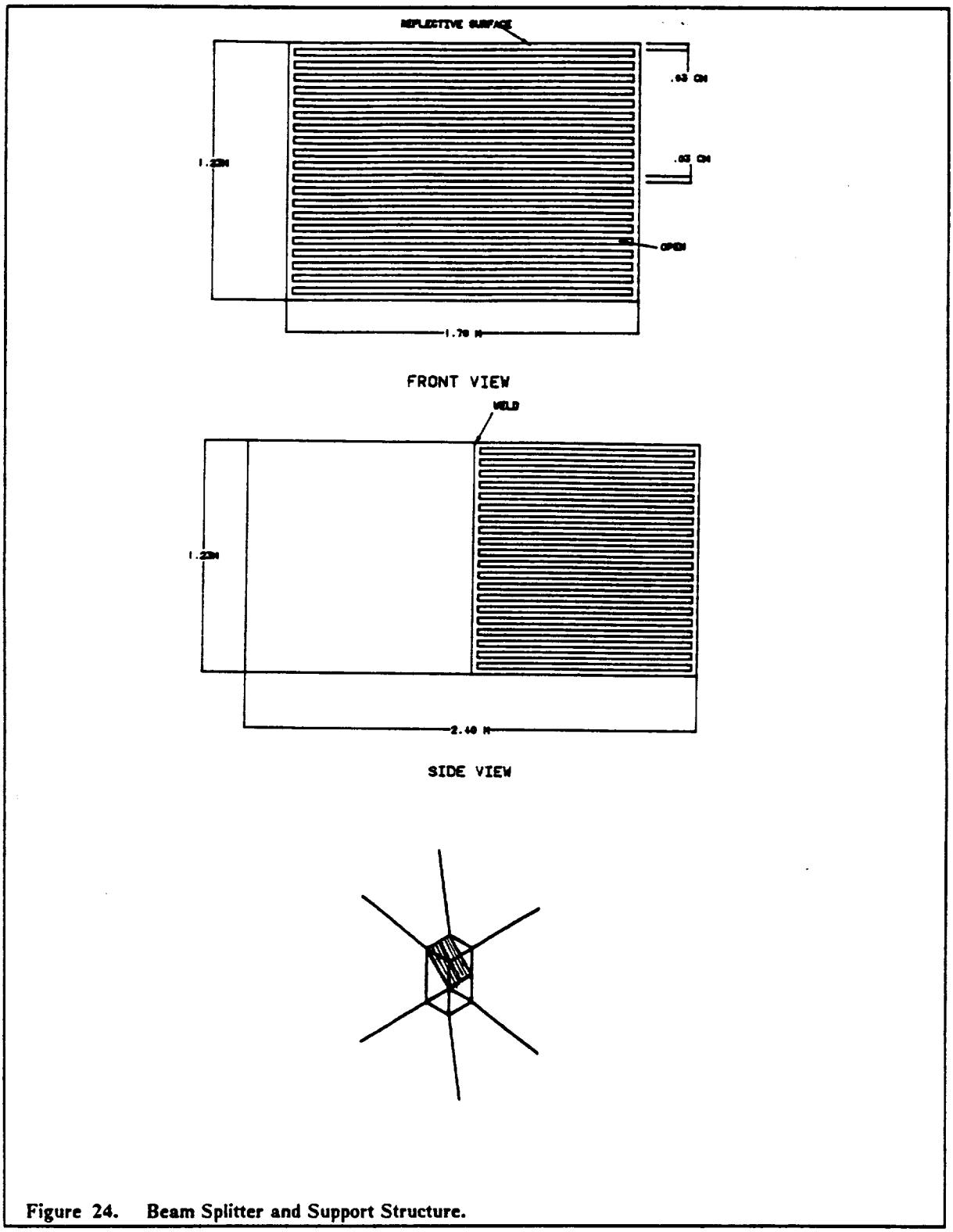

Figure 24. Beam Splitter and Support Structure.

TERTIARY MIRRORS

The design of the third mirrors was critical since each will converge and direct its incident beam into the plasma chamber of the engine. An offset parabolic mirror was chosen for this reason. The construction of the third mirrors is similar to that of the secondary mirror except for the use of a concave reflective surface for the third mirrors (Figure 25).

Tertiary Mirror Surface : $z = 0.066x^2 + 0.066y^2$
Diameter : 1.3 m

The dielectric layers for these mirrors are coated on a 2.5 cm beryllium facesheet which serves as both a substrate and a mounting surface. This offers a reflectivity of 99.9% for the third mirrors.

The use of adaptive optics in the construction of the tertiary mirrors is an attractive option that should be given more study in the future. Addaptive optics enable the the reflected beam to be more sharply focused and centralized in the plasma chamber than a rigid mirror. Thus, a mirror utilizing addaptive optics would increase the efficiency of the engine.

OPTICAL SYSTEM PERFORMANCE

Dielectric coatings offer a 99.9+ % reflective surface but over the two year life cycle of the coating, degradation may cause losses in reflectivity on the order of 1.5%. After this time period the dielectric layers must be reapplied to ensure that no thermal damage will occur.

Primary mirror: The initial reflectivity is assumed to be 99.0%. This value incorporates a 1% loss due the inaccuracies in the curvature of the 24.0 m diameter reflecting surface. Degradation may cause another 1.5% loss after two years, leaving a reflectivity of 97.5%.

Secondary mirror: 99.9% of the incident energy on the secondary mirror is reflected initially, but after degradation this amount decreases to 98.5%.

Beam splitter: Initial reflectivity of the beam splitter is 98.7% degrading to 98.1%.

Tertiary mirrors: The tertiary mirrors are similar to the secondary mirror in that initial reflectivity is 99.9% falling to 98.5% over the two year life of the reflecting surface.

For the thermal analysis of the optical system, the following average reflectivities are used in the calculations: primary mirror 98.0%, secondary mirror 98.8%, beam splitter 99.1%, tertiary mirror 98.8%.

THERMAL ANALYSIS

Thermal analysis of the optical system is important because high absorption of the laser beam can cause deformation in the mirror's materials rendering it less efficient or even useless. In order to analyze the heating of the secondary and tertiary mirrors they were assumed to be plane, circular surfaces with diameters of 1.2 m, and 1.3 m respectively. This assumption simplifies the mathematics in the thermal calculations but, the results are still accurate in estimating the the steady state temperature obtained in the mirrors. The radiant energy impingent on the surface of the mirrors and beam splitter cause the temperature of these surfaces to increase according to the reflectivity, absorbtivity, and transmissivity of the optical material.

The mirror will reach a steady state where it can no longer absorb any of the incoming energy. In order to maintain equilibrium in the steady state, the energy absorbed into a structure must equal the energy removed from the structure by radiation. An energy balance was done in order to determine the steady state temperature. The absorbed energy considered was from the sun's radiation and the laser.

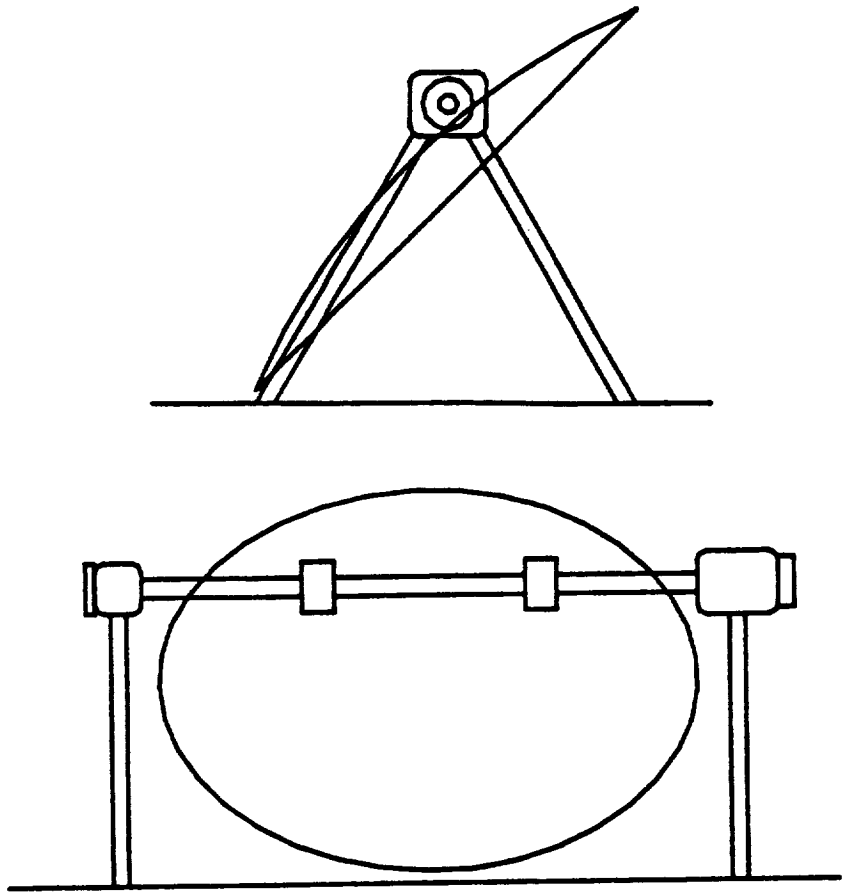

Figure 25. Tertiary Mirror Design.

$$Q + \alpha \times w \times S = 5.669 \times 10^{-8} \times E \times T^4 \times S$$

where:

Q = laser energy absorbed (W)
α = absorbtivity of the mirror
T = steady state temperature (K)
w = heat flux of the sun (W/m^2)
S = surface area of the mirror (m^2)
E = emissivity of mirror surface

Table 10. Conclusion of Thermal Analysis.

Optical device	T_s (K)	Q_a (kW)
Secondary Mirror	1376	200
Beam Splitter	1020	200
Tertiary Mirror	1113	100

From the steady state temperatures of the above optical components, it was determined that a cooling system must be incorporated into the optical train.

Mirror Cooling

Once the need for cooling was established, three possible systems were evaluated: a toroidal radiator, a honeycomb panel heat pipe sytem and a liquid hydrogen cooling system. These systems were required to remove a total of 600 kW of heat energy, 200 kW from the secondary mirror, 200 kW from the beam splitter, and 100 kW from each tertiary mirror. Evaluation of the cooling schemes took into consideration the overall mass of the system, space deployment capabilities, and manufacturing processes.

During the design of the cooling system, it became apparent that the system required to reject 600 kW of energy would add approximately 3000 kg to the vehicle mass. This would have significantly effected the moments of inertia, and the excess mass around the mirror would have required the mirror truss to be strengthened. Therefore, it was decided that cooling the tertiary mirror and the beam splitter could be accomplished using the hydrogen fuel. In this design, liquid hydrogen traveling to the engines passes thru passages incorporated into the rear surfaces of the beam splitter and the back of each tertiary mirror (Figure 26). This raises the temperature of the hydrogen to 408 K. Incorporation of this design into the present fuel feed system only required that the power of the pump be increased to allow the fuel to travel through a longer cooling pipe. The use of the regenerative hydrogen cooling system decreased the total amount of heat removal to the 200 kW produced by the secondary mirror.

Since radiation is the only method of heat rejection in space, the surface area, temperature, and emmisivity become the limiting factors for heat rejection. Stefan-Boltzmann's equation was used to calculate the surface area required for each of the radiators. In calculating the area it was assumed that in 20 years, coatings for the radiators will be capable of producing an emissivity of of 0.85. The maximum temperature of the dielectric surface was restricted to 600 K. This maximum temperature restriction minimizes the thermal deformation in the supporting truss and the degradation of the dielectrics. Using the above information a surface area of 85.058 m^2 was calculated as the minimum area a cooling system would need to reject 200 kW of energy.

Placement of the cooling system was restricted by the need for symmetric loading about the center of mass and the amount of heat radiated back on to the spacecraft. From these restrictions it was determined that the cooling system must be placed around the perimeter of the primary mirror.

The toroidal radiator considered was derived from a low temperature, expandable power radiator (Ref. Chow). This design was incorporated using a large toroid which encompasses the primary mirror (Figure 27). In this design, cooling is provided by pumping water to the secondary mirror where it is vaporized and then returned to the radiator. Heat energy is then transferred to the radiator where the water is condensed and returned to the mirror by a pump.

The radiator is constructed from flexible plastics capable of being rolled into a small volume during transportation and then joined to the LPIV in space. Because the fluid velocity is inversely proportional to the corssectional area of the pipe, an internal pressure of 1 atm was selected in order to produce lower velocities while maintaining a reasonable pipe diameter. This pressure created the need for a wall thickness of approximately 2 mm, which resulted in a structural mass of about 175 kg. Heat is removed by 100 kg of water which serves as the working fluid.

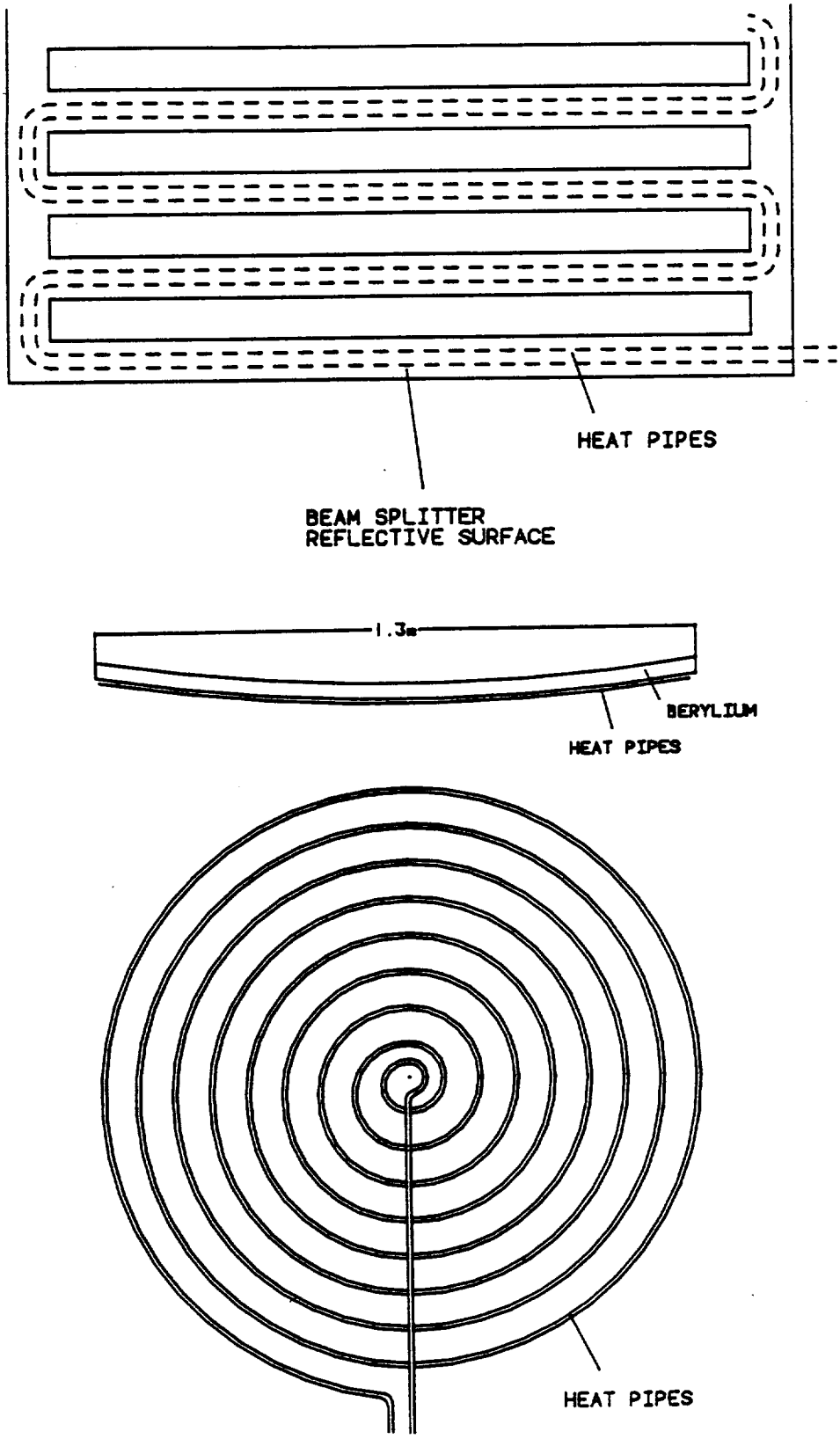

Figure 26. Cooling System for Beam Splitter and Tertiary Mirror

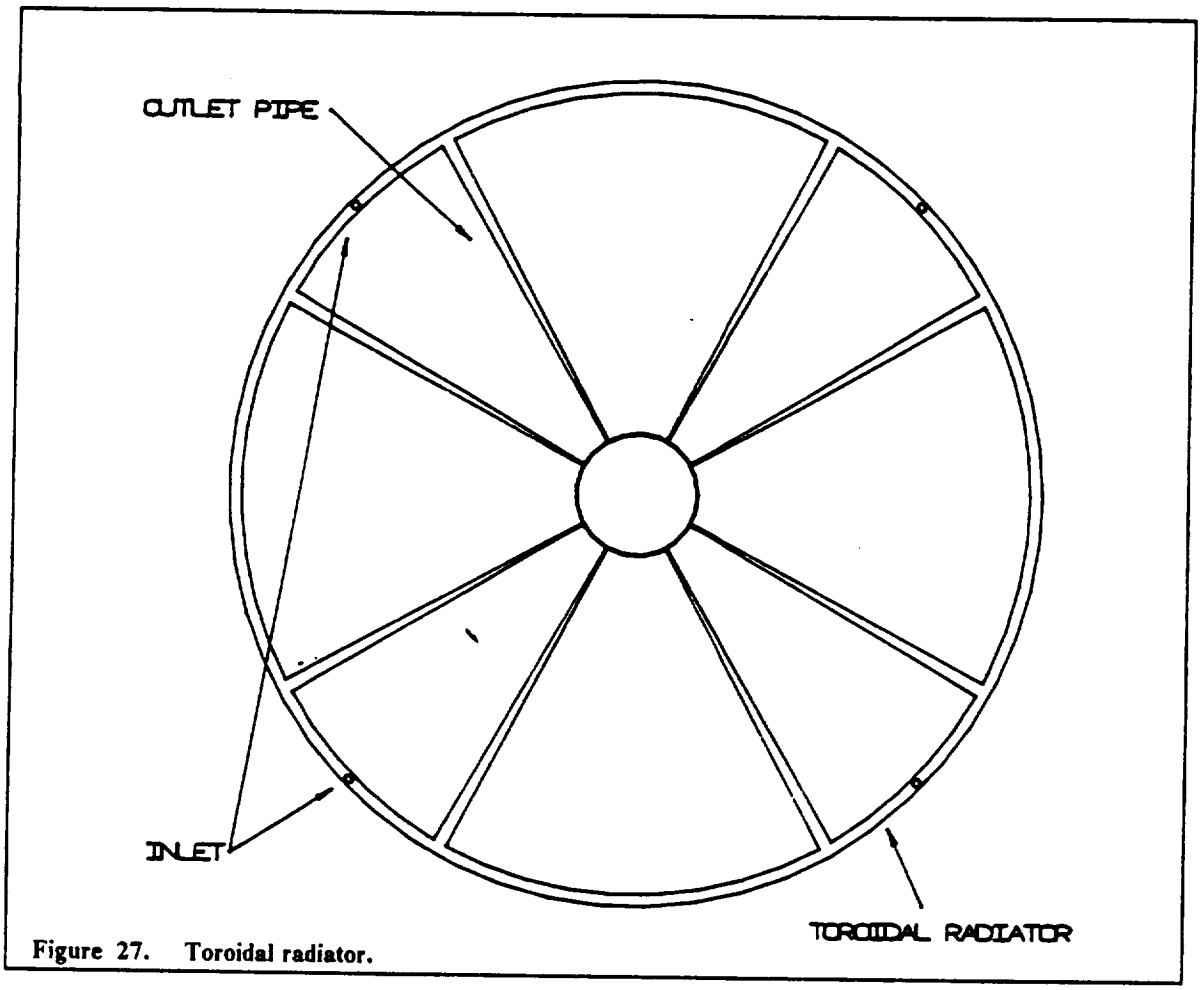

Figure 27. Toroidal radiator.

Although the toroidal radiator has a very low overall mass, the design was rejected due to manufacturing difficulties and a need for a pump to circulate the working fluid. The cooling system which seemed to be best suited for application with the LPIV is based on a honeycomb panel heat pipe proposed by NASA. In the modified configuration, two types of heat pipes are used - a cylindrical heat pipe with an arterial wick (Figure 28) and a honeycomb heat pipe (Figure 29). The function of the cylindrical heat pipe is to provide a two way passage between the evaporator on the back of the secondary mirror and the radiator. The arterial wick is necessary for high performance heat pipes in space because it provides a low pressure path for transporting a liquid. A second wick is used around the heat pipe's inner wall near the evaporator enabling liquid to be distributed evenly around the heat pipe. The vapor leaving the evaporator flows in the area surrounding the artery until it reaches the radiator (honeycomb heat pipe) where it condenses. Pumps are not required in this system because capillary pressure is used to move the fluid through the arterial wick.

A few problems arose when trying to incorporate this type of cooling system into the design of the LPIV. The use of water as the working fluid way cause problems with freezing due to the temperature in the earth's shadow. Possible solutions that may remedy this is to add an antifreeze to the water or to have a heater which would keep the water above its freezing temperature.

The other problems were the interference of the incoming laser beam with the cylindrical heat pipes that run along the tripod supports and the radiator that is positioned around the perimeter of the primary mirror. 2 cm of a multi-layer insulation is used around the cylindrical heat pipe to provide a passage through which the working fluid can pass without changing states. The radiator is mounted behind the primary mirror to protect it from laser beam radiation.

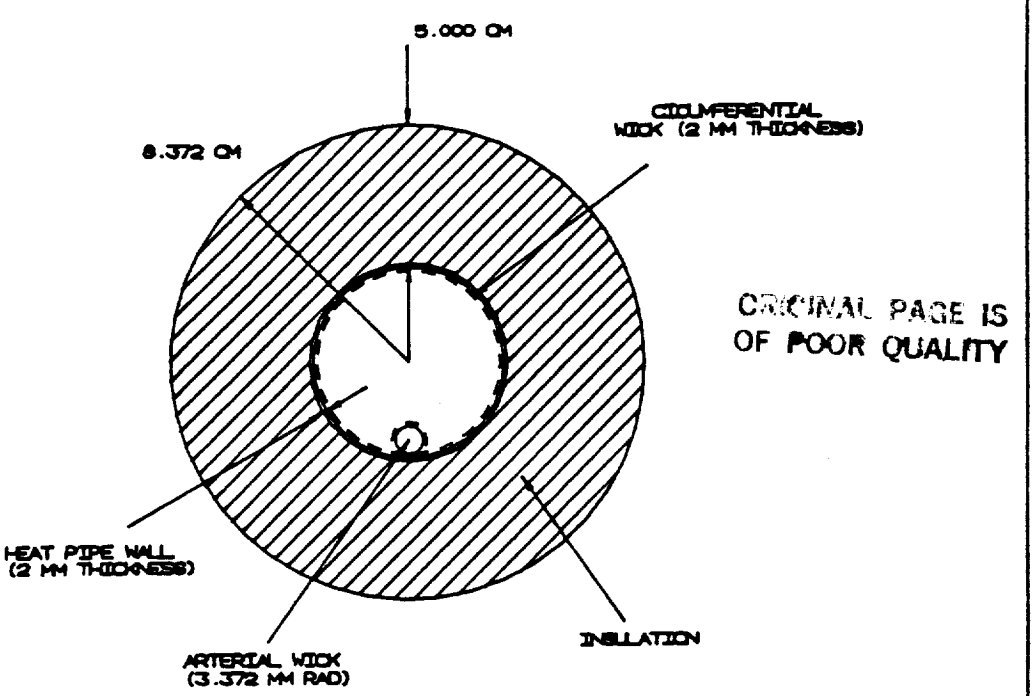

Figure 28. Arterial Wick Heat Pipe

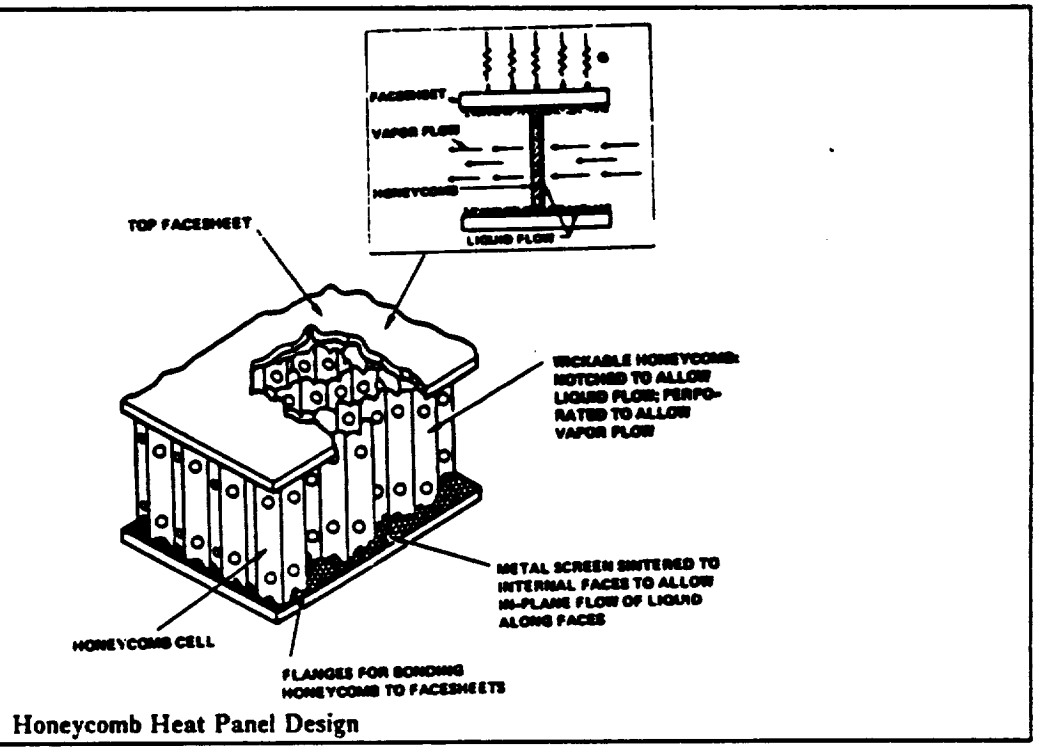

Figure 29. Honeycomb Heat Panel Design

OPTICAL SUPPORT STRUCTURES

The main objective of the optical support structures was to minimize displacement errors occurring along the optical path. Errors occur in the variation of the primary mirror shape, deflection of the secondary mirror tripod support, beam splitter motion, and tertiary mirror displacements. The

secondary mirror tripod support, beam splitter motion, and tertiary mirror displacements. The primary mirror's supports were required to be of minimal mass while providing rigidity. The maximum error allowed in the primary mirror is +/- 0.01 m from the initial contour. Using this criteria two support structures were considered. The first design consisted of six I-beam spokes joined together by a central hub (Figure 30). The individual hexagon panels were then connected together and fastened to the spokes by smaller C- beams. This design provided very high rigidity but was accompanied by a high mass.

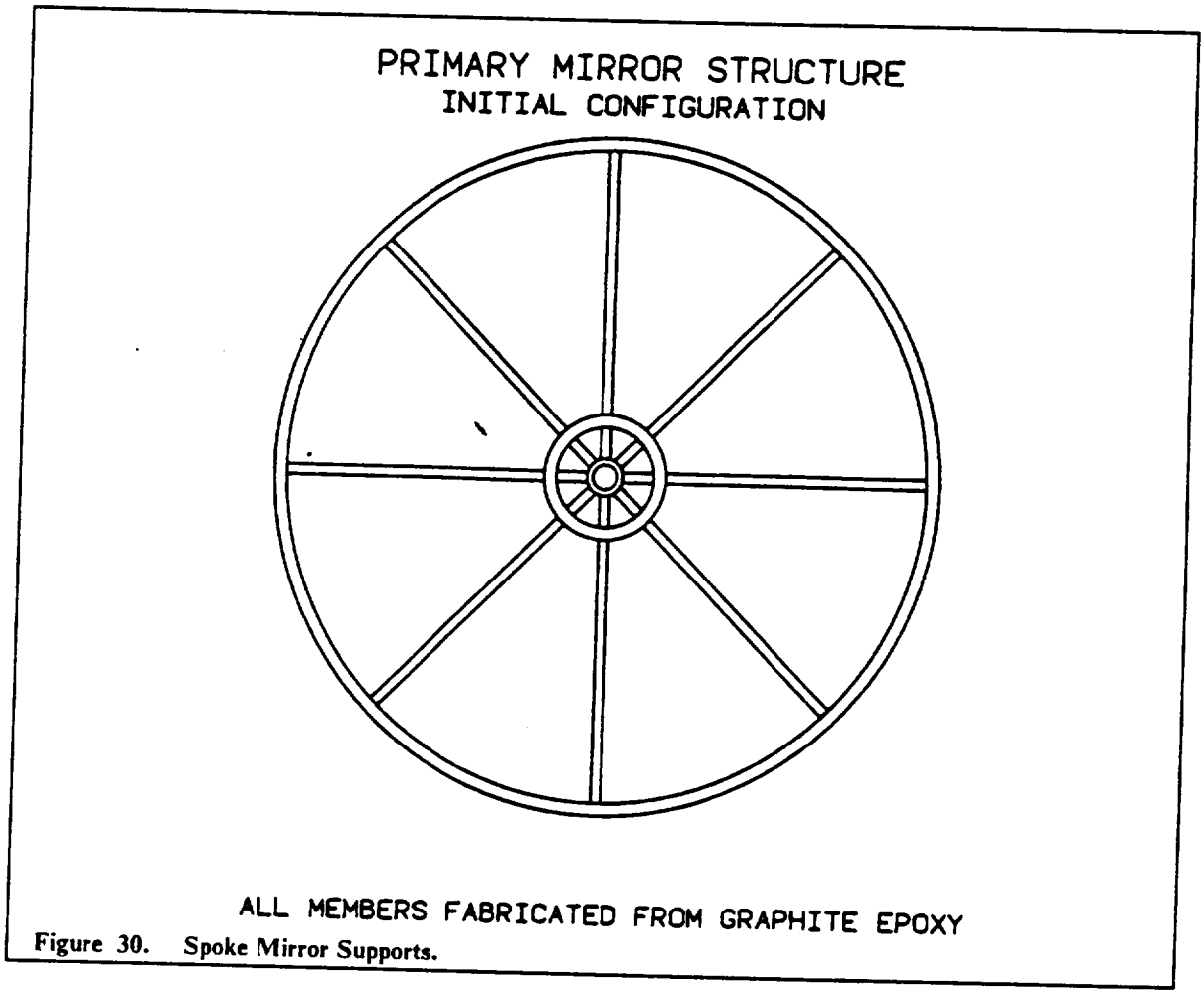

Figure 30. Spoke Mirror Supports.

Another design that was considered was a truss type structure. The truss consisted of tripod support behind each hexagon panel which were interconnected at the tripod vertices by a truss member (Figure 31and Figure 32). Each tripod member was calculated to be 1.670 m in length with an inner and outer radius of 0.0595 m and 0.06 m, respectively. The connecting members were 2.045 m in length with an outer radius of 0.080 m and an inner radius of 0.0790 m. The material chosen for these members was graphite/epoxy with a chromatic acid anodized aluminum foil coating (ref. Dursch). This support design was chosen because it provided the primary mirror with high rigidity and lower mass than the spoke structure (Table 11). The hexagon surface panels are attached to angular C-beams (Figure 34) by a spring pin method (Figure 35). As mentioned in section 3.3 the pins are placed through notched holes in two places on each C-beam. This method of construction will allow easy EVA replacement of individual panels.

The hexagon panels are then joined together by bolting together the C-beams. The hexagon panels are prejoined before launch by machine bolting the C-beams together everywhere except along six joints. The remaining six joints are attached together in space by using a latch jaw mechanism (Figure 36). This structure is then attached to the tripod members by a collet joint fastened to the C-beam. A mass analysis of the primary mirror support structure is presented in Table 11.

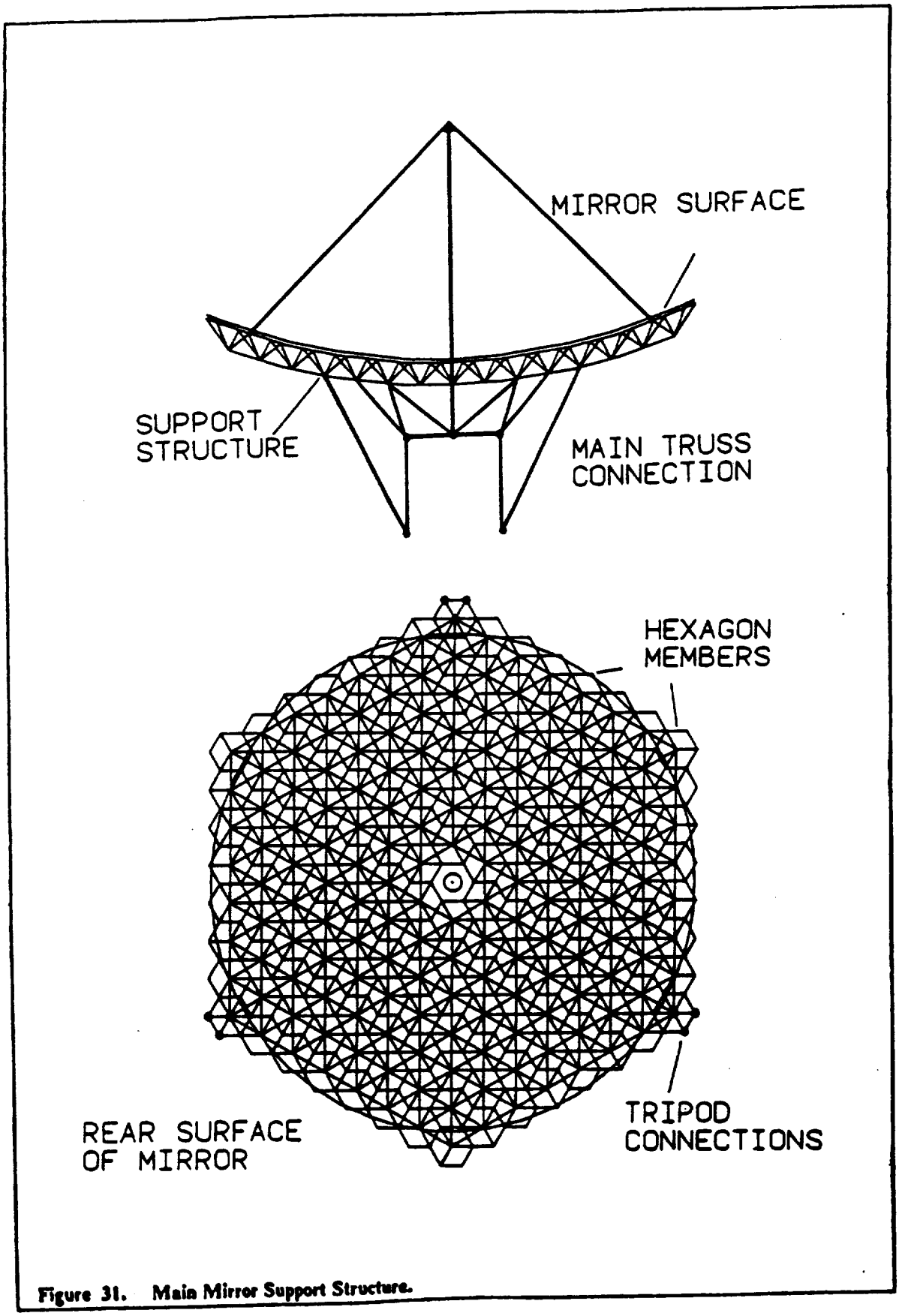

Figure 31. Main Mirror Support Structure.

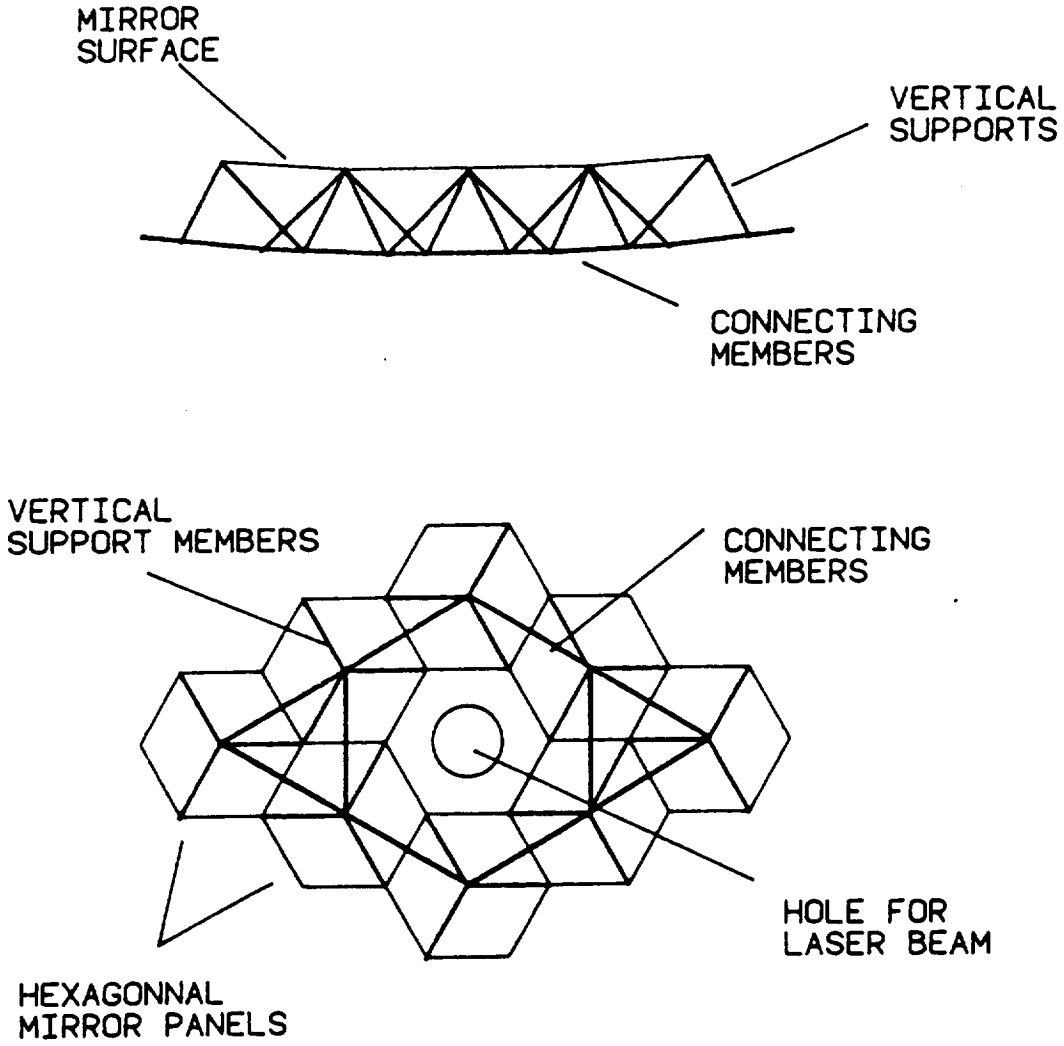

Figure 32. Detailed Main Mirror Support.

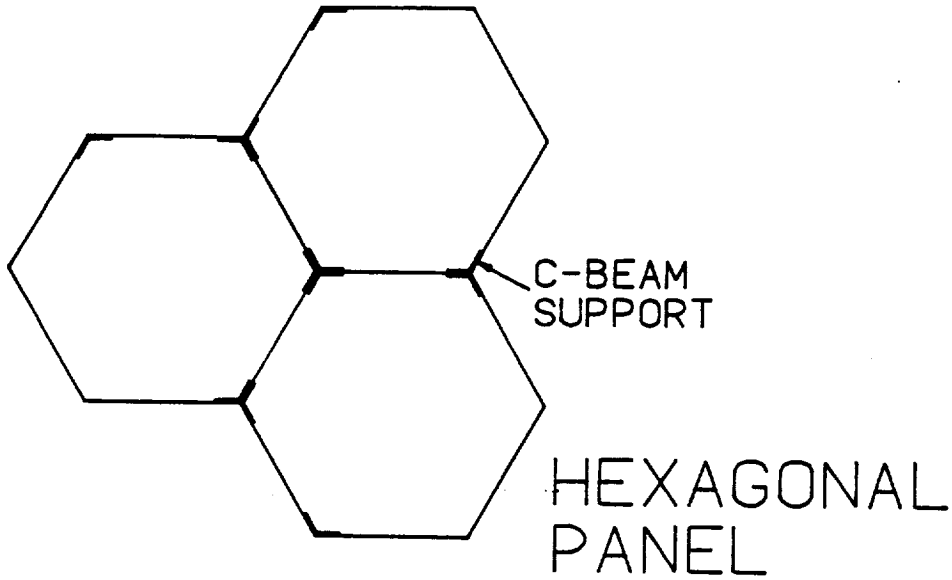

Figure 33. Detail of Hexagonal Panel Assembly

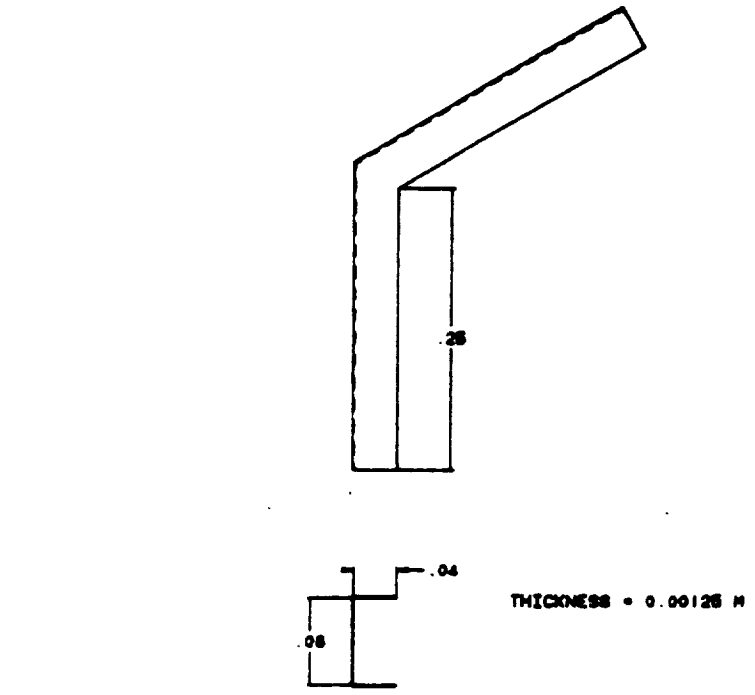

Figure 34. Angular C-beam Support.

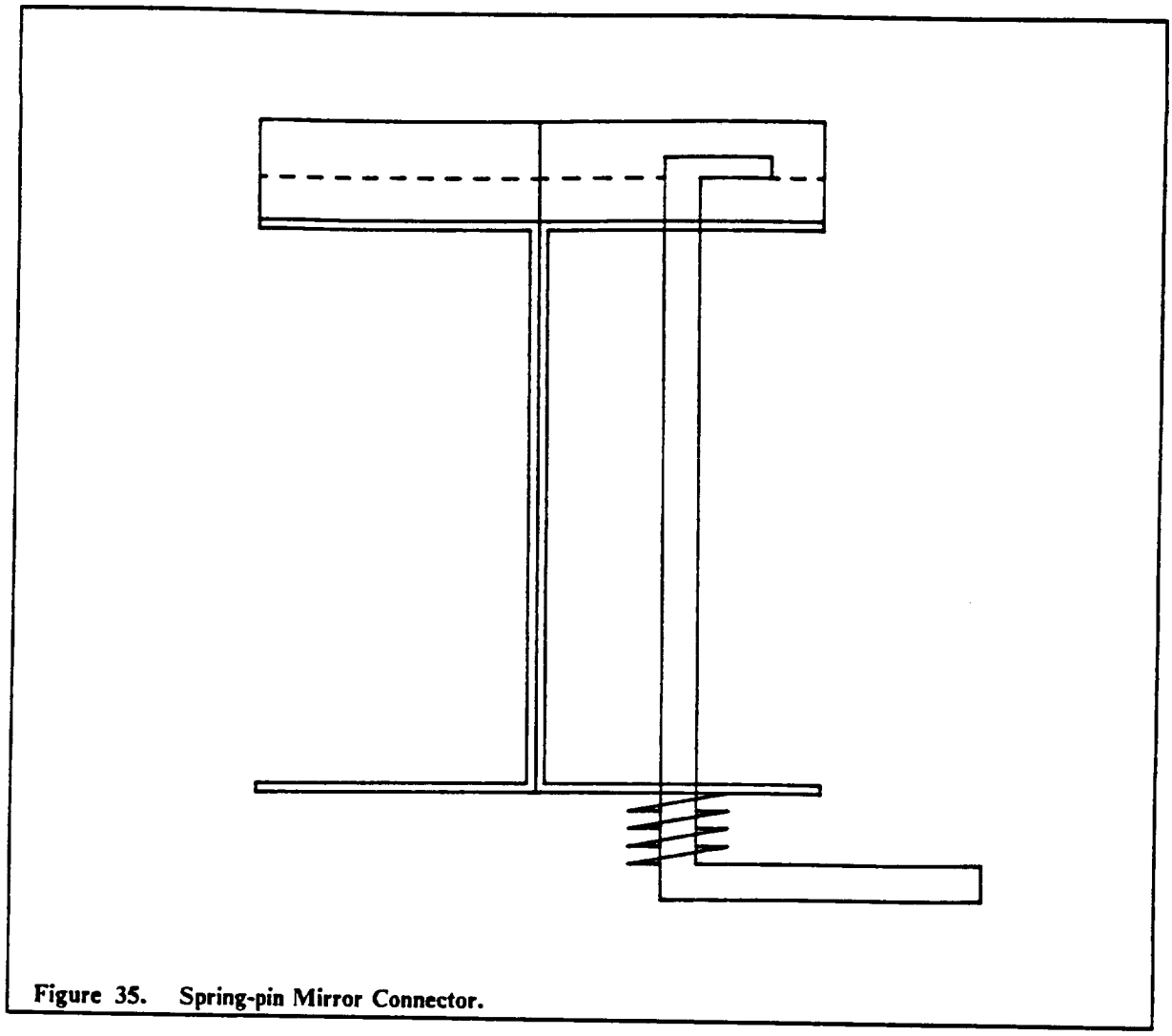

Figure 35. Spring-pin Mirror Connector.

One of the most critical design features of the optical train was the tripod support for the secondary mirror (Figure 37). While considering the possible types of members, a rectangular support and a tri-beam support were analyzed. The rectangular beam was merely a thin tall beam which would resist bending while blocking little of the laser beam. The tri-beam support is constructed from three tubular beams joined together every 4.1 m by small cross members (Figure 38). The tri-beam support was chosen because it provided the best combination of minimal overall mass and high strength. The size of each member is 16.016 m in length, 0.0474 m outer radius, and 0.0023 m in thickness. These members are also constructed from graphite/epoxy with an aluminum foil coating. The analysis which was performed on the tripod calculated the maximum deformation that would occur due to a non-uniform temperature change of 75 K. The largest deflections which result from such loading conditions are less than 0.0005 m. These deflections are well within our limit of error for the optical train. Due to possible errors in the calculation of the change in temperature the accuracy of this analysis may be off. Therefore, the need may arise to compensate for deflections that will decrease the optical efficiency below the minimum acceptable efficiency. A possible solution could be to attach a hydraulic pushrod to the end of each support arm and link this by a computer to the optical system.

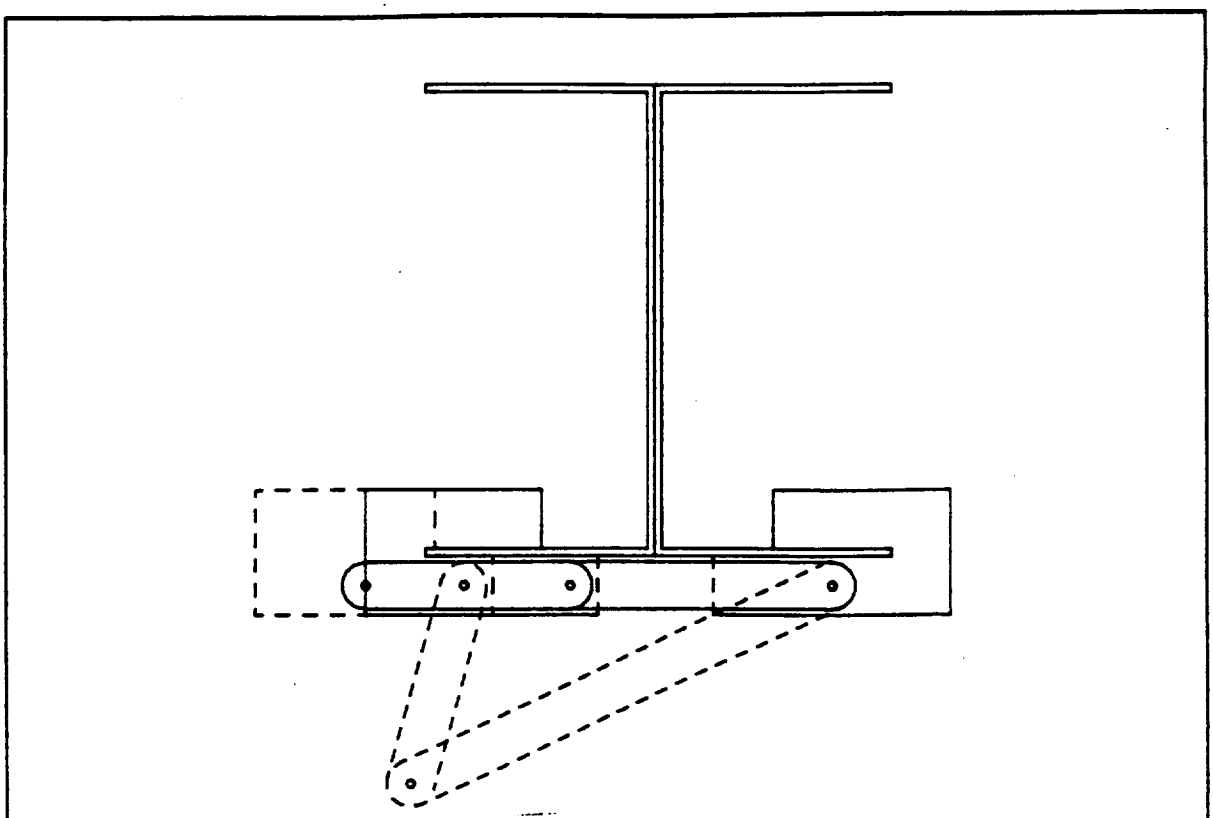

Figure 36. Latch-jaw Mechanism For Space Assembly.

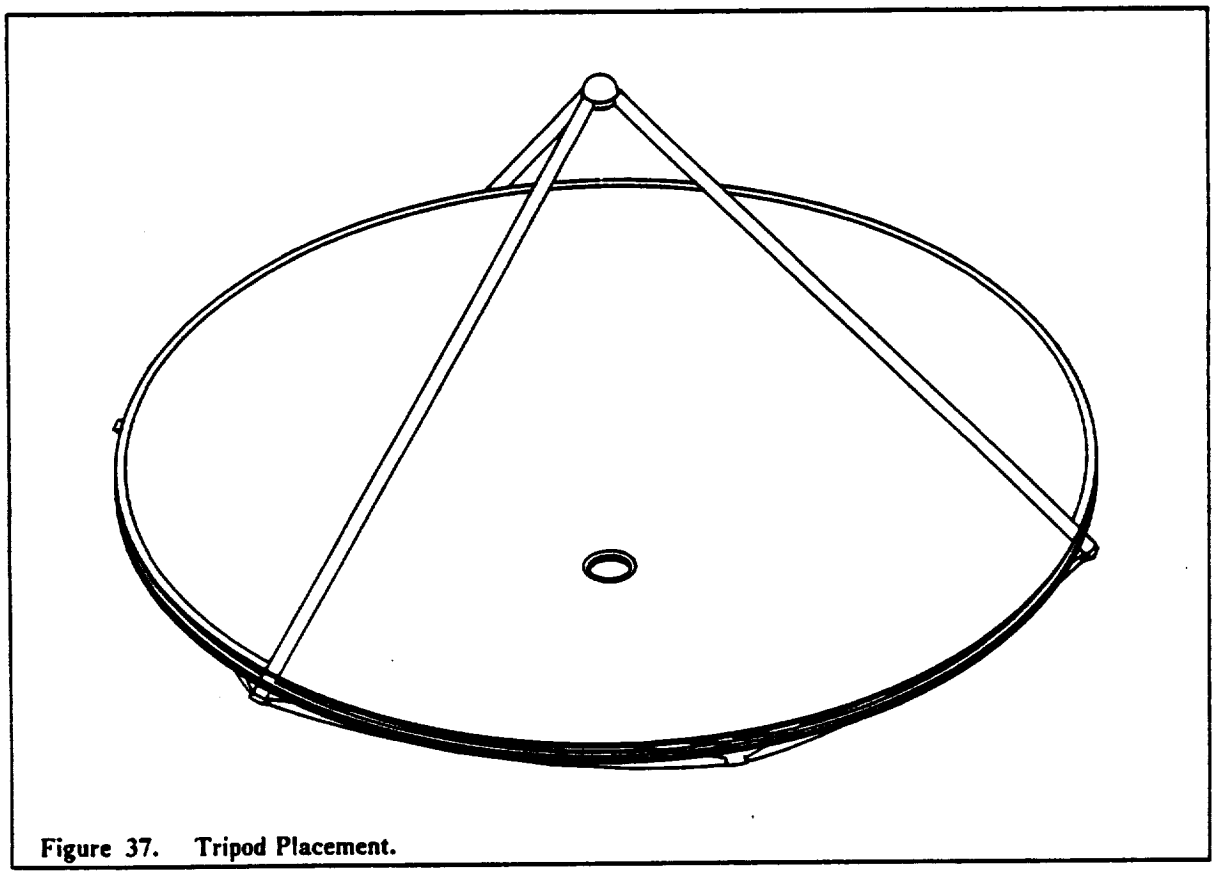

Figure 37. Tripod Placement.

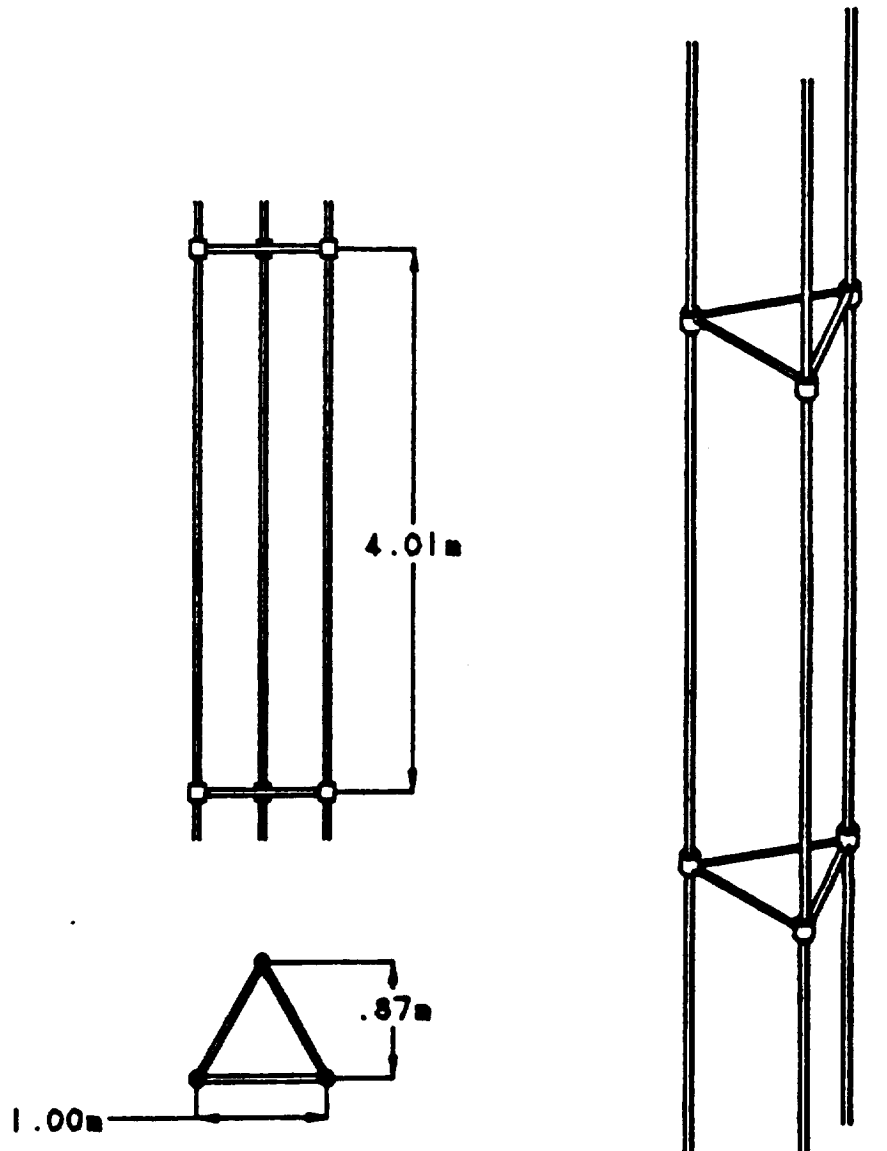

Figure 38. Tripod Tri-beam Supports.

Table 11. Optical Train Masses.

Primary Mirror Masses

Hexagon Panels:

Material	Density (kg/m^3)	Thickness (m)	Area (m^2)	Mass (kg)
Beryllium	1850	0.002	456	1688.5
Dielectrics	2700	3.29×10^{-6}	456	4.1
Gr/Ep	1765	0.002	292	1029.2
Fused Silica	2190	0.013	.00373	8.2
TOTAL Mirror mass				2730.9

C-Beam Corner Joints:

Cross-sectional area:	4.00×10^{-4} m^2
Member length:	0.50 m
Volume:	2.00×10^{-4} m^2
Number of members:	756
TOTAL MASS:	266.9 kg

Truss Structure:

Tripod members

radius:	
inner	0.0595 m
outer	0.0600 m
length:	1.670 m
Cross-sectional area:	1.877×10^{-4} m^2
Number of members:	378
TOTAL MASS	209.1 kg

Connecting members

radius:	
inner	0.079 m
outer	0.080 m
length:	2.045 m
Cross-sectional area:	4.995×10^{-4} m^2
Number of members:	339
TOTAL MASS:	611.2 kg

TOTAL Truss mass	820.3 kg
Total Primary Mirror Mass:	3818.1 kg
Secondary Mirror Mass:	90 kg
Beam Splitter:	85 kg
Tertiary:	110 kg
TOTAL OPTICAL SYSTEM MASS	4103.1 kg

STRUCTURES

INTRODUCTION

Technology in the field of spacecraft structures and materials engineering has experienced a rapid growth in recent years. Materials such as aluminum, used in early space vehicles, have been replaced by composite, metal-matrix, and thermoplastic materials. For certain applications these materials may be preferred over aluminum because of their high strength to weight properties and high modulus characteristics. Due to the strict rigidity requirements of the optical system for the LPIV, proper material selection satisfying the structural integrity requirements of the spacecraft plays a key role in the development of the truss structure. The primary requirement for the structure of the LPIV is that it is able to withstand all inertial, aerobraking, and docking loads. Other objectives for its design include: (1) minimization of structural weight, (2) minimization of dispacements due to thermal loading, and (3) minimization of material degradation due to space environment.

TRUSS DESIGN

In order to develop a main truss structure that will satisfy the mission requirements three types of truss structures were considered, specifically a box truss, triangle truss, and an octetruss. A box type main truss design was proven to be most suitable. One reason why this configuration was chosen over the triangle-type truss was because it withstands torsion better. A reason it was chosen over the octetruss was due to the mass savings incurred in such a design. Two configurations of the box truss considered are shown in Figure 39 (Ref. Kempster).

The main truss is 37.5 m in length and 5.3 m x 5.3 m square in cross section. The overall length of the truss was chosen mainly for placing the engines far enough away from the main mirror to minimize any effects of the plumes. Seven 5.3 m x 5.3 m unit boxes make up the main truss with members connected by aluminum nodes shown in Figure 40.

Material Selection

Three materials considered in the development of the main truss structure are aluminum, boron/aluminum, and graphite epoxy. Strength and stress characteristics as well as high modulus properties are shown in Table 12.

Criteria for suitable material selection include: (1) high strength to mass and stress to mass characteristics, (2) low coefficient of thermal expansion (CTE), (3) low degradation due to the space environment, and (4) product availability and service life.

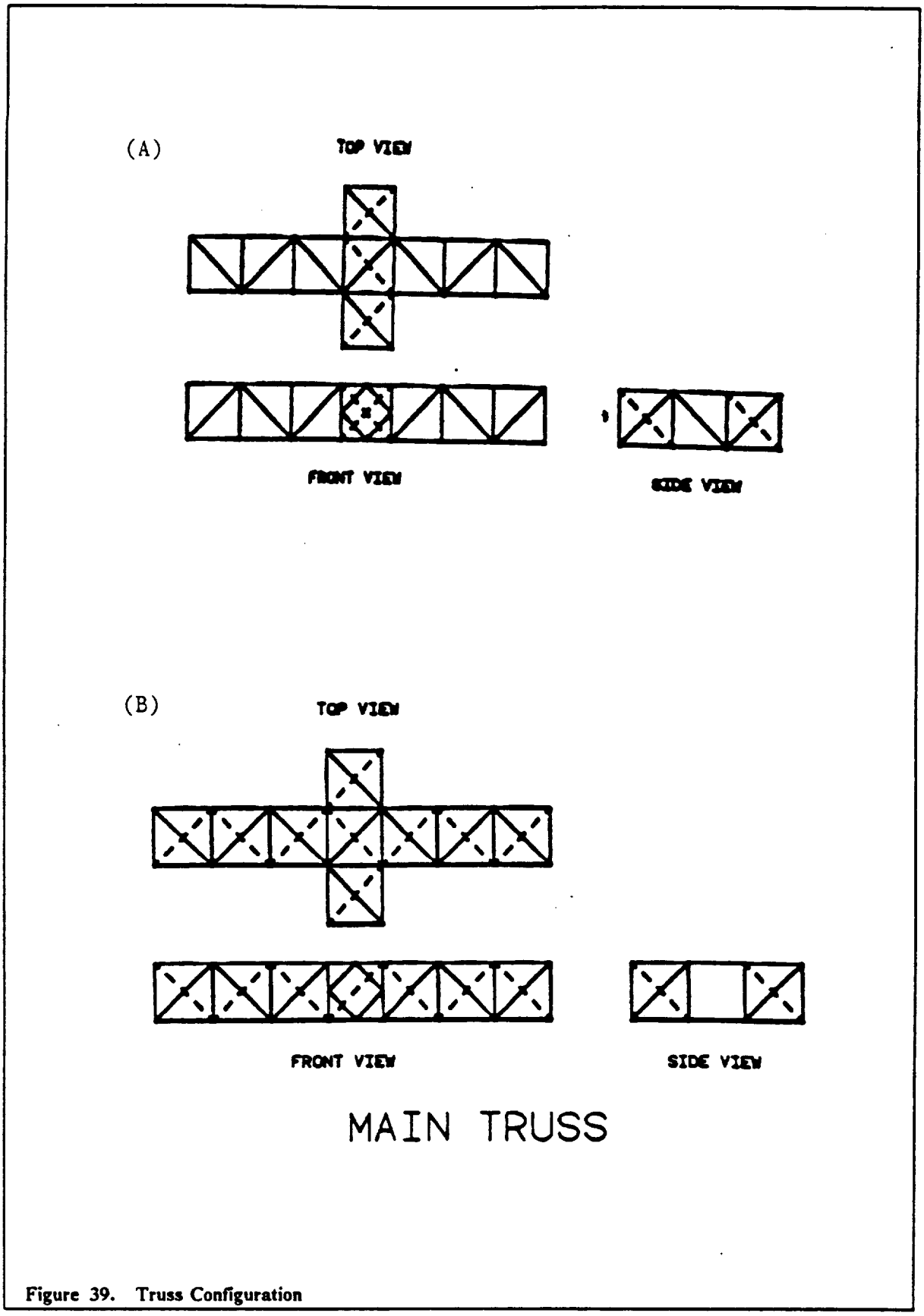

Figure 39. Truss Configuration

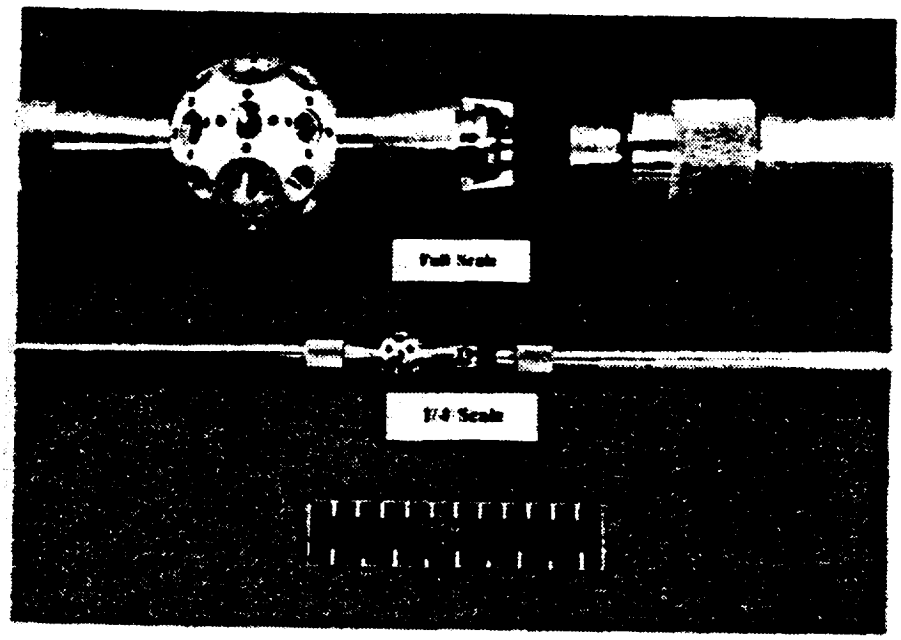

Figure 40. Node Connectors

Table 12. Material Properties

Property	Aluminum	Boron/Aluminum	P75S/934
$E_1(GPa)$	68.9	230.3	262
$E_2(GPa)$	68.9	160	9
$E_1/density$ $(x10^6 m^{2/s2})$	24.6	92.5	148.4
$E_2/density$ $(x10^6 m^{2/s2})$	24.6	64.3	5.1

The graphite epoxy P75S/934 with a $(O_f, \pm 20, O_f)$ layup has been selected because it satisfies all requirements more readily than the other materials. Certain problems with graphite epoxy in the space environment such as outgassing may be dealt with by applying a chromic anodized aluminum foil to the outside of the truss members. Use of this foil not only decreases outgassing but also lowers the CTE. A report by Boeing which tested this graphite epoxy arrangement in a LEO environment indicated that the maximum change in temperature the members will undergo is 67 K and that the foil helps in the reduction of space environment effects such as: temperature cycling, solar radiation absorption, atomic oxygen degradation, vacuum, micrometeoroids, space debris and microcracking due to thermal loading (Ref. Dursch). Graphite epoxy has been used and commercially produced for quite some time now in space applications and has been shown to have a long lifetime of use.

Static Analysis

In order to perform the static analysis on the main truss structure and other structural components, "Structural Analysis Software for Micros" (SSAM) by B.J. Korites has been used. SSAM performs a static finite element analysis utilizing the "direct stiffness" method in order to determine nodal displacements and member forces (Ref. Korites). Assumptions used in the modeling of the truss for analysis are: (1) a statically loaded truss structure, (2) all nodes represent end fittings modeled as frictionless ball and socket joints, incapable of inducing bending in the members (Ref. SLICK),

and (3) engine thrust, payload and mirror assembly inertial loads are distributed over appropriate nodes of the truss.

Due to symmetry, only half of the truss structure needed to be analyzed. Figure 41 shows thrust and inertial loads applied to the truss for analysis. These loads include a factor of safety (FS) of 2 to account for any loads that have not been considered such as dynamic, docking, etc. A worst case thrusting load, diagonal to the box truss, is used for the analyses to determine maximum displacements. Aside from static analysis, SSAM performs thermal analyses of structures. Thermal radiation is the major contributor to structural deformations for the LPIV.

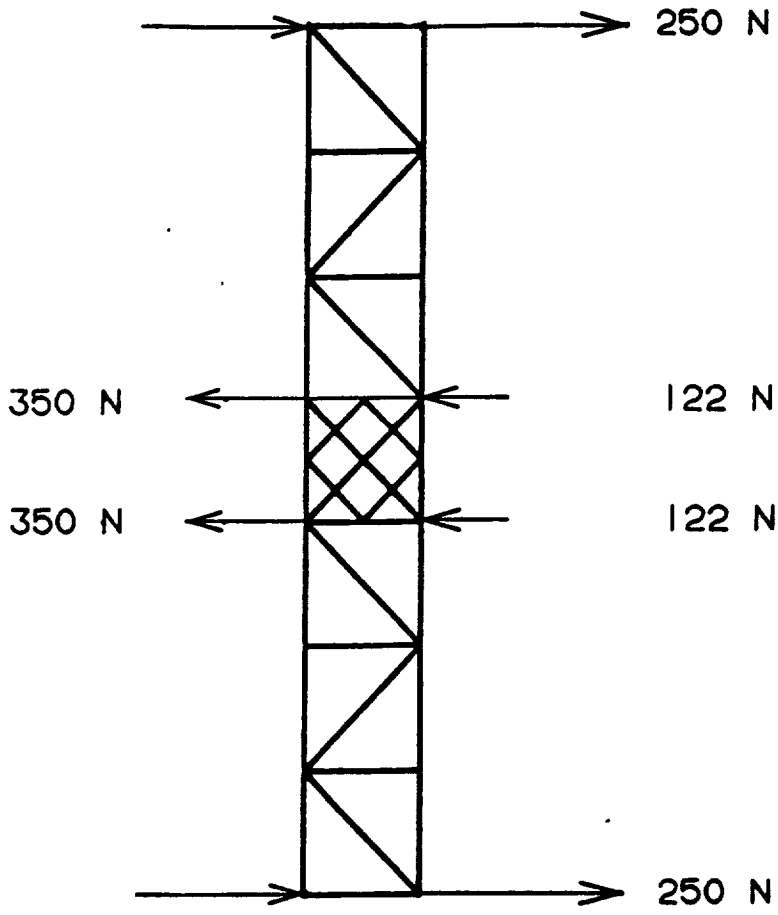

Figure 41. Representation of Thrust and Inertial Loads

Thermal Analysis

Thermal representation of the truss structure in SSAM requires specification of temperature gradients for each member. A worst case scenario is again used to predict maximum thermal loading deformations on the truss. Figure 42 illustrates the scenario. The structure is placed in LEO where it is subjected to the highest changing levels of radiation during its mission. Temperatures of members are obtained when applied thermal loads input into each member reach equilibrium with radiation reradiated from each member. Each member is subjected to solar, earth, and earth albedo radiation in the space environment (Ref. Mahaney). Figure 43 shows a representation of the radiation effects on a member.

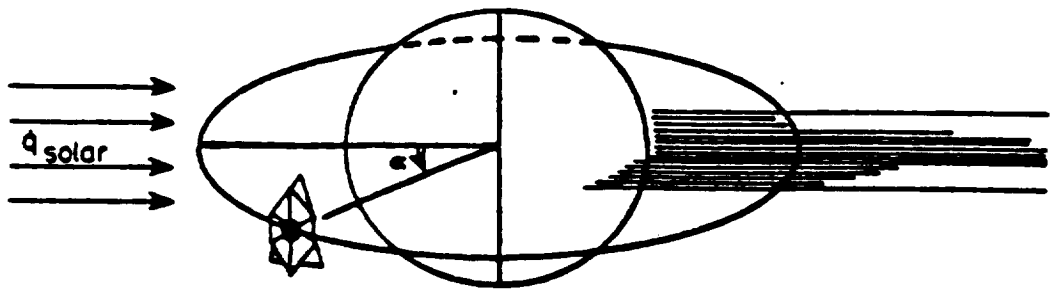

Figure 42. Thermal Loading Scenario

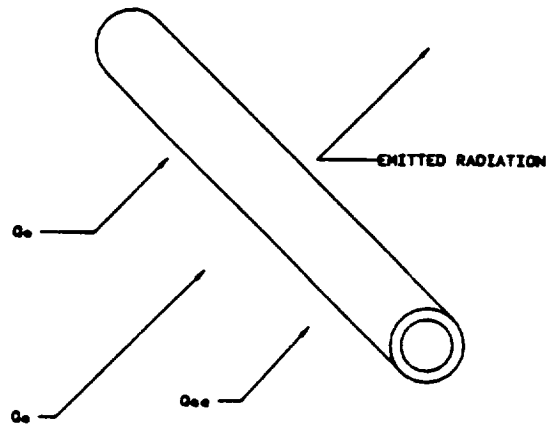

Figure 43. Radiation Effects on Truss Member

Expressions for each type of radiation are:

$$\dot{q} = \sigma \varepsilon T_m^4 \tag{1}$$

$$\dot{q}_s = 1390\alpha \cos\psi \tag{2}$$

$$\dot{q}_e = \sigma\alpha T^4 F \tag{3}$$

$$\dot{q}_a = 1390AF\alpha F \cos\theta \tag{4}$$

where:

$\dot{q}$ - member emitted radiation
$\dot{q}_s$ - solar radiation
$\dot{q}_e$ - earth radiation
$\dot{q}_a$ - earth albedo radiation
σ - Stefan-Boltzmann constant
ε - emissivity of material
α - absorptivity of material
θ and ψ - spacecraft orientation
F - view factor
AF - albedo factor
T_m - member temperatures
T - black body radiation (289 K)

Iteration of the following equation until equilibrium occurs results in the member's temperature under the assumed parameters.

$$\dot{q} = \dot{q}_s + \dot{q}_e + \dot{q}_a \tag{5}$$

Assumptions in calculating the thermal displacements are (Ref. Mahaney): (1) all elements are isothermal (no conduction between members), (2) aluminum joints are disregarded, and (3) material properties are considered constant.

Combined Results

Data obtained from the static analyses was combined with the data obtained from the thermal analyses in order to determine total displacements of the truss nodes. Table 13 shows the results for both trusses analyzed.

Table 13. Maximum Nodal Displacements

Figure	Max. Displacement (mm)
18A	1.314
18B	1.310

Although the second truss of Figure 39 shows less displacement, a mass savings to maximum displacement of 603 (kg/mm) compared to 560 (kg/mm) for the first truss, indicates that the first truss will best meet the mission requirements of the LPIV.

Mass Analysis

As indicated in the previous section, the first truss of Figure 39 has a better mass to displacement ratio than the second truss. The graphite epoxy material selected for the structure meets the rigidity criteria while minimizing overall mass. Table 14 compares masses of the first truss in Figure 39 made up of the different materials considered. Members making up the truss have a 4.74 cm outer radius and a 4.54 cm inner radius and varying lengths of 3.75, 5.3, and 7.5 meters are used in the mass analysis.

Table 14. Mass Savings Analysis

Material	Density (kg/m^3)	Mass (kg)	Percent Savings
Al	2800	1146	0
B/Al	2490	1023	11
P75S/934	1765	734	36

Stress Analysis

Stress analysis was performed using the SSAM program. The program calculates individual and global member stresses of the structure. Using the formula for critical loading of a cylindrical beam, $P_{cr} = (\pi)^2 EI/L^2$, the critical stress calculated is 273.4 kPa. The SSAM program determined the maximum stress the truss encounters to be 138.4 kPa which fell well under the critical stress value. This stress occurs in a vertical member in the first cubical area past the center structure.

MAIN TRUSS SUMMARY

In order to arrive at a good truss structure design, many steps must be accomplished. Overall configuration, material selection, and structural analysis are some of the steps that must be done in order to arrive at a valid design. Data presented through a static analysis indicates that the truss in Figure 44 will be the best suited design to satisfy LPIV project requirements. Member displacements are slight which satisfies structural rigidity requirements for the optical train.

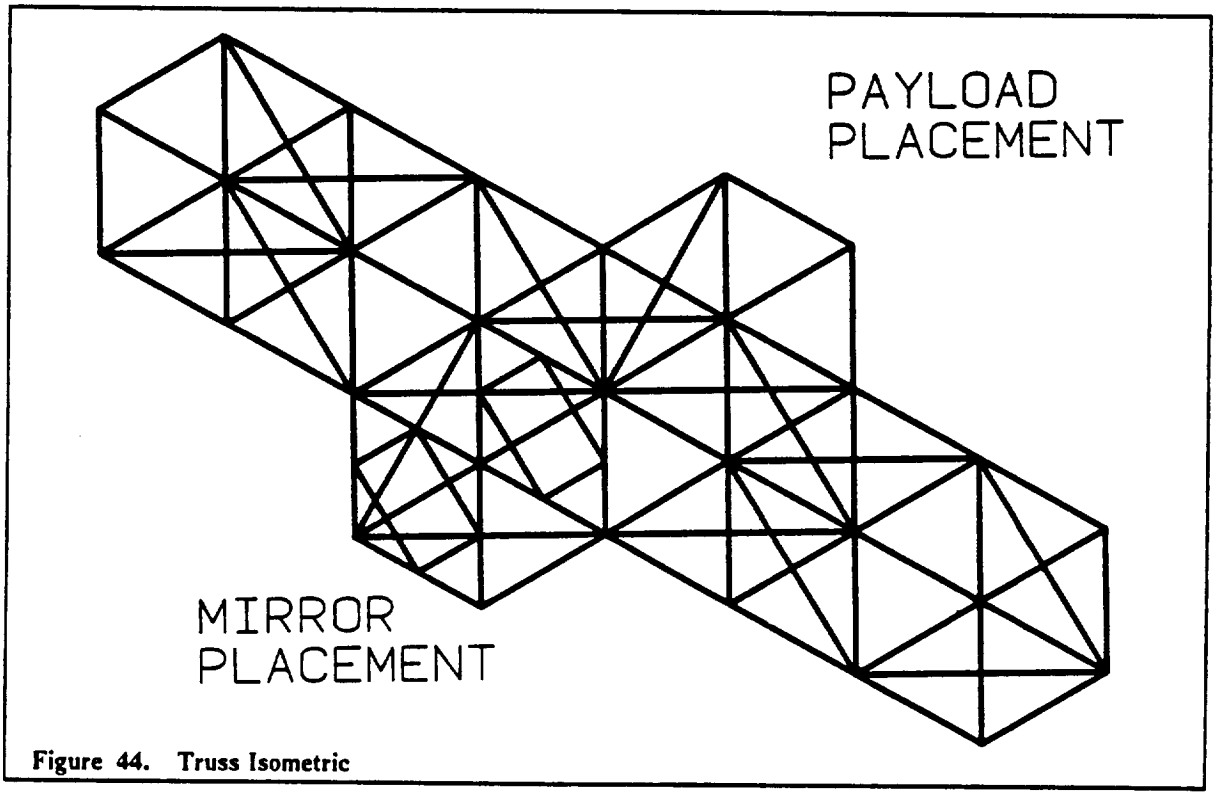

Figure 44. Truss Isometric

Stresses encountered during the trip have been determined to be significantly less than the critical stress determined. Selection of graphite epoxy composite material with the chromic anodized aluminum foil resulted in a minimization of structural weight and degradation due to the space environment allowing for a longer life cycle.

DOCKING MECHANISM

In designing the docking mechanism for the LPIV, the basic objective is to capture and structurally attach together two bodies in space autonomously. For our mission, the LPIV must dock with the orbiting Earth station as well as the station located in lunar orbit. The requirements under consideration are: assuring initial coupling of the two bodies, proper alignment of the ships, absorbing the shock of impact and effecting the link-up of ships while assuring undocking of the ships after termination of the joint flight.

To assure initial coupling and alignment of ships, a range and range rate system is required. This system measures the relative distance from the measuring point to the object during docking and closing maneuvers. To dampen the shock of impact, shock absorbers are properly placed on the docking mechanism.

Range and Range Rate System

Radar and laser devices are common methods for measuring range and range rate of distant objects. However, radar devices have a limited minimum range due to the relatively long time duration of transmitted pulses used for measurement. Also, laser devices require sophisticated targets on the object, but this system may be used if there is no potential damaging effects of the radiation on the targets.

A device invented by Jim Russell, Olin Graham, and Walter Epperly is a good choice since no radar or high powered laser is required (Ref. Graham). As shown in Figure 45 this device consists of a triangulation system for measuring range by means of an opto-electrical camera. Figure 45 illustrates the range and range rate system. The system (10) includes an opto-electric camera (30). A helium neon laser (12) produces a source beam (13) of coherent light which is applied to a beam splitter (16). The beam splitter applies a reference beam (17) to the camera and produces an outgoing beam applied to a first angularly variable reflector (20) which directs the outgoing beam (24) to the distant object. An incoming beam (26) is reflected from the object to a second angularly variable reflector (22) which reflects the incoming beam to the opto-electric camera via the beam splitter. The first reflector and second reflector are configured with respect to the beam splitter so that the distance D travelled by the outgoing beam from the beam splitter and the first reflector is the same as the distance travelled by the incoming beam from the second reflector to the beam splitter. The reference beam produces a reference signal in the geometric center of the camera. The incoming beam produces an object signal at the camera. The difference between the reference signal and the object signal is used, with manual or automatic means, to vary the angle A between the outgoing beam from the first reflector and the reference line (39) between reflecting points of the first and second reflectors and the angle B between the incoming beam from the second reflector and the reference line. The angles A and B are maintained essentially equal. The difference between the reference signal and object signal is used to provide an input to a rotator driven circuit (42) to vary the angles of the first and second reflectors until the reference signal and object signal are coincident. Range R is then determined as $R = D \tan A$.

Docking Mechanism Design

Figure 46 illustrates the docking mechanism configuration (Ref. Burns). The passive half consists of a triangular frame (for stability purposes) with three alignment grooves. The frames are structurally supported by six shock struts for energy attenuation. A simple analysis of shock absorbers is given in Appendix B. The shock struts contain latches to rigidize them after capture. The passive frame will be attached to the space station. The active side consists of a triangular frame with three alignment keys to match the grooves in the passive frame. On three sides triangular capture guides provide guidance for the passive frame to be nested with the active frame. Contoured within the capture guide is the capture and structure latch mechanism. The active frame is mounted to the LPIV truss by fasteners (Figure 47) and epoxy and has a mass of approximately 90 kg. Solenoids in each latch are activated by proximity switches in the face of the active frame. The actuation of

the solenoids release the capture and structure latches to contain and hold the passive frame. Dual motor actuators retract the latches to provide structural rigidity and alignment.

Figure 48 shows the mechanism in three states - ready, capture, and structure latch (Ref. Burns). In the ready position the spring-loaded latch is retracted below the surface of the capture guide. When the passive frame activates three or more of the proximity switches, the frame is within the capture range of the latches. The capture solenoids are actuated and the latches, driven by springs, move to the capture position. The latch drive actuators pull the latch drive link down and clamp the two frames together and engage the alignment keys. The drive actuator springs and solenoids are dual to provide operation after one failure.

Figure 49 illustrates a dual motor rotary actuator which is larger than required for the latch actuator, but serves to demonstrate the dual motor drive concept to be used (Ref. Burns). Both DC motors normally drive through a differential planetary gear train to the output shaft. If one motor fails either by loss of power or jams, the other motor will drive the output shaft at full torque at half the rate. A brake on the armature of each motor prevents backdriving the failed motor with the active motor.

PAYLOAD MODULE

A detachable payload module is required to provide the LPIV with the flexibility to carry a variety of cargo. The shape which best meshed with the LPIV configuration was a cylindrical shape. The dimensions of the module are shown in Figure 50. The radius of the payload module is 2.6 m because it is the largest radius that could be integrated with the placement of the module on the LPIV.

The module is constructed out of boron/aluminum as opposed to graphite/epoxy, because of its higher shear modulus. The payload module is wrapped with two aluminum bands to allow for easy attachment and added structural support. There will also be four hatch beams attached to the inside of the module to prevent fracture due to bending. The walls of the module will be 0.0005 m thick, each band will be 0.002 m thick and will be attached to the module with epoxy. The hatch beams will be 0.001 m thick.

The payload module is attached to the LPIV inside the box truss which extends out from the main truss opposite of the mirror. Around each band, four 0.02 m diameter holes will be drilled. The payload will then be secured to the craft by the insertion of eight latch pins. Overall this payload will allow the LPIV to accomplish a multi-transport role in future.

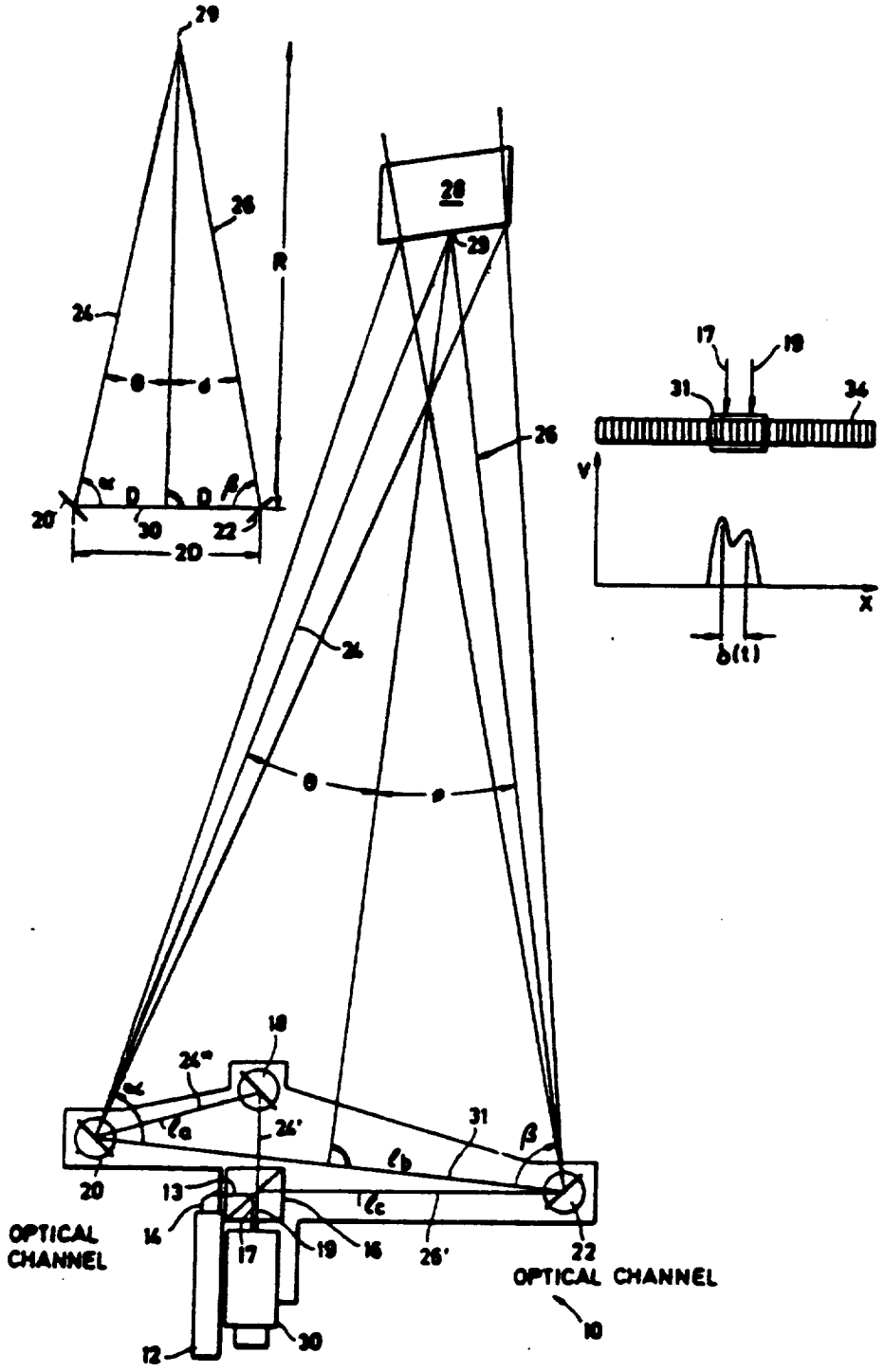

Figure 45. Range and range rate system

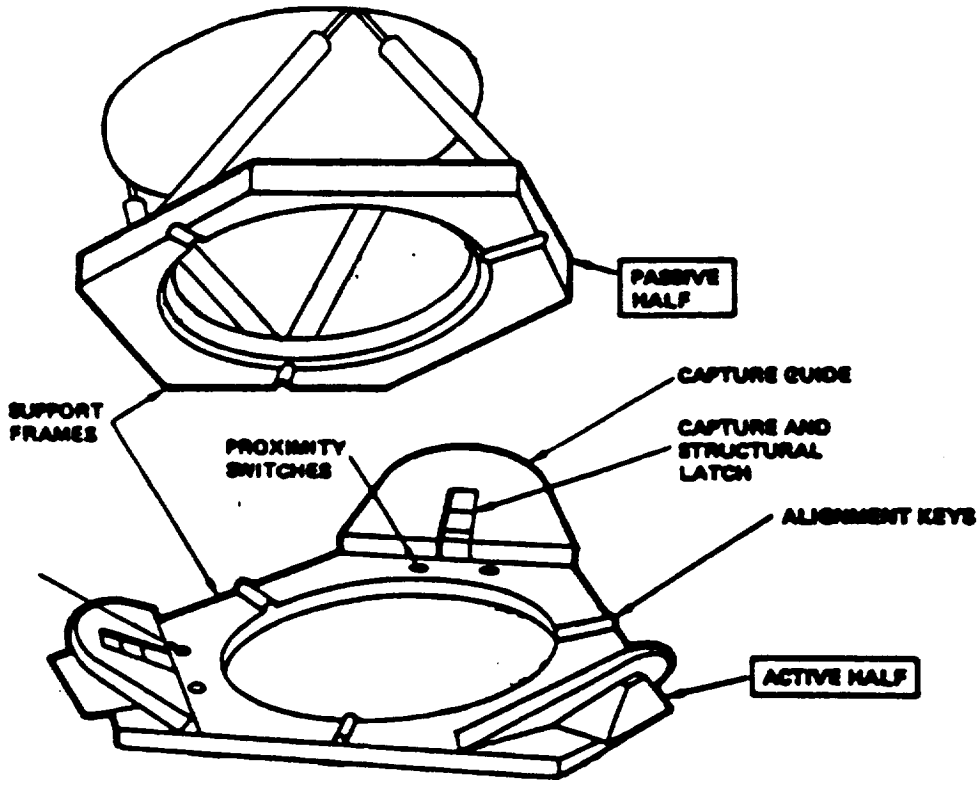

Figure 46. Docking mechanism configuration

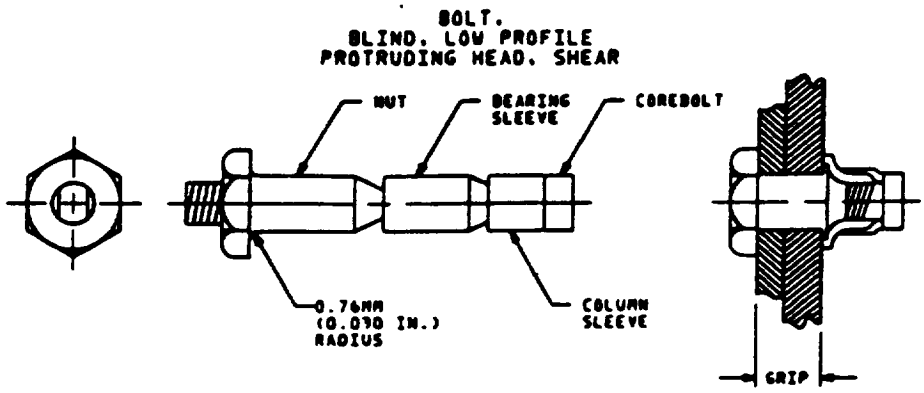

Figure 47. Fastener

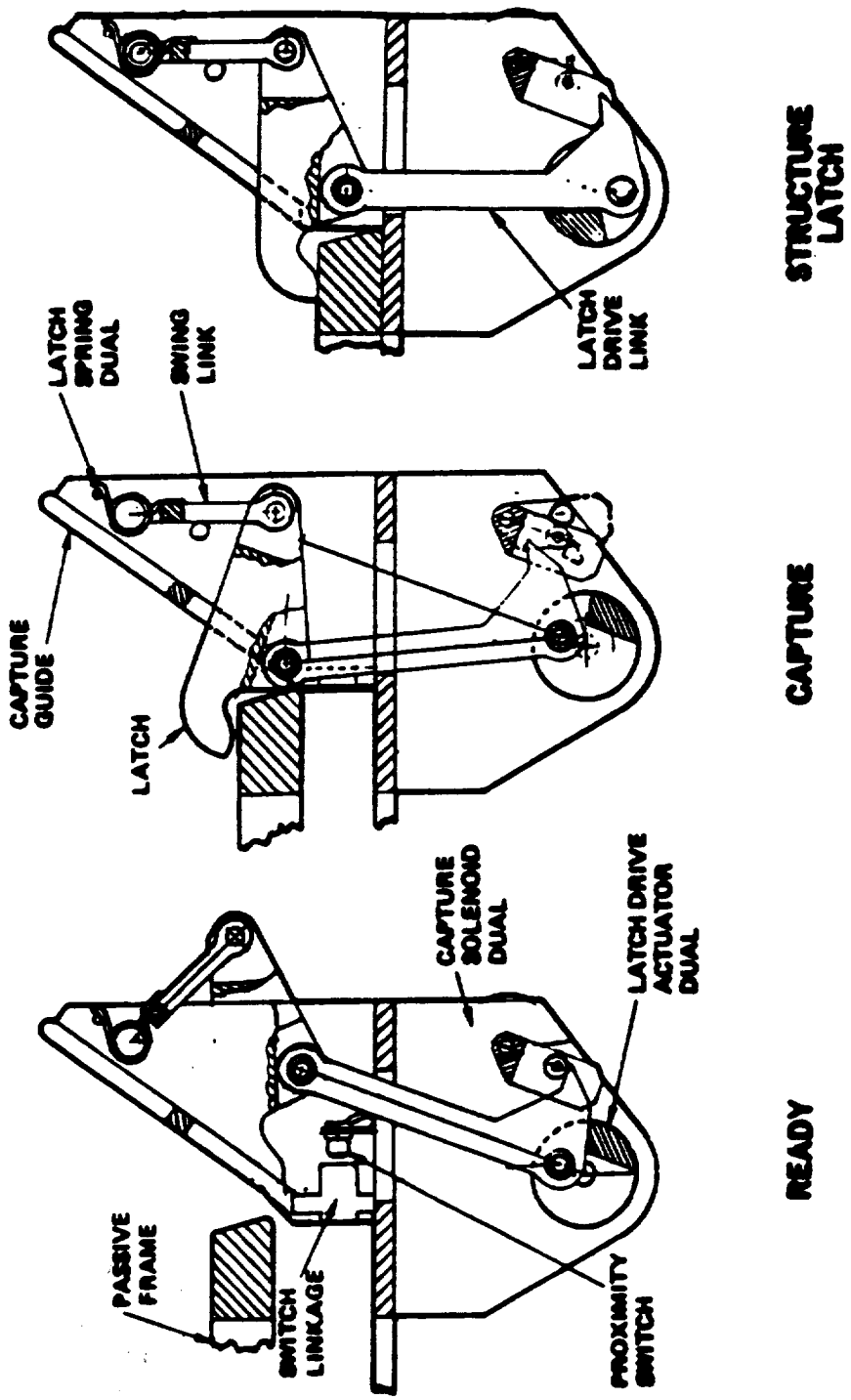

Figure 48. Docking mechanism in three states

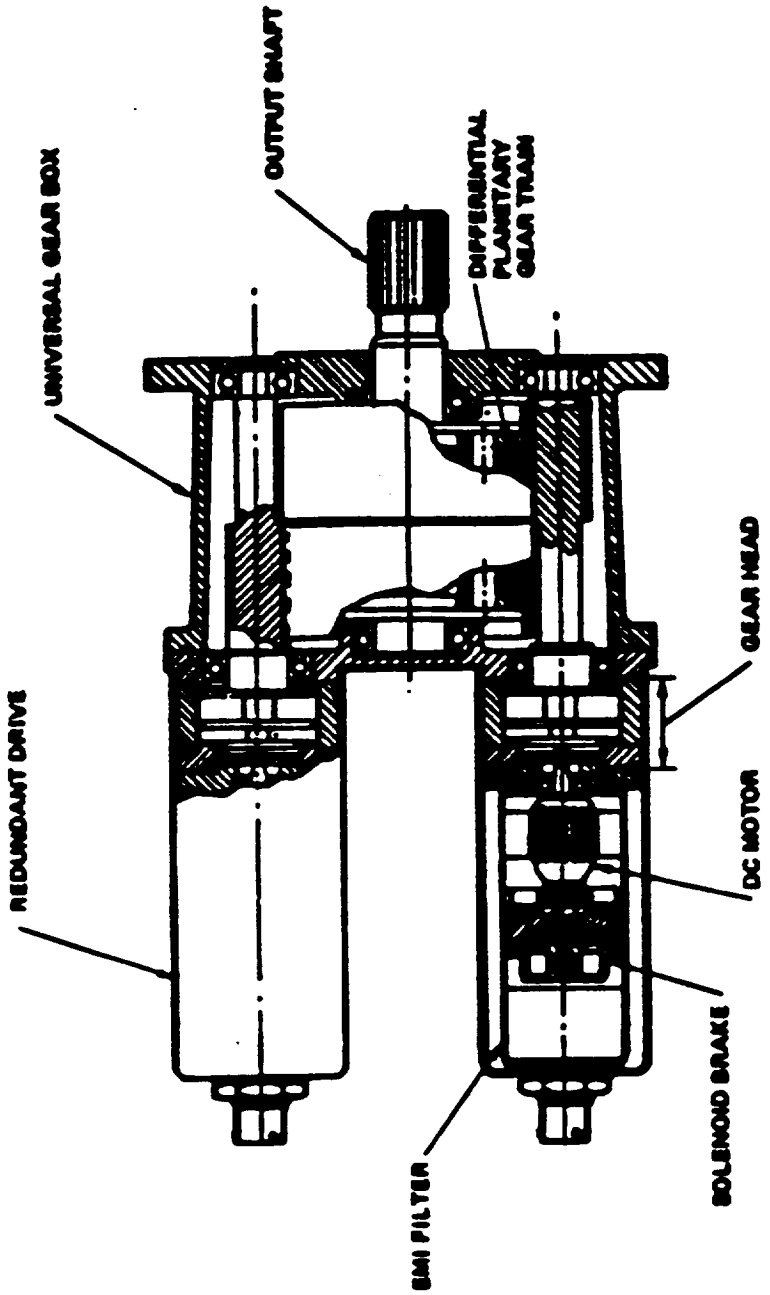

Figure 49. Dual motor rotary actuator

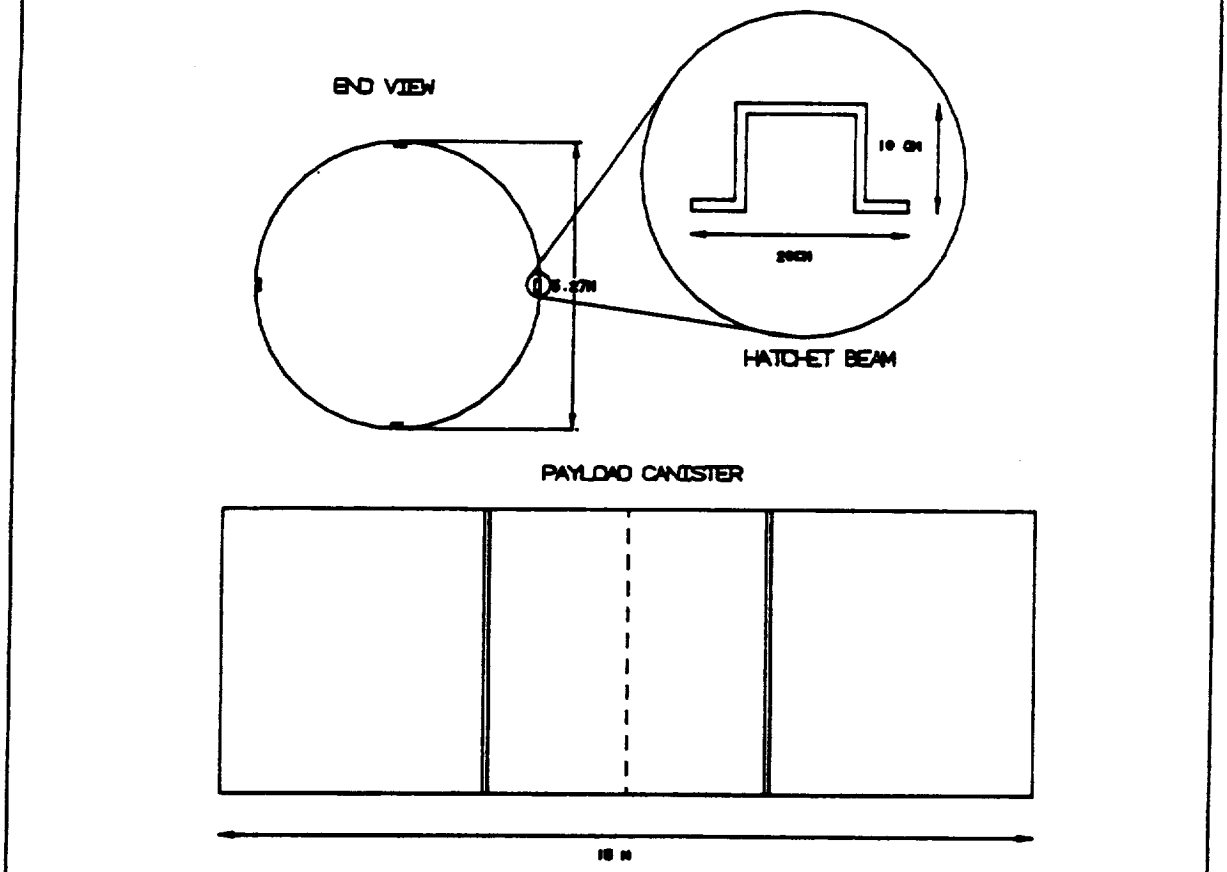

Figure 50. Payload Module

PROPULSION

INTRODUCTION

The concept of a laser powered interorbital transfer vehicle rests on the technology to produce engines that will transfer laser power to the propellant, thus eliminating the need to transport heavy oxidizers. The three methods of converting the laser energy into the thermal energy of the propellant are molecular resonance absorption, particulate absorption process and the inverse Bremsstrahlung (IB) process. Molecular resonance absorption involves seeding the propellant with molecules which undergo transition from their ground state to a higher vibrational energy state by absorbing a photon. This process is very wavelength sensitive, in that only certain chemicals will undergo the appropriate transition for a particular wavelength. The chemicals involved may react with the chamber walls or propellant, and the process has a maximum temperature dependent on the energy state reached (Ref. Boeing).

The particulate absorption process seems to be more favorable than molecular resonance. As its name implies, particles opaque to laser light are introduced into the rocket chamber with the propellant. Since they are opaque, they absorb energy from the light. As the particles heat up, they heat the hydrogen around them eventually forming a plasma. Possible additives include cesium, cesium and water, nitrous oxide and carbon monoxide, and water and carbon monoxide. The carbon monoxide mixtures have been found to be more absorptive at the lower wavelengths such as the one which is of interest to this study ($\lambda = 1.315\mu m$). Particulate absorption has been chosen as a scheme for plasma initiation in the LPIV.

After the plasma is initialized, it will be maintained through the inverse Bremsstrahlung mechanism (and particularly electron-ion IB). The additive is gradually decreased until pure hydrogen is all that remains being injected into the chamber. The IB process works because at very high temperatures, the hydrogen becomes opaque. As the laser beam impinges upon the plasma, the photons transfer their energy through inelastic collisions with the electrons, atoms, molecules and ions of the now opaque hydrogen. This process occurs for any wavelength and has a high temperature limit set only by the laser power (Ref. Boeing). During the process, electrons of the hydrogen are released through the collisions with photons. These electrons then leave the plasma area to impact with the surrounding hydrogen in the chamber, aiding in further heating the hydrogen.

Depending on the optical arrangement, a single plasma or an array of plasmas may be created in the engine chamber. The engines will be of the single plasma type because their small size does not justify the complexity of a multi-plasma system, and most of the present knowledge of the plasma system is on single plasmas. While multi-plasmas may help to increase the heating of the hydrogen, their stability characteristics are obscure. Also considered was the fact that the primary mirror captures the beam off-center, possibly leading to an uneven temperature distribution between the plasmas of a multi- plasma system. This effect is diminished by the use of a single plasma engine. Preliminary research, done on low power argon plasmas has concluded that stable plasmas may be maintained through the use of long focal length lenses as long as the forced convective flow through the chamber is high enough to keep the plasma near the focus. If the flow is not fast enough to accomplish this, the plasma will migrate up the beam away from the focus resulting in an off-axis temperature maximum lower than that which would be achieved were the plasma contained near the focus. Although this upstream movement increases thermal radiation losses from the plasma to the surrounding hydrogen, it lowers power absorption, and decreases the stability of the plasma. Increasing laser power has the similar effect of causing the plasma to move upstream

and, at a point, become unstable (Ref. Keefer). Obviously, very extensive and detailed experiments with a prototype engine will be needed to find an optimum balance of power and flow velocity in order to maintain a stable plasma.

ENGINE DESIGN

Initially, a hybrid system including a chemical rocket for injection from Earth or moon orbit to the earth-moon transfer orbit was planned. The spiral orbit adopted later made this unnecessary due to the fact that the nearly continuous laser engine burn was found to be adequate. The engine parameters have been established on the basis of the assumptions listed in Table 15.

The power of the incoming laser has been assumed to be 15 MW. The power losses through the optical system were assumed as explained in the section discussing the effects of degradation of the reflective surfaces. Previous studies suggest a specific impulse of 1500 seconds as a realistic value with a moderate area ratio of the exit nozzle (Ref. Jeng). It has also been shown that increasing the area ratio beyond 10 does not significantly increase the I_{sp} (Ref. McKay). Thermal conversion efficiency is also based on current literature (Ref. Keefer) and may be conservative for the projected technology level assumed for this project, the year 2020.

Table 15. Basic Data and Assumptions

Power of incoming laser (P)	15 MW
Optical train efficiency H_{opt}	0.948
Thermal conversion efficiency (H_{th})	50%
Specific Impulse (I_{sp})	1500 sec

From the energy equation, the thrust of each laser engine is:

$$T = \frac{(PH_{opt}H_{th})}{(I_{sp}g_e)} = 483.2\,N$$

g_e = acceleration due to gravity at Earth's surface = 9.8 m/sec^2

The propellant mass flow rate is:

$$\dot{m} = \frac{T}{(I_{sp}g_e)} = 0.033\,kg/\,\text{sec}$$

Chamber pressure and bulk temperature have been obtained from approximate 1-D calculations of nonequilibrium flow through a nozzle having an area ratio of 36 and producing a specific impulse of 1500 sec with a thermal efficiency of 50 percent. Initial calculations indicated the values as follows:

chamber temperature, T_o = 4500 K
chamber pressure, P_o = 6.8 atm

Because the absorption of laser energy is strongly dependent on the laser wavelength and gas pressure, it was necessary to examine the absorptivity of the hydrogen plasma at the pressure of 6.8 atm. Based on the studies done on radiant energy absorption (Ref. Caledonie, Pirri), the absorption due to electron-ion and electron-neutral IB was calculated. It was found that by increasing the chamber pressure to 10 atm, the absorption coefficient of 1.315μm can be raised to values ranging from 0.28 cm^{-1} to 0.34 cm^{-1} at temperatures ranging from 17000 K to 20000 K. This will be sufficient to accomplish full absorption in a short distance inside the plasma. To keep the specific impulse of

1500 sec, while the pressure is increased to 10 atm, the chamber pressure should be lowered to about 4400 K.

The size of the laser sustained, hot plasma (> 14000 K) depends on the laser power, flow velocity and chamber pressure. From published data (Ref. Jeng), it has been estimated that at a pressure of 10 atm and a velocity of 20 m/s, the laser intensity required for sustaining a plasma will be around 3.2 x 10^5 W/cm^2. The corresponding diameter of the highly absorbing plasma will be about 5 cm. The maximum diameter of the chamber and the throat diameter have been established from calculations based on high temperature hydrogen data reported by Patch. The main engine parameters are summarized in Table 16.

Table 16. Engine Characteristics

Laser power entering each engine	7.11 MW
Thrust	483 N
Propellant mass flow rate	0.033 kg/sec
Nozzle inlet stagnation temp	4400 K
Chamber pressure	10 atm
Average chamber flow velocity	20 m/sec
Chamber diameter (max)	30 cm
Throat diameter	2 cm
Nozzle area ratio	36

A schematic of the proposed engine is shown in Figure 51. The engine configuration has been selected from evaluation of various options, which differed primarily in optical arrangement for the laser beam entry. A rear entry has been chosen over a side one because it eliminates possible impacting on the opposite wall which may cause a serious wall overheating problem. An initial configuration using a focusing lens as a window to the engine was rejected in favor of an arrangement consisting of a parabolic focusing mirror (tertiary mirror) and a flat window. Such arrangement results in longer focal lengths (which tend to improve plasma stability) and allows more flexibility in focusing ability (by using adaptive optics for the tertiary mirror). Also, the size of the window can be somewhat reduced. A possible candidate for the window material is sapphire, recommended by its high strength and high transmissivity (> 99%).

COOLING

Since the high temperature plasma leads to an intense, mostly radiative heat transfer to the chamber walls, regenerative cooling combined with possibly high reflectivity of the internal chamber surface will be necessary to preserve the integrity of the chamber walls. The hydrogen propellant will be used as the coolant medium. About 20% of the hydrogen delivered to the engine will be injected directly to cool the window (Figure 52). The rest (80%) will be passed through four helical coils to cool the chamber and nozzle walls. The now gaseous propellant is then injected into the engine chamber through rings stationed at various locations along the flowfield (Figure 53). The wall temperature on the gas side is limited by the material properties. Tungsten, considered for this design due to its relatively high ultimate strength at high temperatures and its good heat transfer properties, was assumed to have an upper operational temperature of about 2800 K. Preliminary calculations of the regenerative cooling system have been carried out with the following assumptions:

Temperature of hydrogen entering cooling system = 407 K
Maximum temperature of the hydrogen entering the chamber = 2300 K
Maximum temperature of the chamber internal wall = 2800 K
Pressure at entrance to cooling system = 20 atm
Pressure at injectors to engine chamber = 12.5 atm

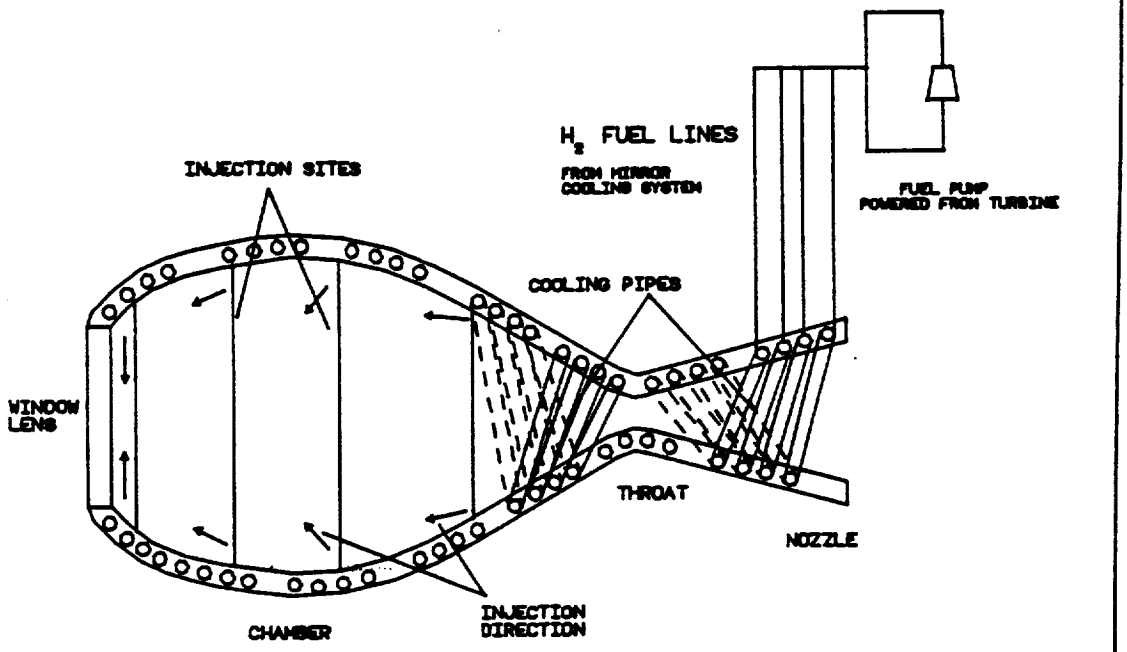

Figure 51. Engine Cross Section

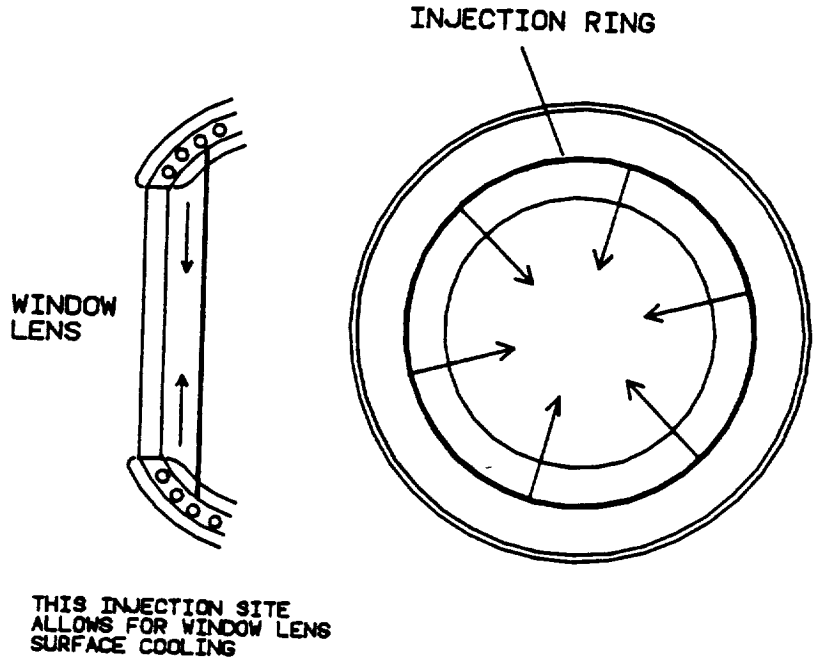

Figure 52. Hydrogen Injection Schematic-Front View

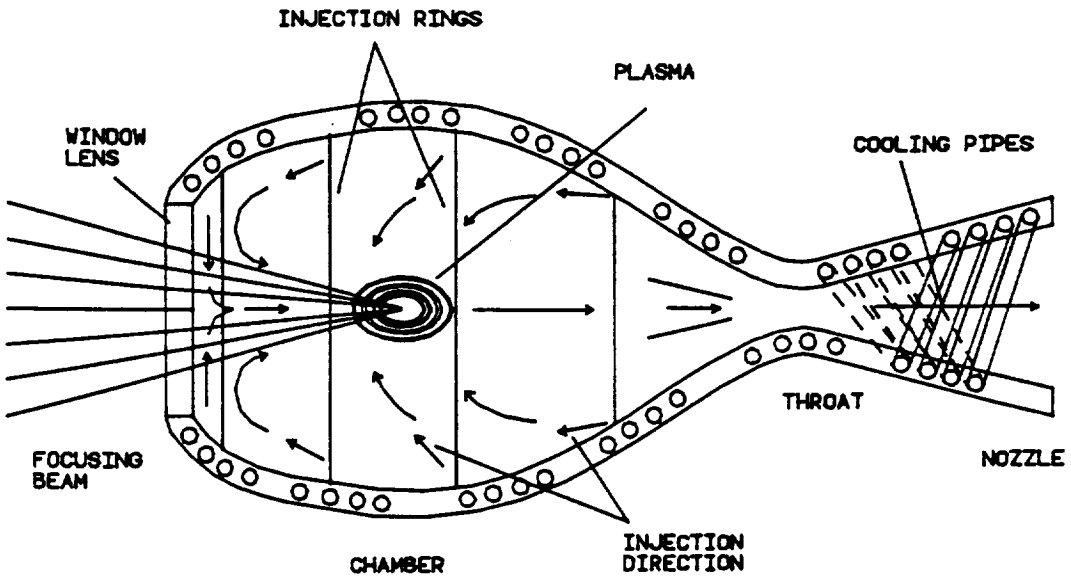

Figure 53. Hydrogen Injection Schematic-Side View

The results have indicated the following parameters for a four helical cooling pipe system.

Length of each helical tubing = 7.5 m
Diameter of tubing = 15 mm

TURNTABLE

One of the requirements for the LPIV is an ability to rotate the engines through 360 degrees. In order to achieve this goal, a turntable is needed at both ends of the main truss to rotate the engines independently from the rest of the ship. In the preliminary design, two types of turntables were considered. The first type utilized a single, centrally located motor assembly which rotated both engines through the use of a rod and gear assembly. This option was discarded due to the problems associated with a telescoping main truss, as prescribed in the aeroassisted version of the LPIV.

The second turntable configuration considered uses two electrical motors to individually rotate each engine. Each engine assembly is connected to a 3 m diameter gear ring, which is attached to the main truss by four graphite epoxy members. The incoming laser beam passes through a hole in the center of the ring, where it is reflected off a tertiary mirror and into the engine chamber. Fuel lines to each engine are flexible, allowing the expansion and contraction necessary as the fuel tanks move along the tracks. The turntable assembly, consisting of the bearing plate, gear ring, supports, and beams are all made of graphite epoxy P75S/934, resulting in a mass of 547 kg and requiring 3.14 W to operate. Both the turntable and engine assembly are shown collectively in Figure 54, and isometrically in Figure 55. The torque and power required to operate the turntable was calculated from the thrust force (483 N), bearing friction and the maximum angular velocity, derived from orbital calculations.

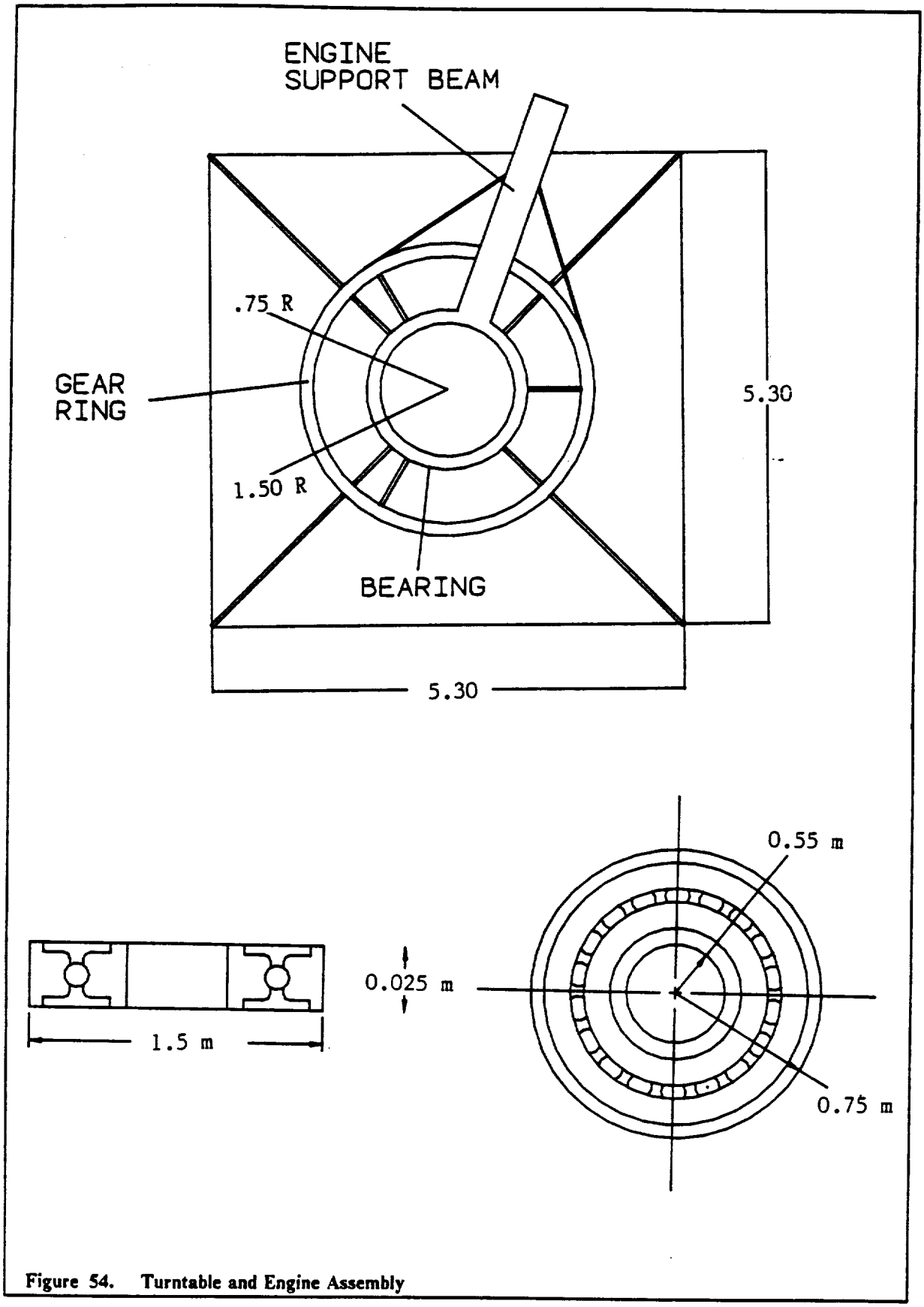

Figure 54. Turntable and Engine Assembly

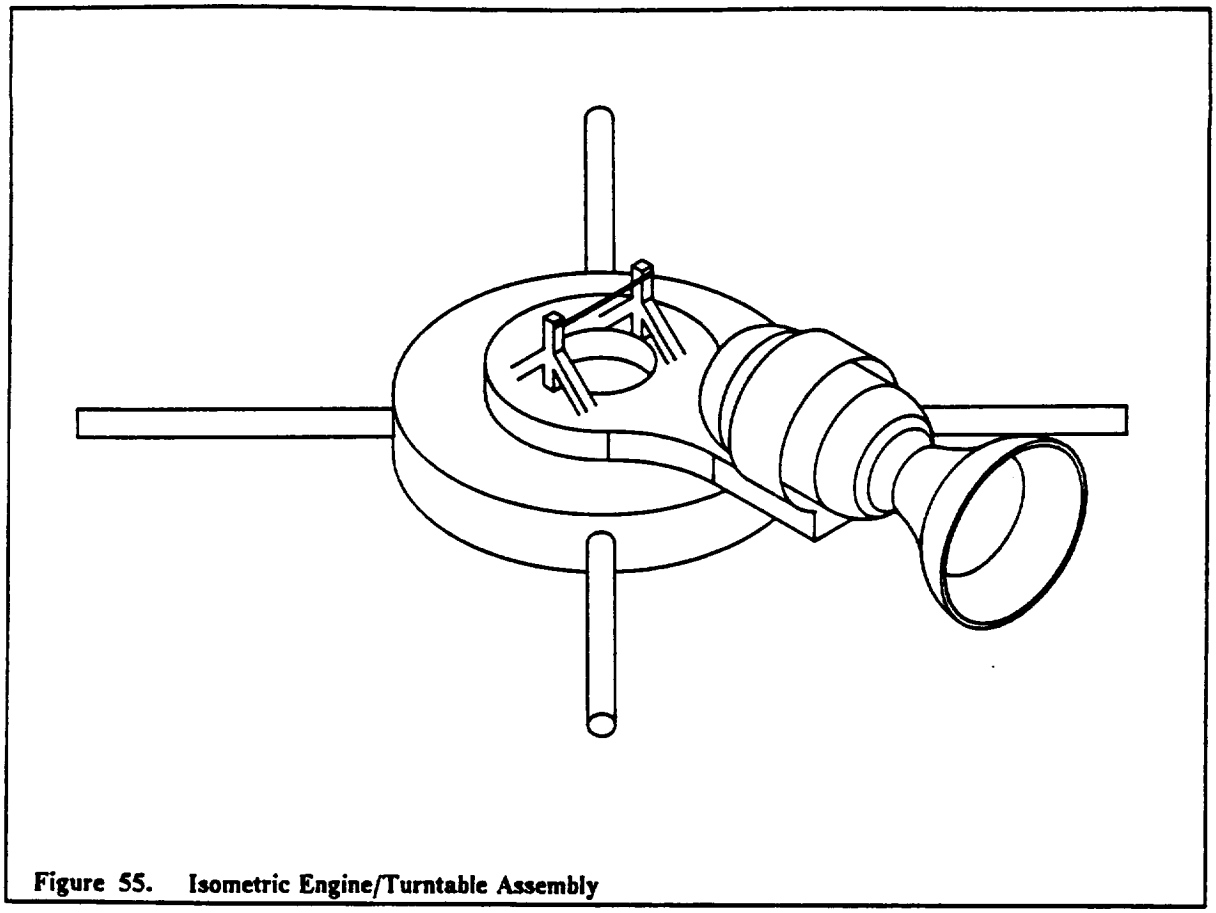

Figure 55. Isometric Engine/Turntable Assembly

Since the turntable must rotate the engine independently from the rest of the ship, it is coupled to the reaction control system operated by a computer to keep the engine oriented correctly. When the engine needs to be turned, the motor will activate and rotate the bearing which, in turn, will rotate the engine to its new position. As the engine turns, the flexible hose, connected from the fuel tank to the engine, will be either extended or contracted depending on the position of the engine by the spring device.

The studies done on this type of propulsion techniques indicate a strong possibility of usage in the near future. Advances in the areas of materials, heat transfer, and plasma studies will no doubt enhance the advantages of this efficient and economical mode of transportation, especially for the steady use of such space vehicles as the LPIV.

REACTION CONTROL SYSTEM

INTRODUCTION

For a vehicle such as the LPIV, attitude control is crucial because of the necessity of maintaining continuous contact with the laser power system. The reaction control system (RCS) provides the LPIV with attitude control and translational mobility. It is required that the RCS provide attitude control during burns of the main engines without generating plumes which might interfere with the optical train. To achieve this, control moment gyros (CMG's) are used to rotate the LPIV's main mirror into alignment with the power satellite to receive the laser beam. For those periods when attitude adjustment is needed and the main engines are not firing, small attitude control rockets are fired to generate the necessary torques. Larger rockets are used to adjust for orbital errors and to provide mobility when docking.

DETERMINATION OF ORBITAL PARAMETERS

Since the LPIV has two planes of symmetry, only rotations about two body axes are required to achieve any desired orientation in receiving the power beam. These axes are depicted in Figure 56. A rotation about the x axis is a roll, while a rotation about the z axis is a yaw. This symmetry is utilized to reduce the number of gyros necessary to provide three-dimensional control of attitude from three to two.

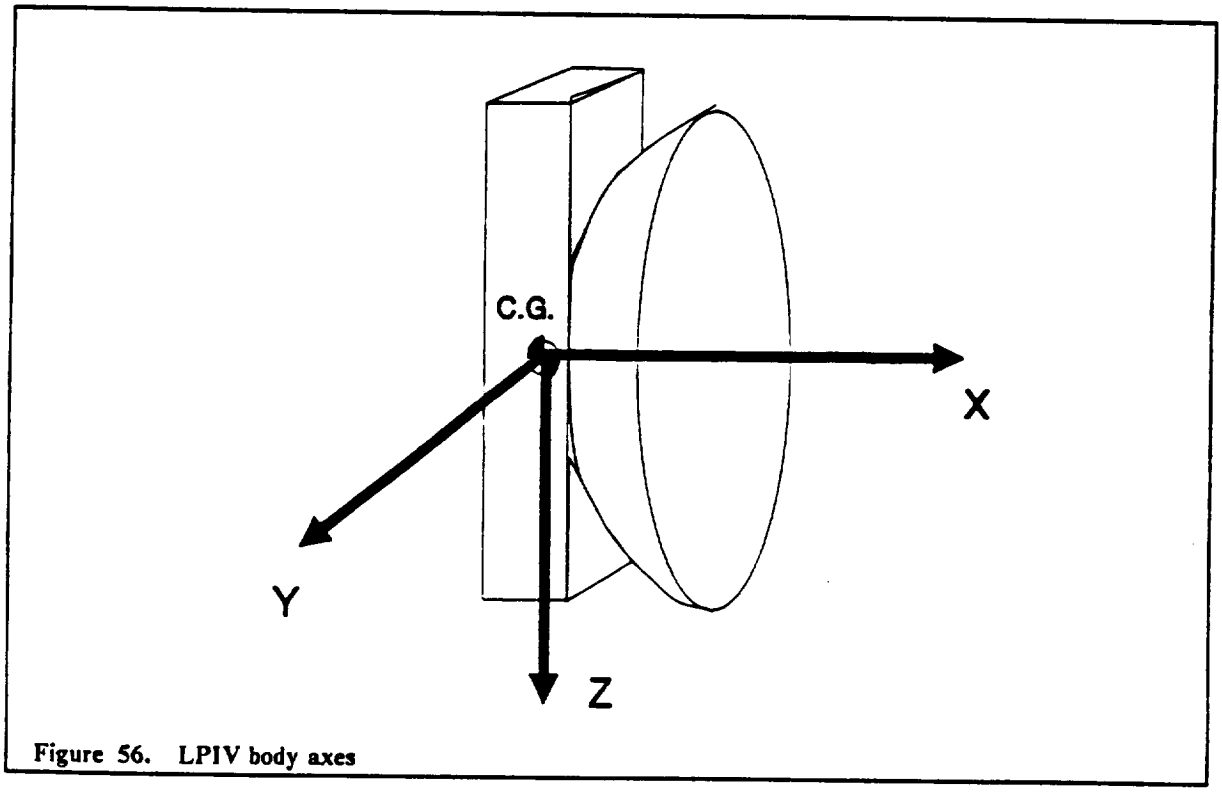

Figure 56. LPIV body axes

Using the global radius vectors of the LPIV and the laser power station (LPS), it is possible to determine the pitch and yaw angles the LPIV has to assume in order to track the LPS. The roll angle is defined as being the inclination of a plane orthogonal to the LPIV's body axis relative to the global xy plane. The yaw angle is simply the anomaly of the power satellite defined in this inclined plane, centered at the LPIV. A graphical depiction of these features is found in Figure 57.

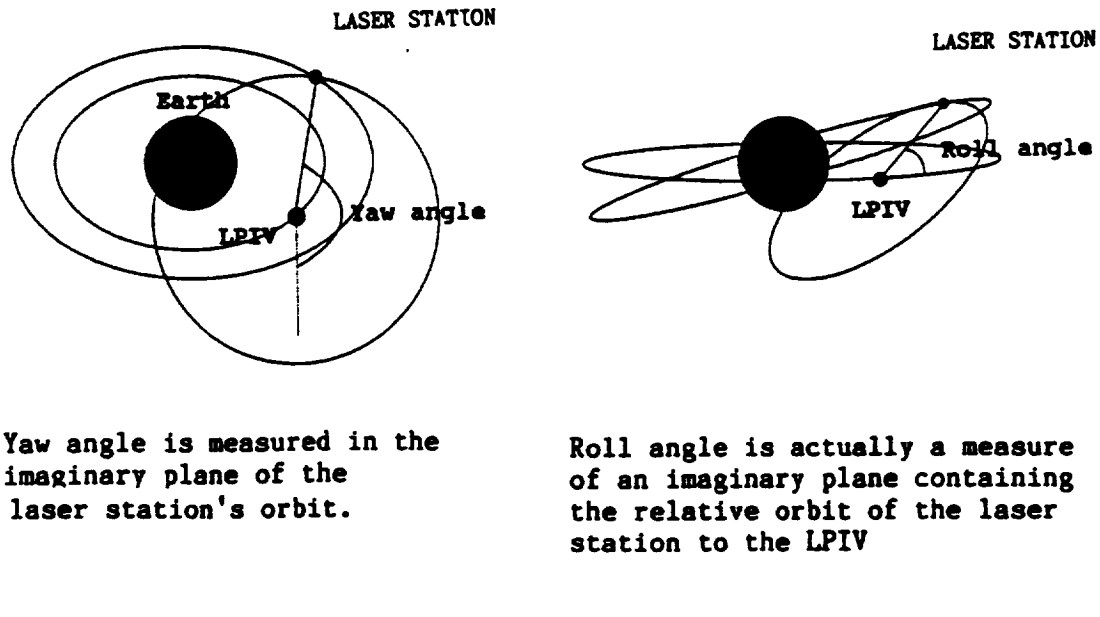

Figure 57. Graphic depiction of yaw and roll angles

Using these angles and the time steps between them, it is possible to calculate the angular accelerations about the roll and yaw axes necessary to achieve the orientation of the next time step. This is done as follows:

$$roll_2 = roll_1 + \omega_{roll}\Delta t + 0.5\alpha_{roll}\Delta t^2$$

Therefore,

$$\alpha_{roll} = 2(roll_2 - roll_1 - \omega_{roll}\Delta t)/\Delta t$$

$$\omega_{roll2} = \omega_{roll} + \alpha_{roll}\Delta t$$

Using these formulae, the angular accelerations needed by the LPIV are known. By multiplying these accelerations by the moment of inertia of the LPIV about the corresponding axis, a required torque is computed which will orient the LPIV as it needs to be. CMG's are the components needed to accomplish this process.

CONTROL MOMENT GYROS

The task of generating the torques necessary for the angular accelerations is performed by the control moment gyros (CMG's). In space, with nothing to work against, a torque cannot be directly applied to the LPIV using a device such as an electric motor. What is needed is some form of 'torque lever' which translates a torque about one axis into an equal torque about another. This

is exactly what a CMG does. An electric motor applies a torque about an axis perpendicular to the spin axis. The momentum of the gyroscope determines at what rate it rotates about that axis (Ref. Nutates). As the gyroscope rotates, it also precesses, that is, it rotates about its other axis which is perpendicular to the spin axis (Ref. Roberson). This concept is illustrated simply in Figure 58. To be used in a spacecraft, the gyroscope should be fixed rigidly to the ship in the direction of precession, so that the whole ship precesses with it. The precession rate is dictated by the applied torque and the moment of inertia of the ship, not just the gyroscope.

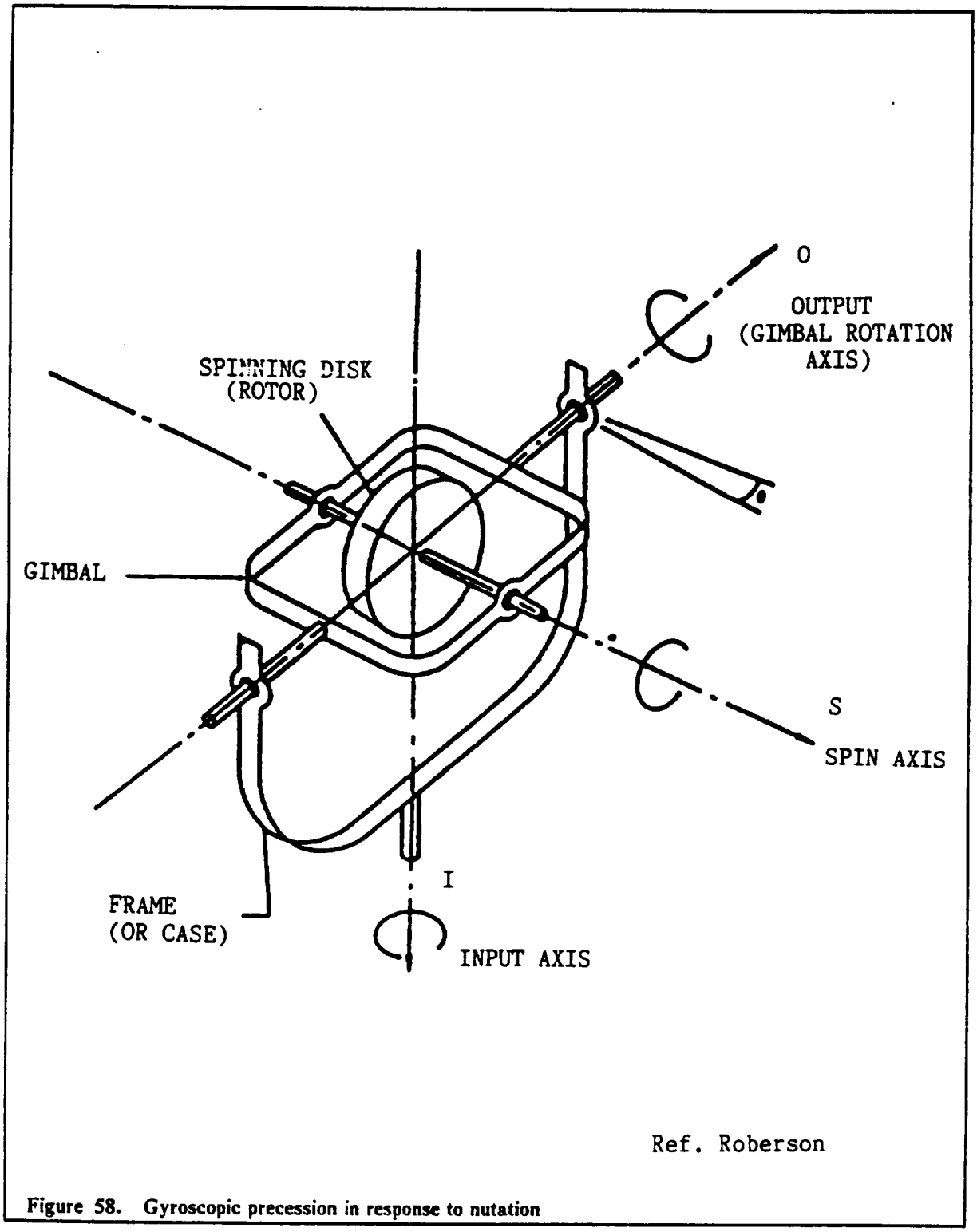

Figure 58. Gyroscopic precession in response to nutation

Should the gyroscope precess a full ninety degrees in either direction, its momentum vector is now parallel to the rotation vector. If this occurs, no amount of rotation will produce a torque. The gyroscope is said to be saturated. The only remedy for saturated gyroscopes is to apply an outside torque before the gyroscopes become saturated. By working the gyros against this torque, it is possible to recover all precessions and set the gyro to zero precession. For this reason, a desaturization rocket system is implemented to complement the CMG's.

Configuration

Two gyros are placed within the boom near the C.G. These are aligned with their momentum vectors perpendicular to the xy and xz planes so that they can provide torques about the roll and yaw axes. The location and orientation of these gyros may be seen in Figure 59.

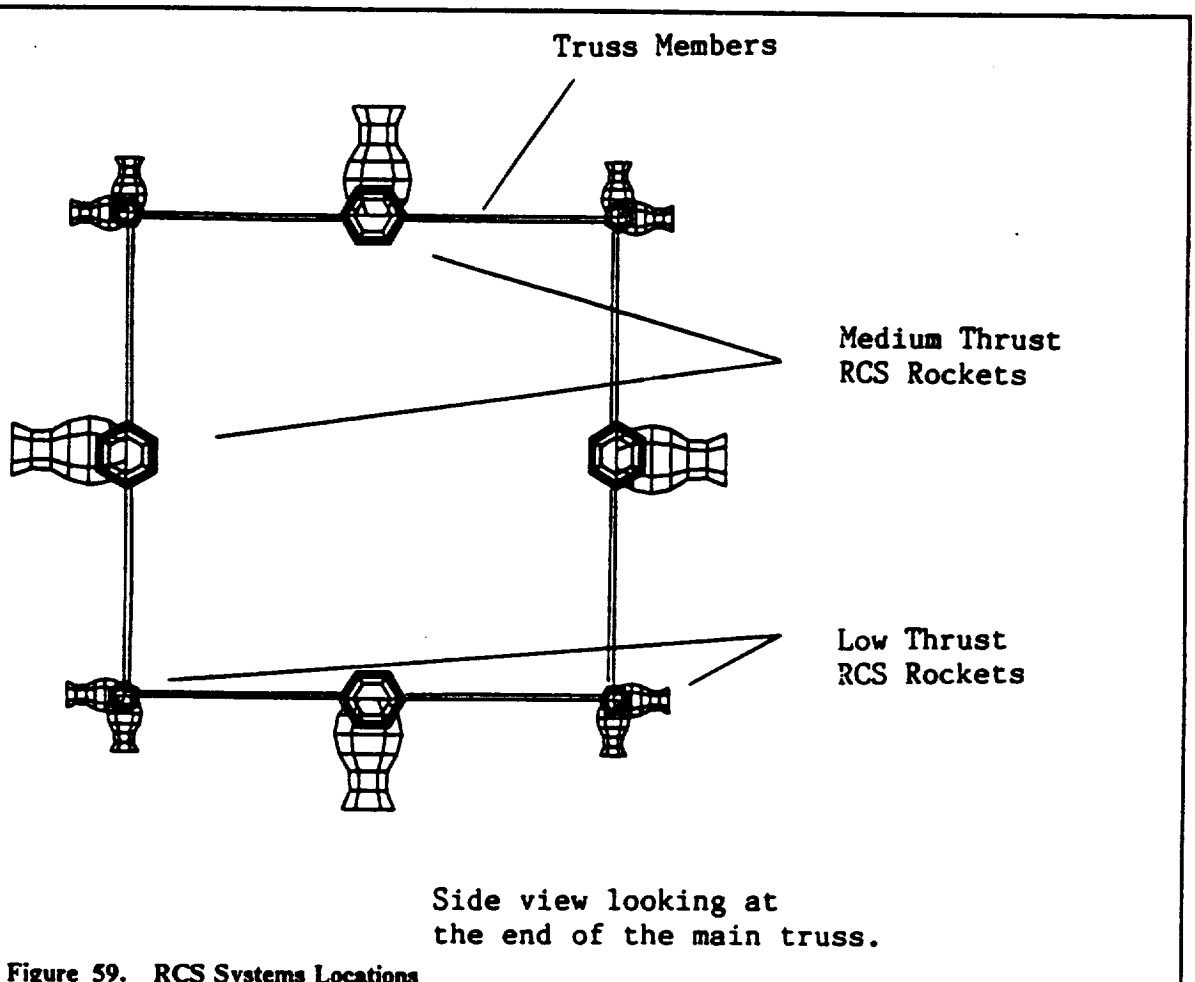

Figure 59. RCS Systems Locations

Precession and torque calculations

By precessing the gyros, the whole ship is rotated to align the primary mirror with the beam from the laser power station. The precession angles needed throughout the orbit are determined directly from orbital data obtained in the computer simulation. Since the gyros directly maneuver the LPIV to the desired angle, knowing the angle makes it possible to determine the precession angles trigonometrically. The only variation to a straight trig solution lies in the fact that an angular spin rate is generated with each acceleration used to obtain the precession angle. Graphical representations of the precession angle as a function of time about both the roll and yaw axes are in Figure 60. The zig-zag nature is a result of computing the accelerations only once every 120 seconds.

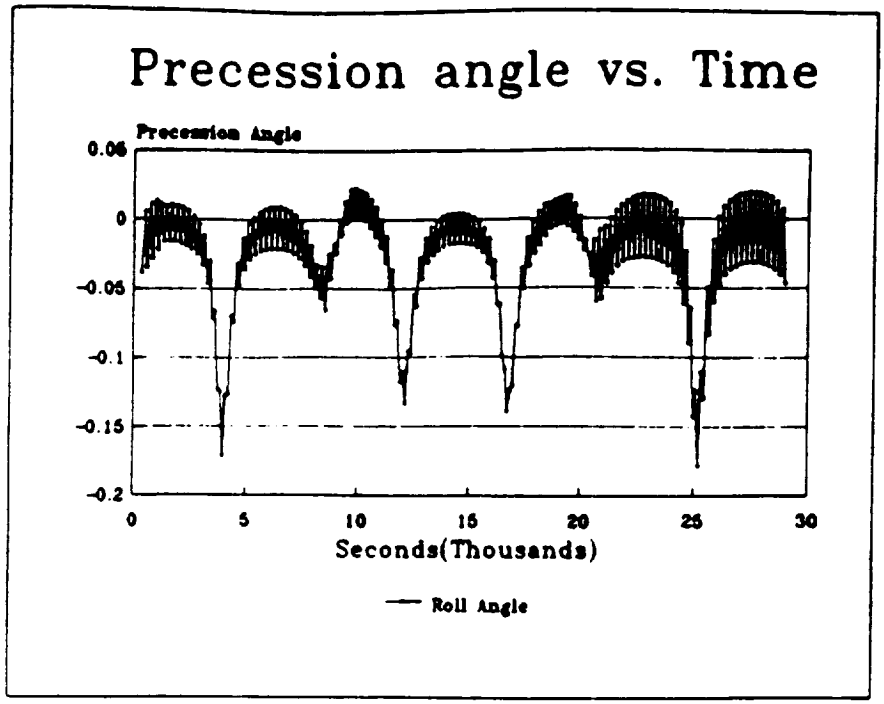

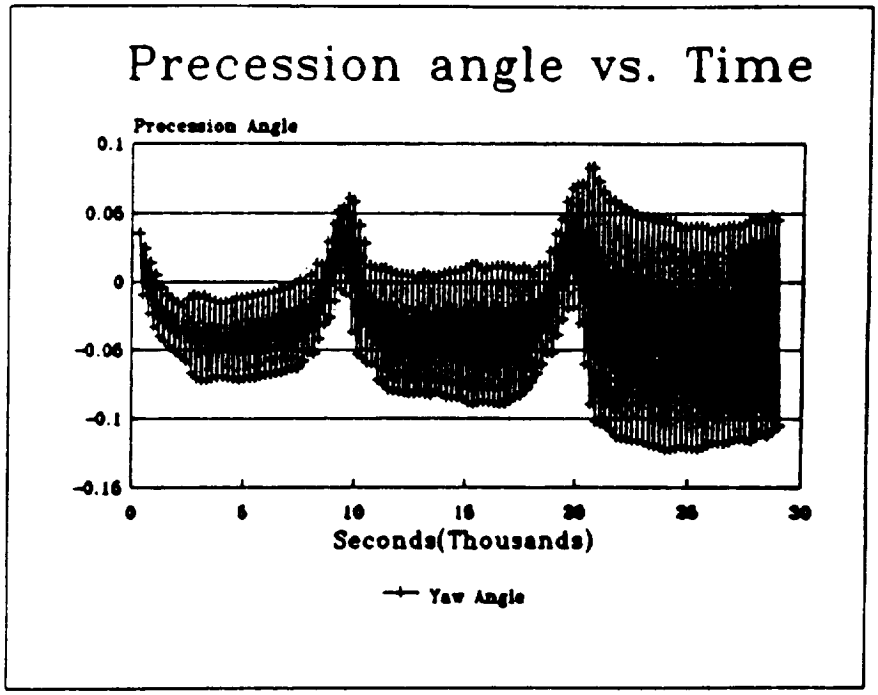

Figure 60. Precession angles as a function of time.

The torques necessary to generate the precessions of each time step are determined by multiplying that axis' moment of inertia by the acceleration required to achieve the desired final angle. Values for the moments of inertia of the craft are given in Table 17.

Table 17. Moments of Inertia

	Non-Aerobraked	Aerobraked
Ix =	1.689×10^6kg-m^2	1.921×10^6kg-m^2
Iy =	1.309×10^6kg-m^2	1.507×10^6kg-m^2
Iz =	1.450×10^6kg-m^2	1.648×10^6kg-m^2

Table 18. Maximum Precession Angle of Gyros

	Precession	Angular rate
Roll	0.22323 rad	-0.00372 rad/ sec^2
Yaw	0.11649 rad	-0.00194 rad/ sec^2

Table 19. CMG Specifications

Angular momentum	305 N-m-sec
Output Torque	305 N-m-sec
Mass	52.2 kg
Size -	
Length	0.89 m
Width	0.57 m
Height	0.24 m
Power -	
Standby	15 W
Quiescent	50 W
Torquing (peak)	250 W

Selection of gyros

The type of gyro selected for the CMG's must be able to output the maximum torque required by the precession accelerations while minimizing power consumption. The mass of the gyro should be kept low, and it should be capable of unlimited rotation.

The maximum precession angles and their associated angular rates are listed in Table 18. The maximum torques specify what torque the selection gyroscope must be capable of delivering. The maximum precession angles are used to determine the greatest possible desaturization that may have to be performed by the desaturization rockets.

The gyro selected for the LPIV is similar to the Sperry M225 (Ref. Sperry). Data for power consumption, weight, etc. are found in Table 19. These specifications differ from those issued for a Sperry M225 in two regards. It is felt that by the time predicted for this vehicle's construction, the same torque levels and momentums will be possible with at least a ten percent reduction in mass and size, without increasing the power requirement. These predictions are responsible for the differences between published data and those in Table 19.

DESATURIZATION ROCKET SYSTEM

Low thrust rockets are used to desaturate the CMG's whenever the LPS is in the Earth's shadow and therefore unable to provide power to the LPIV. The LPS is in the Earth's shadow for forty minutes once during each of its orbits around the Earth. During this time, the desaturization rockets will be fired to generate a torque equal in magnitude and opposite in sign to that necessary to reverse the precession of the CMG's.

Determination of thrust requirements

Knowing that the shadow time for the power satellite is 840 seconds the angular acceleration and the torque required to desaturate the gyro within that time period is computed from:

$$\alpha = 2 \times \phi - \omega \times dt^2$$

$$T = I \times \alpha$$

The propellant chosen for the desaturation rockets is hydrazine, mainly because of its high specific impulse (230 seconds) in comparison to other gaseous monopropellants. A monopropellant is preferred because of its simplicity and high reliability. Hydrazine will be used for attitude control in the space station which the LPIV services. A diagram of a probable attitude nozzle configuration is given in Figure 61 (Ref. Sutton).

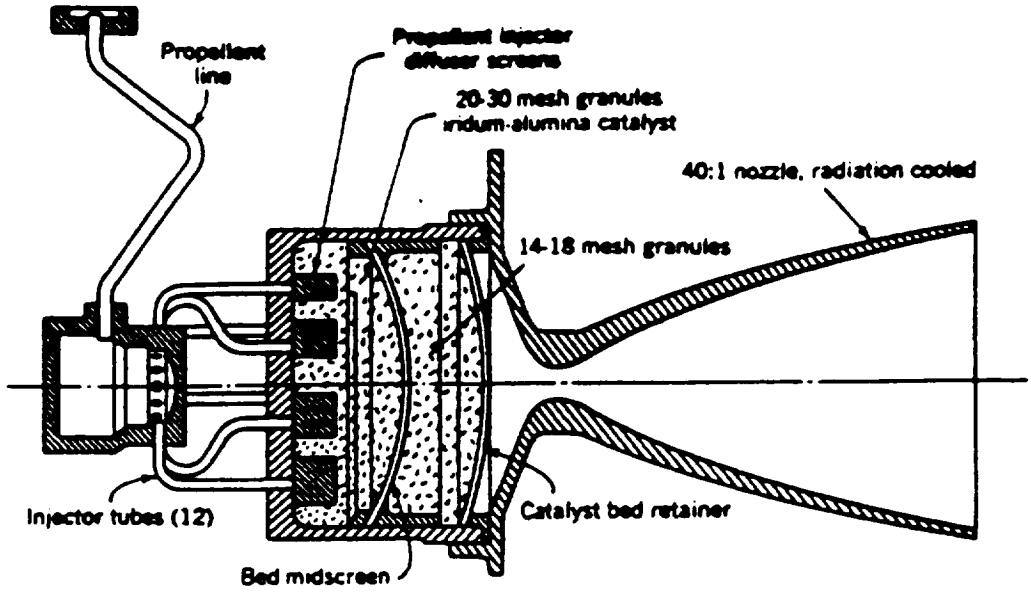

Figure 61. Typical attitude control rocket utilizing hydrazine

Because of their reduced moment arm, a higher level of thrust is required for the yaw rockets to perform the same precession as the roll rockets. Rather than have two separate rocket systems for yaw and roll, the roll burn will be shorter. Thrust levels, mass flow rates, and fuel consumption per desaturization for the desaturization rockets are summarized in Table 20.

Table 20. **Desaturization Rocket Characteristics**

Thrust per rocket	5 N
Specific Impulse	230 sec
Mass flow per rocket(roll)	$2.2x10^{-3}$ kg/sec
Mass flow per rocket(yaw)	$2.2x10^{-3}$ kg/sec
No. of rockets (roll)	4
No. of rockets (yaw)	4
Time of burn (roll)	71.18 sec
Time of burn (yaw)	104.3 sec
Total propellant mass / desaturization	1.45 kg

Configuration

Since the desaturization rockets also provide fine translational control during docking, it is required that they be capable of delivering thrust along all three axes. To achieve this, clusters of rockets are attached to each of the four corners at either end of the main truss. In this manner, four rockets may be fired in any direction to translate the LPIV. The compressed hydrazine is stored in fuel tanks attached to each pod (Figure 59).

Total fuel mass needed is determined by the number of desaturizations to be performed and the amount of maneuvering necessary for docking. During the thrusting period for escape from the Earth's gravitational pull, there are over 50 shadow periods within which it is possible to desaturate the CMG's. Of these, it is considered reasonable that no more than three periods will actually be used to desaturate.

Because of the low thrust levels of the desaturization rockets, they are useful for only the finest control in docking. Using a twenty second burn of all four engines parallel to an axis, and assuming an approximate mass of 40000 kg at lunar capture, the desaturization rockets only provide a velocity change of 0.01 meters/second. This, however, is the type of maneuverability desired for fine control in docking.

MEDIUM-THRUST RCS SYSTEM

For purposes of orbit correction, in particular when the LPIV is docking and when it is preparing to perform the aerobrake maneuver, it is desired to have a rocket system of much higher thrust levels than the desaturization rockets. These rockets exhibit thrust levels approaching that of the LPIV's main engines, since they are to be used as backup engines should the laser fail.

Configuration

Pairs of nozzles are affixed to the truss at its midpoint for each of the four sides on each end of the truss. One nozzle points upward while another is aimed outward from the truss to which it is attached. The rockets most crucial in the event of an emergency during aerobraking will be the two pointing in the negative x direction, towards the aeroshell. These rockets, as well as the other primary RCS rockets are used for translational mobility as well to correct orbital errors, mainly when docking.

Thrust Sizing Determination

Besides providing docking mobility, the RCS system is used as a backup propulsion system for the post-aerobraking maneuver. After the aerobrake assists the LPIV in being "captured" by the Earth,

the LPIV's orbit is circularized back into low-Earth orbit. Normally, this is performed by the laser engines. In the event that the laser engines should fail, however, it is up to the RCS system to apply enough impulse to prevent the LPIV from re-entering the Earth's atmosphere. A diagram of what the RCS should provide for can be found in Figure 62.

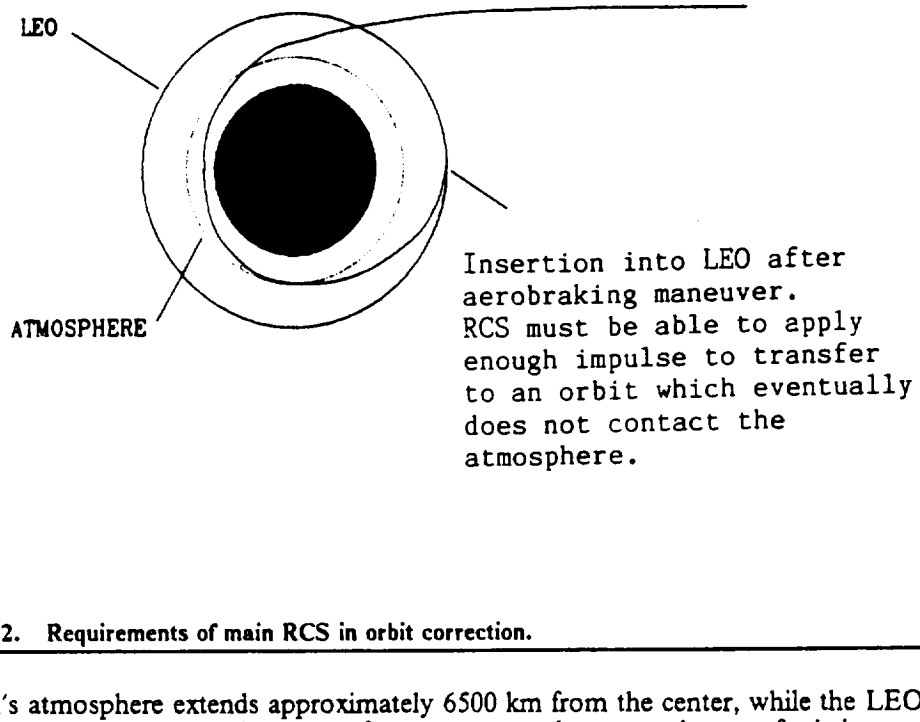

Figure 62. Requirements of main RCS in orbit correction.

The Earth's atmosphere extends approximately 6500 km from the center, while the LEO orbit lies 6750 km from the center. In the event of an emergency, however, the transfer is into an orbit for which perigee lies just at 6500 km, barely avoiding the effects of atmospheric drag. The velocity change needed to execute this emergency maneuver is 90 m/sec, which is what must be delivered by the primary RCS within 2600 seconds.

Another sizing constraint is that the thrust of the RCS rockets should not be much greater than that of the laser engines, since the truss structure is designed for a total force of 2000 N. There is a factor of safety associated with this limitation, so it is reasonable to increase the thrust slightly, particularly for a system that is not expected to be used frequently, if ever.

Fuel Selection and Rocket Properties

The main rocket of the RCS system is a bipropellant, using hydrogen as fuel and oxygen as the oxidizer. Hydrogen is used mainly because of its availability in the LPIV and because the main rocket and the laser engines will never be fired simultaneously. A tank containing the required oxygen for the RCS rockets is located in the center of the truss, near the CMG's.

To be effective, the RCS is capable of executing the orbital change within only one half of the period of the orbit which results from the aerobraking maneuver, even though contact with the atmosphere won't occur for another fourth of the period. This is done as a sort of time-based factor of safety to ensure that the RCS is able to complete the maneuver before the atmosphere is contacted again. Data for the specific impulse and mixture ratio of propellants were obtained from

Sutton's reference. Using known specific impulse and the velocity change requirements, the required mass flow is determined. The fuel mass required is obtained by multiplying the mass flow by the time of the burn. Table 21 lists data for the primary RCS rockets.

Table 21. Main RCS Rocket Characteristics

Fuel	Hydrogen
Oxidizer	Oxygen
Specific gravity	0.26 g/cm^3
Chamber temperature	2400 K
Effective exit velocity	2428 m/sec
Specific Impulse	388 sec
Thrust level required	1350 N
Delta Velocity required	90.0 m/sec
Mass flow rate	0.3647 kg/sec
Total mass to correct	970.0 kg

Knowing the properties of the rocket's fuel and the velocity change it must be capable of delivering, mass flow and thrust levels are easily computed.

Docking maneuverability of the RCS system.

Since the primary RCS rockets have a total thrust of 1350 N in any direction, they are much more capable when it comes to providing docking maneuverability. Using the same burn as was evaluated for the fine rockets as a comparison (20 seconds), it is possible to induce a change in velocity of up to 0.67 m/s in any direction. This is a significant amount and is useful for correcting orbit injection errors.

PROPELLANT TANK AND SUPPORT SYSTEM

INTRODUCTION

The LPIV has two cryogenic tanks containing a total of 35000 kg of liquid hydrogen propellant. Design of the cryogenic propellant tanks focuses primarily on minimizing the mass of the tanks and their support structures while providing adequate insulation to minimize boiloff. Since the mass of the propellant takes up a large amount of the total vehicle mass as a whole, the tanks must be moved strategically so that the center of mass of the LPIV will remain at the same location (midpoint between the turntable centers) as the propellant is depleted. This is done by placing the tanks on tracks that move the tanks along the secondary truss. Due to the translation of the tanks with respect to the entire LPIV, a fuel line system using flexible fuel hoses must be devised in conjunction with cryopumps to deliver propellant to the engines. Considerations must be given to the harsh environment of space, specifically the cyclic temperature fluctuations. Thermal effects and launch loads must be dealt with by proper material selection and structure design.

Propellant Tanks

The initial task of the propellant tanks design was to decide on the shape and size of the tanks. Due to the symmetry of the LPIV, it was required that the propellant be divided into at least two tanks. Three possible combinations of tanks were devised and analyzed using a combination of spherical tanks and cylindrical tanks with spherical caps. Each combination must contain a total of 495 m^3 which is the volume required for 35000 kg of liquid hydrogen. The results were as follows:

Table 22. Comparison of Possible Tanks Configurations

	Total Surface Area (m^2)	Dimensions (m)
2 cylindrical tanks w/ spherical caps	352.8	5.0 diam 14.25 length
2 spherical tanks	380.0	7.8 diam
4 spherical tanks	479.9	6.1 diam

The selection was narrowed down to two choices of either the two cylindrical or two spherical tanks because of the savings in mass (i.e. least total surface area). The cylindrical tanks had the advantage of fitting within a 5m by 5m truss used for the LPIV main structure but difficulty arose in creating the support structure and implementing these tanks onto a track system. To do so would require the truss to be lengthened to support the cylindrical tanks and thus would have added more mass. Moreover, the center of mass of the tanks would be difficult to determine because of fuel sloshing over the length of the cylindrical tanks and creating considerable instability in the LPIV. This is the major reason for not using the cylindrical tanks because for the LPIV to work, exact determination of the center of mass is required. The solution was to use two spherical tanks because

spherical tanks would reduce sloshing by nature and minimize shifting of the center of mass because of the shorter length dimension.

Track System Selection

Initially, a gear track system and chain drive system were being considered. It must be noted that the track would have to support a tank having a mass of 20000 kg .The gear track system was designed using two tracks containing gear teeth which extend along the secondary truss. The tank would be moved along the tracks by means of motorized gear wheels mounted on the tank platform. This gear track system was eliminated because too much stress would be exerted on the gear teeth during acceleration. A chain driven system appeared to be a possibility but the design seemed prone to failure because of the length of the chain that would be required. As a result, a rotary to linear motion track had to be designed. The screw track and actuator was adapted for the LPIV and it seemed to be the most suitable for this purpose.

TANK MATERIAL

The LPIV tanks will be fabricated from a new low-density aluminum-lithium alloy, 2090 series (or its future derivative) developed by Alcoa (Ref. Torre). This material has proven in tests to be better than the more well known 2219 aluminum currently being used. The technique of forming the tank is by spin forming a disc into a one-piece hemisphere. Two hemispheres will then be joined by a major weld at the dome halves to create the spherical tanks. The interior is designed such that it will support slosh baffles in order to minimize sloshing loads. All support structures will be built, tank assembled, and the insulation applied as a complete process because the tank is an integrated structure. The tanks and their assembly must be manufactured on the ground because of the manufacturing complexity. The whole assembly is then carried to orbit by a second generation shuttle requiring a larger payload area than the present shuttle.

SUPPORT STRUCTURE

The aluminum tanks are supported by S-glass/epoxy composite struts which are in turn connected to the graphite/epoxy frames (Figure 63). The glass/epoxy struts are used because of their low thermal conductivity which helps to minimize the boil-off due to external heat conducted to the tanks. The struts are attached to the tanks by a step chem milling pattern combined with welding techniques. The other ends of the struts are connected to the tank structure using titanium rod-end fittings. This fitting allows for movements of the struts as the tanks contract or expand due to thermal effect or pressurization. The graphite/epoxy frame is made up of twelve section members. The members are joined at the corners by titanium fittings (Figure 64). All struts and frame members are hollow cylindrical composite sections. The members would also have protective coating such as those use for the LPIV main truss structures.

Table 23. Dimensions of Tank and Supports

Tank Diameter	7.8 meters	
Thickness	1.17 millimeters	
Dry Mass of Both Tanks	1025 kilograms	
	S-Glass/Epoxy Struts	Graphite Epoxy Struts
Length	5.5 meters	8.0 meters
Radius	5.6 centimeters	6.8 centimeters
Thickness	0.7 centimeters	0.8 centimeters

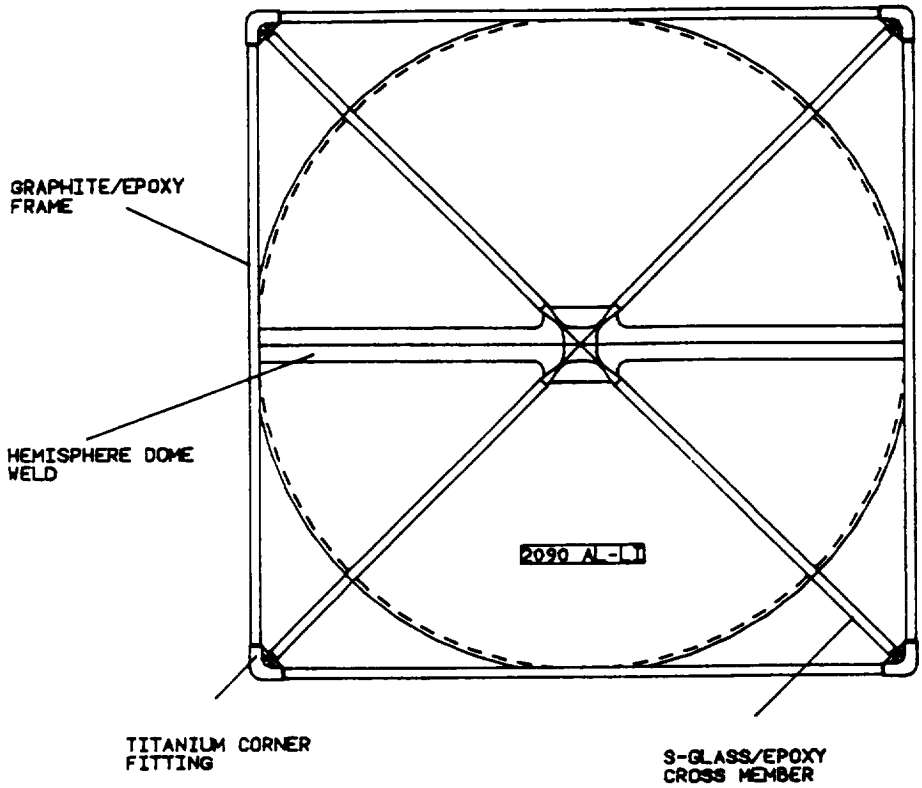

Figure 63. Cryogenic Tank and Structure.

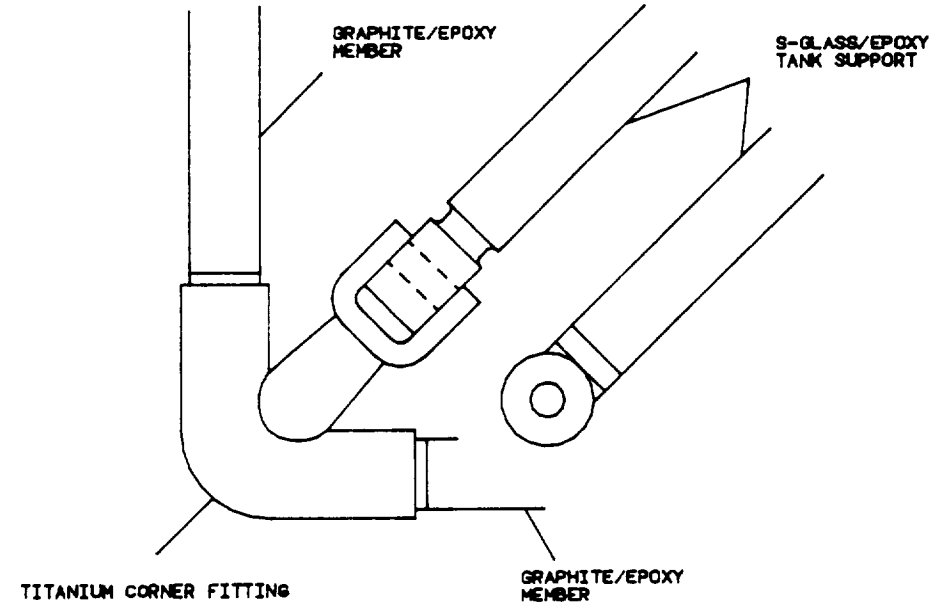

Figure 64. Titanium Joint Fitting

INSULATION

In insulating the propellant tanks, two schemes were considered - the all multi-layer insulation (MLI) and MLI/foam combination. The major deciding factor in selecting either one was to consider the mass of insulation required for each system.

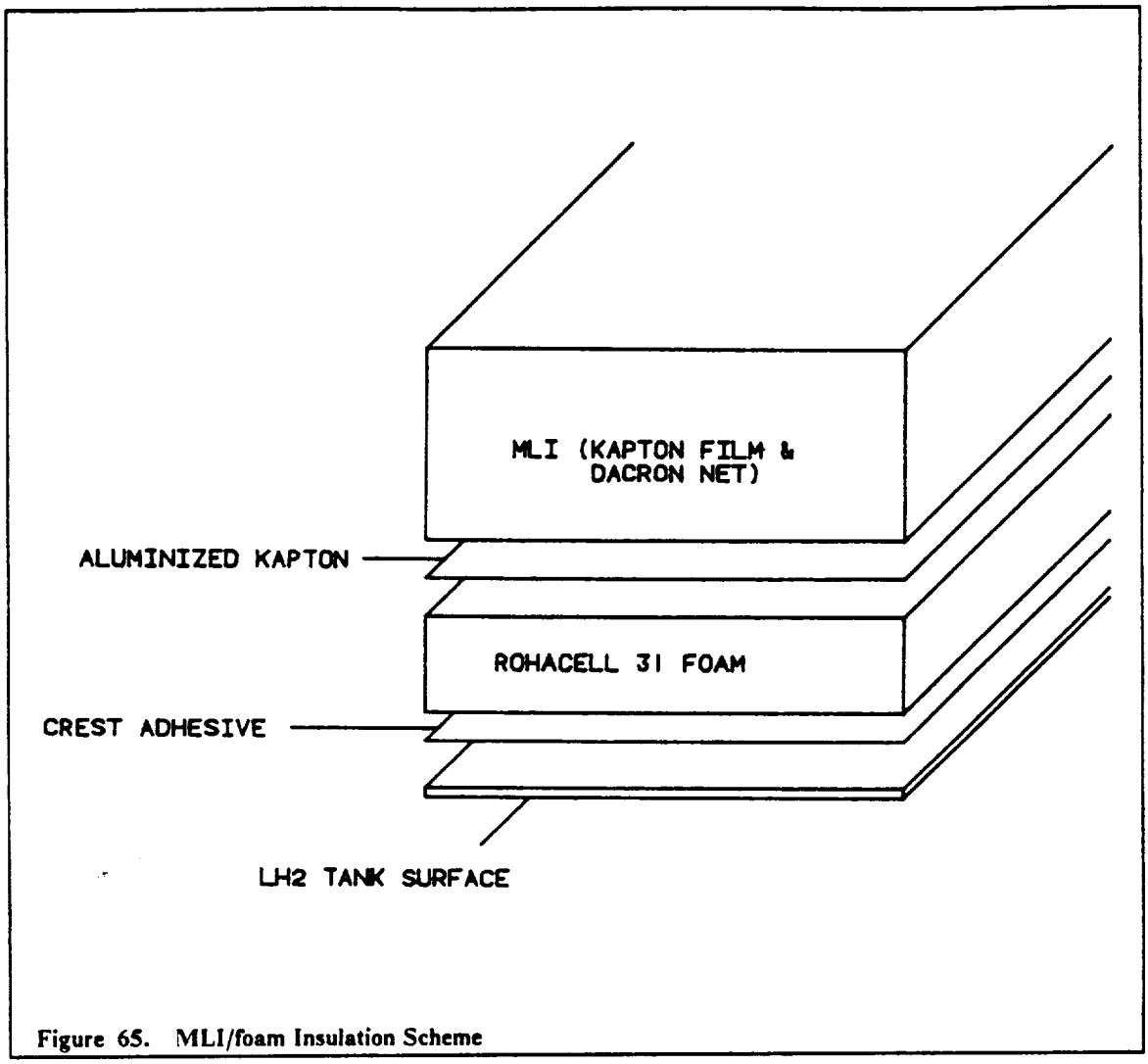

Figure 65. MLI/foam Insulation Scheme

The MLI/foam system was selected over the all MLI system because of the lower surface density and expected greater potential for future improvement.It should be noted, however, that the all-MLI insulation has a better perfomance in terms of longer lifetime. Nevertheless, since the LPIV has been designed such that the propellant tanks can be removed completely from the LPIV, any maintenance of the tank insulation would not require a complete overhaul of the LPIV. Due to this ease of tank maintenance, it was only to the LPIV's advantage that the mass saving using the MLI/foam should be taken. Complete details of the particular type of MLI/foam chosen here were researched by a joint NASA/Boeing contract (Ref. Kramer). The MLI is made of alternating layers of metallized Kapton film and Dacron net spacers. This particular type of MLI is state of the art and has been flown and tested extensively as cryogenic insulation. Between the MLI and the foam is a gas-impervious barrier film bonded over the outside of the foam. This barrier entraps volatile materials in the foam that could escape into the MLI and degrade its performance. This barrier would be made of aluminized Kapton.

The foam used is the Rohacell 31. This foam has also been studied in numerous tests to be superior in performance compared to others. It is manufactured in sheets which are cut and then fit to the contour of the tank by heat forming. Finally, the foam is adhesively bonded to the tank surface using a process called vacuum bagging. The foam insulation around the tank mounting supports must allow for movement of the support struts. These movements are caused by thermal contraction and expansion of the tank and supports, tank pressurization and vibration due to launch loads.

In order to reduce the external temperature of the tank due to solar radiation, a special paint is sprayed on top of the MLI to reflect the heat from the tank. The paint used for this particular design is a silicate bonded paint containing zinc orthotitanate pigments, Zn_2TiO_4, called YB-71 (Ref. Herada). The YB-71 paint is sprayed to a thickness of 8 mils which will provide a reflectance of 94 percent. It has been determined by experiment that this thickness gives the optimal performance for the paint. Finally, a layer of Mylar is applied to protect the paint surface from micrometeorite collisions.

Boiloff

The thickness of the MLI/foam required for the tank was determined by allowing 1 percent boiloff. Boiloff is the propellant that is vaporized within the tank due to the heat flux into the tank. Thus for the duration of the LPIV mission of fifteen days, approximately 350 kg of liquid hydrogen will be lost or vented. The boiloff/insulation calculations are presented in the appendix and results are given in Table 24.

Table 24. Insulation Dimension and Masses

MLI Thickness	1.840 cm
Foam Thickness	0.184 cm
Mass of Insulation for Both Tanks	268 kg

TRACK SYSTEM

The track system of the propellant tanks uses two T-tracks which extend along the secondary track which will support the tanks and their structures (Figure 66 and Figure 67). The tanks will be moved along the tracks by means of a center screw track with an actuator connected to the fuel tank support platform.

Due to the geometry of the system, the screw track could only be supported by the ends so it was designed as a secondary track used only to move the tanks to the desired location along the track. The main T-track would support the fuel platform carrying the fuel tanks and the stresses exerted by the tanks during acceleration . For strengths and low mass, the screw track and T-track will be made of high strength composite material. The current leading material is graphite/epoxy but it should be noted that almost certainly a newer material with better strength and stiffness with lower mass will be available in the 20-year time frame.

The T-track is connected to the LPIV along the secondary truss at the joints used to connect the truss members. More track supports are needed at intervals between the joints to reinforce the tracks since these supports will be the only thing holding the entire track and propellant tank to the LPIV. As for the screw track, it would have support only at the ends since the actuator will travel its entire length. Sizing of the T-track and screw track is estimated using basic material property of the graphite/epoxy and mass estimate is acquired from the corresponding results.

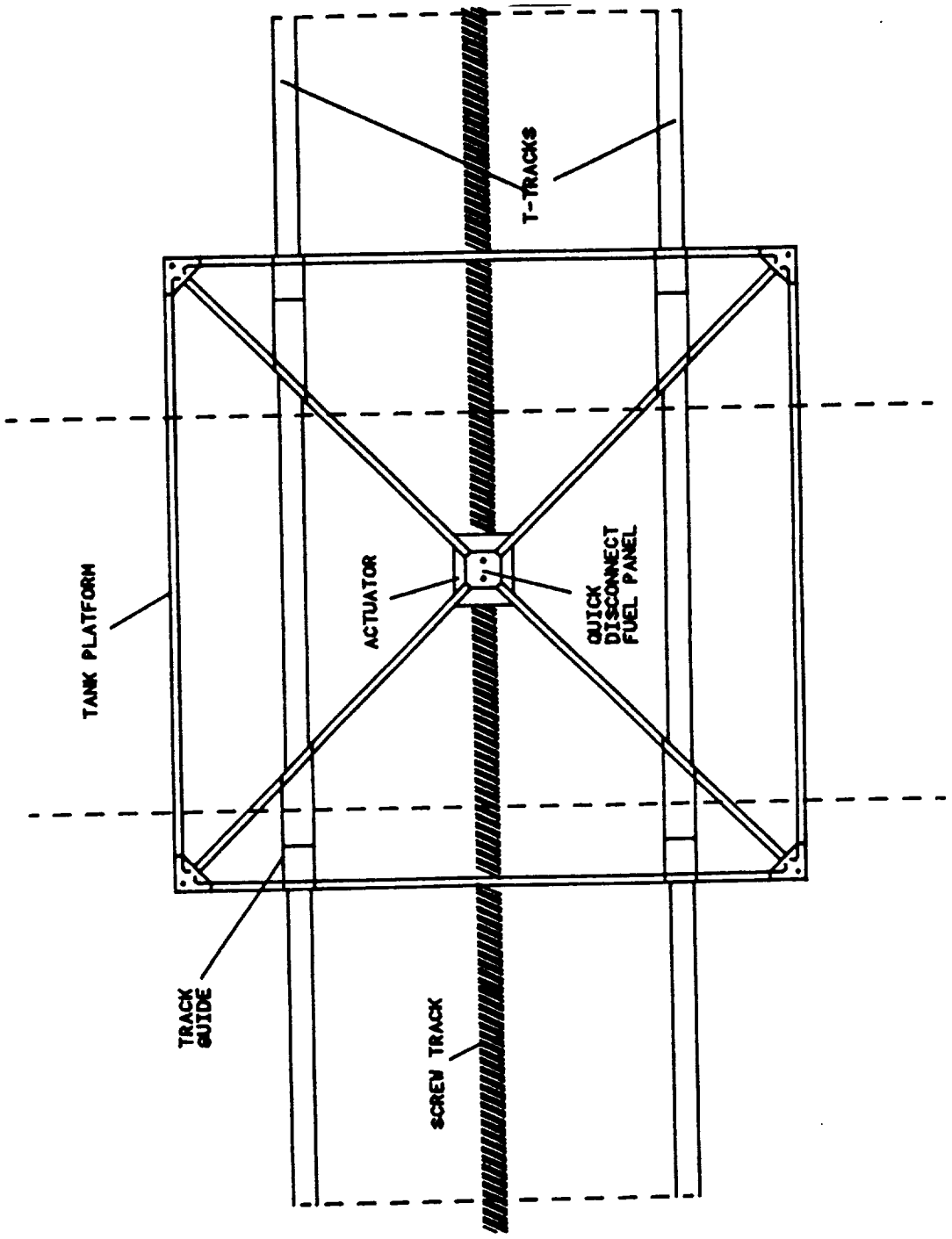

Figure 66. Top View of Track System

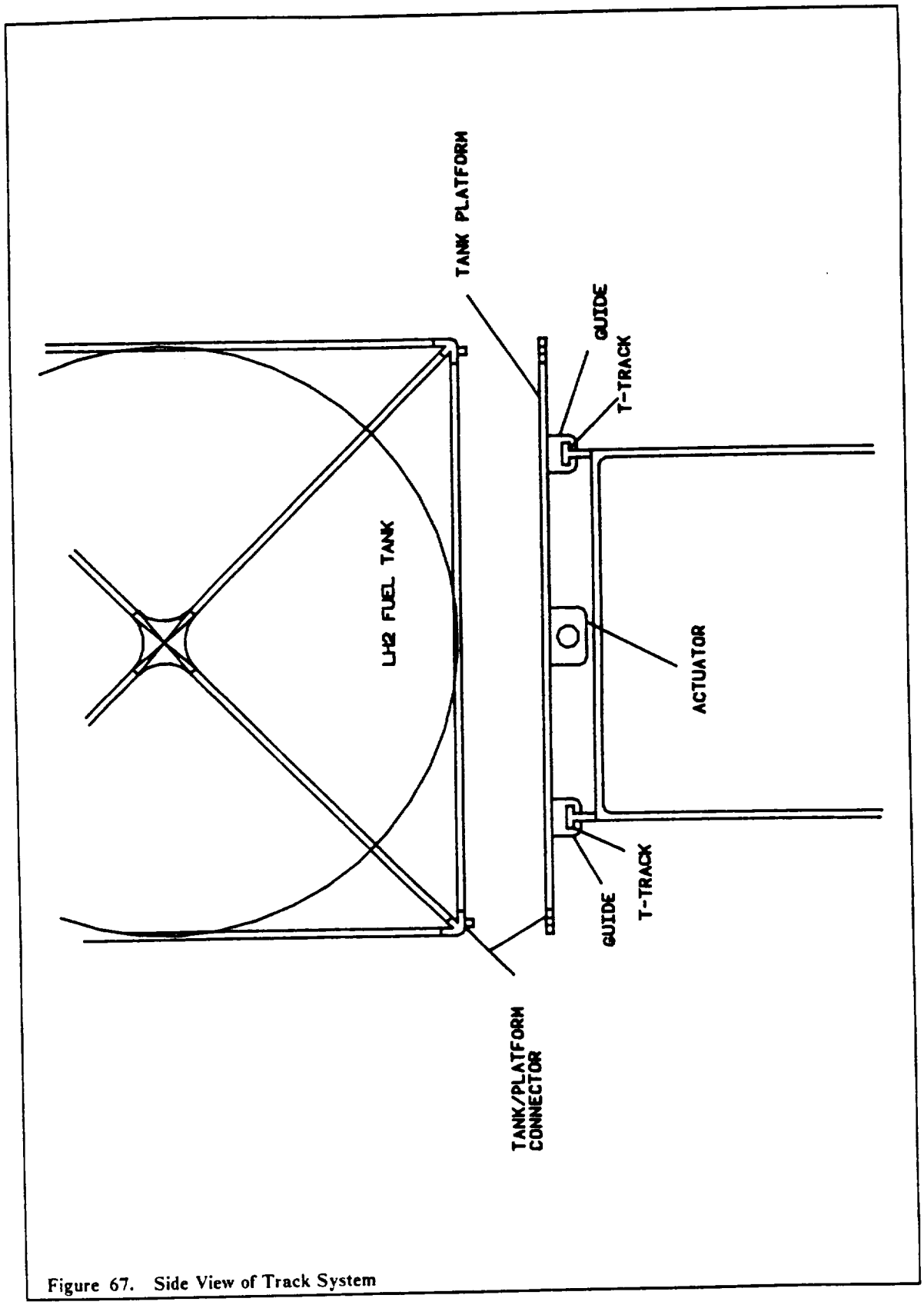

Figure 67. Side View of Track System

The actuator designed for the LPIV is made from a combination of cams, rollers, and gears (Figure 68) and will provide very accurate positioning. It will be driven by a high torque reversible electrical motor. The maximum power requirement for each actuator is 5 W each or 10 W for both actuators. The actuator works by activating the motor which will turn the rotating cam and the locking nut at the same time. The rotating cam advances the entire actuator which will move the tank platform and the turning locking nut will lock the actuator in place preventing any reverse reaction. Each actuator has been designed to havetwo separate cam/nut systems for movements in advance and reverse direction powered by the same motor. The reversible motor allows for the use of one motor for both travel directions.

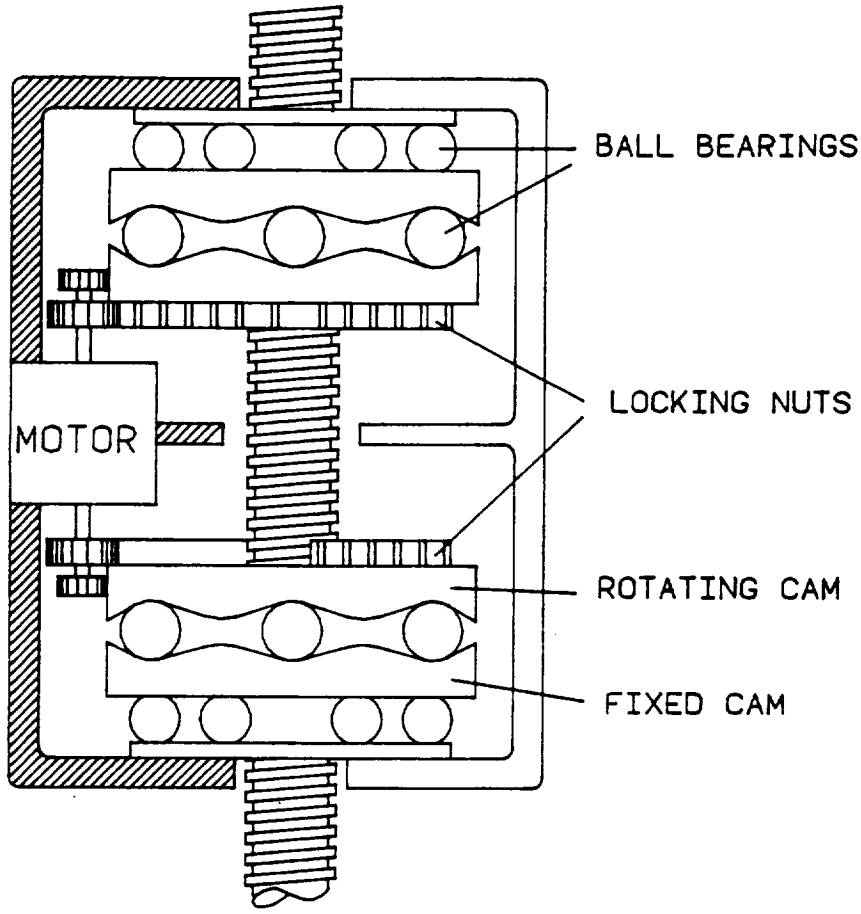

Figure 68. Actuator

The propellant tank platform serves as a propellant tank holder and is permanently attached to the tracks. The platform is attached to the screw track and T-tracks by the actuator and four guides, respectively. The platform will be made of composite graphite/epoxy tubes connected by fittings at the corners in a manner similar to the tank structures. However, these fittings will only have one degree of freedom each fitting contains a male-female latch devised to lock the tank in place after attachment. These latches can be operated by electrical pulses to either a closed or open position to attach or release the fuel tank from the platform. The platform will also have a quick disconnect panel for fuel flow between the tank and the LPIV.

The four guides on the platform will hold the platform and tank to the T-tracks. These guides will require a rolling and braking mechanism so that they can move freely when the actuators are activated and clamp to the T-tracks when the actuators stop. Table 25 gives the masses of the complete track system.

Table 25. Mass Estimates for Track System	
T-tracks	300 kilograms
Screw Tracks	150 kilograms
Actuators	80 kilograms
Tank Platform	290 kilograms
TOTAL	2190 kilograms

PROPELLANT FEED SYSTEM

The propellant feed system is responsible not only for necessary and precisely controlled supply of the hydrogen to the laser engine but also for the cooling of the engine walls and/or beam splitter and the tertiary mirrors. As such, the propellant feed system is one of the crucial components of the LPIV. Two candidates for the propellant feed system are electrically driven pump system and turbopump powered by the hot dydrogen bled from the cooling system. The first system requires an electrical power of nearly 3 kW and its total mass is much greater than the turbopump system. Therefore, the latter system has been selected under the assumption that improvements in technology over the next 20 years will greatly enhance the reliability of the rotating turbomachinery.

The LPIV will use two turbopumps, one at each end of the truss for each engine. The use of two pumps instead of one simplifies the problem of balancing the LPIV center of mass; also, each turbopump should be located near the engine because the turbine uses hydrogen bled from and discharged back into the engine cooling jacket.

Propellant will be fed to the pumps from the pressurized tanks. The propellant inside the tanks will be maintained at low pressure presently determined to be 5 psia since this is known to be the lowest practical pressure while still providing a net positive suction head at the pump inlet. The turbopumps must increase the pressure of the propellant from 5 psia (.34 atm) to about 367 psia (25 atm). This will be the pressure required for the propellant to overcome the friction in going through the cooling and injection into the engine. An electric motor will be used to initiate the rotation of the pump until the operational speed is achieved. The required pumping power is:

$$P_p = \dot{m}_p \frac{P_d}{\eta_p} \rho_p$$

where $\dot{m}_p$ - propellant mass-flow rate
P_d - pressure differential
η_p - pump efficency (assumed 0.7)
ρ_p - propellant density

which results in a value of 1.34 kW. The turbine is driven by a small fraction of hydrogen diverted from the engine cooling system at a location where the hydrogen temperature is around 1050 degrees Kelvin. The pumping power must be equal to the shaft-power ouput P_t of the turbine (after accounting for the mechanical effiency η_m of the possible speed reducing gear) given by

$$P_t = \eta_m \eta_t B \dot{m}_p C_{pt} \delta T_t$$

Here B is the propellant fraction to drive the turbine, δT_t is the temperature drop across the turbine, C_p is the average specific heat and η_t is the energy- conversion efficiency of the turbine. Assumming $\eta_t = 0.8$, $\eta_m = 0.9$, $\wedge \delta T_t = 75^\circ K$ one can determine B = 0.05 i.e., about 5 percent of the total hydrogen flow or 20 percent of the hydrogen which goes through one helical cooling "coil" is needed to drive the turbine. The hydrogen discharged from the turbine is reintroduced back to the cooling coil.

While no detailed configuration are presented, approximate estimates of the turbopump systems have indicated that both the turbine and the pump will be of very small sizes and will have to operate at very high speeds. The single-stage turbine will use a rotor with the blade tip and blade root diameter of approximately 2 and 1.5 cm and the operational speed may be around 80,000 rpm. A

A small centrifugal pump will have an impeller designed so as to optimize the suction specific speed. A near 1:2 speed reduction gear may be required for matching of turbine and pump.

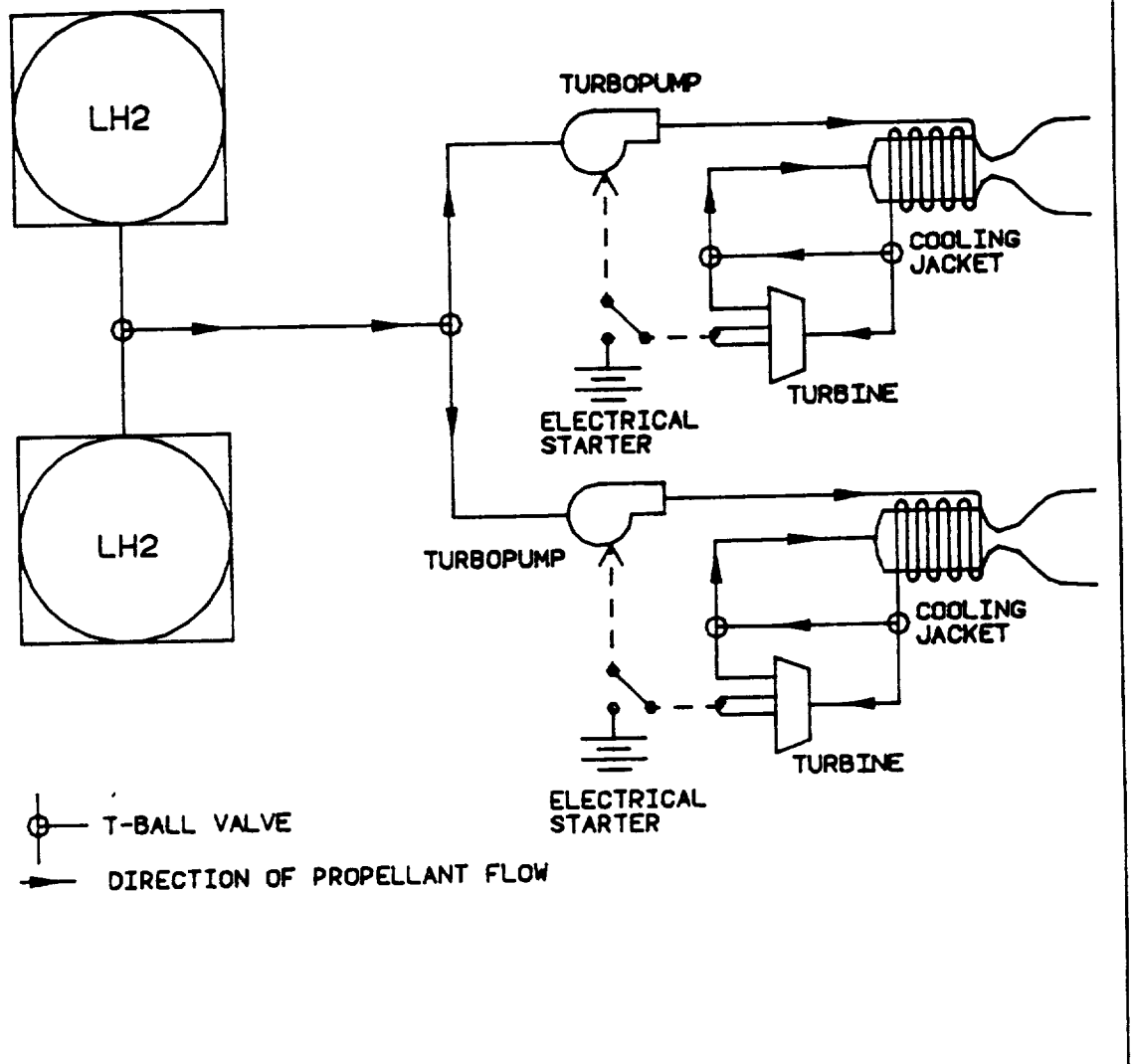

Figure 69. Fuel feed system

Fuel Lines

Since the propellant tanks will be moving along the tracks, it is necessary to devise a scheme to install fuel lines which would run between the tanks and the laser engines. The only solution for this scheme is to employ flexible fuel hoses (Figure 70). The scheme required 8 meters of flexible fuel hoses. The proposed design requires that the material retain flexibility at 21K without degradation and that the hose will be under axial stress in keeping the fuel lines straight at all times. This is because all the slacks must be taken up by the spring mechanisms so that they will not interfere with the tank movement. Thus, an assumption is made that in the alloted time frame, a material will be available suitable for use in the propellant transport scheme.

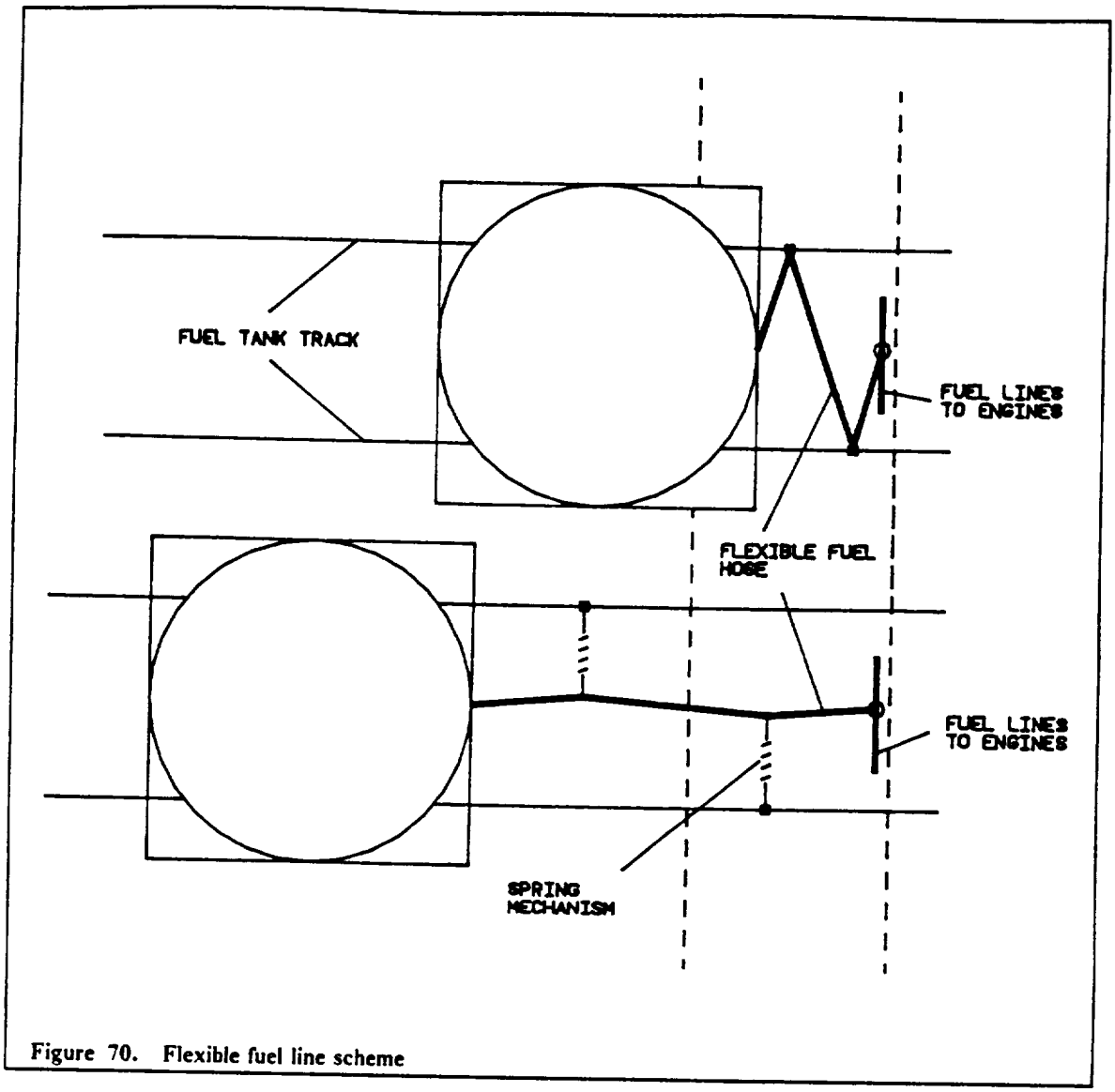

Figure 70. Flexible fuel line scheme

Table 26. Mass Breakdown of Propellant Feed System (for two engines)

Turbopumps (including gears)	10 kilograms
Electric starting motors and gears	25 kilograms
Valving and propellant lines (w/ insulation)	100 kilograms
TOTAL	135 kilograms

Refueling

Refueling the LPIV is a simple process of disconnecting the entire empty propellant tank and its structures from the platform and reconnect a full tank. The quick disconnect scheme will allow the LPIV to have a very short turn-around time plus any maintenance on the tanks will not decommission the entire LPIV vehicle. The tanks may be refilled at convenience and stored aside for refueling other LPIVs.

SUMMARY

Perhaps the main problem encountered in the design of the LPIV propellant tank and tracks has been the material selection. Certain advances need to be made in the materials fields before these system can be realized. Lighter materials exhibiting high strength and stiffness will be very desirable. Also, the material must not succumb to thermal loading due to space solar radiation and long term space atmospheric degradation. All these requirements are interrelated and should be viewed with equal importance for the entire system to function.

ACQUISITION, POINTING AND TRACKING (APT) SYSTEM

INTRODUCTION

Laser powered vehicles place stringent demands on the acquisition, pointing, and tracking (APT) system. It is this system which enables the LPIV to capture the power made available to it from the remote laser power station. The APT system must not only maintain the laser beam on target throughout the LPIV's period of powered flight, but also be able to locate the beam when it must begin receiving from a different power source.

The APT system relies heavily on three other systems of the craft, the communication system, the on board computer and the RCS system. The communication system is used to establish an initial link between the LPIV and the LPS and assists in narrowing the volume of error in which the LPS is contained. The computer is used to calculate the positions of the laser power stations and the LPIV given the orbital data. The RCS system is used to maneuver the vehicle into a position from which it can receive the power beam.

The other primary components of the APT system consist of the optical receiver, the optical transmitter, the fine pointing gimbal assembly, and several photodetectors. These subsystems work together to insure that the power which is being transmitted thousands of kilometers from the LPS is received at the window of the engines to be converted to thrust in the most efficient way possible.

SYSTEM REQUIREMENTS

There are two factors which must be taken into account by the APT system, the angle with which the laser beam radiates upon the primary mirror and the offset of the beam from the center of the reflector. The primary reflector is a paraboloid; therefore, only if the beam is received parallel to the axis of symmetry can it be focused onto the secondary mirror and proceed along the optical train to the entrance of the engines.

For maximum efficiency, the beam should also be offset from the center of the primary reflector. The reason for this comes from the configuration of the optical train and the erratic thermal loading of the tripod that may result due to the laser beam. The secondary mirror is positioned in the center of the parabolic reflector near the focus and causes a central obstruction of 1.13 m^2. The laser beam spot size will be typically less than 15 m in diameter with the most intense part being directly in the center (Figure 71). In order to avoid blocking out this most powerful part of the beam and take advantage of the maximum power available, the beam is offset from the center.

The APT system must be accurate to 23 m over a distance of 100000 km. This corresponds to an angle of 0.23 μm. It is projected that by the year 2010, when the LPIV is ready for deployment that the accuracies on the order of 0.1 microradians will be possible due to advances in the fields of vibrational control and spacecraft attitude control.

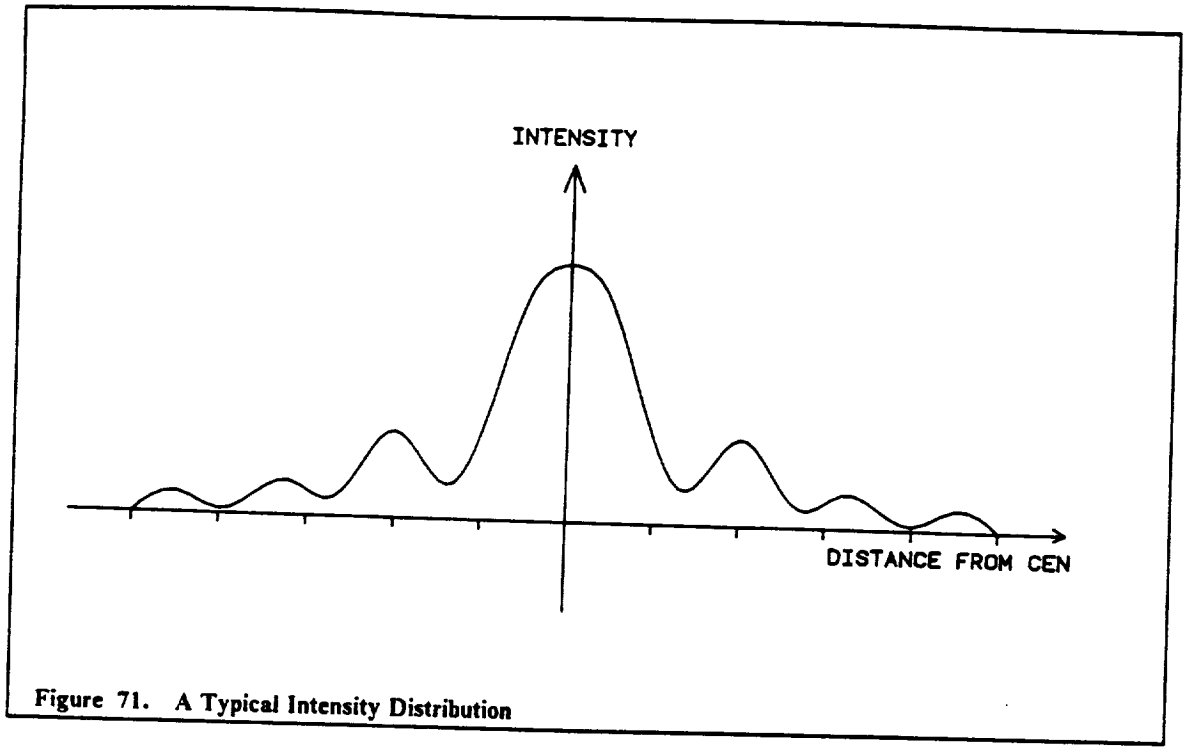

Figure 71. A Typical Intensity Distribution

SYSTEM CONFIGURATION

The APT subsystems work together to accomplish three basic tasks: establish a two way link with the LPS, aim the primary mirror to receive the beam, and process data to calculate positions of the LPIV and laser power stations.

The Link

Working to establish the link are the communication system, the optical transmitter and optical receiver. The communication system is employed only in the initial stage of acquisition to instruct the LPS to emit its pilot beam and begin its search pattern. A detailed discussion of its configuration and other functions can be found in the following chapter on communications.

The optical transmitter and receiver are located on the back of the secondary mirror and share the same optics (see Figure 72). The transmitter is a Neodymium: YAG (yttrium, aluminum, garnet) laser with a frequency doubler. Nd: YAG is the most conventional solid-state laser. Its efficiency is only 0.4 percent but its lifetime is 4 to 5 years and is highly reliable. It normally emits light at a wavelength of 1.064 μm. By doubling the frequency, we half the wavelength thus making it emit radiation at .532 μm (Ref. Katzman). This accomplishes three goals. First, it causes the wavelength to be much more separated from that of the iodide power beam which emits radiation at 1.315 μm. In this way, noise and interference are limited. Second, the smaller wavelength allows the optics themselves to be smaller which cuts down on mass. Finally, the smaller wavelength boosts the antenna gain (discussed in chapter 9) which lowers the power requirements (Ref. Hacker). At this wavelength and with the antennas on the LPS and the LPIV, the Nd: YAG laser needs only 40 W of power to send a coherent signal to the LPS.

The receiver is effectively a simple 20 cm reflector telescope designed by Eastman Kodak (Ref. Katzman). It must be modified only slightly to allow for the quadrant photodetector to be placed in the proper position behind the primary mirror. A dichroic beam splitter is located in the path of the oncoming beam which allows most of the radiation incoming at 1.315 μm to pass through while reflecting most of the outgoing radiation at 0.532 μm.

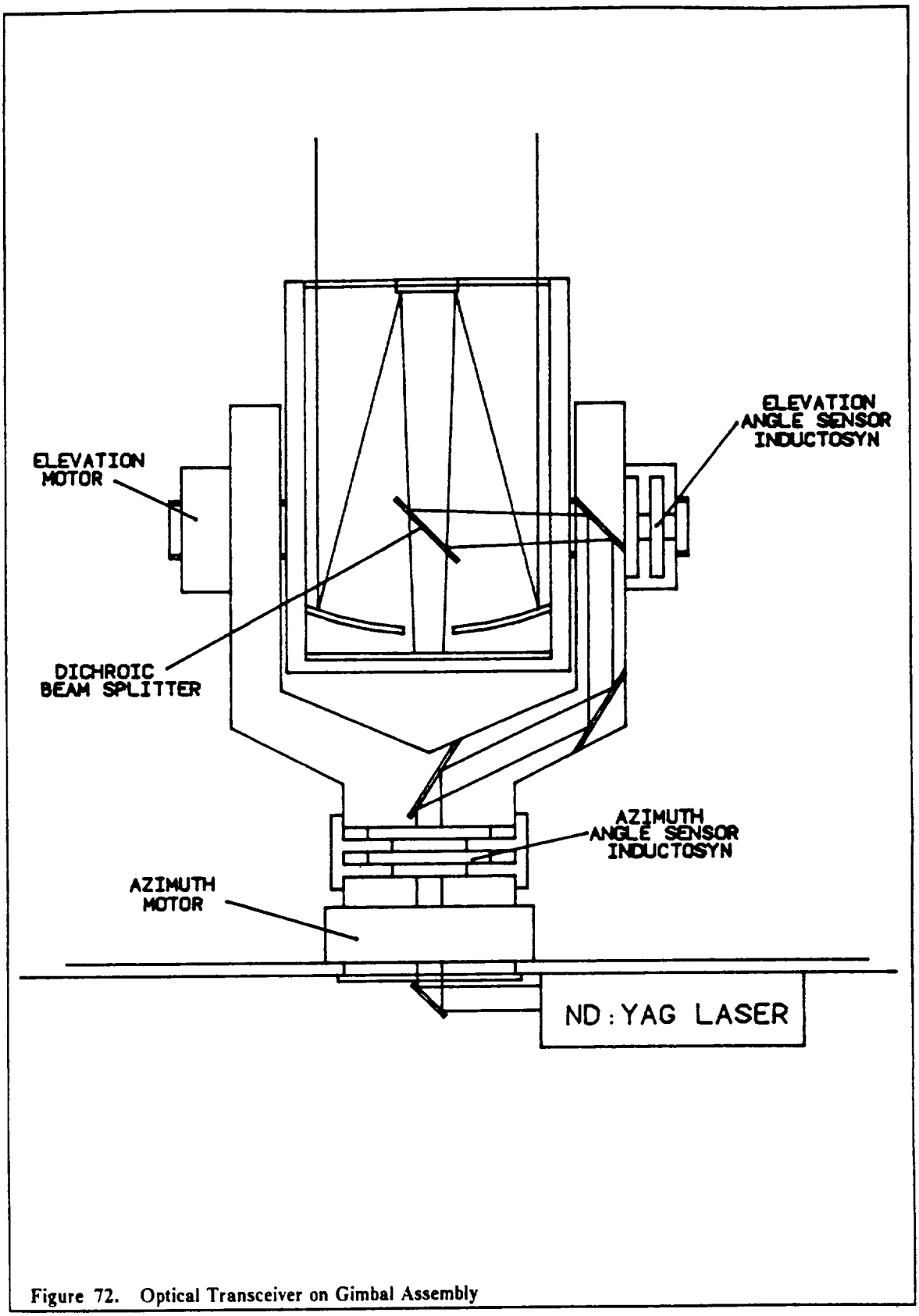

Figure 72. Optical Transceiver on Gimbal Assembly

The Aim

The telescope is mounted on a gimbal assembly with two degrees of freedom about the azimuth and elevation (Figure 78). This gimbal assembly along with the photodetectors and the RCS system make up the aiming portion of the APT system. The gimbal assembly is used for the fine pointing of the optical receiver and consists of an azimuth motor and an elevation motor each with its own induction angle sensor. The azimuth has full 360° mobility and the elevation has a field of view of just over 30°. Both the azimuth and elevation are controlled by induction motors built into the gimbal assembly. These induction motors consume only 12 W of power each.

The quadrant photodetector which will be located in the telescope is pictured in Figure 73. It operates on the principle that when the beam is on center, the radiation in each quadrant will be equivalent. They are constructed of four independent avalanche photodiodes (APDs). In order to locate the beam vertically, the energy in the lower two quadrants is subtracted from that of the upper two quadrants and the difference is divided by the total energy. For horizontal location, the same is done between the right and left quadrants. These coordinates are then relayed to the computer which may then instruct the RCS system or the LPS of the appropriate action to take to center the beam.

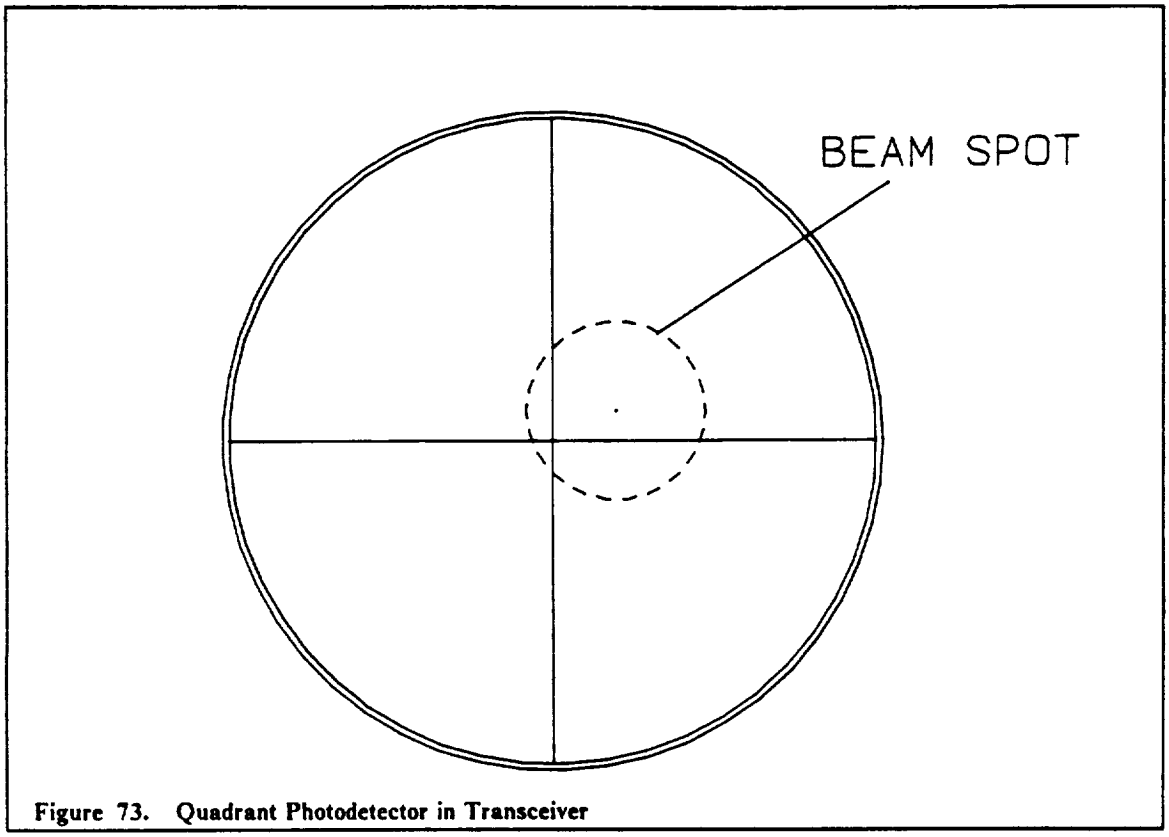

Figure 73. Quadrant Photodetector in Transceiver

There is a system of photodetectors in addition to the quadrant photodetector in the telescope which work together to insure proper beam alignment. They are located around the perifery of the primary mirror in two rings at 20° intervals. The outer ring is located two meters from the edge of the primary mirror and the inner ring is located two meters inside of the outer ring. The photodetectors in each ring are APDs covered by a dielectric filter tuned to a wavelength of 1.315 μm corresponding to the wavelength of the power beam. APDs were selected for the photodetectors because of their small size of close to one inch, their high reliability, and their compatibility with light at the given wavelength (Ref. Katzman). If the beam is properly offset, at least one of the photodetectors on the inner ring will be activated and none of those on the outer ring will be activated. This dictates that at least one edge of the beam spot is between the two rings (Figure 74). This beam position is maintained by the RCS system.

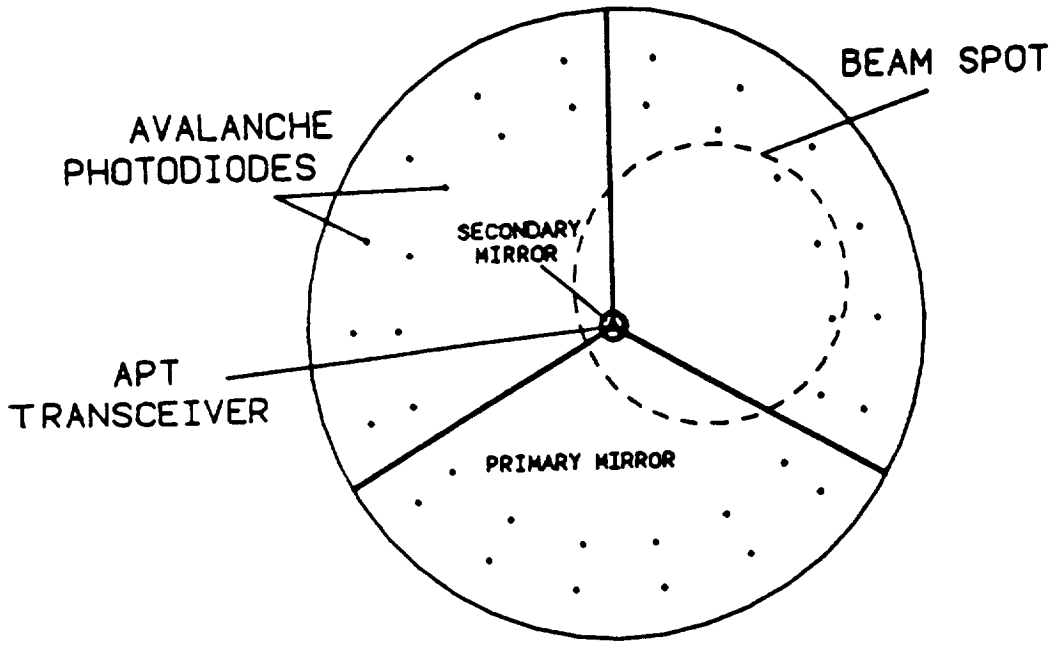

Figure 74. Proper Positioning of Beam Spot

The Computer

The on-board computer is used to calculate the position of the power station from which the LPIV will receive the beam. A sophisticated program called SIGHT has been written by a member of our group for this purpose and will be used as a model for the full system which will be integrated into the LPIV. To accomplish this the computer must be given the complete orbital data for all of the power and relay stations and be able to solve for their position at any time using the data from the on board clock. In order to correct for small errors and to account for orbital variations, this data is automatically updated every time the APT system locks onto the LPS, and it can be directly changed using the communication system from the space station or from mission control.

TYPICAL APT SCENARIO

Because the LPIV will be receiving its power from any one of several LPSs it must be able to calculate the position of any one of these at any time with a considerable degree of accuracy. During a typical mission the LPIV may change the station from which it receives power thirty to fifty times. The APT system should therefore be optimized in order to minimize the thrusting time lost during the acquisition stage.

Once the mission has begun, the LPIV can operate completely autonomously until it reaches the end of its mission, provided that initial orbital data is correct and that all systems remain fully operational. For the following discussion of how this is accomplished, please refer to the mission flowchart of Figure 75 and Figure 76.

Aiming of the LPIV

The first step is for the onboard computer to calculate the relative positions of the laser stations. This is done using two star tracking devices located on opposite sides of the primary mirror and the preprogrammed orbital data for the LPSs. When this is accomplished the computer determines which is the best power station to lock onto based on relative positions, relative velocities, and length of time possible to receive without having to switch again. The LPIV then orients its primary mirror in the direction of the power station while keeping its engines pointed along the flight path.

Acquisition of the Pilot Beam

In order to expedite the acquisition stage, a pilot beam is first fired through the same optics that the laser beam will be fired through. The pilot beam must be of similar wavelength in order to pass through the filters and give correct readings on the photo detectors. The power beam is a high power iodide laser having a wavelength of 1.315 μm. A low power semiconductor laser of InGaAsP with a typical wavelength of 1.3 μm was selected for the pilot beam.

To begin the acquisition process, the power station emits a defocused pilot beam. This defocusing enables the beam to cover the entire error volume (Figure 77a). The optical receiver on the LPIV begins a search pattern for the power station and continues repeating it until the pilot beam is detected. The laser transmitter then emits a return beam to illuminate the power station (Figure 77b). The power station continues searching for the LPIV until the return beam is detected (Figure 77c). Then the pilot beam is focused to the actual size that the power beam will be (Figure 77d) (Ref. Popescu).

Pointing of the LPIV

The LPIV APT system and the power station remain locked on to each other while the LPIV reorients its primary mirror to receive the beam. Once the primary mirror is correctly oriented, the pilot beam should be on target with the engine. It should also be offset in order to insure that the most powerful part of the beam, the center, is not blocked by the central obstruction. The two rings of optical detectors check for this offset and the RCS makes any corrections necessary. At this point when the pilot beam has been properly oriented and offset and the APT optical receiver has been locked into position the acquisition stage is complete and the tracking stage begins.

Tracking of the power beam

Because the laser beam is so much more powerful than the pilot beam, a filter must be placed in front of the optical receiver in order to protect the quadrant photo detector from the intense radiation of the iodide laser. When this has been done, the LPIV is ready to receive the laser beam.

During the tracking stage, the APT system is in constant closed loop communication with the LPS. The APT system is continuously informing both the LPS and the RCS system of appropriate actions to take to maintain proper beam positioning.

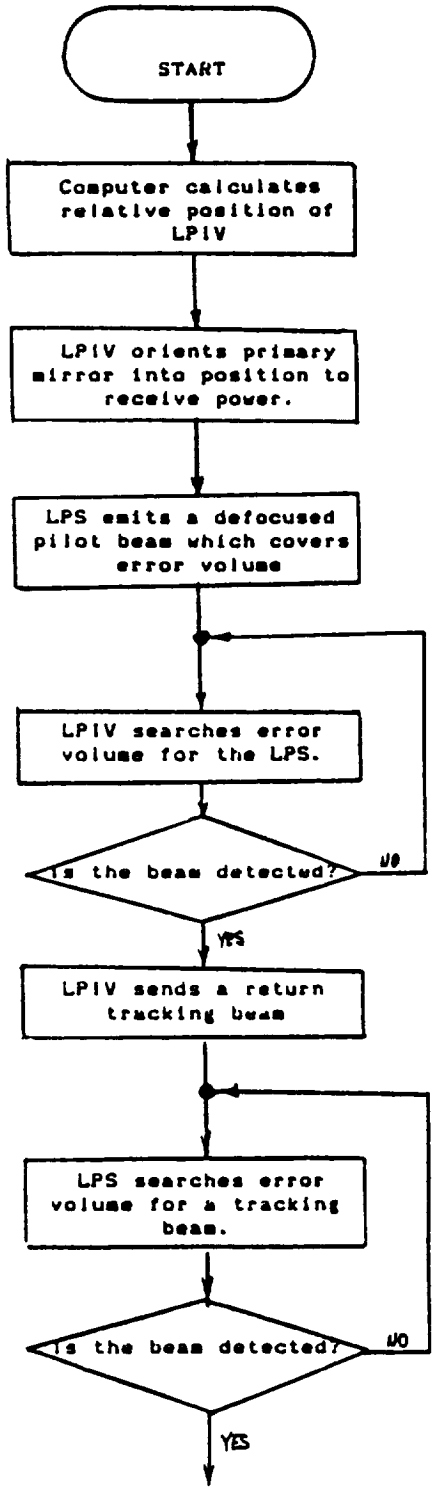

Figure 75. APT Flowchart of Typical Mission

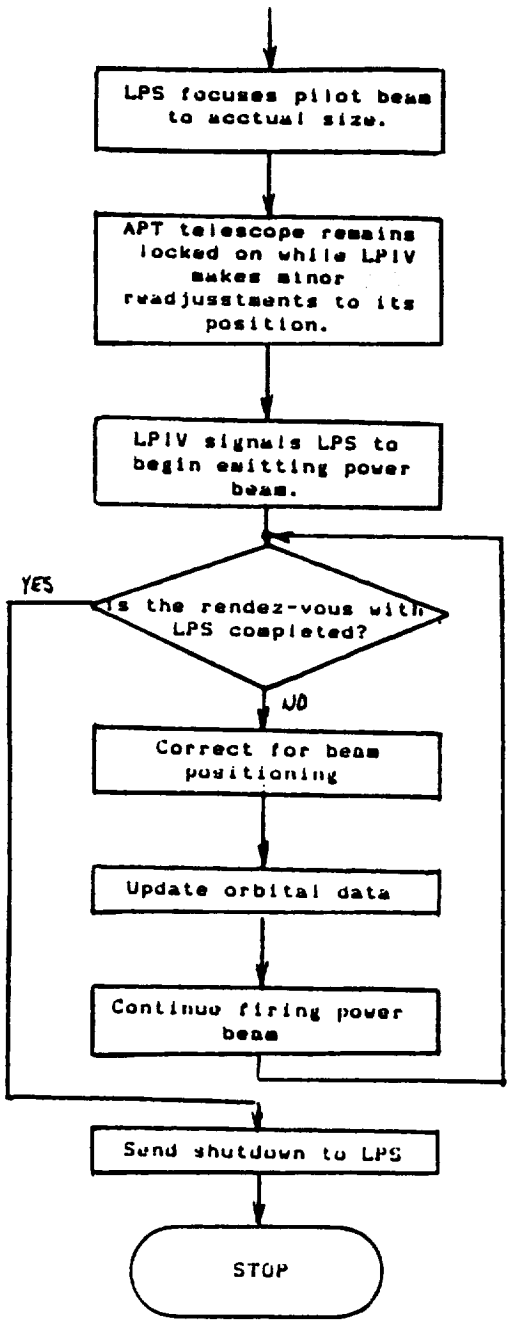

Figure 76. APT Flowchart of Typical Mission (continued)

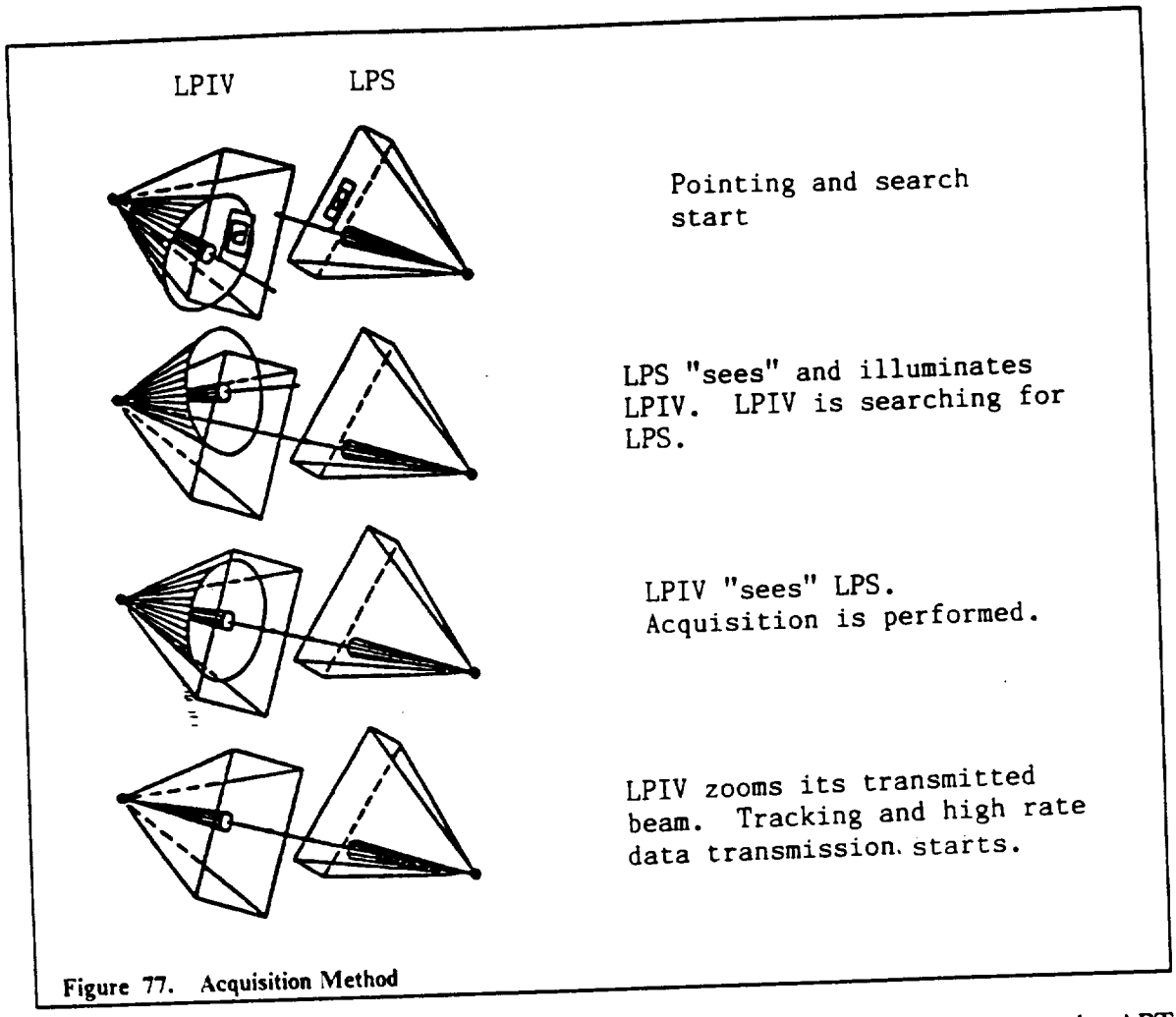

Figure 77. Acquisition Method

This process of maintaining proper positioning continues until the computer instructs the APT system to send the shutdown signal. This may be done for one of three reasons: (1)the LPS and the LPIV may move so that the earth is between them making it necessary to switch power stations, (2) the relative positions and velocities of the two vehicles may make it more advantageous to begin receiving from another power station, or (3) the LPIV may reach the end of its powered flight stage and enter the coasting stage.

THE LEAD AHEAD PROBLEM

Due to the finite speed of light and the long distances which may exist between the LPS and the LPIV it is necessary to calculate the angle by which the LPS must lead the LPIV when sending the beam so that it is received on target. In order to estimate this lead ahead angle, we need to know the velocities of the LPS and the LPIV.

The LPS is in a circular orbit at one earth radius. According to the equation for circular speed

$$V_{cs} = \sqrt{\frac{\mu}{r}}$$

Where r is the radius of the orbit or 12756 km and μ is the gravitational constant equal to 398600 km^3/sec^2. This corresponds to a velocity of 5.59 km/sec.

There are two cases which deserve consideration here. The first is when the LPIV is farthest from the LPS during powered flight. At this point, the signal travel time is the longest. The maximum

distance between the two vehicles during powered flight is approximately 100000 km. At this distance the LPIV is traveling at a speed of 2.524 km/sec in the same direction as the LPS. It takes light only 0.33 seconds to travel this distance. Assuming that the velocities are linear (this is a good assumption within a small time step) and also assuming that the response times of the vehicles are negligible (much less than .33 sec), their relative velocity is 3.63 km/sec corresponding to a change in relative position of 1.21 km. Solving for the lead angle from the equation

$$\phi = \tan^{-1}\left(\frac{2 \times 1.21}{10^5}\right) = 24.2$$

microradians.

From these calculations it becomes obvious that lead ahead must be considered. In order to calculate the angle, the computer uses the preprogrammed orbital data to calculate the position and velocity of the LPS. The LPIV knows its own velocity from the data provided by the accelerometers, and its position is determined by the star trackers. Given this data, the computer can calculate the relative angle between the transmitter and the receiver and adjust the APT system accordingly.

SUMMARY

The APT system is a vital subsystem of the LPIV. Because of its importance, Reliability and accuracy have been the two primary considerations in its design. Individual components have been selected for their high durability and long projected life. Secondary considerations included mass and power requirements. A list of these specifications is included in Table 27.

Table 27. Table of Masses and Power Requirements

Mass of telescope	19 kg
Mass of laser	4.5 kg
Mass of gimbal assembly	65 kg
Mass of mount	10 kg
Mass of all APDs	6.5 kg
Total Mass	105 kg
Power of laser	40 W
Power of gimbals	24 W
Total Power	64 W

COMMUNICATION SYSTEM

INTRODUCTION

The communication system of the LPIV has three basic functions: Telemetry, Tracking, and Command (TTC) (Ref. Evans). Telemetry is used to monitor the vehicle's status during the course of its mission. The computer on board continuously gathers information regarding the health of the LPIV and sends it back to either the earth based mission control station or the space station to be analyzed. The TTC system assists in tracking the vehicle by establishing an initial link with the laser power station for the purposes of course pointing. TTC may also be used to command the vehicle for manuevering during docking or initial firing, to update the orbital flight data, or to change orbits.

The mission of the LPIV dictates that the vehicle be pointed toward the laser station continuously during powered flight. During this time, the positioning of the vehicle is strictly governed by the location of the laser station regardless of the location of the space station, or the direction of flight. For the LPIV to be able to establish a link directly with the space station or mission control it would have to be equipped with at least two antennas in order to avoid blocking the transmission by another part of the vehicle. It would also require a completely separate acquisition, pointing, and tracking (APT) system for use by the TTC system.

In order to avoid such problems, it is necessary for the laser station to have the capability of serving as a repeater station for satellite transmission from either the space station or mission control. Because the laser station will be continuously tracking the LPIV and the space station will be tracking the laser station, this will eliminate the need for a separate APT system. It also enables the communication link to be uninterrupted for a much longer period of time because the antenna will not fall into the shadow of the vehicle (Ref. Pratt).

The repeater at the laser station is, of course, only employed during powered flight of the LPIV. During the coasting stage, the LPIV may orient itself to point in the direction of transmission.

For the purposes of this paper, the links from the laser station to the space station and to mission control are left out with the assumption that current communication satellites such as INTELSAT (INternational TELecommunications SATellite) can be used to establish these links. Only the link between the repeater at the laser station and the LPIV is discussed here.

SYSTEM REQUIREMENTS

Because the LPIV is an unmanned craft, there is no need for voice transmission, only data. Digital communication systems are best suited for this function. A digital TTC system requires that the signal be modulated and coded. Modulation is the technique used to convert the 1's and 0's of a binary system to an analog signal so that it can be transmitted at radio frequencies. Coding of the signal is usually advantageous because it helps to reduce the noise in the signal and provide more accurate data transmission (Ref. Evans).

The distances through which the LPIV will have to communicate make directional antennae a necessary component. An omnidirectional antenna may be employed for establishing the initial link, but power restrictions make directional antennas the only choice for regular communications (Ref. Pratt).

By the time that the LPIV is placed in service, it is assumed that the higher ends of the spectrum will be in more practical use. A higher frequency means a shorter wavelength and a smaller antenna size, so in the interest of minimizing mass, a frequency of 40 MHz will be used for the link from the laser station to the LPIV with a return link at 60 MHz.

The number of subsystems of the LPIV that will be communicating on the same bandwidth requires that some multiple access technique be employed. The simplest and most established is a frequency-division multiple access (FDMA) technique. This involves dividing the bandwidth up into several narrower bandwidths with a small space between them and using each division as a separate channel (Ref. Roden). This is the technique which will be employed on the LPIV TTC system.

MODULATION AND CODING

Several methods of modulation exist for representing a digital signal with an analog wave. Three were considered for the LPIV: amplitude shift keying, frequency shift keying, and phase shift keying. Primary criteria for selection of a method included tolerances to noise, complexity of necessary equipment, and success of already established systems.

Frequency shift keying (FSK) makes use of curves of different frequencies to represent 1's and 0's. This method has been shown to be the most tolerant of signal noise (Ref. Evans).

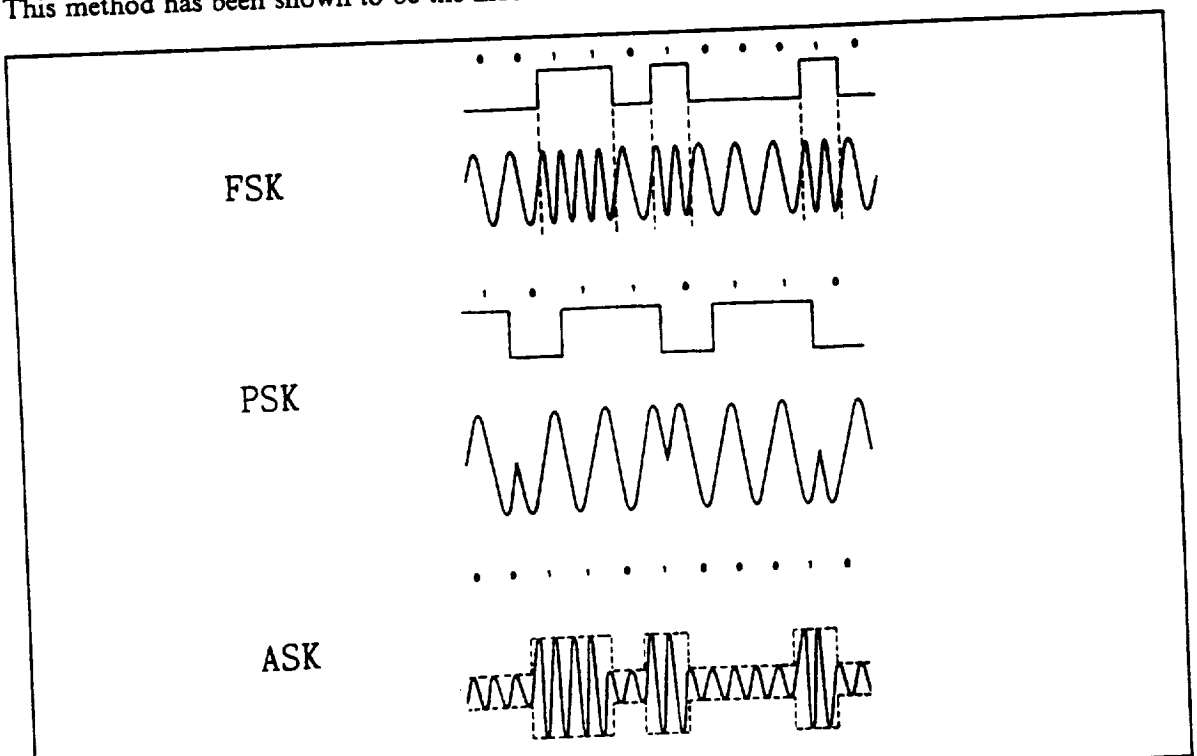

Figure 78. Frequency Shift Keying

Phase shift keying (PSK) represents the 1's and 0's of the digital signal with cosine waves of different phases. Although at a basic level, PSK is not as tolerant of signal noise as FSK, it can be expanded by adding more possible phase shifts. In other words, normally a binary PSK system represents a 0 with one wave and a 1 with an identical wave 180 ° out of phase. It is possible to expand this system to represent two bits at a time by adding a node at 90 ° and one at 270 °. Each phase shift can then represent a combination of two bits and thus a built-in method of error checking. This is called a quaternary PSK (QPSK) and is the modulation technique which will be used by the

LPIV. An incentive for using this system is that this is the system that has been recommended by the LinCom Corporation for use on the space station (Ref. Ratcliff).

Coding is a method of error correction used in reducing the bit error rate of a signal. The study of coding methods is much too extensive for this limited discussion, so it will only be briefly mentioned. One method of coding has been so widely used that it is almost considered an industry standard. This is the convolution code with a constraint length of 7, and a rate of 1/2. The length is a measure of the complexity of the code and the rate is a measure of how much redundancy is added. Using this code the signal to noise ratio needed to produce a given BER can be reduced by as much as 50 percent (Ref. Evans).

ANTENNAS

In any communication system the antenna is the primary factor governing power requirements. Generally, the larger the antenna, the less power is required. This presents a tradeoff especially pertinent to spacecraft; that is, by increasing the area of the antenna, the required power is lowered but the mass of the antenna and support structure is increased.

Antenna Gain Theory

When we say that a larger antenna requires less power, we actually mean less power density, or less power per unit area because the power is distributed over an area which increases with distance. If more of this power is intercepted by the antenna, then the power density need not be as great. This effect is known as antenna gain and plays a vital roll in the calculations for both transmission and reception.

If a signal is produced by a single point, the signal spreads out evenly over a sphere of radius d where d is the distance from the point of propagation to the point of interception. If a directional antenna is used to concentrate a portion of the signal in a given direction then the expression for antenna gain is given by the following equation:

$$G = \frac{4\pi A\eta}{\lambda^2} \tag{9.1}$$

where η is the antenna efficiency, λ is the wavelength, and A is the area of the antenna. For a parabolic reflector η is between 50 and 75 percent. For our calculations we will use a conservative η of 50 percent. As evidenced from the equation, antenna gain is inversely proportional to the square of λ. In other words, a smaller λ will produce a higher gain. At the writing of this paper frequencies of less than 20 GHz are in practical use and frequencies up to 100 GHz have been used on rare occasions. It is assumed that by the 21st century frequencies in the range of 40 to 60 GHz will be in common use. We have therefore selected for the LPIV frequencies of 40 GHz for receiving and 60 GHz for transmitting. These correspond to wavelengths of 0.0075 m and 0.005 m respectively. We will base our calculations for this section on a λ of .005 m.

From equation 9.1 then G = 251000 A. In signal calculations we frequently use decibels, abbreviated Db, to make calculations simpler. By definition

$$X(Db) = 10\log(X) \tag{9.2}$$

When the values above are substituted into equation 9.1 and G is then converted to its decibel value we get

$$G = 54 + 10\log(A) \tag{9.3}$$

Notice that when working in decibels, products and quotients may be expressed as sums and differences thus greatly simplifying calculations.

Antenna Placement

Unfortunately, if the antennas are not facing each other then no advantage is gained by this factor. This is often the case for spacecraft before an initial link is established. When the LPIV is deployed or after it is forced to switch relay stations it may be pointed in totally the wrong direction or even spinning. In order to initially make contact, the LPIV must also be equipped with a small omnidirectional antenna. This antenna need not be sophisticated at all because it is used simply to establish contact until the directional antennas are facing each other. It does not have to receive or transmit any data but only some reference signal that can be recognized on the other end (Ref. Pratt).

It is suggested that the directional antenna used be of the asymmetric, or offset, type to minimize the problems due to the central obstruction of the axisymmetric type. It should be located at the periphery of the primary reflector at 90 degrees from the main truss as shown in Figure 79. By placing the antenna at this point we are getting it as close to the primary mirror as possible without blocking the power beam and as far as possible from the engines in order to minimize blockage of the signal and deterioration of the antenna by exhaust particles. The reason for this is so that when the APT system has properly aligned the craft for powered flight, the antenna will be aligned as close to boresight as possible with that of the laser station.

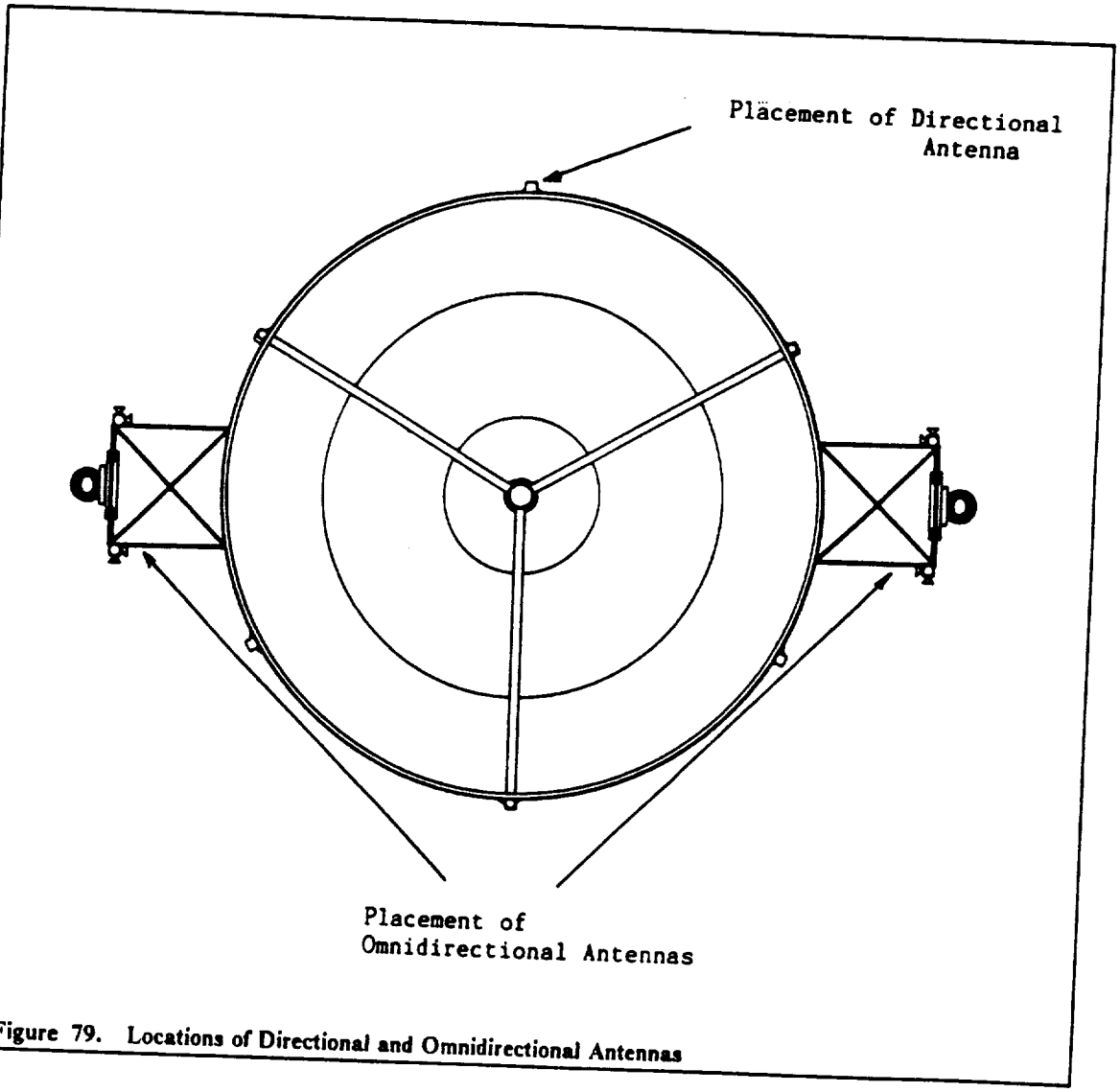

Figure 79. Locations of Directional and Omnidirectional Antennas

In order to insure that initial contact is easily made, an omnidirectional antenna should be placed at each end of the truss so that no matter what happens to the craft, at least one of the antennae will remain in view. These antennae and their wiring may weigh up to 4 kg and since they are only used for very short periods of time, their power requirements are negligible.

THE LINK EQUATION

The link equation is used to estimate the power collected at the receiving end of a radio frequency crosslink. All the terms are expressed in decibels and therefore can be added and subtracted depending on whether they are gains or losses according to the equation

$$P_r = P_t + G_t + G_r - L \tag{9.4}$$

The terms are the power of the receiver P_r, power available from the transmitter P_t, the antenna gain at the transmitter G_t, the antenna gain at the receiver G_r and the free space loss L.

The free space loss is that loss simply due to the distance the signal must travel and is calculated according to the equation

$$L = \frac{\lambda^2}{(4\pi d)^2}$$

In decibels, the equation is

$$L = -20\log(\frac{4\pi d}{\lambda}) \tag{9.5}$$

At an absolute maximum distance of 400,000 km L = 240 DbW. Assuming the same values as before and that the gains at each end are the same, we have

$$P_r = P_t + 108 + 20\log(A) - 240 = P_t + 20\log(A) - 132 \tag{9.6}$$

Now, the critical value is the value of the signal to noise ratio. This value in decibels is calculated according to the following equation:

$$\frac{C}{N} = P_r - 10\log(kT_sB) \tag{9.7}$$

Where k = Boltsman's constant = 1.3810^{-23} = -228.6 Db and T_s is the noise temperature which is about 3000 Kelvin for space systems and B is the bandwidth which is 100 MHz. When these values are substituted into equation 9.7 we get

$$\frac{C}{N} = P_t + 20\log(A) - 18 \tag{9.8}$$

For data transmission, it is necessary that this quantity be on the order of 20 Dbs. Substituting this into equation 9.8 it is easy to see the power/area tradeoff.

$$P_t = 38 - 20\log(A)$$

As an example, for a 2 m diameter antenna, P_t = 28Db W or 639 W. For a 4 m antenna, P_t is only 40 W.

It is estimated that the mass of the antenna and support structure would be approximately 10 kg/m^2. When this is compared with the overall mass of the LPIV it is a very small component. It is therefore desirable to sacrifice mass to gain power. For this reason, a three meter antenna should be used on the LPIV. This gives a power requirement of less than 126 W and a mass of 70 kg. A summary of data for the proposed communication system is included below.

Quantity	Value	Explanation
d	400,000 m	maximum distance
η	.50	minimum efficiency
λ	0.005 m	Wavelength at 60GHz
D	3 m	diameter of antenna
A	7.0686 m^2	area of antenna
m	70 kg	mass of antenna
B	100 MHz	bandwidth
C/N	20 Db	carrier/noise ratio
P_t	126 W	power of transmitter

SUMMARY

The telemetry, tracking and control system of the LPIV serves some of the most important functions during the mission of the vehicle. Through the TTC system we are able to monitor the details of the mission from thousands of kilometers away. We are able to give the LPIV special instructions so that it can cope with unusual circumstances such as a change in its preprogrammed mission or an inoperable LPS. The system has been designed so that the LPIV may carry on uninterrupted communications throughout the course of its mission using as little power as possible.

The primary considerations in the design of the TTC system were reliability and power requirements. By enabling the LPS to function as a repeat station, the need for a lot of complicated electronics has been alleviated. The system proposed is designed simply. It incorporates no moving parts which frequently require maintenance or repair, and the solid-state electronics keep the overall mass to a minimum.

AEROBRAKE DESIGN

INTRODUCTION

One configuration for the LPIV under consideration is the use of planetary aerobraking in order to achieve a velocity decrement without the costly expenditure of propellant, thereby reducing the necessary amount of hydrogen. The aerobrake process involves entering a planet's atmosphere (in this case the Earth's), whereby the vehicle becomes an aerodynamic body. The reduction in velocity comes from the drag acting on the surface of the aerobraked vehicle. The goal is to reduce the velocity of the vehicle enough so that it leaves the atmosphere at a circular speed corresponding to a low Earth orbit, or more specifically, an orbit matching that of the proposed space station.

The design of the aerobrake must take into consideration the following criteria: first, the mass of the added aerobrake structure should not exceed the amount of fuel which would be saved by the aerobrake procedure; secondly, the structure should be able to withstand both the forces and thermal loadings which the vehicle would encounter during atmospheric entry, primarily at perigee; thirdly, the aeroshell should adequately protect the existing LPIV vehicle from excessive forces and temperatures; and finally, the aerobrake should be refurbishable if damage should occur, with the requirement that the entire structure be designed for transport into and assembly in a space environment.

AEROASSISTED VEHICLE CONFIGURATIONS

There are various classifications of aero-assisted vehicles which have been hypothesized; generally these configurations fall into three groups based on their aerodynamic property of L/D, or lift-to-drag ratio. The high L/D group, similar to what the proposed NASP plane will look like, is designed for orbit to ground missions involving large inclination changes, a requirement not needed by the LPIV mission. The moderate L/D configuration shown, also known as the Aeromaneuvering Orbit-to-Orbit Shuttle (AMOOS), has a blunt nose which acts to reduce the heat flux over the nose of the vehicle upon entry. Finally, the low L/D configuration, commonly referred to as an aerobrake, uses its geometry to create lift and trim characteristics which help to guide the vehicle along its atmospheric trajectory. It has a slightly curved, blunted nose to aid in the reduction of stagnation point heat fluxes on the surface of the aerobrake. The three configurations are shown together in Figure 80.

This latter configuration suits our configuration best due to its geometry and aerodynamic capabilities. The LPIV project deals with aerobraking into Earth's atmosphere in order to slow the vehicle, enabling it to rendezvous with the space station in a circularized low earth orbit of approximately 407 km. The large umbrella shaped aeroshell is best fit to protect the delicate mirror assembly,the main truss structure and laser engines. The aerobrake will serve to create a buffer layer which will shield the vehicle. Regarding the construction of the aerobrake, there exists the possibility of making the aeroshell rigid, or inflatable. The latter option, also known as a ballute, has the advantage of a relatively low mass compared to the rigid aerobrake, but was discarded due to the difficulties in reusing such a configuration. A ballute must usually be jettisoned after usage due to the complications arising from trying to repack an inflatable structure. The rigid option was chosen for its higher performance characteristics, as well as reusability, because it is a permanent feature on the LPIV which needs little refurbishment from mission to mission.

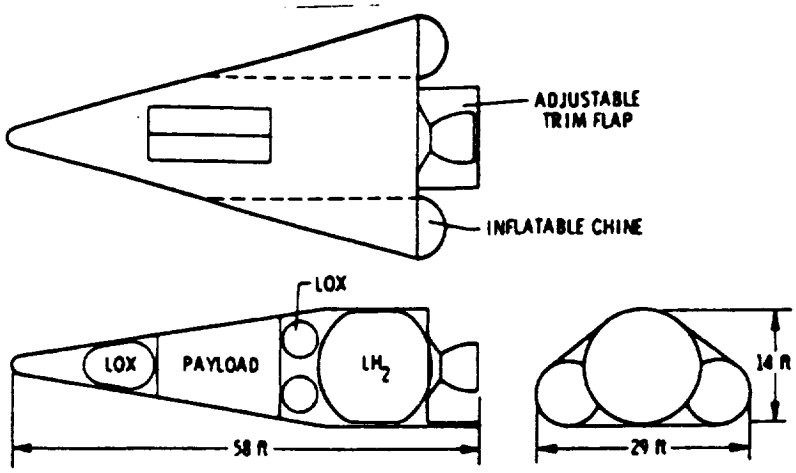

AOTV with high L/D capability

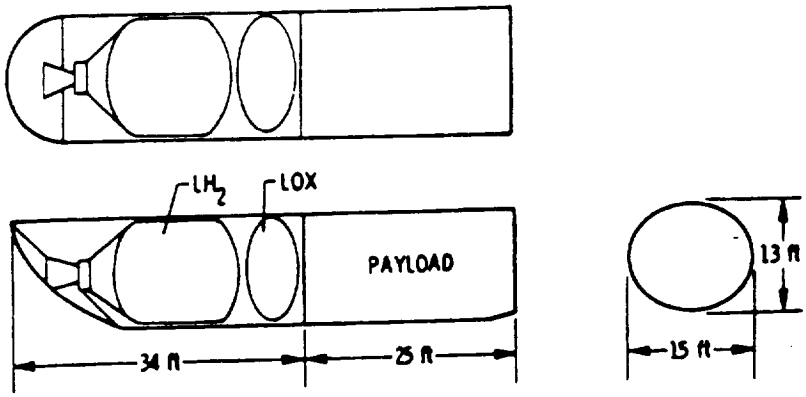

AOTV with moderate L/D capability

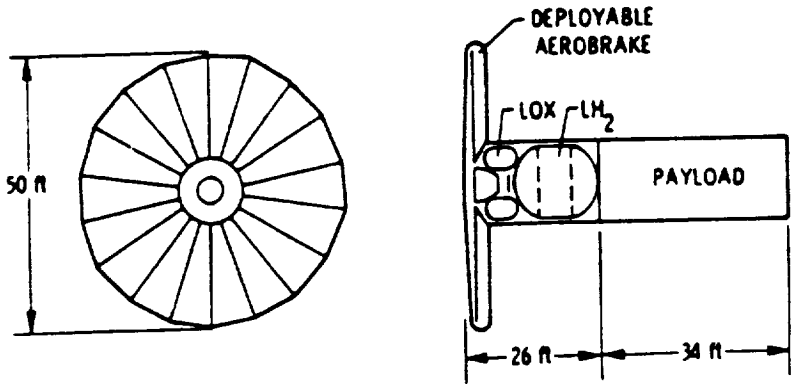

AOTV with low L/D capability

(Ref. Menees, Davies, Scott)

Figure 80. High, Moderate, Low L/D Configuration AOTV's

AEROBRAKE GEOMETRY

Originally, a raked elliptical cone geometry (Figure 81) was chosen due to its excellent aerobraking and aeromaneuvering capabilities. Numerous studies (Ref. Menees, Davies, Scott), have been done on the use of blunted raked conics in aeroassisted flight trajectories, and from these reports exact geometries and aerodynamic capabilities can be obtained. However, by using an asymmetrical shape for the aeroshell, a stable center of mass is difficult to maintain upon rotation of the engines, thereby negating the advantages of the chosen configuration. Therefore, a non-raked elliptical conic was used instead. The equation used for the geometry was

$$\frac{x^2}{25} + \frac{y^2}{289} + \frac{z^2}{289} = 1, \qquad (1)$$

where x is coordinated along the vehicle's primary axis (through the main mirror assembly), and y, z are normal to x. This function creates a smooth surface which is 34 meters in diameter, and 5 meters deep. The nose of the aeroshell is very blunt, thereby reducing stagnation point heat fluxes as well as spreading the temperature and energy distributions more evenly over the surface of the aerobrake. The current geometry is shown in Figure 82.

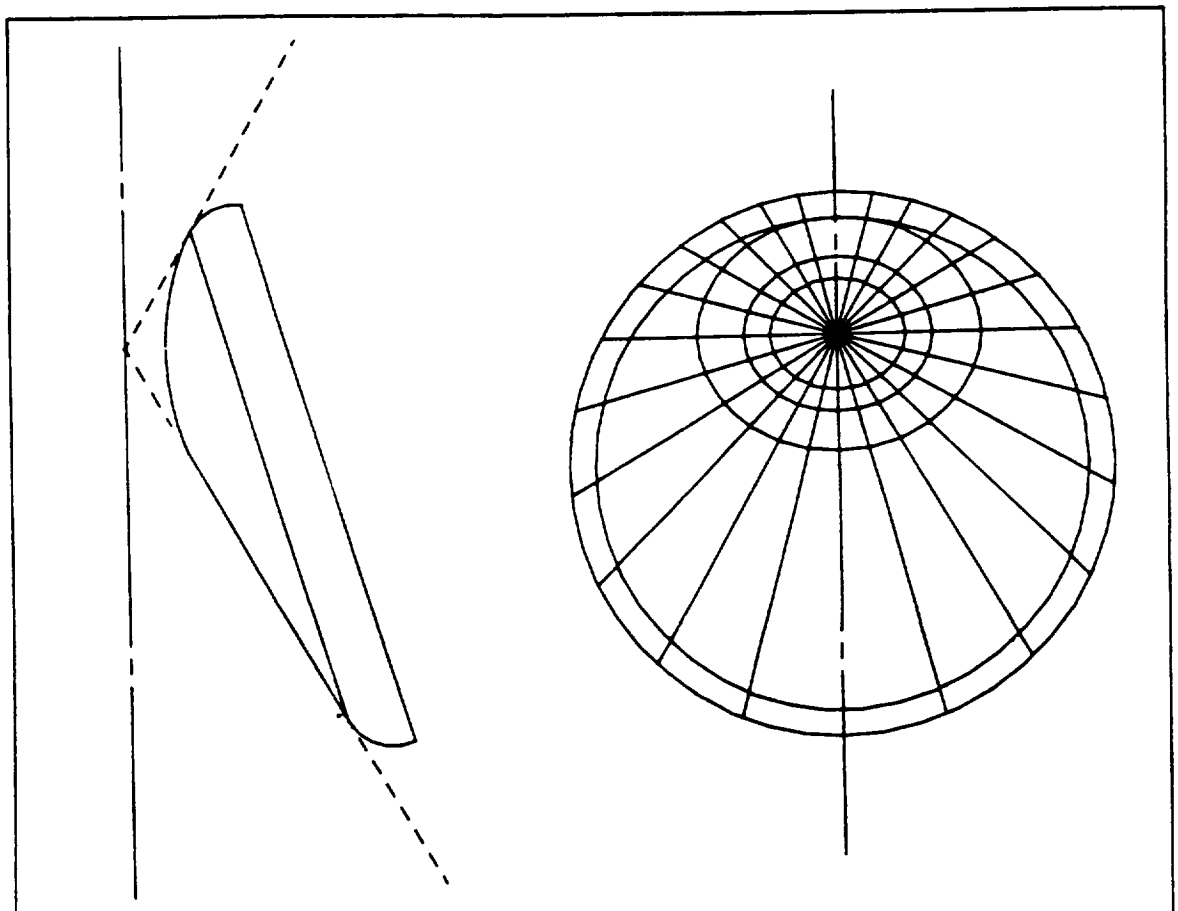

Figure 81. Raked Off Elliptical Cone Aerobrake

The symmetry of this design requires that the aerobrake assembly have tilting abilities, in order to have variable aerodynamic capabilities. This would be done by allowing the aerobrake support truss to pivot slightly about the y axis of the aeroshell. The tilting action will alter the L/D property of the aerobrake by as much as + /- .2.

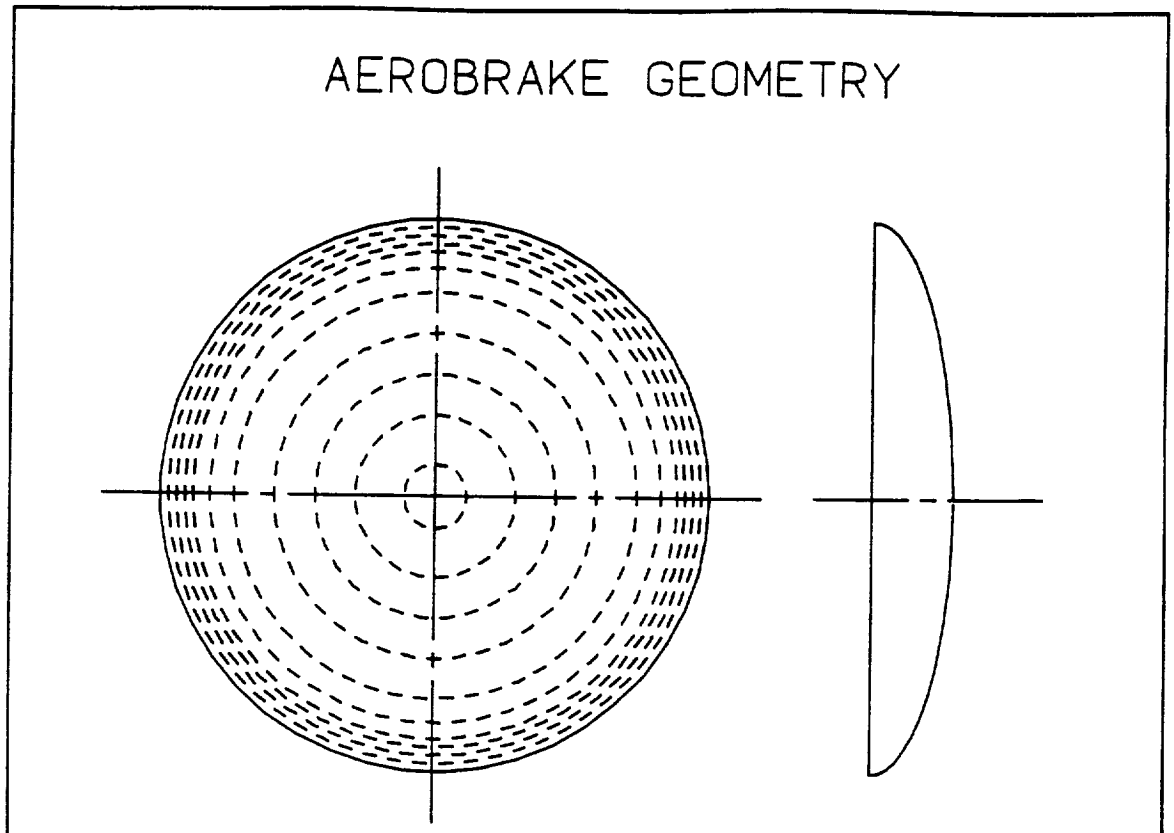

Figure 82. Symmetric Elliptical Aerobrake

AEROBRAKE SIZING

The main requirement which determined the actual size of the aerobrake was that it adequately protect the mirror and truss assembly located behind it. The LPIV vehicle enters the atmosphere at very high velocity (M > 10), causing the air it comes into contact with to heat the vehicle through convective and radiative heat transfer. The increased heating rates and temperatures caused by this viscous layer of gases must be reflected or dissipated by the aerobrake surface. The layer of hot air leaves the aerobrake surface where it expands to form a wake. The air expands off of the edge of the aeroshell at approximately a 15° angle, relative to the angle of attack of the vehicle. The mirror and main truss assemblies must not come into contact with this wake because the resulting temperature increases would cause large deformations in the structures, if not failure.

Initial calculations were done to size the aerobrake for protection of both the mirror and main truss structure. Results yield a diameter of 47 m to adequately protect both structures. The aerobrake was then made to house the payload bay, in effect shortening the length of the LPIV vehicle. By incorporating telescoping capability to the main truss structure, the necessary diameter of the aerobrake is reduced to 34 m, a large reduction in both size and mass. The main truss will retract so that it no longer extends beyond the edge of the aerobrake, and as this process is necessary only during the actual aerobraking stages when there is no laser propulsion, the engines' ability to fire is not interfered with.

AEROBRAKE PLACEMENT

The location of the aerobrake was determined to be aft of the payload storage bay. Placement anywhere else on the LPIV would intervene with the laser beam reception by the mirror, or dis-

ruption of the plasma engines. The aerobrake structure is centered along the thrust axis of the vehicle to maintain symmetric thrusting properties.

AEROBRAKE TRAJECTORY

Any kind of aero-assisted trajectory quickly becomes a very difficult topic for analysis; the calculations must combine standard orbital mechanics with aerodynamics. The vehicle in question first becomes a lifting body when it reaches a position about 122 km above the Earth, where the first traces of atmospheric density are detectable (Figure 83). At this stage, drag and heat fluxes are at a minimum. In fact, most of the deceleration and certainly the maximum heating occurs at perigee of the orbit, where the density is the highest. Most literature place a limit of about 76 km as the minimum altitude an aerobraked vehicle should fly in order to avoid massive convective and radiative heating.

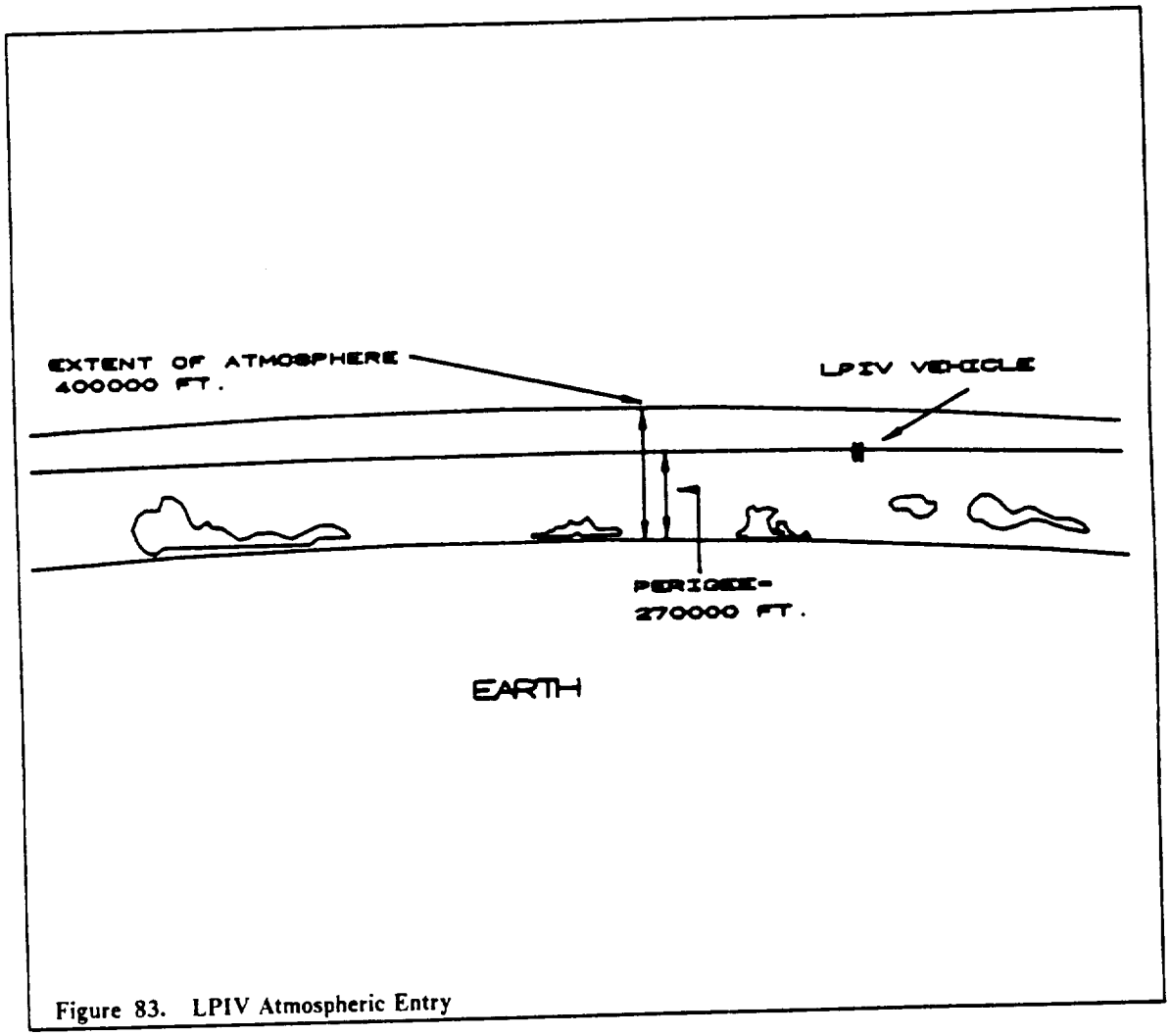

Figure 83. LPIV Atmospheric Entry

In a return orbit from the Earth with a perigee of 82 km, the LPIV vehicle will encounter the Earth's atmosphere at an eccentric anomaly of 9.03°. Its velocity at this point is around 10980 m/s, and begins a velocity and altitude profile which is similar to Figure 84. The entire aerobraking procedure can last from 3 to 12 minutes (Ref. Dauro), depending on such parameters as entrance velocity, flight path angle, and perigee altitude.

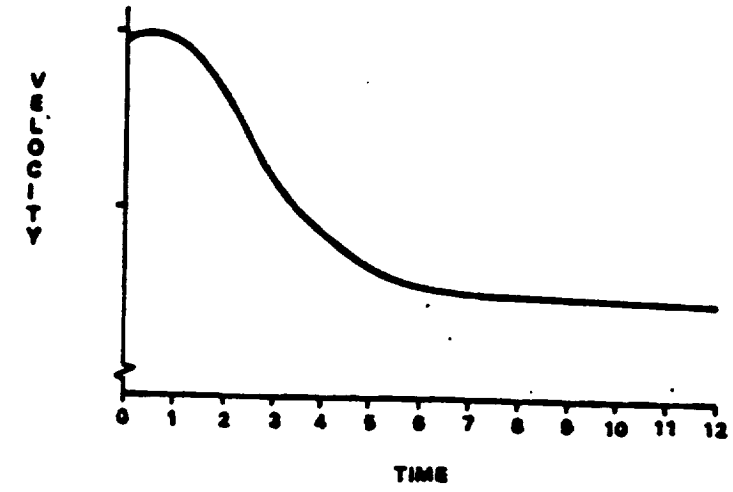

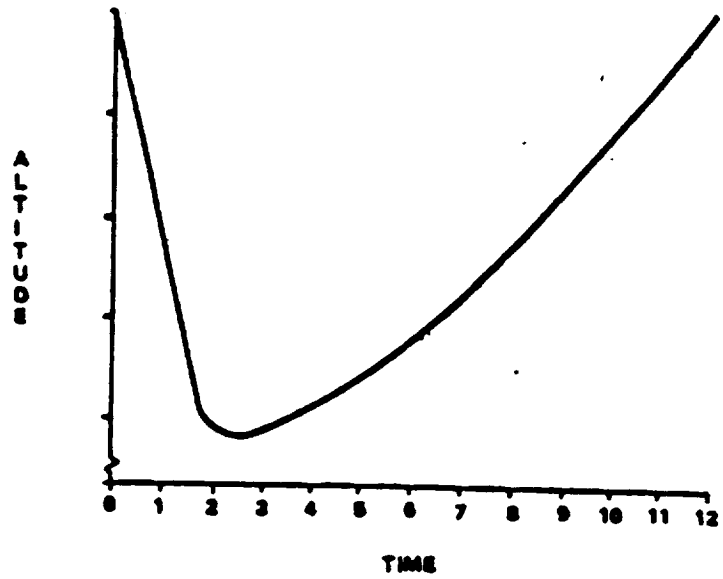

Figure 84. LPIV Velocity/Altitude Profile (Ref. Menees, Davies, Scott)

In order to circularize about the space station in a 220 n mi. (407 km) orbit, the LPIV must exit the Earth's atmosphere with a velocity of 7620 m/s, requiring a reduction in velocity of almost 3350 m/s. Multiple atmospheric passes are possible to obtain the required reduction in velocity with lower heating values, as shown in Figure 85.

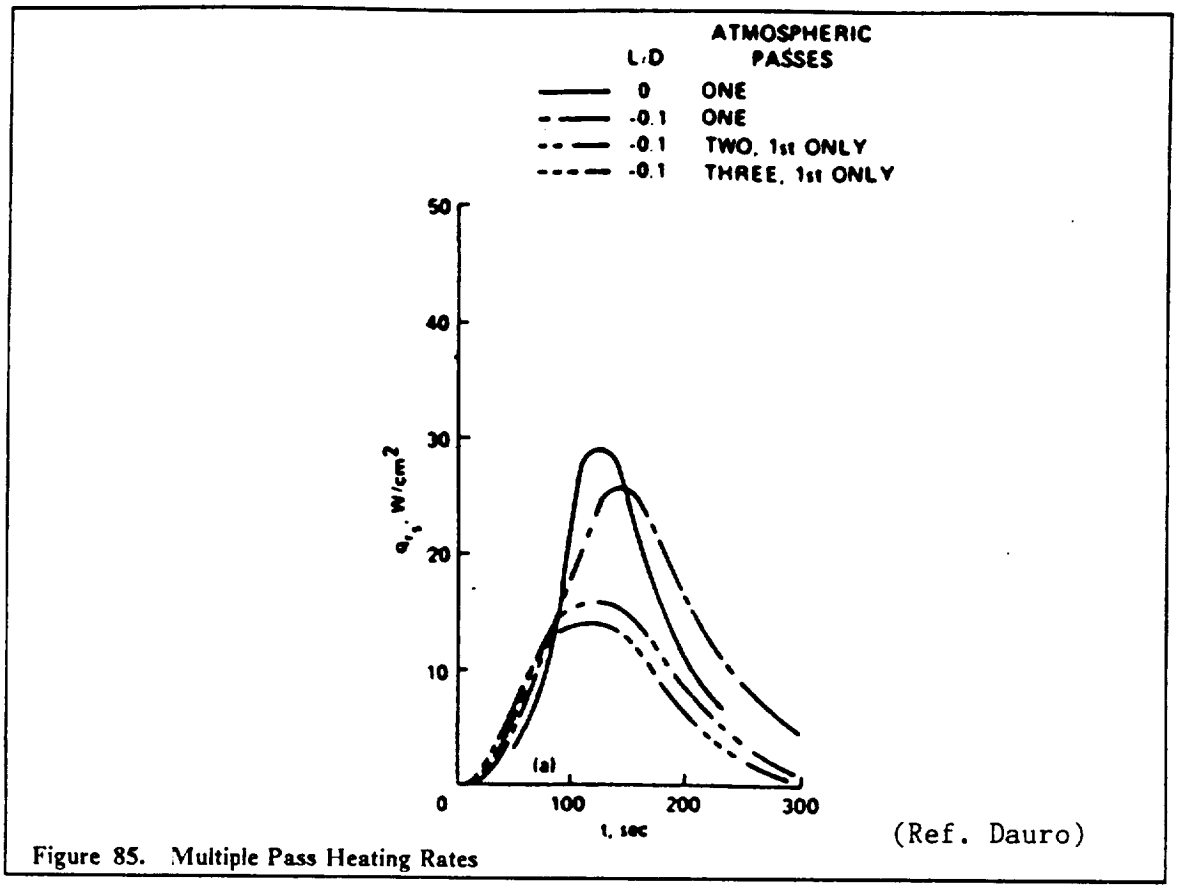

Figure 85. Multiple Pass Heating Rates

AEROTHERMODYNAMIC ANALYSIS

After determining the geometry of aerobrake, corresponding aerodynamic and thermal characteristic properties of the shield were calculated using Newtonian methods. Pressure coefficients along the surface were calculated and plotted using the hypersonic flow relation

$$Cp = 2\sin^2\theta \tag{2}$$

where θ is the angle the outward pointing normal at an element dA makes with the oncoming flow (Figure 86). The resulting pressure distribution is symmetric about the y-axis, and is plotted in Figure 87. Published data showing aerodynamic data for a low L/D version of an aerobrake was used to show performance over a wide range of angles of attack (Table 28). The symmetrical shape means that at $\alpha = 0°$, there is no lift or pitching moment acting on the aerobrake, and the structure must be tilted to give it aeromanuevering capabilities. The L/D ratio is therefore variable, but would be set at a value of .1 ($\alpha = 10°$) during aerobraking to give the best performance characteristics. Aerodynamic properties over varying angles of attack are shown in Figure 88.

These numbers represent rough approximations based on published data; a more detailed analysis was not done due to the complexity of the equations involved, as well as time limitations. They are shown merely to display the probable range of performance abilities which could be expected for such a configuration.

Table 28. Aerodynamic Properties

Performance characteristics at $\alpha = 0°$

L/D = 0.00	$C_{Y\beta} = -.0050/°$
$C_L = 0.00$	$C_{n\beta} = .0023/°$
$C_D = 1.48$	$C_{l\beta} = .0030/°$
$C_M = 0.00$	

Reference Area (area projected onto yz plane)

$$A = 907.92 \text{ m}^2$$

Ballistic Coefficient $(m/C_DA) = 19.83\ kg/m^2$ (based on an estimated mass of 26650 kg = dry mass + payload; no fuel)

The heating analysis was based on published data for aerobraked missions similar to the LPIV's. The majority of heat fluxes acting on the surface of the aeroshell during aerobraking are convective in nature; the highest energy level occurs at perigee of the trajectory, when atmospheric density is the greatest. A preliminary equation was used to first calculate an approximation of the maximum stagnation heat flux, which acts at the center of curvature at the ellipsoidal portion of the aerobrake (Ref. Scott). The equation used is highly dependent on the ballistic coefficient m/C_DA, and is given as

$$\dot{q}_{max} = (1/\sqrt{R_N})7.3(m/C_DA)^{0.467}(L/D)^{-0.242} W/cm^2 \quad (3)$$

Using the previously shown ballistic coefficient, this maximum heating comes out to be 23.0 W/cm^2 , a tolerable amount of energy. A similar equation was used to calculate the heating along the aerobrake trajectory. The surface heat flux distribution is shown in Figure 89, indicating the highest heating rates at the center and outer edge regions of the aerobrake surface.

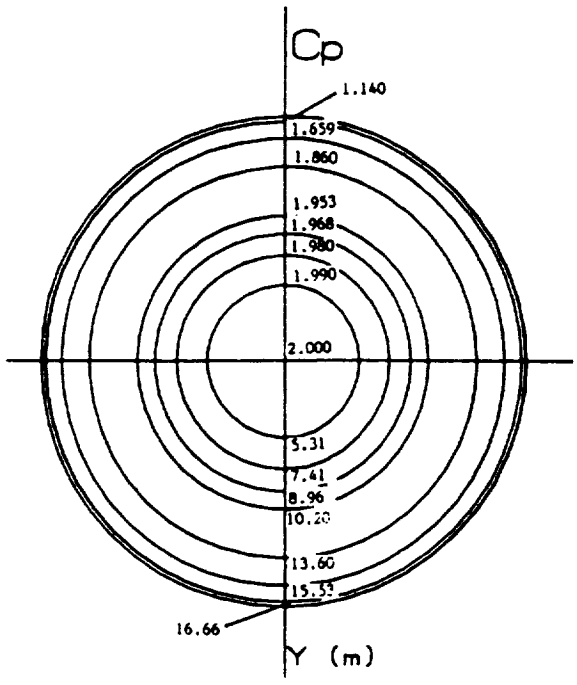

Figure 87. Pressure Distribution

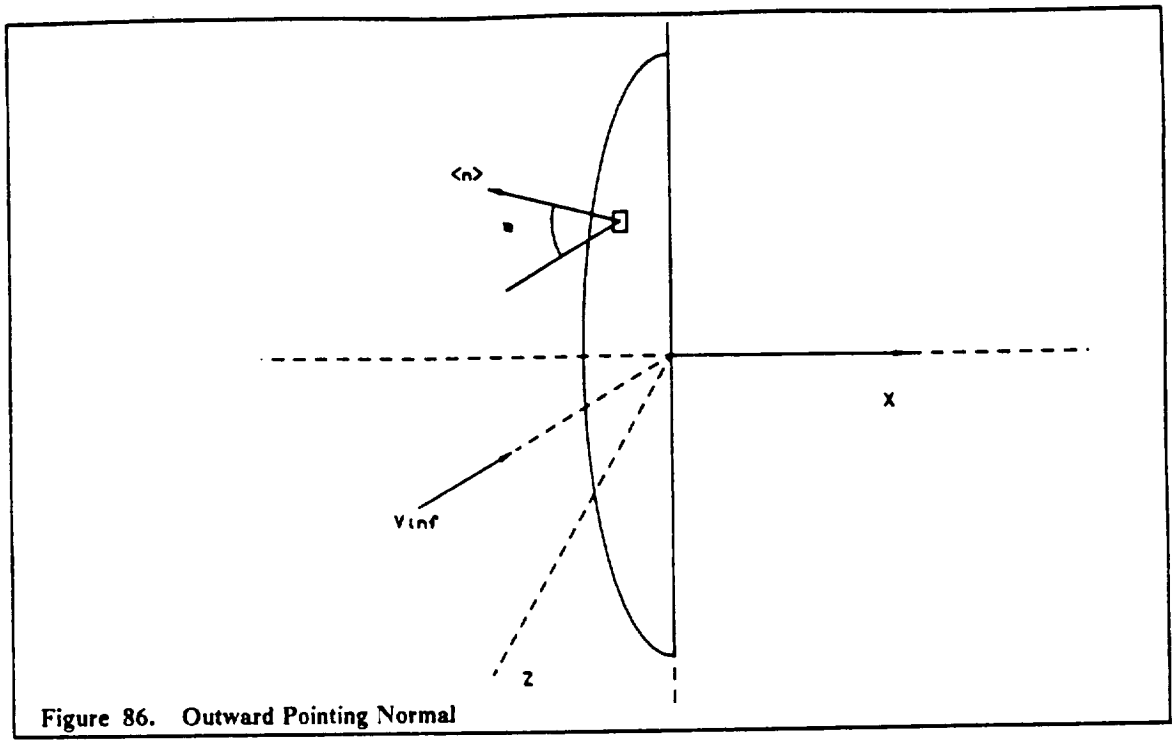

Figure 86. Outward Pointing Normal

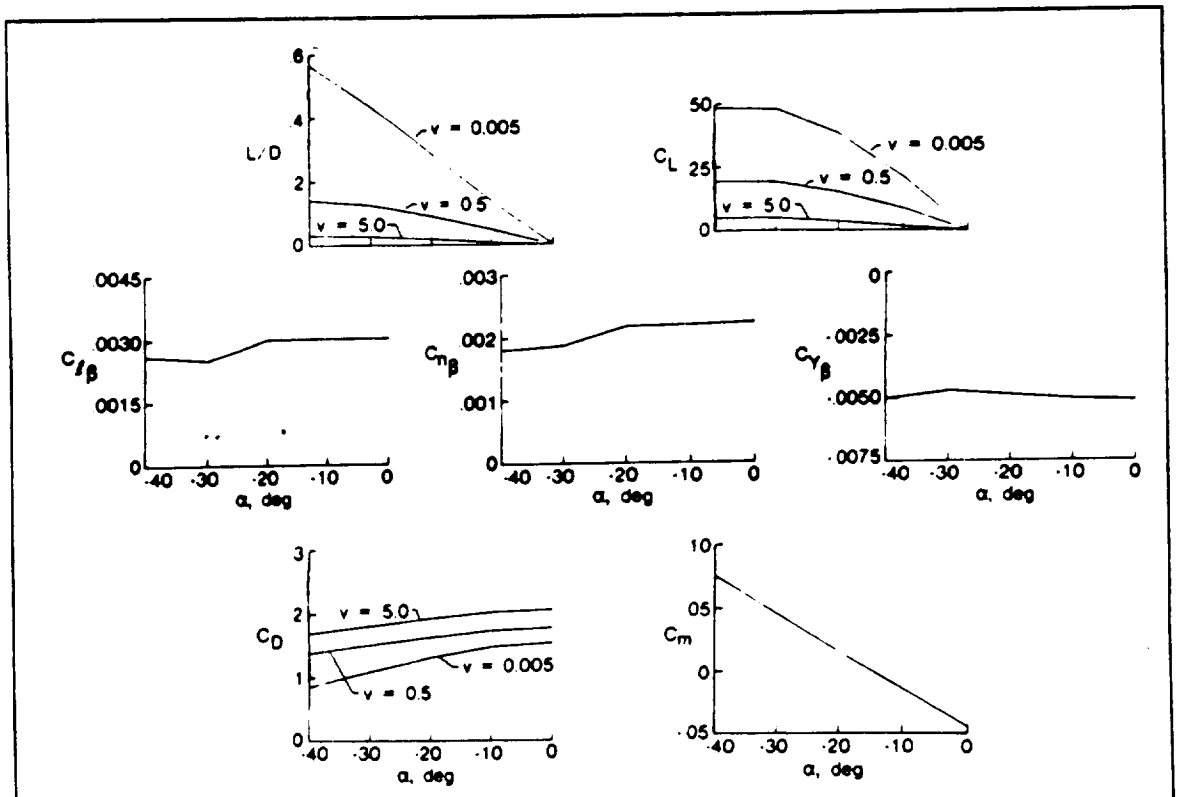

Figure 88. Aerodynamic Performance Tables

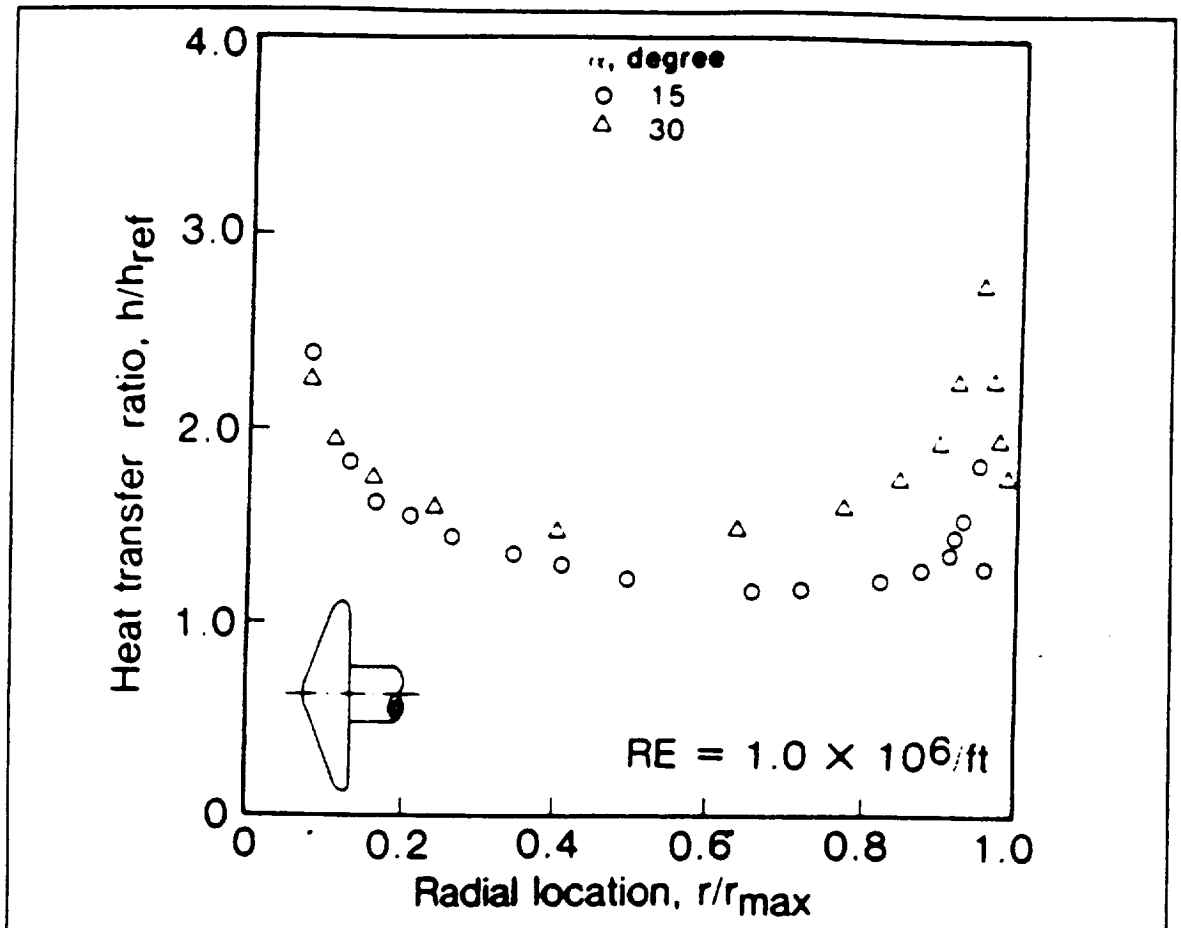

Figure 89. Surface Heat Flux Distribution

AEROBRAKE TRUSS DESIGN

The design for the truss which will serve to support the aerobrake is a simple set of crossing frames based on a similar report done here at VPI (Ref. VPI,1987). The symmetrical features associated with this design allow for the support truss to be made up of only two different frames, which are then repeated in a cross hatched pattern (Figure 90). The truss is designed to match the contour of the inside of the aerobrake surface, as well as provide enough room to store an adequate sized payload within the aerobrake shell. The structure is shown in its components in Figure 91. The truss members are treated as two force members, either in compression or tension loading.

Member Description

Each member of the truss design will be of a graphite epoxy material, a composite undergoing much research and with high hopes of usefulness in space applications. The cross sectional area of each member is .0006967 m^2 , giving a mass of about 1.23 kg/m. This size is adequate to withstand over 6 g's before failing, a condition not likely to occur in this scenario.

Based on the shape of each truss frame and the density of graphite epoxy, a total mass of the truss structure was calculated to be 800 kg, a very acceptable number considering the fuel savings achieved by aerobraking.

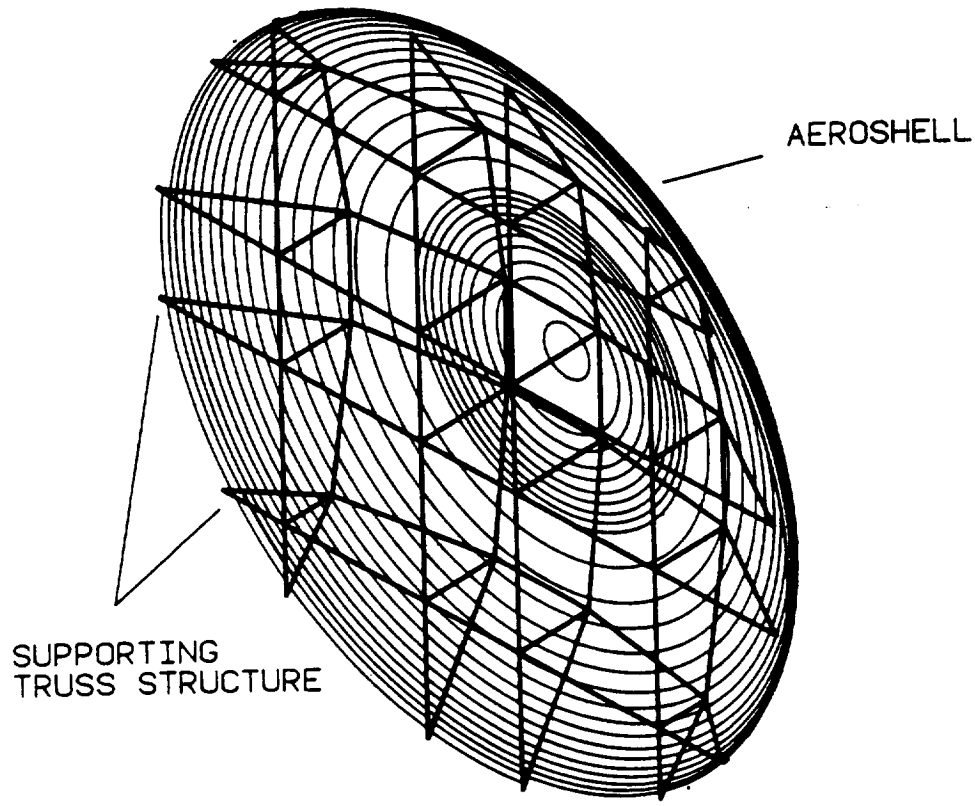

Figure 90. Support Truss Layout

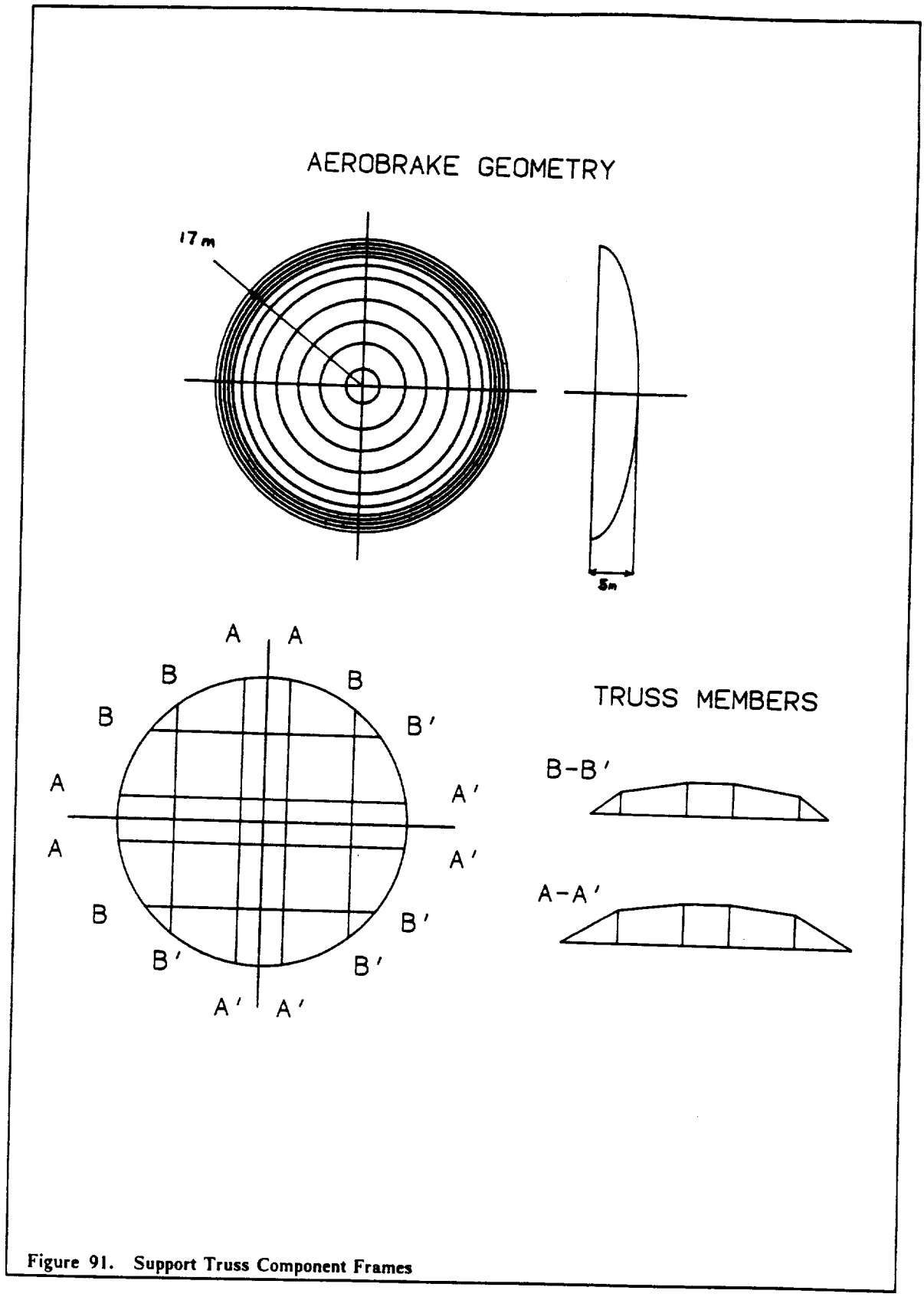

Figure 91. Support Truss Component Frames

Joint Description

The joint which will connect each member to another is the same as used by the 1987 VPI group (Figure 92). It consists of a titanium fitting which is fastened to the end of each member with an adhesive. By using an isotropic material such as titanium, the stress concentrations can be tolerated easier by the fittings than a shaped graphite epoxy end, reducing chances of failure at a joint. The joints are basic revolute pin joints, allowing only one degree of freedom.

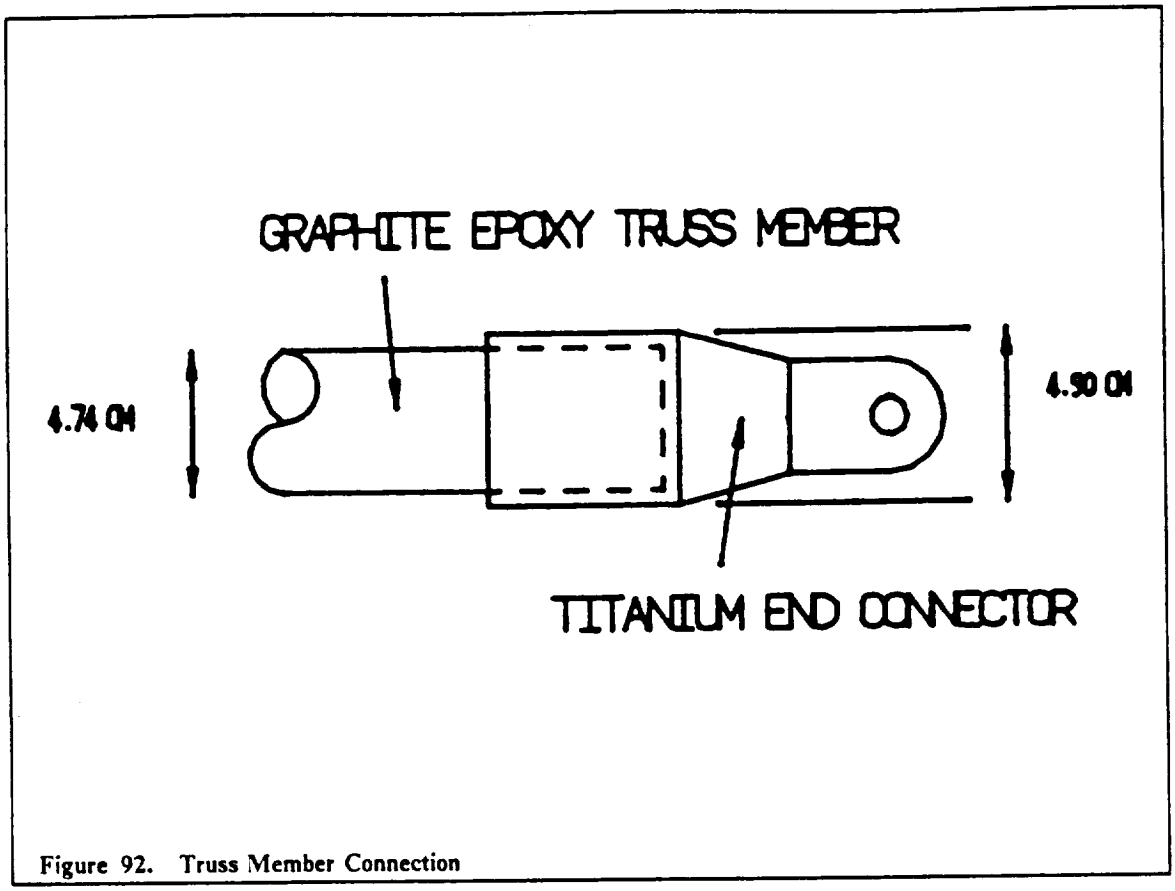

Figure 92. Truss Member Connection

Telescoping Truss

The structure which supports the aerobrake shell was made deep enough so that a payload bay could be located inside the aerobrake itself, thereby helping to reduce the required diameter of the aerobrake. With this configuration, however, comes the problem of payload recovery once docked at the space station. Retrieving the payload canister is difficult since it is now encased within the aerobrake support structure.

This problem is remedied by using a telescoping truss which can be extended once docked at the space station, or in orbit at the moon. The four central support truss members are made up of two concentric cylinders (Figure 93), which are locked into position during flight by a male-female connection (Figure 94). When the time comes for removal of the payload canister, the pins are retracted, and an electrically driven piston located in a cylinder perpendicular to the driveshaft then hydraulically pushes the aerobrake structure out and away from the rest of the LPIV vehicle. There are four such motor/piston assemblies for the aerobrake structure, with a combined power of 32 W. The canister is then exposed for easy removal, and installation of another module can be completed in a short amount of time.

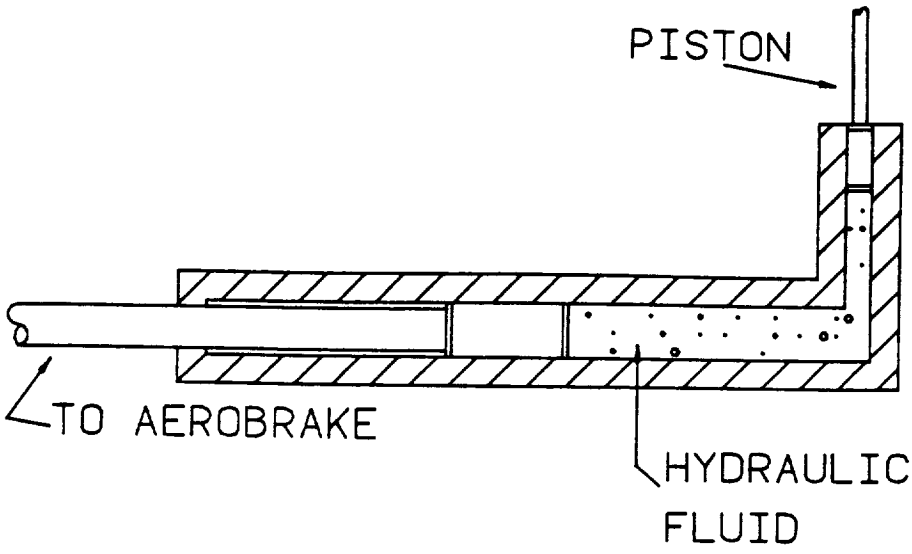

Figure 93. Telescoping Truss Schematic

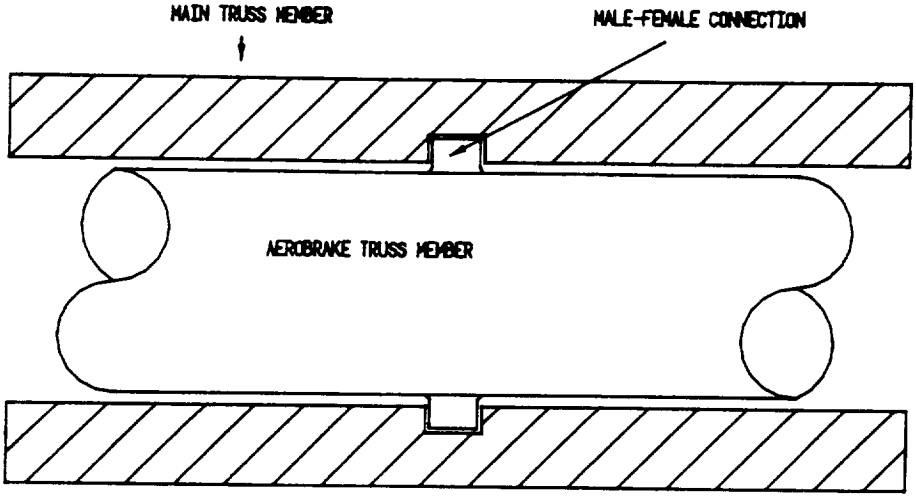

Figure 94. Telescoping Member Connection

Another major modification to the unaerobraked option of the LPIV involves telescoping the main truss during the aerobrake procedure (Figure 95). This action brings the truss and engine assembly in towards the axis of the vehicle, serving to protect the assembly from the expanding wake off the aeroshell, as well as reduce the necessary diameter of the aerobrake to protect the structure. The engines in this position could not be fired, and any required manuevering would have to be done by the RCS systems. Again, the use of small motors would be used to power a flywheel which would cause the telescoping action. The required power of these motors is small, around 3.6 W each.

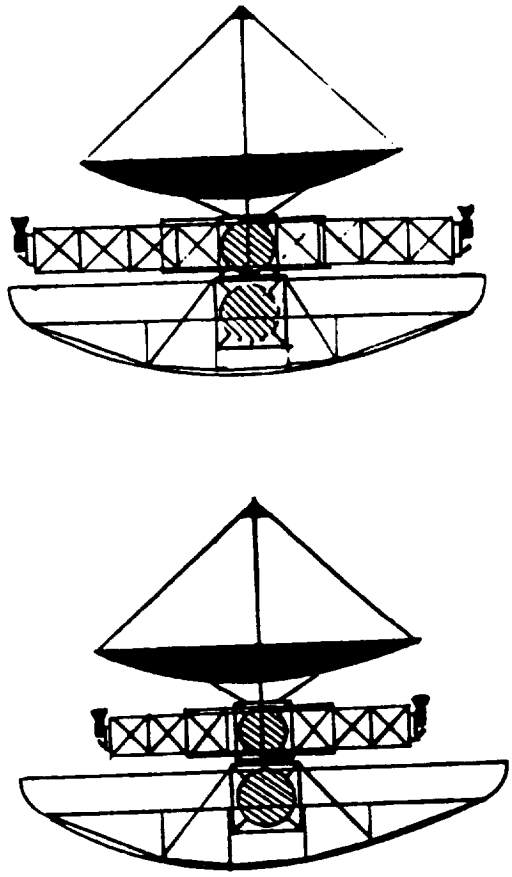

Figure 95. Telescoping Main Truss

RIBBING

The first stage of the thermal protection system, or TPS, is the ribbing which will support the actual covering on the aerobrake, as well as add strength to the existing truss underneath. The beams which will span sections of the aerobrake will need to conform to the shape, as well as withstand the distributed loads acting on them. Using a similar shape designed by the 1987 VPI group, the rib sections will also be made of graphite epoxy and are connected in square 6.8 m blocks, which are then attached to the truss structure in an alternating parallel-perpendicular pattern (Figure 96). The total ribbing assembly has a mass of around 550 kg.

The individual beams are connected at 2 m intervals for parallel sections, and two connections are made at each perpendicular intersection (Figure 96). The connections are L shaped plates made of high grade titanium, in order to withstand the stresses involved in the aerobraking process. This pattern allows for an easy installation/removal process, as well as being modular in nature to facilitate any refurbishment necessary. The members are all small enough so storage and transportation into space via the shuttle is possible.

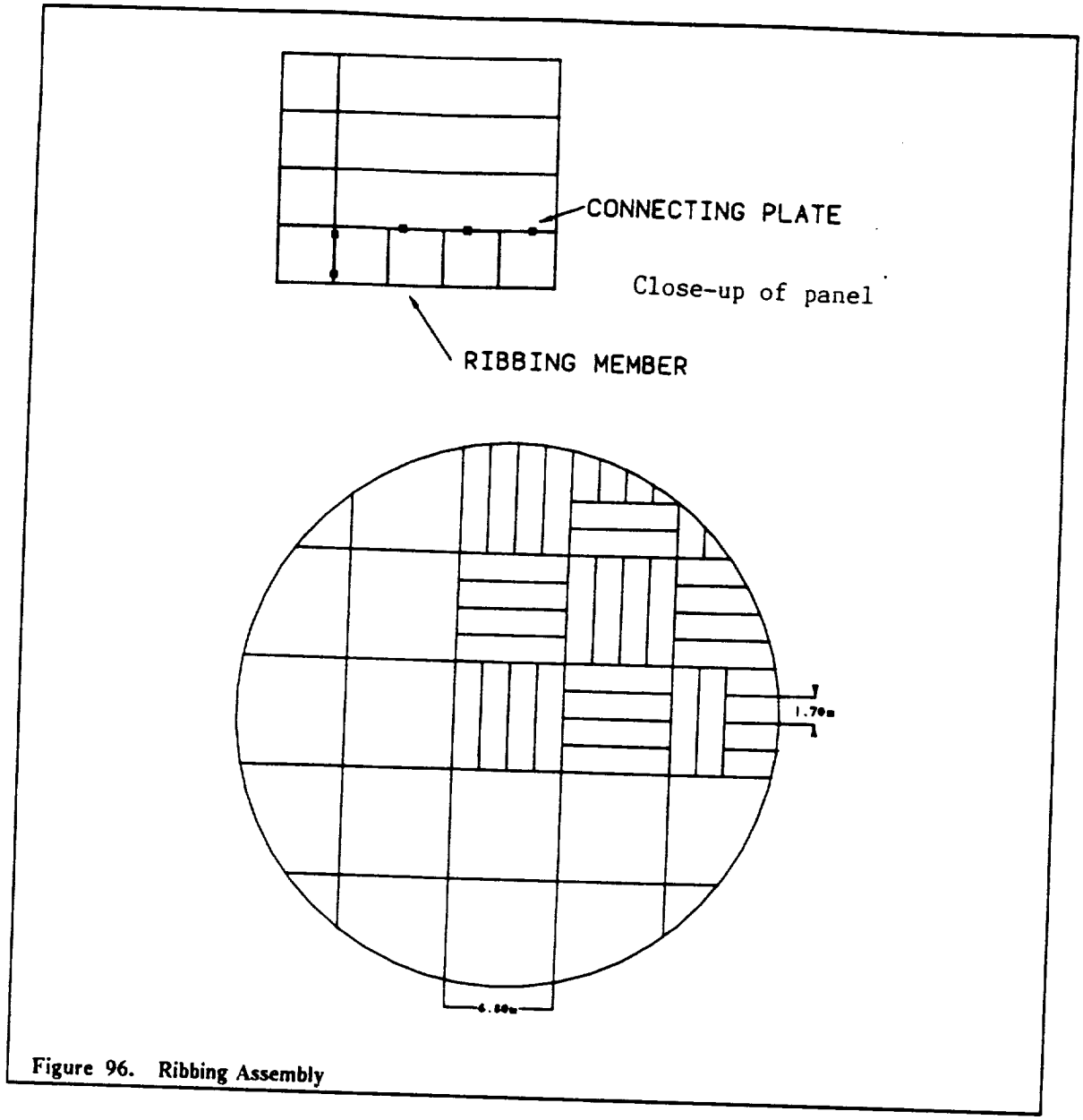

Figure 96. Ribbing Assembly

THERMAL PROTECTION SYSTEM (TPS)

The material which will serve to protect the vehicle from the temperature extremes encountered during aerobraking should be of course able to withstand temperatures on the order of 1500-2000 K, as well as being reflective enough to dissipate a good portion of the radiative heat flux which will also be acting on the surface.

Carbon based materials have exceptional abilities to withstand temperatures, however they are lacking in the area of reflective properties. For this reason, ceramic materials were chosen as the outermost covering on the aerobrake, with a variety of materials underneath, all acting to dissipate the convective energy heating the aerobrake. A prime requirement is that the TPS get rid of enough energy so that the graphite epoxy truss underneath does not fail due to thermal loading.

The current design, modeled after the Mars mission vehicle designed two years ago (Ref. VPI), involves a layered covering over the ribbing; it consists of an outer layer of a highly reflective, heat

resistant material such as the colloidal silica particulate coating used on the space shuttle. Its unit mass is .3378 kg/m^2, giving a mass of about 95 kg. Directly underneath is an insulator such as Nicalon, Nextel, or silica cloth. Nicalon is the best choice due to its heat resistance as well as radiative properties (Ref. VPI). At .1762 kg/m^2, its mass is approximately 50 kg.

The next layer is primarily responsible for protecting the inner structure of the aerobrake. The material should have low thermal conductivity properties, as well as be able to reflect most of the heat acting on it back to the Nicalon layer above it. Possible materials for this layer are Nextel cloth and Q-felt (silica fiber).

The final layer is a membrane stretched over the support structure which serves to absorb any heat from the Q-felt or Nextel layer, as well as radiative heat occurring from the wake behind the aerobrake. The combined layers are shown in Figure 97.

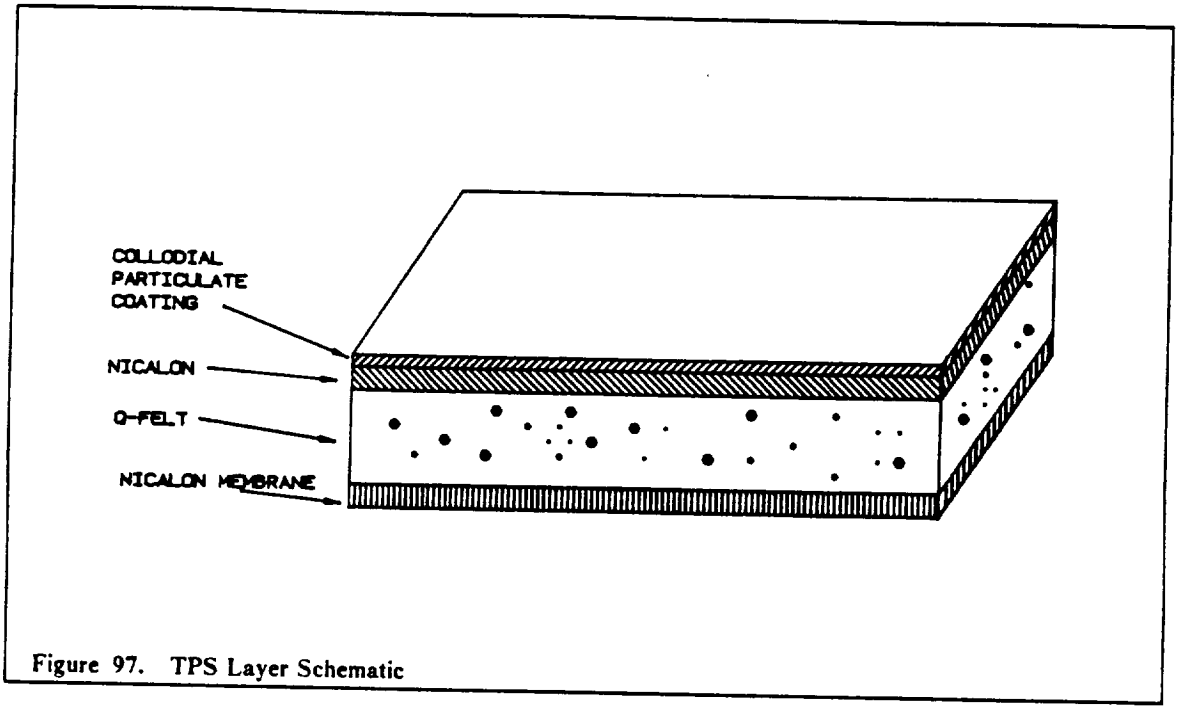

Figure 97. TPS Layer Schematic

TRANSPORTATION AND ASSEMBLY IN ORBIT

The structure is designed so that the largest section would be part of the support truss (about 7.6 m), giving the ability to be broken down and transported into low earth orbit via a space shuttle, where it is then assembled and fitted to the LPIV vehicle. The ceramic shield may be rolled up for transportation, but methods have been suggested in which the cloth is cut into sections which will be joined together in orbit. Presumably there will be existing facilities in space which can handle such construction in space, but most of the fabrication will be done on Earth to minimize the effort required in orbit.

SUMMARY

The use of an existing planetary atmosphere to slow an orbital spacecraft has long been an idea explored by NASA due to the fuel and mass savings which can be taken advantage of with such a procedure. This design uses a very lightweight, durable structure which is large enough to protect some of the more fragile assemblies found on the LPIV from the punishing extremes of an atmospheric entry. Aerobraking is a feasible technique for spaceflight which should be in use within the

next 20 years. This project serves to show such feasibility as well as provide a visualization for the goals set down by this program. Table 29 gives the additional mass of the aerobrake design.

Table 29. Mass Breakdown

Support Truss	800 kg
Ribbing	500 kg
TPS Layers	2200 kg
Total Mass:	3500 kg

ELECTRICAL POWER SYSTEMS

In determining the power source needed for the electrical systems used for the LPIV, photovoltaic solar cells, storage batteries, and fuel cells were considered. The basic requirements considered are a lightweight, dependable power source with high reliability, high energy and power densities, long life, and maintainability. Table 30 provides the power requirements for all the electrical systems to be used on the LPIV.

Table 30. LPIV Electrical Power Requirements

Component	Power (Watts)
Gyroscopes	250
Pointing/Tracking system	200
Turntable motor	15
Main truss telescoping motors(4)	7
Track actuator	5
Communication system	70
Aerobrake telescoping motors(4)	32
Receiver/Preprocessor	25
Range and range rate system	25
Central processor	20
Tracking sensors	20
Total	669 W

Photovoltaic cells have provided the electrical power for almost every spacecraft the United States and the Soviet Union have launched in the first decade of the Space Age. For missions which will be completed in a few weeks or less, primary batteries and fuel cells may be used in space vehicles; however, for missions longer than that, their weight and volume penalties simply become too great (Ref. Angrist). Because of their low individual outputs, solar cells are generally not used singly but are connected in panels or arrays. An optimum power-to-mass ratio of 200 W/kg would require about a 60 m by 4 m panel (Ref. Angrist). This type of array would be much too large to use on our configuration as well as depending too much on solar energy since the maximum amount of solar energy could not be intercepted for our vehicle. Also, a sun sensor and tracking mechanisms would have to be added, thereby adding more mass. Although they have energy densities of up to about 300 W/kg (Ref. Mantell), storage batteries cannot be used since the capacity of a storage battery is governed by the size and weight of electrodes which store chemical energy, which accounts for much of the size and weight of the battery itself (Ref. Mantell). The fuel cell is a form of a storage battery in which the chemical energy is stored as a fuel in a reactant tank outside the cell and is fed to, or removed from, the electrodes when required. The electrodes are not changed in any way when the cell is operated. In this way, the capacity is governed only by the size of the fuel tanks, and the battery size is related only to the rate of conversion or power output. Fuel cells also have longer lifetimes and provide more power (if the power required is greater than 200 W) than storage batteries (Ref. McDougall). Therefore, fuel cells were chosen as the main power source. The fuel cell system will be attached to the main truss behind the beam splitter.

In the 1960s, there was renewed interest in the fuel cell when the space programs required compact power sources. This resulted in the efficient, reliable, and very expensive power systems used with success in the Gemini and Apollo space missions. The cells that have been most extensively developed are those that use hydrogen as their fuel and oxygen as the oxidizer. The highest theoretical

output from such a system is about 3600 W/kg (Ref. Mantell). As an illustration, Allis-Chalmers has successfully developed a liquid-cooled 5000 W fuel cell module for space use (Ref. Mantell). As shown in Figure 98 there is an electrode support or current-carrying plate made of corrosion-protected magnesium. This positions the electrode, serves as a manifold to distribute gas to the electrode area, and conducts current externally.

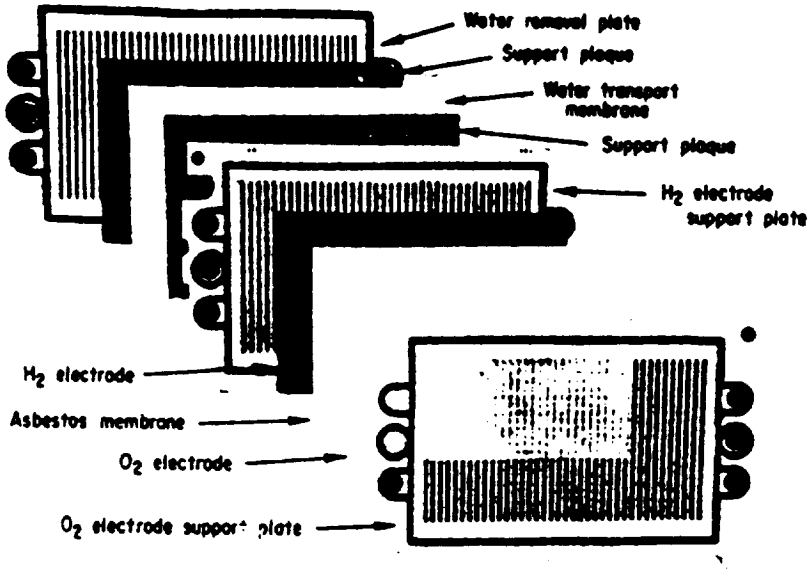

Figure 98. Cell construction (Allis-Chalmers)

The anode is a sintered nickel plaque, catalyzed with a mixture of platinum and paladium. The cathode or oxygen electrode is powdered silver, supported in plastic. The capillary matrix filling the space between electrodes is asbestos saturated with 35 percent potassium hydroxide.

In operation, water must be continually removed. If too much water is removed, the cell will dry up. The components or water removal are water-transport membranes saturated with 45 percent potassium hydroxide (KOH), two porous support plaques, and a plastic water-removal plate similar to the support plate. Two end plates and tie bolts complete a single cell.

Figure 99 is an assembly drawing of a four-cell module.

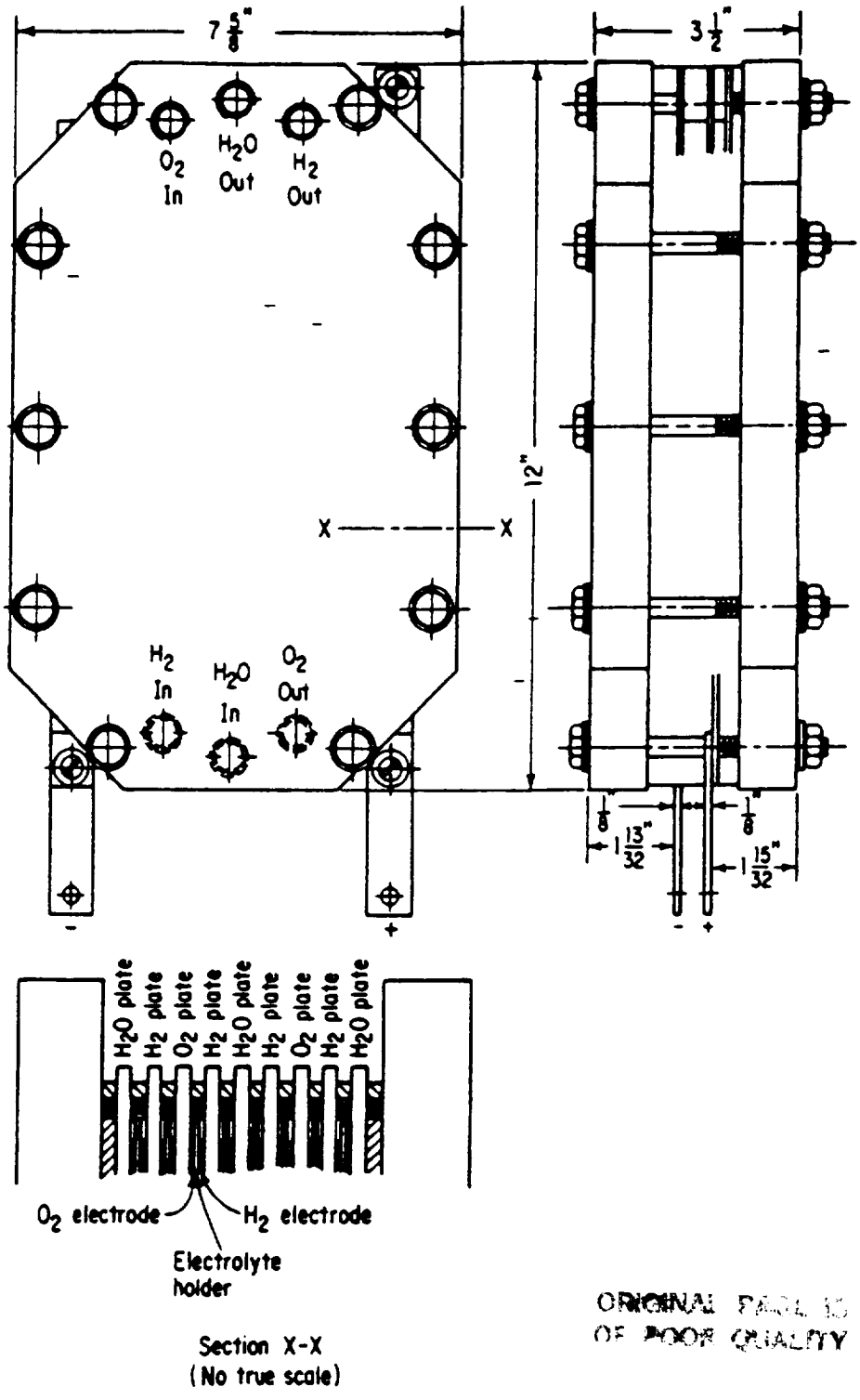

Figure 99. Assembly drawing of a four-cell member

DESIGN SUMMARY

In this report, major design aspects for the LPIV have been addressed. It has been attempted to demonstrate the feasibility of a resuable orbital transfer vehicle of this nature. A highly efficient optical train utilizing dielectrics can effectively transfer the power of a remote laser beam to be used in the creation of a sustained plasma in the engine's chamber. Optimal mission scenarios have reduced the trip time while still maintaining high propellant efficiency. With the promising advances made in composite structural technology, it will be possible to develop a long lifetime structure that will maintain the optical integrity of the vehicle.

The symmetric configuration simplifies the orientation problem for a spacecraft to collect a laser beam from any direction. The spacecraft can perform a two axes maneuver to accomplish proper beam alignment. Additionally, movable propellant tanks allow for a stable center of mass. Without the added mass of fuel oxidizers, the LPIV can ferry significant amounts of cargo readily between low earth and lunar orbits. This is necessary for long term support of the proposed space platforms. The following table summarizes the vehicle and performance characteristics of the LPIV. Further investigation for laser powered orbital transfer vehicles has been demonstrated by our results.

Characteristics of the All-Propulsive LPIV

Propulsion:	
Laser Power	15 MW
Optical train efficiency	94.8
Thermal conversion efficiency	50
Specific Impulse	1500 sec
Propellant flow rate	2 @ 0.033kg/s
Thrust	2 @ 483 N
Masses (kg):	
Vehicle dry mass	12300
LEO to LLO payload	16000
Initial propellant at LEO	35000
Initial propellant at LLO (for return trip)	17784
Overall vehicle loaded	63300
Propellant used for LEO-LLO trip	17216
Propellant used for LLO-LEO trip	14881
Performance:	
LEO-LLO trip time	8 days
LLO-LEO trip time	9 days
LEO-LLO payload mass ratio	.338
LLO-LEO payload mass ratio	.532
Overall structural coefficient	.26

Appendix A

The Multi-Impulsive Elliptical Transfer method

Begin at LEO:

$$V_{cs}=\sqrt{\frac{\mu}{r}} = 7.68522\,\frac{km}{\sec}$$

Period at LEO:

$$2\times\pi\times\sqrt{\frac{R_{LEO}^3}{\mu}} = 88.257\,\min$$

$$120^\circ = \frac{1}{3}\times Period = 29.419\,min = 1765.15\ \sec$$

This is the time of burn assumed using a thrust, T = 900 N assumed to act at perigee.

$$\Delta V = \frac{T}{m_{LPIV}}\times\Delta t = 0.03209 km/\sec$$

$$E = \frac{V^2}{2}-\frac{\mu}{r} = -\frac{\mu}{2\times a}$$

$$\Delta E = \frac{\Delta V^2}{2}-\frac{\mu}{r}$$

$$h = r_p\times v_p = r_a\times v_a$$

$$e = \sqrt{1+\frac{2\times e\times h^2}{\mu^2}}$$

Using the equivalent impulsive thrust, centered at perigee, successive ΔVs were applied to the trajectory. The results yielded 17 ellipses for the transfer orbit to GEO. Assuming close to circular speed, a miminimum energy impulsive thrust was applied to reach a lunar intercept by a Hohmann transfer including a circularization burn.

$$E_t = \frac{-\mu}{r_1+r_2}$$

$$V_1 = \sqrt{2\times\frac{\mu}{r_1}+E_t}$$

$$V_{cs1} = \sqrt{\frac{\mu}{r_1}}$$

$$\Delta V = V_1 - V_{cs1}$$

$$TOF = \pi\times\sqrt{\frac{a_t^3}{\mu}}$$

(Ref. Baite, Mueller)

The Stepwise Spiral Approximation

Initial Conditions:

$$r(0) = r_o$$

$$\phi(0) = 0$$

$$\dot{r}(0) = 0$$

$$\dot{\phi}(0) = \sqrt{\frac{\mu\gamma}{r_o^3}}$$

$$M(0) = M$$

Thrust force and equations of motion:

$$F_r - M_t g_r + M_t r\dot{\phi}^2 - M_t\ddot{r} = 0$$

$$F_\phi r - \frac{d}{dt}(M_t r^2\dot{\phi}) = 0$$

Replacing one revolution of a spiral by a circle of average radius, the total energy gained on this circle is given by:

$$\Delta E = F\Delta s = F(2\pi r)$$

Then, $E = E_{kin} + E_{pot} = \frac{1}{2} M_t g_r r$

therefore, $\Delta E = \frac{1}{2} M_t g_r \Delta r$

where; $\Delta r = \frac{4\pi r F}{M_t g_r}$

or, $\Delta r = \frac{F4\pi}{M_t \mu\gamma} r^3$

The time for one revolution of the spiral is:

$$\tau_r = 2\pi\sqrt{\frac{r^3}{\mu\gamma}}$$

trajectory with initial conditions:

$$\dot{r}(0) = \frac{\Delta r}{\tau_r} = 2\frac{F}{M_t}\sqrt{\frac{r^3}{\mu\gamma}}$$

and

$$\dot{\phi} = \sqrt{\frac{\mu\gamma}{r^3}}$$

(Ref Stulhinger)

Appendix B

Shock Absorbers

To analyze the shock of impact, a set of angular and rectilinear springs and dampers were modeled and the values of the spring constants and damping factors computed by use of the following equations (Ref. Ih):

angular stiffness and damping:

$$K_A = \omega_A^2 \left(\frac{I_1 I_2}{I_1 + I_2} \right)$$

$$D_A = 2\eta_A \omega_A \left(\frac{I_1 I_2}{I_1 + I_2} \right)$$

linear stiffness and damping:

$$K_L = \omega_L^2 \left(\frac{M_1 M_2}{M_1 + M_2} \right)$$

$$D_L = 2\zeta_L \omega_L \left(\frac{M_1 M_2}{M_1 + M_2} \right)$$

where:

$M_1 \wedge I_1 = LPIV$ *mass & inertia*

$M_2 \wedge I_2 =$ *space station mass & inertia*

$K_A \wedge K_L =$ *angular & linear spring constants*

$D_A \wedge D_L =$ *angular & linear damping factors*

$\omega_A \& \omega_L =$ *angular & linear natural frequencies*

$\zeta_A \& \zeta_L =$ *angular & linear damping ratios*

Using (Ih):

$$\omega_A = 0.003 Hz$$

$$\omega_L = 0.030 Hz$$

$$\zeta_A = 0.707$$

$$\zeta_L = 0.707$$

$$I_1 = 5.561 x 10^6 kg - m^2$$

$$I_2 = 5.259 x 10^6 kg - m^2$$

$$M_1 = 6.070 x 10^4 kg$$

$$M_2 = 2.535x10^6 kg$$

gives:

$$K_A = 24.331N - m/radians$$

$$D_A = 1.147x10^4 N - m/radians/s$$

$$K_L = 53.352N/m$$

$$D_L = 2.515x10^3 N/m/s$$

Appendix C

Determination of Precession Angle

Given two angles at which the LPIV must be oriented within a single time step, the acceleration, and ultimately, the torques needed to achieve this orientation may be determined.

θ_1 = initial angle of orientation

θ_2 = final angle of orientation

I_x = moment of inertia about axis of rotation

ω_x = angular rotation rate about axis

α_x = angular acceleration about axis

δt = time step size in seconds

Using the basic kinematic equation :

$$\theta_2 - \theta_1 = \omega_x \times \delta - t + 0.5 \times \alpha_x \times \delta - t^2$$

From this we obtain:

$$\alpha_x = 2 \times \gamma\theta_2 - \theta_1 - \omega_x \times \delta - t/\delta - t^2$$

This is the formula used to compute the angular accelerations needed to be undergone by the LPIV at each time step. These accelerations are used again in the calculation of the necessary torques and the precession angles associated with applying them. Torque about the axis = $\alpha_x \times I_x$ Precession angle, ϕ_2, is determined using the angular rate and acceleration previously computed, plus the previous precession angle, ϕ_1:

$$\phi_2 = \phi_1 + \omega_x \times \delta - t + 0.5 \times \alpha_x \times \delta - t^2$$

It is also important to update the angular rotation rate at each time step:

$$\omega_2 = \omega_1 + \alpha_x \times \delta - t$$

Using these basic equiations the precession angles of the gyros for the entire voyage may be calculated.

Sizing of Desaturization Rockets

Assuming that the fuel for the RCS rockets is chosen, and therefore the specific impulse is known, it is a simple matter to determine the mass flow and thrust levels of an RCS system capable of desaturating the CMG's. Preliminary analysis of the minimum thrust level needed to completely desaturate the CMG's within one shadow period showed a thrust level of less than five Newton's. To satisfy the requirement that the RCS be in some way capable of translating the LPIV, the thrust

level chosen is five Newtons. Knowing both the thrust and the specific impulse, the mass flow of both the roll and yaw rockets is determined by:

$$\dot{m} = \frac{T}{(I_{sp} \times g)}$$

The total mass of propellant used in desaturization is determined by the amount of time the rockets are thrusting. The angular acceleration equals the torque divided by the moment of inertia. From this data, the time is determined:

$$-(max.precession) + \omega_x \times 3{:}03\ a.m. + 0.5 \times \alpha_x \times 3{:}03\ a.m.^2$$

The time is computed by solving for the quadratic roots.

Appendix D

Tank Dimensions and Mass

Mass of LH_2 required = 35,000 kg
Density of LH_2 = 70.8 kg/m^3
Volume req'd = Mass/Density = 494.35 m^3
For spherical geometry:

$$V = \frac{4}{3}\pi R^3$$

$$S = 4\pi R^2$$

Thus for two spherical tanks $V_{pertank} = \frac{1}{2} V_{total}$

By simple algebra
R = 3.9 m
D = 7.8 m
S = 383.3 m^2

Using the data for the Al 2090 (Ref. Torre):
E = 7.584 x 10^4 MPa
σ_{ult} = 2.237 x 10^4 MPa
Density = 2547 kg/m^3

For the spherical tank:

$$\frac{\sigma_{max}}{F.S.} = \frac{pr}{2t}$$

where
σ_{max} - maximum allowable stress
p - tank pressure (5 psia)
r - radius of tank (3.89 m)
t - tank thickness
FS - factor of safety (1.5)

Solve t = .00117 m or 1.17 mm

Mass of tank = Total surface area x thickness x Density
= 1125 kg

Insulation Dimension and Mass

Given the condition of 1 percent total boiloff from 35,000 kg of fuel, the heat flux $\dot{q}$ for this boiloff to take place is calculated using

$$M_{vf} = \frac{\dot{q}\theta}{h_{fg}}$$

where

M_{vf} - mass of fuel vented (1 percent of 35,000kg or 350kg)
θ - length of mission (15 days)
h_{fg} - heat of vaporization of LH_2 (499 kJ/kg)
$\dot{q}$ - total heat transfer

solving $\dot{q}$ = 135 W

Calculating the heat flux due to solar radiation on the tank:

$$\dot{q} = Aq''\varepsilon$$

where

$\dot{q}$ - total heat flux to the tank
A - area of tank expose to solar radiation(191.7 m^3)
q"- solar radiation constant (1400 W/m^2)
ε - emissivity of tank (0.06 since the paint is 94 percent reflective)

solving $\dot{q}$ = 16 kW

Using the Stefan-Boltzmann law to find the temperature on the surface of the tank

$$\dot{q} = \sigma A T^4$$

where

$\dot{q}$ - total heat flux (16000W - 135W = 15,865W)
σ - Stefan-Boltzmann constant (5.67 $x10^{-8}$ W/m^2K^4)
A - area expose to solar radiation (191.7 m^2)
T - absolute temperature

solving T = 195 K and let this be the temperature beneath the paint surface

The MLI thickness can then be determined from the equation:

$$\dot{q} = \frac{kA(T_1 - T_2)}{t}$$

where

$\dot{q}$ - heat flux
k - thermal conductivity of the insulation (0.03 W/m*K)
A - area expose to solar radiation (191.7 m^2)
T_1 - temperature of the tank surface (195K)
T_2 - interface temperature of the MLI/foam (144K)
t - thickness of MLI required

Note that this equation was derived for the MLI/foam scheme assuming the temperature of the liquid hydrogen to be 21K.

Solving for t_{MLI} = .0184 m or 1.84 cm

The nominal ratio of t_{foam}/t_{MLI}(nominal) = 0.1

thus t_{foam} = 0.184 cm
Density of MLI = 35.08 kg/m^3
Density of Rohacell foam = 30.0 kg/m^3
Mass of insulation = $SurfaceArea_{total} \times (t_{foam} \times density_{foam} + t_{MLI} \times density_{MLI})$
= 268 kg

Mass of Structures

Density of graphite/epoxy = 1685 kg/m^3
Density of S-glass/epoxy = 2490 kg/m^3

Mass of member = $\pi(R_2^2 - R_1^2) \times length_{member} \times Density_{member}$ where
R_2 - outer radius
R_1 - inner radius

Table 31. Tank Structures and Track Mass Calculations

	No. members	r2 (cm)	r1 (cm)	l (m)	Total Mass (kg)
Fuel tank support:					
Graphite/epoxy	12	6.8	6.0	8	520
S-glass/epoxy	24	5.6	4.9	5.5	760
Fuel tank platform:					
Graphite/epoxy	4	6.8	6.0	8	170
Graphite/epoxy	4	6.8	6.0	5.65	120
Track system estimate:					
Graphite tracks	4	X-Area =	6cm^2	8	300
Screw track	2	8	7.5	8	150
				Grand total mass	2020

Power Requirements

For the actuator, the power calculation is done in the case which would require the actuator to do the most work. This is when the tank is full and must be moved opposite the direction of acceleration of the LPIV at 1 mm/s along the track. This speed is selected, which is considered fast by operating standard, so the tank will be able to move along the entire track in less than two hours for servicing purpose.

Total Mass to be moved = approx. 20,000 kg
Maximum acceleration of LPIV = Thrust/Mass
= 1000N/60,000kg = .016667 m/s^2
F = Ma
Velocity at which tank must be moved = 0.001 m/s
Power = Force*Velocity = 5 W or 10 W for two actuators

For the fuel pump, the power requirement was calculated using the equation:

$$HP_{input} = \frac{QH \times SG}{K}$$

where
HP - horsepower input
Q - delivery ($\dot{m}_{fuel}$ = 0.0681 kg/s)
H - total head on delivery side
SG - specific gravity of fuel (70.8 kg/m^3)
K - constant (= 33 for Q in gal/min and H in ft)

The head was calculated given that the pressure must be boosted from 0.3atm to 20 atm. The calculated head was determined to be 9.8 ft. Note that all units must be converted into English

units before the equation can be employed. Solve HP = 1.73 hp or 1.29 kW for each turbopumps or a total of 2.6 kW.

REFERENCES

AAAS/AAS Special Astronautics Symposium, Berkeley, Calif., 1965. Recent Developments in Space Flight Mechanics, vol 9.

Angrist, Stanley W. Direct Energy Conversion, Fourth Edition. Allyn and Bacon, Inc. Boston. 1982.

Ayers, Schuyler R., Morel, Donald E., and Sanborn, James A., "Development of Composite Facets for The Surface of a Space-based Solar Dynamic Concentrator".

Bate, Roger and Mueller, D. *Fundamentals of Astrodynamics*. Dover Publications, New York, NY. 1971.

Belew, "Skylab", U.S. Government Printing Office, Washington, D.C.

Bendix, Guidance Systems Division, "Double Gimballed CMG's".

Boutemy, J. C. "Use of CCD arrays for Optical Link Aquisition and Tracking" Optical Systems for Space Applications. vol. 810, no. 34, April 1987.

Boyce, W. E. and DiPrima, R. C. *Elementary Differential Equations and Boundary Value Problems*, John Wiley & Sons, New York, NY. 1986.

Burns, G., "Space Platform Advanced Technology Study," NASA Report, N81-20146, 1981.

Cerimele, Christopher: A Simplified Guidance Algorithm for Lifting Aeroassist Orbital Transfer Vehicles. NASA, Houston, Texas, 1984.

Chapman, D.R. "An Approximate Analytical Method for Studying Entry Into Planetary Atmosphere", NACA TN 4276, 1956.

Cheatwood, F. McNeil, et al. "Geometrical Description for a Proposed Aeroassist Flight Experiment Vehicle", NASA Technical Memorandum 87714, 1986.

Dauro, V.A. "Aerobraking", Marshall Space Flight Center, 1979.

Davies, C.B., Park, C. "Aerodynamic and Thermal Characteristics of Modified Raked Off Blunted Cone", AIAA-86-1309, 1986.

Dursch, H., Hendricks, C., "Development of Composite Tube Protection Coatings," Boeing Aerospace Co., 1986.

Dursch, Harry W. and Hendricks, Carl. L., Protective Coatings for Composite Tubes in Space Applications," NASA report N87-18669, 1987.

Ebwright, R. N. et al., Conceptual Design and Analysis of Orbital Cryogenic Liquid Storage and Supply System. NASA Report N81-25118. May 1981.

Escobal, P.R. *Methods of Orbit Determination*. New York, John Wiley and Sons, Inc. 1965.

Evans, B.G. Satellite Communication Systems. Peter Peregrinns Ltd., London, United Kingdom. 1987.

Fleischman, G.L., Peck, S.J., Tanzer, H.J., "Advanced Radiator Concepts Utilizing Honeycomb Panel Heat Pipes," Hughes Aircraft Co., NASA Report N87-12747, 1987.

Goodger, E.M., "Principles of Spaceflight Propulsion", Pergamon Press, Oxford, 1970.

Graham et. al., "Range and Range Rate System," NASA Report, N87-22708, May, 1987.

Grigull, U., and Sandner, H., Heat Conduction, Hemisphere Publishing Corporation, Washington, 1984.

Gruwald, A. J. and Ellis, S. "Interactive Orbital Proximity Planning System", NASA Technical Paper 2839, Ames Research Center, Moffet Field, California. 1988.

Hacker, G. "System Considerations for an Optical Intersatellite/ Interorbit Link Based on Nd: YAG Laser Technology, Optical Systems for Space Applications. vol. 810 no. 24. April 1987.

Hamilton, H.H., Weilmuenster, K.J. "Calculation of Convective Heating on Proposed Aeroassist Flight Experiment Vehicle", AIAA-86-1308, 1986.

Herada, Yoshiro, Space Stable Thermal Control Coating. NASA Report N83-17711. November 1982.

Holman, J. P., Heat Transfer, McGraw-Hill Book Company, New York, 1986.

Ih, Che-Hang C., Wang, S.J., "Dynamic Modeling and Adaptive Control for Space Stations," NASA Report, N86-16251, 1986.

Irvine, Thomas B., Nall, Marsha M., and Seidel, Robert C. "Solar Dynamic Power Systems for Space Station," NASA/DOD Technology Conference, Nov. 18-21, 1986.

Jones, J. B. et al. Engineering Thermodynamics. John Wiley & Sons, Inc: New York, 1986.

Katzman, Morris. Laser Satellite Communications. Prentice-Hall, Inc., Englewood Cliffs, NJ. 1987.

Kempster, K.B., Babel, H.W., "Space Station Truss Strut tube Design," AIAA SDM Issues of the International Space Station, 1988, p.3.

Kern, R. U. Kugel, E. Hettlage, "Control of a Pointing, Acquisition, and Tracking Subsystem for Intersatellite laser Links ISL2" Optical systems for Space Applications. vol. 810

Korites, B. J. Structural Analysis Software for Microcomputers," Kern International, Inc., 1975.

Korites, B.J., "Structural Analysis Software for Micros," Kern International, 2nd ed., 1987.

Korsmeyer, D. "Trajectory Determination and Characterization of a Cislunar Low-Thrust Spacecraft." Large Scale Programs Institute, Austin, Texas. 1987.

Kramer, T.J. et al., Evaluation of Propellant Tank Insulation Concepts for Low-Thrust Chemical Propulsion Systems. NASA Report N84-20634. April 1984.

Mahaney, J., Thornton, E.A., Dechaumpai, P., "Integrated Thermal-Structural Analysis of Large Space Structures," Presented at the symposium on Computational Aspects of Heat Transfer in Structures, NASA LaRC, 1981, pp.179-198.

Mantell, C. L. Batteries and Energy Systems. McGraw-Hill Company. New York. 1983.

Mayo, Edward E, et al. "Newtonian Aerodynamics for Blunted Raked Off Circular Cones and Raked Off Elliptical Cones", NASA TN D-2624.

McDougall, Angus. Fuel Cells. John Wiley and Sons. New York. 1976.

Menees, G.P. "Design and Performance Analysis of a Conical Aerobrake Orbital Transfer Vehicle Concept", Progress in Astronautics and Aeronautics, Vol.96, 1984.

Menees, Gene P. "Thermal Protection Requirements for Near-Earth Aeroassisted Orbital Transfer Vehicle Missions", Progress in Astronautics and Aeronautics, Vol.96, pg.257.

Menees, Gene P., Chul Park, and John Wilson. "Design and Performance Analysis of a Conical Aerobrake Orbital Transfer Vehicle Concept", Progress in Astronautics and Aeronautics, Vol.96, pg.286.

Menees, Gene P., and Kevin Brown. "Aerothermodynamic Heating Analysis of Aerobraking and Aeromaneuvering Orbital Transfer Vehicles", Progress in Astronautics and Aeronautics, Vol.96, pg.338.

Meyer-Arendt, Jurgen R., Introduction To Classical and Modern Optics, Prentice-Hall, New Jersey, 1984.

Oglevie, Ronald: Autonomous Flight Control for Low Thrust Orbital Transfer Vehicles. Irvine Technology Group, Irvine, Calif., 1986.

O'Shea, Donald C.,Ed., "Selected Papers on Optomechanical Design," vol. 770, 1988.

Pitts, W.C., and M.S. Murbach. "Thermal Response of an Aeroassisted Orbital Transfer Vehicle with a Conical Drag Brake", Progress in Astronautics and Aeronautics, Vol.96, pg.361.

Powell, Richard W. ,et al. "Performance Evaluation of the Atmospheric Phase of Two Aeromaneuvering Orbital Transfer Vehicles", Progress in Astronautics and Aeronautics, Vol.96, pg.143.

Ratliff, James E. "FDMA System Design and Analysis for the Space Station" NASA/ Lyndon B. Johnson Space Center. Houston, TX 1986

Roberson, Robert. "Attitude Control", Advances in Space Science and Technology, 1960.

Roden, Martin. Analog and Digital Communication Systems. Prentice-Hall, Englewood Cliffs, NJ 1985.

Scott, C.D., et. al. "An AOTV Aeroheating and Thermal Protection Study", Progress in Astronautics and Aeronautics, Vol.96, 1984.

Scott, C.D., et al. "Aerobraking Orbital Transfer Vehicle", NASA N86-20471.

Sperry Flight Systems, "Control Moment Gyros", May, 1982.

Stuhlinger, Ernst. "The Flight Path of an Electrically Propelled Space Ship." Army Ballistic Missile Agency, Huntsville, Ala., 1957.

Sutton, George. "Rocket Propulsion Elements", Wiley-Interscience, New York, 1986.

Tietz, J.C., Kelly, J.H., "Development of an Autonomous Video Rendezvous and Docking System," Martin Marietta.

Torre, Chris N, Low-Pressure/Lightweight Cryogenic Propellant Tank Design for the Space-Based Orbital Transfer Vehicle. AIAA Paper 86-0915. 1986.